SYNTHESIS AND CHARACTERIZATION OF ELECTRODEPOSITED NICKEL BASED ALLOYS AND THEIR NANOCOMPOSITE COATINGS

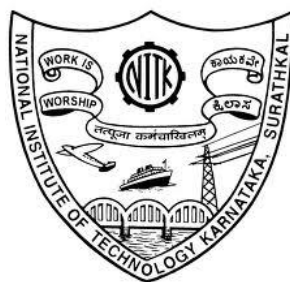Thesis

Submitted in partial fulfillment of the requirements for the degree of

DOCTOR OF PHILOSOPHY

By

LIJU ELIAS

DEPARTMENT OF CHEMISTRY

NATIONAL INSTITUTE OF TECHNOLOGY KARNATAKA,

SURATHKAL, MANGALURU – 575 025

August, 2017

DECLARATION

By the Ph.D. Research Scholar

I hereby *declare* that the Research Thesis entitled "**Synthesis and Characterization of Electrodeposited Nickel Based Alloys and Their Nanocomposite Coatings**", which is being submitted to the **National Institute of Technology Karnataka, Surathkal** in partial fulfillment of the requirements for the award of the Degree of **Doctor of Philosophy** in **Chemistry** is a *bonafide report of the research work carried out by me*. The material contained in this Research Thesis has not been submitted to any University or Institution for the award of any degree.

LIJU ELIAS
Register number: 138026CY13F06
Department of Chemistry
National Institute of Technology Karnataka, Surathkal

Place: NITK-Surathkal
Date : 02-08-2017

CERTIFICATE

This is to *certify* that the Research Thesis entitled "**Synthesis and Characterization of Electrodeposited Nickel Based Alloys and Their Nanocomposite Coatings**", submitted by **Liju Elias** (Register No: **138026CY13F06**) as the record of the research work carried out by him, is *accepted as the Research Thesis submission* in partial fulfillment of the requirements for the award of degree of **Doctor of Philosophy**.

Dr. A. Chitharanjan Hegde
Research guide
(Signature with date and seal)

Chairman-DRPC
(Signature with date and seal)

__Dedicated to my beloved Family and__

__Teachers who taught me right from kindergarten till today...__

Thanks for all, who inspired the hope in me;

Ignited my imagination;

And be a reason for instilling in me – a love of learning.

ACKNOWLEDGEMENT

My special thanks are due to my colleagues Dr. Yathish Ullal, Dr. Vaishaka R. Rao, Ms. Sandhya S. and Ms. Akshatha S. for their encouragement and cooperation.

I take this opportunity to thank my all friends from NITK like, Mr. Praveen Naik, Ms. Medhashree H., Ms. Ansari Rasheeda M., Dr. Gibin George, Mr. Arun Augustin, Dr. Goutham Sarang, Mr. Ahammed Rizwan, Dr. Manojkumar N., Mr. Abhinav K. Nair, Mr. Sreejesh M., Mr. Nimith K. M., Mr. Siby Thomas, Mr. Prashanth Huilgol, Dr. V. Ansal, Mr. Ramu Geddavalasa and Mr. Ramu Srikakulapu among many for their company, love and affection. I must also remember all my teachers and every great soul who has perhaps anonymous for passing their knowledge to me in shaping my mind and developing confidence in me.

Special thanks to my family. Mere words cannot express how grateful I am to my parents, Mr. Alias E. D. and Mrs. Leela Alias for all sacrifices they made on my behalf. Their prayers gave me the endurance to sustain this far. Above all I humbly thank God Almighty, who showered the choicest of his blessings to complete this endeavor.

LIJU ELIAS

Abstract

This thesis titled '*Synthesis and Characterization of Electrodeposited Nickel Based Alloys and Their Nanocomposite Coatings*' is a comprehensive approach for improving the corrosion resistance and electrocatalytic activity of binary alloys, namely Ni-W and Ni-P. New alkaline citrate baths have been optimized for the electrodeposition of Ni-W and Ni-P alloy coatings through standard Hull cell method, using glycerol as a common additive. The effect of bath composition, deposition current density (c. d.), pH and concentration of additive on the coating properties were studied. The corrosion resistance of monolayer alloy coatings were improved to many folds of its magnitude through multilayer approach by depositing in layers, having alternatively different composition. Further, the benefit of magnetoelectrodeposition (MED) has been explored for improving the coating characteristics of Ni-W alloy. The conditions of MED have been optimized for maximizing the corrosion protection efficacy of Ni-W alloy coatings. The effect of magnetic field (B) on coating characteristics, in both intensity and direction have been tested. A significant change in the deposit characters have been observed due to increase in the limiting current density (i_L), explained by the magnetohydrodynamic (MHD) effect. The electrocatalytic activity of the alloy coatings towards hydrogen evolution reaction (HER) and oxygen evolution reaction (OER) were tested using electrochemical methods. The HER efficiency of the coatings was further enhanced by different methods such as electrochemical dissolution, MED, magnetic field induced HER (MFI-HER), and by nanoparticles incorporation. All depositions were carried out for the same duration (10 min) for comparison purpose. The corrosion resistance and electrocatalytic activity of Ni-based alloy coatings and their nanocomposite coatings were compared in relation to their composition, surface morphology and phase structure. The process and product of electrodeposition were characterized using different analytical techniques, like SEM, XRD, EDS etc. The performance of the coatings have been compared and discussed with Tables and Figures, supported by plausible mechanism.

Keywords: *Electrodeposition; Ni-W; Ni-P; MED; corrosion study; HER and OER; MFI-HER; nanocomposite coatings.*

CONTENTS

LIST OF FIGURES

iii

iv

LIST OF TABLES

xii

NOMENCLATURE

°C	Degree Celsius
µm	Micrometer
A	Ampere
AC	Alternating current
B	Magnetic field
c.d.	Current density
CCCD	Cyclic cathode current density
CCE	Cathode current efficiency
cm	Centimeter
CMM	Composition modulated multilayer
CMMA	Composition modulated multilayer alloy
CP	Chronopotentiometry
CR	Corrosion rate
CV	Cyclic voltammetry
CV's	Cyclic voltammograms
CVD	Chemical vapour deposition
DBT	Dual bath technique
DC	Direct current
dm	Decimeter
E_{corr}	Corrosion potential
ED	Conventional electrodeposition
EDL	Electrical double layer
EDS	Energy dispersive spectroscopy
EEC	Electrical equivalent circuit
EIS	Electrochemical impedance spectroscopy
E_{pa}	Anodic peak potential
E_{pc}	Cathodic peak potential
FESEM	Field emission scanning electron microscopy

F_L	Lorentz force
FTIR	Fourier transform infrared spectroscopy
FWHM	Full-width half maximum
GMR	Giant magnetoresistance
GO	Graphene oxide
HER	Hydrogen evolution reaction
ICDD	International commission on diffraction data
i_{corr}	Corrosion current density
i_L	Limiting current density
i_{pa}	Anodic peak current density
i_{pc}	Cathodic peak current density
JCPDS	Joint committee of powder diffraction standards
K	Kelvin
kHz	Kilohertz
M	Molarity
MBE	Molecular beam epitaxy
MED	Magnetoelectrodeposition
MFI-HER	Magnetic field induced HER
MHD	Magnetohydrodynamics
mHz	Millihertz
min	Minute
mL	Milliliter
mM	Millimolar
$mm\ y^{-1}$	Millimeters per year
MS	Mild steel
mV	Millivolt
MWCNT	Multi-walled carbon nanotube
nm	Nanometer
OCP	Open circuit potential
OER	Oxygen evolution reaction
PVC	Polyvinyl chloride

PVD	Physical vapor deposition
PVP	Poly(vinyl pyrrolidone)
R_{ct}	Charge transfer resistance
rGO	Reduced graphene oxide
s	Second
SBT	Single bath technique
SCE	Saturated calomel electrode
SEM	Scanning electron microscopy
SNS	Silver nanoparticle sol
T	Tesla
TCE	Trichloroethylene
TEM	Transmission electron microscopy
UV-Vis	Ultraviolet-visible
V	Volt
Wt.%	Weight percent
XRD	X-ray diffraction

INTRODUCTION AND LITERATURE REVIEW

This chapter gives a brief introduction to electrodeposition and its applications. An overview of electroplating process, its controlling parameters and advancements in electrodeposition are also included. The theory of electrodeposition, with a special emphasis on principles of alloy deposition and modern methods of electroplating such as composition modulated multilayer (CMM) deposition and magnetoelectrodeposition (MED) are explained. An introduction to corrosion and electrocatalysis along with the application of electrodeposited coatings towards corrosion protection and electrocatalytic water splitting reactions are also discussed. The importance of Ni-based alloys for corrosion resistance and electrocatalytic activity are reviewed in brief. Finally, the motivation of the present research work with its scope and objectives are also presented.

1.1 ELECTROPLATING TECHNOLOGY

Surface science is an interdisciplinary subject in materials science which deals with the surface of solid matter, and finds applications in chemistry, mechanical engineering, electrical engineering etc. Surface engineering basically involves changing of surface properties to reduce the degradation over time. This is accomplished by making the surface robust to the environment or application in which it will be used. Surface finishing is a promising engineering technique in this regards to enhance the surface properties by applying a thin complementary layer on the surface of the bulk material. Such finishing treatment can ensure enhancement in material properties like durability, decorative appeal, electrical conductivity, chemical resistance, tarnish resistance etc. Though many surface finishing technologies are available, electroplating has been evolved as a promising technology over recent decades due to its development from an art to an exact science. The wide acceptability of electroplating in practical science and engineering is evident from the ever increasing number publications in this field. Electroplating, or electrochemical deposition deals with the synthesis of thin solid films

from dissolved species by alteration of their oxidation states accomplished using external power source [Kanani 2004]. In other words, it can be defined as the process of depositing the metal/alloy onto the surface of a substrate by electrochemical reduction of metal ions by passing direct current (DC) through their electrolyte solution. The advantages such as low cost, formation of thicker deposit, convenience in depositing on complex shapes, easiness in controlling and modifying the deposit character etc., making it more attractive.

The ultimate aim of electroplating technology is to develop the plated film with desired mechanical, physical and chemical properties that meet many applications. Many extensive works in the field of electroplating technology have already been published, focusing on their electrochemical study. In addition to the traditional use of electroplating technology for surface finishing, it is now used to develop materials/coatings of high performance by exploiting the incredible benefits of this method [Dini 1993]. Today, electroplating technology is responding in both revolutionary and evolutionary ways due to ever increasing demand in industry. It has turned into an important means for developing nano/micro structured materials showing variety of functional properties. Some of the technological areas in which electroplating finds important place are: macro and micro-electronics, optics, optoelectronics, Giant magnetoresistance (GMR) and sensors of most types, to name only a few among many [Schwarzacher 2006].

A number of key industries such as automobile industry (which uses for example chrome plating to enhance the corrosion resistance of metal parts) adopt electroplating, even where other methods, such as evaporation, sputtering, chemical vapor deposition (CVD), physical vapor deposition (PVD) etc. are available, due to genuine reasons of economy, accuracy, reproducibility and convenience involved in the process. Due to rapid progress seen in the field of electroplating, in terms of new advanced methods of deposition like composite electrodeposition, magnetoelectrolysis, sonoelectrolysis etc., electroplating emerged as one of the leading-edge technologies today [Schwarzacher 2006, Luo et al. 2006]. Moreover, the precise knowledge on process and product of electroplating became possible due to modern instruments.

1.1.1 History of electroplating

Volta's discovery of the chemical way to produce electricity in 1799 led to a wide interest of electrolysis. The Italian chemist Luigi Brugnatelli introduced electroplating first through depositing gold using Voltaic Pile. Forty years later, John Wright of Birmingham, England discovered that potassium cyanide as a suitable electrolyte for gold and silver electroplating. The electroplating process was first patented by cousins Henry and George Richard Elkington [Schlesinger and Paunovic 2006]. Thereafter several patents were issued for electroplating in the year 1840. In the initial stages, the electroplating was mainly focused on the deposition of copper from its simple salts, whereas by 1850's electroplating methods for the development of bright nickel, brass, tin and zinc were commercialized for engineering and specific applications. The next new wonder in terms of electroplating came as economical jewellery, when the process was applied to costume jewellery in 1857 [Schlesinger and Paunovic 2006]. The laws introduced by Michael Faraday in 1833 and Walther J. Nernst in 1898 are the fundamentals of electrodeposition [Kanani 2004]. Since then, the electroplating technology has developed progressively, and today it has emerged as a multidisciplinary subject of mechanical, materials and electrical engineering in co-ordination with applied chemistry [Luo et al. 2006].

1.2 PRINCIPLES OF ELECTROPLATING

Generally, galvanostatic electrodeposition, by applying a constant current between the electrodes is widely used than the potentiostatic electrodeposition method. In the case of potentiostatic electrodeposition, deposition carried out at controlled and constant potential, where the stoichiometry of the product needs to be strictly controlled. The control over potential in such cases is attained using a reference electrode, whereas it is not required for galvanostatic electrodeposition [Dini 1993]. A simple galvanostatic electrodeposition unit, containing an electrolyte, two electrodes and a DC power source is shown in Fig. 1.1. By convention, it can be stated categorically that the cathode is always the electrode at which a reduction process like metal deposition or hydrogen evolution takes place. Similarly, the anode is always the electrode at which oxidation like metal dissolution or oxygen evolution takes place. The cathode is the one where

the metal (or alloy) is deposited, and anode can be coating metal itself or semiconductor or non-metallic conductor such as graphite. The primary purpose of this is to complete the electrical circuit, and as metal cations are removed from solution as the metal, one or more balancing processes must take place at the anode to remove anions and thereby maintaining overall charge neutrality in solution. The anode may or may not fulfill the second function, which is to provide a source of fresh metal to replace what has been removed from solution by deposition at the cathode [Dini 1993, Kanani 2004].
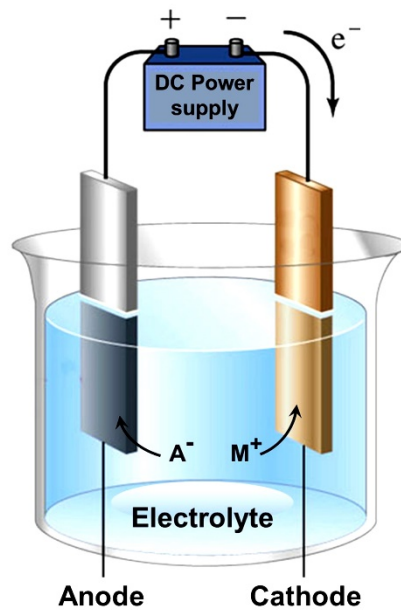
Fig. 1.1- Schematic of a simple DC electroplating unit

The reaction proceeding near the electrode surface is completely controlled by the current passed. The cations move towards the cathode where they are discharged and deposited as metal/alloy (Equation 1.1). The anode undergoes depletion at the same time to replace the metal ions removed and thereby maintaining a constant metal ion concentration in the electroplating bath (Equation 1.2). The overall mechanism is known as electrolysis. However, in the case of insoluble anodes such as stainless steel and platinum, oxidation of water takes the lead [Schlesinger and Paunovic 2006].

$$M^{n+} + ne^- \rightarrow M \ (lattice) \tag{1.1}$$

$$M \rightarrow M^{n+} + ne^- \tag{1.2}$$

The fundamental principles of electrodeposition are based on Faraday's laws of electrolysis. The main advantages of electrodeposition technique over other coating

4

methods like, easiness in making coatings as thin as possible with uniform thickness, smooth surface with decorative appeal, dense and the fine-grained structure, good adhesion to the substrate, high corrosion resistance, less internal stress, sufficient ductility, high hardness and strength, high wear resistance, uniform and low coefficient of friction etc. making it more attractive [Kanani 2004, Schlesinger and Paunovic 2006].

1.2.1 Faraday's laws of electrolysis

The whole concept of electrodeposition is governed by much celebrated laws of electrochemistry, called Faraday's laws of electrolysis. The laws relate the current flow, time and equivalent weight of the metal with the weight of the deposit, as stated below:

1.2.1.1 Faraday's first law of electrolysis

The mass of substance deposited/dissolved at an electrode during the electrolysis is directly proportional to the quantity of the electricity consumed at the electrode according to the Equation 1.3. The quantity of the electricity is the electric charge measured in coulombs.

$$m = \frac{QM}{zF} \tag{1.3}$$

Where, m is the mass of the deposit produced at the electrode (in grams) and Q is the electric charge (in coulombs) required for the process, M is the molar mass of the substance, F is the Faraday constant (96,485 C mol^{-1}), z is the valence number of the ions involved in deposition.

1.2.1.2 Faraday's second law of electrolysis

The second law states that, for a given quantity of electric current passed through different electrolytes, the mass of the metal deposited or dissolved at an electrode is directly proportional to the electrochemical equivalent weight of the metal deposited/dissolved, according to the Equation 1.4.

$$m = \frac{A \times I \times t}{z \times F} \tag{1.4}$$

Where, *A* is the atomic weight of the metal deposited or dissolved, *I* is the actual current passed in ampere, *t* is the time in seconds, *z* is the valence number of ions involved in the reaction and *F* is the Faraday constant (96,485).

1.3 ROLE OF DIFFERENT VARIABLES ON PROCESS OF DEPOSITION

Electrodeposition is one of the most attractive methods for the synthesis of new materials with tailor-made properties on wide range of base metals. Though it is very simple to execute with low cost, the process of electrodeposition is very complex due to the unusually large number of critical elementary steps and operating parameters which control the overall process. The main factors which can influence the process of plating are: *i)* metal salt and electrolyte concentration, *ii)* deposition current density (c.d.), *iii)* temperature, *iv)* agitation, *v)* polarization, *vi)* pH of the electrolytic bath, *vii)* substrate effects and *viii)* nature of anode [Kanani 2004, Luo et al. 2006]. A large number of variable apart from these can also affect the structure and properties of deposits, however, the above are of greater significance in electroplating process.

i) Metal salt and electrolyte concentration

The most important variable that can influence the coating properties is the concentration of the metal salt or metal source in the electroplating bath. In the case of alloy deposits, the composition of the alloying elements in the coating depends largely on the concentration of the two or more parent metals in the bath. In general, the ratio of metals in an electrodeposited alloy differs considerably from their ratio in the electrolytic bath. Whereas, under some special conditions, the ratio of metals can be the same in both the bath and the alloy deposit [Parthasaradhy 1989, Kanani 2004].

ii) Current density

The deposition c.d. is one of the main factors affecting the structure and morphology of the electrodeposited coatings. The c.d. is important not only in determining the deposition rate, but also in the size and distribution of the crystallites. In general, an increase in deposition c.d. can enhance the less noble metal content in the deposit. The extent of influence of c.d. on coating characteristics is likely to be greater in simple primary salt solutions than in complex solutions [Parthasaradhy 1989, Kanani 2004].

6

iii) Agitation

Agitation during the process of electrodeposition is of crucial importance to enhance the deposition rate by minimizing the retarding effect due to concentration polarization. An increase in agitation usually increases the amount of more noble metal in the alloy plate. Agitation decreases the cathode layer thickness and thereby brings more number of fresh noble metal ions to the cathode surface and, which leads to an increase in the proportion of the more noble metal in the deposit [Parthasaradhy 1989].

iv) Temperature

An increase in bath temperature usually tends to increase the proportion of more noble metal in the alloy deposit, as same as the effect observed when agitation of the bath is increased. The increase in temperature decreases the polarization of the more noble metal, relatively more than the polarization of the less noble metal [Parthasaradhy 1989].

v) Polarization

The polarization is a common phenomenon result in decreasing the efficiency of the plating bath during deposition. The evolution of hydrogen taking place at the cathode surface during alloy deposition has significant effect on the polarization, and thereby the composition of the alloy deposited. If the hydrogen evolution is more, the potential of the cathode may be determined almost completely by the hydrogen evolution reaction during alloy deposition [Kanani 2004]. In such cases, even increase in current also can enhance only hydrogen evolution rather than deposition, leading to poor efficiency of alloy deposition with a minor change in composition of the deposited alloy. Whereas, if the overpotential for hydrogen evolution is high, the current corresponds to the individual metal deposition become close to limiting values leading to enhanced deposition [Parthasaradhy 1989].

vi) pH of the electrolytic bath

The pH of plating bath is a significant parameter which can affect the deposit character obtained at the cathode surface. The pH of the bath can be either acidic or basic according to the bath constituents and the type of metal ions to be deposited [Kanani 2004]. Maintaining the bath pH at the same value obtained by dissolving all the bath constituents or making a slight variation from this value is more preferable than

introducing a large variation in the plating bath pH. The bath pH fixing is more concerned to the stability of electrolyte during deposition, i.e., there is possibility for precipitation of the hydroxides of the metals at higher pH. The plating baths operating at very low pH may show low efficiency due to more hydrogen evolution. The required pH of the bath can be adjusted using suitable buffers [Parthasaradhy 1989].

vii) Substrate effects

The surface characteristics of the substrate is also a principal factor affecting the crystal growth during deposition. The proper surface preparation of the cathode before plating can enhance the efficiency of deposition and thereby the quality of the deposit. Normally, the individual crystallites in the coating often adopt an orientation determined by the underlying substrate. In a similar manner, the size of crystallites in the deposit can also be influenced by that of the crystallites in the substrate [Parthasaradhy 1989].

viii) Nature of anodes

The nature of anodes used for plating process is equally important in determining the coating characteristics. The anodes fall in two categories, sacrificial anodes and permanent anode. The sacrificial anodes are made of same metal that is being deposited, and which can anodically dissolve into the plating solution and replace the metal ions which have been deposited at the cathode [Parthasaradhy 1989]. Whereas, the second type is electrochemically inactive and it can act only as a conducting electrode. In this case, the metal ion depletion from the plating bath is compensated by adding the metal source in the form of metal salts [Kanani 2004].

1.4 ELECTROPLATING BATH

The electrodeposition of metal coatings is usually based on aqueous electrolytes, known as electrodeposition baths or simply, baths. Their primary constituents are metal salts of the metal to be deposited; in most cases, they are either acidic or alkaline to promote conduction, and in some cases, it is buffered. In order to optimize the deposit properties, a small amount of additives, or complexing agents are used [Parthasaradhy 1989]. Many electrolytes used in metal finishing are based on complexes. The metal deposition is brought about either by current flow from an external power source, or by the addition

of strong reducing agents, which set up a coupled anodic and cathodic reaction. Depending on which is the case, the terms 'electrodeposition' and 'electroless deposition' are used. In both the cases, the composition and operating parameters of the bath are crucial in attaining a good quality deposit.

1.4.1 Optimization of plating bath

In principle, electroplating of a metal/alloy is not a simple dip and dunk process. It is probably one of the most complex processes known because of the unusually large number of critical elementary phenomena, or process steps involved [Schlesinger and Paunovic 2006]. Generally, a practicable method for electrodepositing any metal/alloy involves three steps; preparation of the surface to be plated, optimization of the plating bath and finally deposition from the proposed bath. In this, the most important step is concerned with the development of a suitable plating bath. This requires a practical knowledge of the electrochemistry of elements, the solubility of their salts, and the chemistry of their complexes. Since all necessary information on the process of alloy deposition is usually not available, the researcher must draw on the analogy with known successful procedures for deposition as a guide, and to make a large number of electrolytic experiments on solutions. Such a research may be partly empirical, and therefore a tendency exists to ignore it. Hence, due to lack of some quantitative guiding principles, the electroplaters are required to rely on some semi-empirical procedures upon which generalizations and theories can be built [Dini 1993]. In this regard, Hull cell experiment is widely used as a practical tool for plating bath optimization.

1.4.1.1 Hull cell - An invaluable analytical tool in electroplating

Hull cell, named after its inventor Richard Hull, has been brought into practice in electroplating industry as early as 1939 [Kanani 2004]. The Hull Cell is a miniature plating unit designed to produce cathode deposits on a panel that correlates the characteristics of the plating bath being evaluated [Lima et al. 2012]. The schematic diagram of Hull cell (267 mL) is shown in Fig. 1.2.
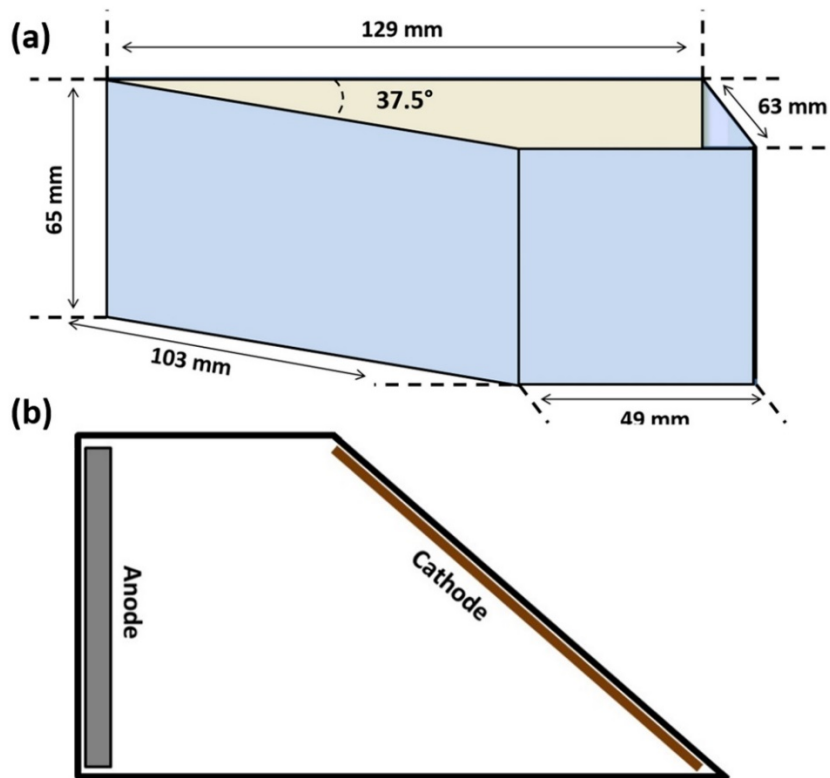
Fig. 1.2- Hull cell for optimization of plating bath: a) plan view, and b) top view

From Fig. 1.2, it may be seen that Hull cell is a miniature electrodeposition tank, in which the cathode is angled with respect to the anode as shown in Fig. 1.2(b). As a result, when a voltage is applied across the anode and cathode, the resulting current density will vary along the length of the cathode, being highest at the point it is closest to the anode. The c.d. distribution in Hull cell panel is shown in Fig. 1.3.
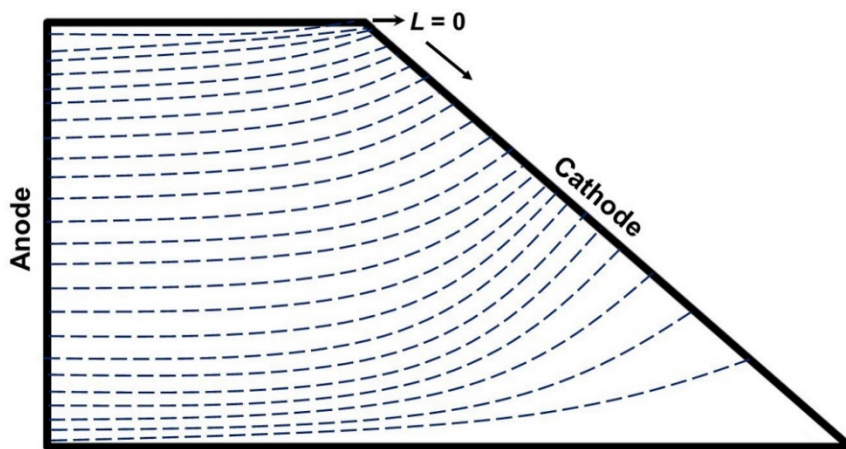
Fig. 1.3- Current density distribution in Hull cell panel (Adopted from Lima et al. 2012)

The c.d. at required point on the Hull cell panel can also be calculated using the Equation 1.5.

$$I = C(5.10 - 5.24 \log L) \tag{1.5}$$

Where, I is the c.d. in A dm^{-2} at any point on the cathode, C is the cell current used for the test, and L is the distance in 'cm' at a point on the cathode, where the c.d. is desired to achieve. In this way, one can, within a single test run, assess the effect of varying c.d. Accordingly, after such a run, the cathode was removed and inspected. Interpretation of the 'as plated' cathode panel give rapid information about brightness levels, irregular plate deposits, uniformity of deposits, coverage, throwing power, impurities, and plating bath chemistry [Lima et al. 2012]. Depending upon the bath chemistry as analyzed, condition of the panel relative to brightness, hardness, uniformity, burning, etc., modification by controlled additions can be made to the Hull cell plating solution and procedures can be repeated. Changes caused by addition to the Hull cell will duplicate results to be expected by the same proportionate additions to the main plating bath. Correlations of properties such as hardness and thickness of the coatings in the given deposition time, temperature and c.d. will also tell the optimum plating range to obtain deposit of desired properties [Kanani 2004, Lima et al. 2012]. Within the limits of recommended operating parameters of a particular plating solution, the Hull cell will duplicate what is actually occurring in the main plating unit. Correlation of the 'as plated' panel and the '*Hull Cell Scale*' allows rapid, non-destructive testing of plating solutions for research, preventative maintenance, troubleshooting, and quality control [Lima et al. 2012].

1.4.2 Characteristics of electrolytic bath

The covering power, throwing power and cathode current efficiency (CCE) are the very important characteristics of an electrolytic plating bath to obtain a bright coating for industrial applications.

i) Covering power

In electrodeposition, the term covering power of an electrolyte describes the extent to which it can cover the entire surface of the substrate, with reasonably uniform thickness [Dini 1993]. The metal deposition begins only above certain deposition potential, which mainly depends on the nature of the depositing metal and the substrate surface. There

is a minimum c.d. for an electrolytic bath to show the covering power. The covering power of the plating bath and its dependency on deposition c.d. can be determined using Hull cell experiment [Brenner 1963]. The covering power of an electrolytic bath is largely a reflection of the energy of nucleation at the work surface. The composition and operating parameters of the plating bath, and the nature of the substrate are the factors mainly influencing the throwing power. Generally, covering power increases with deposition c.d. and decreases with temperature [Brenner 1963, Kanani 2004].

ii) Throwing power

The depositing metal/alloy coating doesn't grow uniformly at the same rate across the surface due to various factors which influences the rate of deposit growth. The throwing power of an electrolyte is its ability to lay down, as nearly as possible, a uniform thick deposit across the substrate surface [Dini 1993]. The more is its ability in this, the better is the throwing power. The plating bath to show good throwing power, it should have good covering power. The throwing power of an electrolyte depends mainly on the primary and secondary c.d. distribution in the system, i.e., current distribution according to Ohm's law and overvoltage, respectively [Kanani 2004].

iii) Cathode current efficiency

The CCE or Faradaic efficiency of a metal/alloy plating bath can be calculated from the weight of the deposit plated for a known time, at a known current and knowing the electrochemical equivalents of the deposited metal/alloy using the Equation 1.6 [Dini 1993]. According to Faraday's law, the amount of deposit formed at the electrode is exactly proportional to the total quantity of electricity passed. However, simultaneous occurrence of several reactions at the cathodic site can affect the efficiency [Kanani 2004].

$$CCE \ = \ \frac{w \times 100}{E_a \times c} \tag{1.6}$$

Where, w is the weight of the metal/alloy deposit in grams, E_a is the electrochemical equivalent weight of the metal/alloy, c is the amount of electricity passed in Coulombs. The CCE is a fractional value, usually expressed as a percentage of the current passing through an electrolytic cell (or an electrode) that accomplishes the desired chemical reaction. In plating, usually increase in the deposition c.d.

decreases the CCE. Whereas, increasing metal content in the electrolyte, bath temperature and agitation leading to an increases in the CCE [Kanani 2004].

1.5 MASS TRANSPORT MECHANISMS IN DEPOSITION

During electrodeposition, when a deposition c.d. is applied across the two electrodes in an electrolytic cell containing optimal electrolyte, the metal ions in the solution moves towards the cathode and get deposited. At the same time, the anions present in the solution moves in the opposite direction, i.e., towards the anode. Thus, current flows through the solution by virtue of the movement of ions, known as the ionic current or electrolytic conductance [Brett and Brett 1993]. In the case of electrodeposition, the mechanism and the rate by which the metal ions are delivered at the cathode from the bulk of the solution is of great importance. The ionic transport within the electrolyte depends on various factors and hydrodynamic conditions near the cathode surface [Schlesinger and Paunovic 2006]. There are mainly three mass transport mechanisms involved in the delivery of metal ions to the cathode surface during deposition such as; migration (under a potential gradient), diffusion (under a concentration gradient) and convection (movement of the electrolyte solution itself) [Kanani 2004].

i) Migration

When a particular deposition c.d. is applied across an electrolytic solution during electrodeposition, assuming that the solution shows same conductivity at all points in the solution. Then, the potential gradient is given by the voltage across the solution (excluding overvoltage) divided by the distance between the electrodes. The rate of the ionic movement in the solution is determined by the magnitude of potential gradient, and such movement of ions under potential gradient is called migration [Brett and Brett 1993]. This effect operates throughout the solution, anions being electrostatically attracted to the anode, and cations to the cathode. The collision of ions with solvent molecules and the viscous drag due to the formation of hydration sheaths around the ions impedes the rate of migration [Kanani 2004].

ii) Convection

The mass transport results from the movement of the bulk solution is called the convective mass transport. It can be achieved by stirring the plating bath either through

mechanical agitation or through the advent of other methods like ultrasound, magnetic field etc. The effect due to convective mode of mass transfer ceases near the electrode surface, i.e., where the stagnant or diffusion layer formed [Brett and Brett 1993]. The effective movement of ions across the diffusion layer can be effected only through diffusion. The convection becomes important in electrodeposition due to its effectiveness in reducing the diffusion layer thickness. The stronger the agitation or stirring, thinner will be the diffuse layer [Kanani 2004].

iii) Diffusion

The final step of mass transfer just before the process of deposition at the cathode surface is the movement of ions across the diffusion layer. The driving force behind this diffusion is concentration gradient, in other words chemical potential [Brett and Brett 1993]. Under open circuit conditions, the concentration of the depositing species remains the same both at the electrode surface and in the bulk of the solution. However, once deposition c.d. is applied, the concentration of the metal ions get depleted at the electrode surface, leading to the formation of a concentration gradient. Hence, the tendency of the depositing species to move from a high concentration region to a lower concentration are the driving force for the diffusion process, as explained by the Fick's law of diffusion [Schlesinger and Paunovic 2006]. Generally, diffusion is assumed as the only significant mass transport mechanism operating within the Nernstian layer. The thickness of the diffusion layer or Nernstian layer decreases under forced convection [Kanani 2004].

1.5.1 Influence of mass transport on electrodeposition

During electrodeposition, the metal ions (M^{n+}) have to be transported from bulk electrolyte to the cathode surface. In general, this mass transport occurs by diffusion, convection, and migration [Brenner 1963]. Close to the electrode surface, the primary mass transport process is diffusion. In other words, the rate of deposition is limited by the transport of metal ions [Schlesinger and Paunovic 2006]. The limiting or the maximum current density of deposition can be given by the Equation 1.7.

$$i_{L} = \frac{nFD}{\delta}c_{b} \qquad (1.7)$$

Where, D is the diffusion coefficient of the depositing species, c_b is the bulk concentration of the M^{n+} ions in the solution, n is the number of electrons involved in

the reaction, δ is the diffusion layer thickness (according to the Nernst diffusion layer model) and F is the Faraday constant. The limiting current density (i_L) is having great practical significance in metal/alloy deposition since the type and quality of the deposits depend on the relative values of the deposition c.d. and i_L. Moreover, in the case of alloy deposition, the i_L values are very significant factor which influencing the composition of the coating [Schlesinger and Paunovic 2006].

1.6 MECHANISM OF ELECTRODEPOSITION

The process of deposition of metal/alloy on the substrate surface from an aqueous electrolyte of its salt solution is an exceptionally interesting case of change of state. The four possible rate controlling steps such as charge transfer, diffusion, chemical reaction and crystallization, are involved in the deposition process whereby a positively charged metal ion, on reaching at the cathode become transformed into an atom at the electrode/electrolyte interface and takes its place in the growing crystal lattice [Dini 1993]. This solid, compact, metallic layer of deposit can be achieved by two different processes: *i)* electrodeposition process, in which electrons are provided by an external power supply, and *ii)* electroless (autocatalytic) deposition process, in which a reducing agent in the solution is the electron source, without using any external power supply. Among which, electrodeposition finds significant industrial significance than electroless method due to the obvious limitations of electroless plating, such as use of expensive reducing agent, a high operating temperature and difficulty in controlling the deposition rate [Kanani 2004].

The electrodeposition process is more complex, involving a number of intermediate stages such as: *i)* transfer of the hydrated metal ions or complex from the bulk solution to the cathode surface, *ii)* stripping of the hydration sheath of the metal ions after reaching at the electrode/electrolyte interface, *iii)* charge transfer with the formation of the adsorbed atoms at the cathode surface, *iv)* formation of the crystal nuclei by the diffusion of the adsorbed atoms at the cathode surface, *v)* fusion of the thermodynamically stable crystal nuclei to form a metallic layer [Kanani 2004], as shown in Fig. 1.4.

15
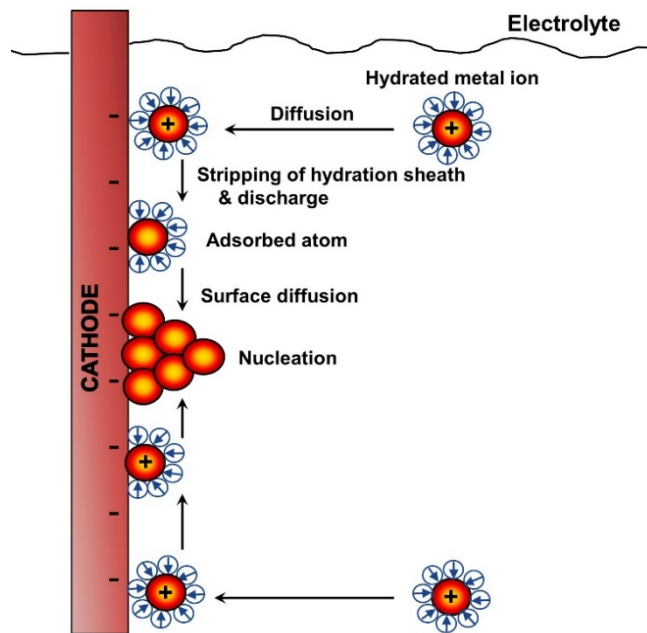
Fig. 1.4- The simplified depiction of the individual steps involved in the overall process of electrodeposition (Adopted and modified from, Schlesinger and Paunovic 2006)

The transport of metal ions from the bulk solution to the work-surface is primarily due to convection and then due to diffusion, within the Nernstian layer. The diffusion of the adsorbed ions to the adsorbed atom through charge transfer takes place spontaneously within the diffusion layer, at the electrode/electrolyte interface. Though the metal ions lose most of their charge by this process, a part of hydration sheath remains with the adsorbed atoms due to residual charge. Further, the nucleation occurs through diffusion controlled migration of the adsorbed atoms leading to crystal growth or electrocrystallization, once the nuclei attained a critical size [Schlesinger and Paunovic 2006].

1.7 COATING CHARACTERISTICS

1.7.1 Hardness

The hardness or microhardness measurement of the electrodeposited coatings are very much important in evaluating the properties and predicting their usefulness. The changes in structure or composition of alloy coatings can be directly identified from the variation in microhardness values. Vickers microhardness measurements are the widely used method due to its less sensitivity towards errors arising from elastic properties than

in other methods [Aruna et al. 2009, Schlesinger and Paunovic 2011]. Whereas, the microhardness values are highly dependent on the specimen preparation, measurement, plating solution, deposit quality and the load applied. A small deviation in any of these controlling factors can lead to inconsistencies and contradictions. To get reasonably reliable microhardness values, the following three criteria's should be maintained: *i)* the deposit thickness should be at least ten times the depth of the indent (otherwise it may reflect the hardness of the substrate rather than the coating), *ii)* the distance between the indent and the substrate should be kept at least half of the diagonal of the indent to minimize the 'anvil' effect, *iii)* microhardness should be represented as an average of multiple measurements made in different parts of the specimen [Brooks et al. 2008, Aruna et al. 2009].

1.7.2 Deposit thickness

The thickness of the electrodeposited coatings is also an important characteristic which can affect its functional properties. The coating thickness can be theoretically evaluated by considering the volume of the deposit. Since volume *V* of the deposit is the product of plated area *a* and thickness or height *h* of the deposit, it allows to get $h = V/a$. Further, the volume of the deposit is related to its weight *w* and density *d* of the deposit by the relation, $d = w/V$. Therefore, we can correlate both the relations as in Equation 1.8.

$$h \ = \ \frac{V}{a} \ = \ \frac{w}{ad} \tag{1.8}$$

Where, the weight of the deposit *w* can be calculated from Faraday's second law. Hence, by knowing the deposition time in seconds, the thickness *h* at a given c.d. can be calculated using the relationship given in Equation 1.9 [Schlesinger and Paunovic 2006].

$$h \ = \ \frac{w}{ad} \ = \ \frac{ZQ}{ad} \ = \ \frac{ZIt}{ad} \tag{1.9}$$

1.8 FACTORS AFFECTING COATING PROPERTIES

The properties of coatings, of either metal, or alloy, can be tailored by adding other constituents into the electrolytic bath called additives. They can be divided into groups, based on their function as: *i)* primary and secondary salts, *ii)* brightening

agent, *iii)* complexing ions, *iv)* buffer compounds *v)* levelling agents and *vi)* salts promoting the anode solubility [Schlesinger and Paunovic 2006]. For a metal or alloy deposition, any one/or many of the above additives work synergistically to impart better quality to the deposit.

1.8.1 Effect of additives

Additives in the electroplating bath can affect the deposition and deposit growth as adsorbates, adsorbed substances, at the cathode surface. The adsorption of the additives on the substrate surface can be either chemical or physical in nature. These adsorbed additives can influence various factors in the deposition process such as, the concentration of deposit growth sites on the surface, concentration of adions on the surface, the diffusion coefficient of metal ions D and the activation energy of the surface diffusion of adions. Therefore, the additives greatly influence the electrodeposition kinetics and growth mechanism of the deposits. The quantity of additive agents required is surprisingly small and their action is often specific for a particular bath. Significant levelling of the grooves on the substrate surface can be achieved by the use of proper additives through uniform current distribution [Dukovic and Tobias 1990, Madore and Landolt 1996]. In metal finishing, bright and highly reflective surfaces can be achieved with the use of brightening agents for both decorative and functional performance [Weil and Paquin 1960]. The brightness of a coating is its optical reflecting power, and it is measured by the amount of light reflected specularly as shown in Fig. 1.5.
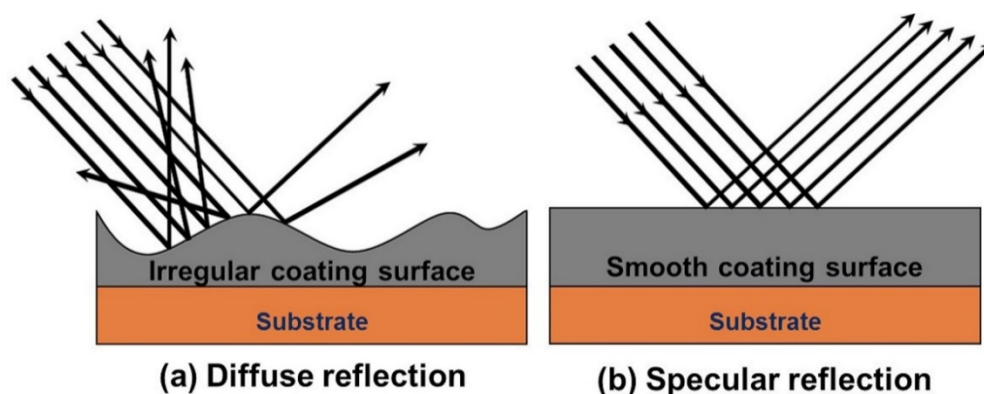
Fig. 1.5- Reflection on coating surface: a) diffuse reflection on rough surface, and b) specular reflection on smooth surface

Brightening can be defined as the ability of an electroplating solution to produce fine deposits which consist of crystallites smaller than the wavelengths of visible light, i.e., smaller than 0.4 μm [Liebreich 1935] and having oriented grain structure [Blum 1921]. A small grain size is a necessary, but it is not a sufficient condition for brightness; at the same time, not all fine-grained deposits are bright. The brightness depends on the degree to which morphological components of the surface of electrodeposits are in the same plane [Weil and Paquin 1960].

1.9 ALLOY PLATING

According to the metal handbooks, alloy can be defined as; "A substance that has metallic properties and is composed of two or more chemical elements of which at least one is a metal" [Brenner 1963]. The concept of alloy plating has come into existence due to the pursuit of achieving a better quality to simple single metal coatings. Chemical reactivity and corrosivity of electrodeposited alloys usually lie between that of the constituent metals. An alloy is usually more reactive than its nobler constituent and less reactive than its baser constituent. The functional properties of electrodeposited alloys depend on their chemical composition and on their structure in the micro and nanoscale [Kanani 2004]. Many factors could affect the composition and microstructure of electrodeposited alloy. Alloy deposits, however, produced, offer certain advantages over single metal deposits like; enhanced corrosion resistance due to greater density and finer grain structure, a combination of properties of the individual constituents, new properties unlike the individual constituents, tailor-made properties by proper selection of the constituents etc.

Today, electrodeposition of alloys is of great interest in many industrial applications like, automotive industry, due to their higher guarantee against corrosion attack than pure metal coatings. In practice, the usage of pure metals is very rare in manufacturing of finished products or semi-manufactures, since they fail to fulfill the required range of desired property. Only using an alloy of two or more metals, or metals and non-metals, the best combination of properties can be achieved. Alloy deposition in the atomic level usually implies the insertion of foreign atoms into the lattice structure of the parent metal, and generally in this the parent metal present in the highest amount. From this, depending on the type and the amount of foreign atom inserted, a

range of modified crystal lattices may result. The technique of alloy deposition can effectively be used to improve the properties of the base metals like; appearance, mechanical properties, wear and abrasion resistance, hardness, electrical and thermal conductivity, reflectivity, electrical, magnetic and corrosion resistance etc [Brenner 1963, Berkh et al. 2014]. The factors influencing the properties of electrodeposited alloys are schematically represented in Fig. 1.6.
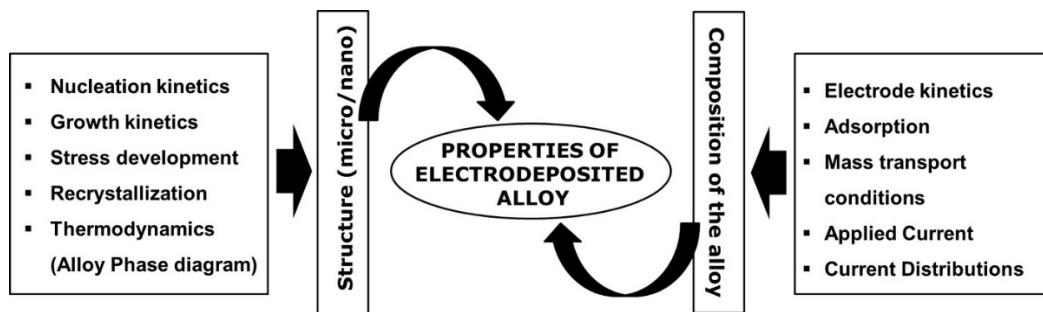
Fig. 1.6- Schematic diagram showing the factors influencing the properties of electrodeposited alloy coatings

1.9.1 Types of alloy deposition

Brenner (1963) classified the alloy systems into various types according to their deposition behavior and the factors which influence the composition of the electrodeposited alloys. The classification is essentially based on thermodynamic and kinetic considerations. He reported a major distinction exists between *normal* system, in which more noble species (with a more positive rest potential) deposits preferentially, and *anormal* system, in which the less noble species is favored. The *anormal* behavior includes *anomalous* and *induced* types of codeposition [Younes and Gileadi 2000, Eliaz and Gileadi 2008]. Accordingly, the alloy plating can be broadly classified into five types: *i)* Regular codeposition, *ii)* Irregular codeposition, *iii)* Equilibrium codeposition, *iv)* Anomalous codeposition, and *v)* Induced codeposition.

i) Regular codeposition

This type of deposition is characterized by the deposition being under diffusion control. The regular codeposition is most likely to occur in baths in which the equilibrium potentials of the metals are not far apart and with metals that do not form solid solution [Brenner 1963]. The percentage of the more noble metal in the deposit is increased by those agencies that increase the metal ion content of the cathode diffusion layer like,

increase in the total salt content of the bath, decrease of deposition c.d., elevation of bath temperature, increased agitation of bath etc.

ii) Irregular codeposition

In this type, the effect of plating variables on the composition of the deposit is much smaller than that of regular codeposition. It is related to systems in which deposition is not under diffusion control. The rate of deposition in these systems is controlled by irregularities of the potentials of metals in solution. It is most likely to occur with the solution of complex ions [Brenner 1963].

iii) Equilibrium codeposition

This type of deposition is characterized by the deposition from a solution, which is in chemical equilibrium with both of the parent metals. Cu-Bi and Pb-Sn alloys fall in this category. This is the only type of deposition in which the ratio of metal content in the deposit (plated at low c.d.) is equal to their ratio in the solution. The alloys, which do not have equilibrium with both the parent metals, belongs to either regular or irregular plating systems [Brenner 1963].

iv) Anomalous codeposition

In the case of electrodeposition of Zn alloys with Fe-group metals, the wt.% of Zn in the deposit is much higher than that in the electrolytic bath. However, one would expect to obtain an electrodeposits of nearly pure Ni due to its strong thermodynamic nobility, i.e., the reduction potential of Zn is -0.76 V and Ni is -0.25 V. Generally, under most practical conditions; the ratio of the less noble metal (Zn) to the nobler metal (Ni) in the deposit is not larger than that in the bath. However, this abnormal behaviour in special cases is known as *anomalous codeposition*, described by Brenner (1963). Anomalous codeposition is rather rare, and is frequently associated with the electrodeposition of Zn-M (where M stands for Ni, Co and Fe) alloys and mutual alloys of iron group metals, namely Fe-Ni, Fe-Co and Co-Ni. The phenomena deserve a considerable amount of study, since its explanation would greatly advance our knowledge of electrode polarization [Eliaz and Gileadi 2008].

v) Induced codeposition

It occurs with metals like Mo, W, V, Ti, P etc., which cannot be deposited alone from their simple salt solutions. However, these metals readily codeposit with the iron group

metals. The deposition of alloys like Ni-Mo, Ni-Ti, W-Co, Ni-W etc., are typical examples of this type of codeposition [Younes-Metzler et al. 2003]. The term induced codeposition was coined by Brenner (1963) to describe a situation where, 'a metal that cannot be deposited alone from its aqueous solution is codeposited in the presence of another metal, forming an alloy'. Metals which stimulate the deposition are called *inducing metals*, and the metals which do not deposit by themselves are called *reluctant metals*. It was applied first to describe the electroless deposition of Ni-P alloys, and later for electroplating of the alloys of W and Mo with the Fe-group metals (Fe, Co and Ni) [Brenner 1963]. Several hypotheses have been reported to explain the mechanism of the induced codeposition. Among them, the most favoured hypothesis is ennobling of the deposition potential of *reluctant metal* by virtue of the formation of a solid solution or inter-metallic compound. It was further assumed that the formation of a solid solution of *reluctant metal* with the Fe-group metal involves a sufficient decrease of free energy to shift the deposition potential of *reluctant metal* to more positive (more noble) potentials. This hypothesis is considered to be more acceptable, and referred to as the shift of the deposition potential [Younes-Metzler et al. 2003, Eliaz and Gileadi 2008].

1.9.2 Advantages of alloy plating

The ever increasing number of scientific and technical publications on the subject of alloy plating shows its practical application in various engineering fields. The vastness of the number of possible alloy combinations and their concomitant practical applications making this field of research more attractive. The alloy deposition can ensure coatings with enhanced properties that cannot be obtained from single metal plating. They can be denser, harder, more corrosion resistant, more protective, tougher and stronger, more wear resistant, better in magnetic properties, more suitable for subsequent electroplate overlays and conversion treatments, superior in antifriction applications etc [Brenner 1963]. The alloy coatings developed at a particular deposition c.d. by keeping all other variables constant will be of same composition always. Such coatings are called monolithic, or alternatively called monolayer alloy coatings. Nowadays, the development of ternary alloy coatings are attaining more scientific

interest due to their promising material properties over binary coatings [Younes and Gileadi 2000].

1.10 ELECTRODEPOSITION OF COMPOSITE COATINGS

Composite coatings are found to be a very auspicious and briskly developing field of great importance, both in research and practical applications. The rigorous development of the composite coating technology allows the production of metal matrix coatings with various homogeneously dispersed phases, which can impart synergistic properties of the matrix and the guest material [Gan 2012, Kuang et al. 2013, Badrayyana et al. 2015]. Electrodeposition is a promising method in this regard for the development of composite coatings with homogeneously dispersed particles (micro/nano) in the metal matrix compared to the other methods, such as powder metallurgy, metal spraying and nitriding or vacuum deposition [Low et al. 2006, Walsh and Ponce de Leon 2014]. The composite electrodeposition is also called 'inclusion plating', to denote the codeposition of insoluble inorganic particles (ceramics, metal based particulates, fibers etc.) dispersed in the plating bath along with the metal ions [Low et al. 2006]. A variety of metal/alloy matrix composite coatings have been reported for various applications. The composite plating can be traced back to as long ago as 1928 in a study of a Cu-graphite coating for automotive applications [Williams 1966].

Electrodeposition has been emerged as a versatile and convenient route over the last decade for the synthesis of a variety of nanomaterials like nanocrystalline deposits, nanowires, nanotubes, nanomultilayers and nanocomposites [Low et al. 2006]. The composite coatings can ensure enhanced material and tribological properties along with improved electrical resistance, giant magnetoresistance, microhardness etc [Watanabe 2004]. This attractive properties of the composite coatings making it useful in various applications like, in printed circuit boards, in memory storage systems, in micro-electro-mechanical systems etc. and these have been the focus of numerous studies [Low et al. 2006]. The improved physical and electrochemical characteristics of the composite coatings extended its use to electrode material synthesis for electrocatalysis and photocatalysis. The codeposition or inclusion of nanoparticles into the metal/alloy matrix is dependent on many factors like particle characteristics (particle concentration, surface charge, type, shape, size), electrolyte composition (electrolyte concentration,

additives, temperature, pH, surfactant type and concentration), current density and hydrodynamics [Watanabe 2004].

Many literature are available on the composite electrodeposition including a variety of particles with size ranging from 4 to 800 nm like, aluminium dioxide (Al_2O_3) [Webb and Robertson 1994, Steinbach and Ferkel 2001, Lozano-Morales and Podlaha 2004], chromium (Cr), diamond (C) [Wang et al. 2005a, Wang et al. 2005b], silicon carbide (SiC) [Zimmerman et al. 2002a, Zimmerman et al. 2002b], gold (Au) [Wang et al. 2014], silicon dioxide (SiO_2) [Kondo et al. 2000], zirconium dioxide (ZrO_2) [Möller and Hahn 1999], titanium dioxide (TiO_2) [Li et al. 2002, Li et al. 2005], silicon nitride (Si_3N_4) [Li and Li 2003] etc. Among the many reported nanocomposites of metals/alloys, copper and nickel based composites are getting more attraction, due to their wide applications.

1.10.1 Sol-enhanced electrodeposition

Sol-enhanced electrodeposition is yet another promising method to overcome the limitation of composite electrodeposition, in achieving a homogeneous dispersion of the colloidal particles within the metal/alloy matrix. Theoretically, the incorporation of the second-phase particles (inclusions) can be much more effective in reinforcing the composite coating, if the particles are superfine/nano in nature than micro [Watanabe 2004]. The nanosized inclusions can give high dispersion and strong interaction with the metal or alloy matrix, and thereby enhanced material properties [Iqbal and Ashiq 2007]. Whereas, in composite electrodeposition, to attain good dispersion of the nanoparticles, powder suspension in the electrolytic bath has to be physically maintained in the solution by vigorous agitation, air injection, ultrasonic vibration, or by adding surfactants. However, it is very difficult to achieve good suspension of the added nanomaterials within the plating bath without causing agglomeration due to its very large surface area. In this regards, sol-enhanced deposition attains importance to develop composite coatings with homogeneously dispersed nanomaterials.

Sol-enhanced deposition works by combining the benefits of sol-gel process and composite electrodeposition. Sol-gel process has been widely utilized for the preparation of nanosized particles of uniform size [Stöber et al. 1968, Livage 1999]. Sol-enhanced composite electrodeposition can be carried out by adding a small amount

of in situ liquid phase synthesized uniform nanoparticles into the metal/alloy plating bath. This can offer better dispersion of the nanoparticles within the plating bath and hence, can provide an opportunity for the in-situ formed nanoparticles to integrate immediately into the metal/alloy deposit along with depositing metal ions to form a nanocomposite coating [Watanabe 2004]. This leads to a highly dispersive distribution of nanoparticles in the coating, avoiding the agglomeration of nanoparticles [Watanabe 2004, Qiu et al. 2007].

The sol-enhanced deposition of TiO$_2$ based composites has been widely studied for various applications [Ogihara et al. 1989, Qiu et al. 2007, Chen et al. 2010a, Wang et al. 2014]. The mechanical properties of the metals alloys are reported to be enhanced to a greater extent after the incorporation of TiO$_2$ nanoparticles through sol-enhanced electrodeposition than conventional composite electrodeposition [Chen et al. 2010b].

1.11 MODERN METHODS OF ELECTRODEPOSITION

Electrodeposition is a well-known coating technique to tune the shape of microcrystals, control their growth and their composition for developing metal/alloy/composite coatings with tailor-made properties. A common method to manipulate the deposit property is by introducing a suitable additive into the plating bath, which can preferentially adsorb on specific crystallographic planes and alter the growth mechanism [Brenner 1963]. Apart from that, by bringing variations on the mass transfer process during deposition can also offer coatings with enhanced materials characteristics. In this regards, development of multilayer coatings and magnetoelectrolysis are promising methods to synthesize new materials with advanced properties. The development of such new materials is driven by the fundamental principles such as: *i)* periodic modulation in mass transport process at cathode brings a periodic modulation in composition of the deposited coatings, according to the basic principle of electrodeposition, *ii)* the material property of the coatings towards corrosion resistance and electrocatalytic activity can be increased substantially by increasing the surface area of the coatings, according to the basis of nanotechnology (the increase in surface area can be achieved either through layering or by composite electrodeposition), *iii)* the enhanced mass transport at the electrode/electrolyte interface can result in the formation of coatings with high reluctant metal content than in

conventional methods. Keeping in view of the above points, the development of composition modulated multilayer alloy (CMMA) coatings and magnetoelectrodeposited (MED) alloy coatings can ensure significant enhancement in materials properties compared with the conventional coatings.

1.12 COMPOSITION MODULATED MULTILAYER ALLOY COATING

Today, in search of efficient surface coating materials for better corrosion protection, the focus has been given for development of compositionally nano-modulated multilayer, or simply nanolaminated alloy coatings in place of their conventional monolayer (monolithic, or homogeneous) coatings. These coatings are popularly called as CMMA coatings, consisting of a sequence of two metals/alloys, alternately deposited one above the other [Brenner 1963, NabiRahni et al. 1996, Roy 2009], as shown in Fig. 1.7. They are developed by pulsing periodically the current/voltage during deposition. The nanolaminated alloy coating technique gaining interest amongst the researchers due to genuine reasons of low cost and greater flexibility to tailor the properties, like thickness of the coating and ability to control the texture and interfaces. Generally, nanolaminated multilayer alloy coatings developed electrochemically exhibit better electrical, magnetic, optical, chemical and mechanical properties quite distinct from their monolayer (monolithic/bulk/non-nanostructured) alloy counterpart [Tench and White 1984, Idrissi et al. 1994]. Even though techniques such as evaporation, molecular beam epitaxy (MBE) and sputtering are some of the common methods still in use for development of multilayer coatings, their high cost and practical difficulties made the multilayer coatings by electrolytic process more popular [Brenner 1963, Roy 2009]. The CMMA coating technology has grown in the past decades as a promising and exciting extension to the range of surface coatings and associated applications.
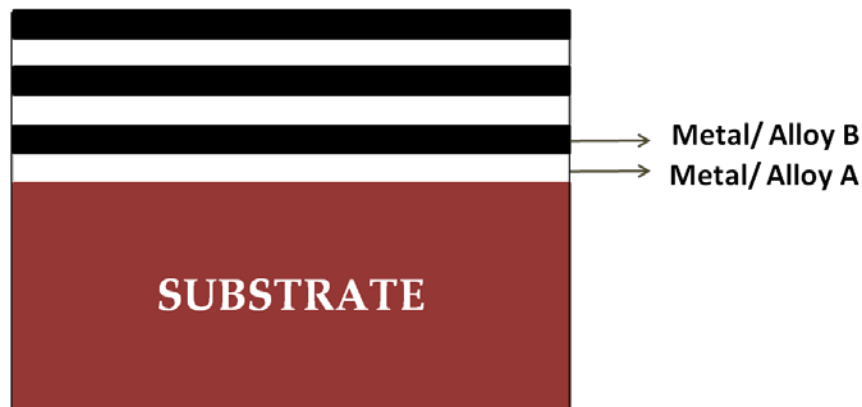
Fig.1.7- Schematic of multilayered coating having alternate layers of two metals/alloys A and B

The multilayer deposition was first reported by Blum (1921) by demonstrating the deposition of alternate Cu and Ni layers with tens of microns thick, from two different electrolytes. Later on Brenner (1963) deposited Cu/Bi by varying deposition c.d. Thereafter numerous research works were reported on CMMA coatings [Simunovich et al. 1994, Zabludovsky et al. 1996, Zabludovsky and Shtapenko 1997, Thangaraj et al. 2009, Ullal and Hegde 2014b, Pavithra and Hegde 2012, Shetty et al. 2016], among which Zn-Ni system is the most widely studied one [Venkatakrishna and Hegde 2010, Yogesha et al. 2011, Rao and Hegde 2013].

In CMMA coatings, each individual layers have a distinctive role and a suitable combination of coating parameters can be used to enhance the final product performance without increasing the total coating thickness. The composition and thickness of each individual layer can be manipulated to optimize the desired property of the multilayered coating [Zabludovsky and Shtapenko 1997, Rao and Hegde 2014]. The betterment in the properties of multilayer coatings lies in the control of mutual diffusion of the neighbouring layers after deposition. However, it is also possible to vary the deposition condition to produce a predetermined compositional gradient in the as-deposited condition. These film materials may possess unusual, but novel properties, making them very important from a practical standpoint. Due to the increased effect of surface, or interface arising from the exceptional thinness of the individual layers of the CMMA coatings, it can exhibit large deviations from bulk behavior, which raises the total properties of the composition modulated multilayers (CMMs) compared to their monolayer counterparts [Leisner et al. 1996, Lee et al. 2015]. Since the layering is

achieved at near atomic dimensions, the developed nanostructured multilayer alloy coatings attain remarkable and sometimes unique properties which are not attainable in normal metallurgical alloys [Yang et al. 1977, Leisner et al. 1996].

1.12.1 Development of CMMA coatings

There are two main approaches for the development of CMMA coatings, and they are: *i)* Dry process, and *ii)* Wet process/electrolytic method.

i) Dry Process

The dry processes used for the development of CMMA coatings are, CVD, PVD, sputtering, MBE, laser ablation and normal temperature evaporation. Many coatings such as Si-Nb and Co-X (where, X = Au, Pd or Cu) have been reported using the PVD method. Though, all these methods have their own significance and applicability, the drawbacks in productivity are significantly higher and severe restriction for depositing on rough substrates also exists. Hence, finding other alternatives became inevitable for the development of CMMA coatings [Leisner et al. 1996].

ii) Wet process/electrolytic method

The development of CMMA coatings from aqueous electrolytes through electrochemical method are called wet process. This process is more attractive, and equally promising with the added advantages over dry process such as: *i)* the processing cost is low and is applicable even to curved and recessed substrates, *ii)* simplicity of the facility for metal deposition and mass production, moreover, thick coatings can be deposited (>100 µm) with high deposition rates (up to about 5 nm/ minute), *iii)* the depositions can be controlled precisely and reproducibly in intended way using advanced power sources, iv) being a cold process, the risk of interdiffusion between layers is low. In spite of the above advantages, metal finishing processes using traditional electrolytes have some limitations and disadvantages also. The main limitations are: *i)* the range and quality of coating that can be produced is limited due to complicated bath chemistry (metal salts, complexing agents, buffering agents, inert electrolyte, and additives), *ii)* the large number of variables making the process of optimization and control little complicated, *iii)* the metal ions with reduction potential below that of H^+ have either low current efficiencies or cannot be electroplated at all

from aqueous solutions [Roy 2009]. Hence the electrodeposition of many important metals such as Al, Mg, W and Ti from aqueous bath is precluded. Multilayer deposition can be accomplished electrolytically by two methods, namely: *a)* Single bath technique (SBT), and *b)* Dual bath technique (DBT) [Leisner et al. 1996].

a) Single bath Technique

The most common technique for electrodeposition of CMM coating involves the use of a single electrolyte containing two or more metal ions. Pulsed currents/potentials are applied to preferentially reduce one of the metals, so as to form alternating (nearly) pure metallic layers [Roy 2009]. The more noble metal ion is usually present in a solution in very small quantities, typically in millimolar (mM) concentration, which limits the plating rate of the noble component. The less noble component, on the other hand, is kept close to its solubility limit (or at least at a high concentration). The molar ratio of the two materials in the electrolyte is typically 1:40 - 1:100. By maintaining such a difference in metal ion concentration, the noble material is plated under mass transfer controlled conditions, and the less noble component is deposited under kinetic control. During the period when the less noble component is discharged, the noble component is also codeposited [Leisner et al. 1996]. Hence, in SBT, it is possible to deposit alternate layers of alloys of same metals, but of different composition using same electrolyte through proper manipulation of deposition c.d. Though this method is the most widely used technique, it shows some limitations like, displacement reactions between two metallic compounds, i.e., which may dissolve away a portion of less noble metal and replace it with more noble metal. Further, it is impossible to obtain deposits of pure less noble metal layers because the noble metal always codeposits to some extent during less noble metal deposition. Another limitation is that the metal ions in the electrolyte should have reduction potentials that are sufficiently far apart so that nearly pure layers can be selectively deposited and hence, the selection for multilayer coating is limited [Roy 2009].

b) Dual bath technique

In dual bath techniques, the deposition is carried out using two different plating baths. The obvious technique to plate a variety of metal multilayers is to use different electrolytes to plate the individual metals. This can be achieved by plating a substrate

in a particular bath, and then transferring the substrate to another electrolyte where a second metal is plated, and so on. If two metals are plated alternately, then the substrate can be transferred back and forth between the two electrolytes to build up a multilayer structure [Leisner et al. 1996]. Any combination of films can be formed in this technique, provided each metal/alloy should deposit individually. The DBT offers a wide choice in the selection of components and allows the deposition of components in an unalloyed form. Ternary and quaternary alloys can also be electrodeposited easily by this method. The practical advantages of a dual bath system are enhanced, when the layers are close to the micron scale, but operating costs and degree of automation needed higher sophistication as the thickness of the individual layers is decreased. However, the major drawback is substrate transfer, which leads to bath contamination. It also includes different phenomena, such as dissolution, reaction displacement, outside pollution and formation of metal oxides during the intermediate rinsing which can adversely affect the properties of deposits [Roy 2009].

The DBT, due to its practical reason is suggested for relatively thick coatings (>50 nm layer thickness) and SBT is for coatings of thinner modulation thicknesses. In SBT, the substrate is always remaining in the electrolyte and hence, there is no risk of mutual bath contamination due to substrate transfer. Both techniques have their own advantages and disadvantages, however, the drawbacks of the DBT have been deemed to outweigh the benefits, so that the SBT approach is commonly used [Leisner et al. 1996].

1.13 MAGNETOELECTROLYSIS

Magnetoelectrolysis, or simply magnetolysis works by employing magnetic induction and electrolysis together - two basic concepts applied in a new way. The superimposition of magnetic field *(B)* in electrochemical processes have large practical significance [Fahidy 1983]. The topic is inherently interdisciplinary, including the concepts of electrochemistry, hydrodynamics and magnetism. The results are sometimes surprising, and their elucidation can lead to unexpected insights into fundamental electrochemical processes, as well as new practical applications. Basically, magnetolysis covers four major aspects of electric/magnetic field interactions. They are: *i)* magnetic field effect on electrolyte properties, called

magnetohydrodynamic (MHD) effect, *ii)* electrolytic mass transport, *iii)* to a smaller extent on electrode kinetics and *iv)* nature of electrodeposit [Steiner and Ulrich 1989]. The MHD effect, arises mainly due to Lorentz force (force acting on charged ions moving in an electromagnetic field) is responsible for the effects of *B* on electrochemical processes [Monzon and Coey 2014].

1.13.1 Lorentz force

The effective force acting on a charged particle '*q*', moving with a velocity '*v*' in an electric field of density '*E*' and a magnetic field of flux density *B* is given by Lorentz force (F_L) [Fahidy 1973, Monzon and Coey 2014]. The Lorentz force is the force sustained by a charged particle when moving in an electromagnetic field, and it can be represented as in Equation 1.10.

$$\vec{F}_L \ = \ q\vec{E} \quad + \ q\vec{v}\vec{B} \tag{1.10}$$

The first part of the equation represents the well know electric force and is straightforward and depends on the applied c.d. (*i*). Under the conditions of common electrochemical processes, the current density is determined solely by the Faradaic current to a very good approximation. The second part is the magnetic force, its magnitude depends on the angle between *B* and *v* (or *i*, since the ions move in the direction of applied current). The magnitude of magnetic force is given by '*F = qvB* sinθ'. When the angle between magnetic field and c.d. is 90˚ (θ= 90˚, i.e., *B* and *i* are perpendicular to each other), the magnetic force is maximum and hence the effect of Lorentz force also becomes maximum. When θ= 0, i.e., *B* and *i* are parallel to each other). However, the electromagnetic body force, the Lorentz force, results from the vector product of *i* and *B* (Equation 1.11) [Fahidy 1973, Koza et al. 2008].

$$F_L \ = \ i \times B \tag{1.11}$$

Therefore, when the direction of the *B* is perpendicular to the line of electric force, the Lorentz force changes the direction of charged particles cutting through the line of magnetic force [Fahidy 1983].

1.13.2 Right-Hand rule

According to well-known right-hand rule of electromagnetism, the effective force acting on moving charged particle, in a direction perpendicular to the applied B is perpendicular to the plane of both. i.e., the Lorentz force is perpendicular to the direction of both v and B [Bund et al. 2003, Koza et al. 2008]. The diagrammatic representation of famous right hand rule is shown in Fig. 1.8. To find out the direction of the effective force acting on the charged particles under i and B, applied perpendicular to each other, point the thumb in the direction of v (or direction of i) and fingers in the direction of B. Then the effective force is operating outwards from the palm as shown in Fig. 1.8(a). Further, to confirm the exact direction of the effective force, curl the fingers and rotate into the plane of B, then the thumb points the direction of effective force as shown in Fig. 1.8(b).
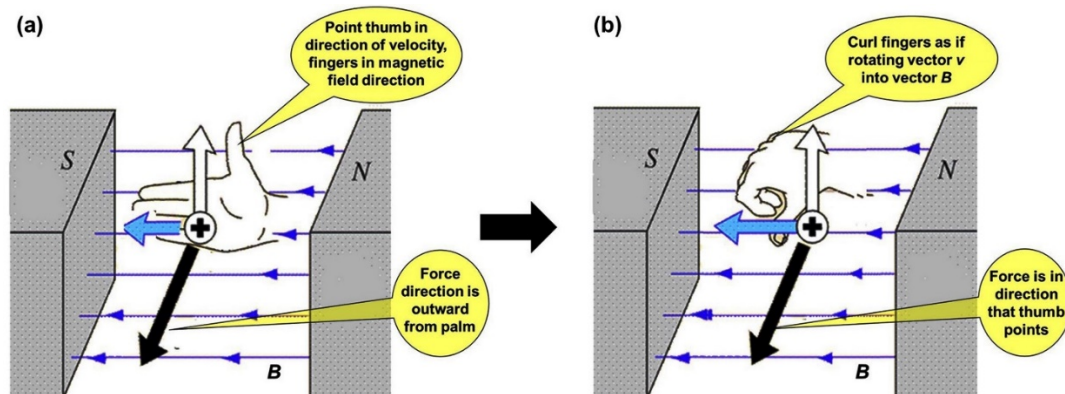
Fig. 1.8- Schematic of the right-hand rule, which governs direction of effective force acting on charged moving particle in perpendicular B; a) the direction of effective force is outward from palm, and b) the force is in the direction that thumb points

1.13.3 Magnetic field effects on mass transfer

The term 'mass transfer' denotes the transport of ions or molecules by the combined effect of diffusion, eddy diffusion and convection, if excluding the contribution of migration to the process [Fahidy 1973]. The mass transfer is commonly called free convection, when there is no agitation, or mixing happens only as a result of the difference in density or concentration at different points within the fluid. Whereas, mass transfer process due to mechanical stirring is called 'forced convection' [Tobias et al. 1952]. The mass transfer process from the bulk of the solution to the electrode-solution

interface depends on electrolyte motion, shape and position of the cell, and other operating parameters [Mohanta and Fahidy 1976, Bund et al. 2003]. In this regards, the effect of magnetic fields on electrolyte solutions has intrigued numerous researchers since Faraday's pioneering but inconclusive observations [Fahidy 1983].

MHD or magneto fluid dynamics is the branch of science dealing with the study of dynamics of electrically conducting fluids like plasmas, liquid metals and electrolytes (salt water) in the presence of applied B. The basic concept of MHD is that the applied B can induce currents in a moving conductive fluid, which in turn polarizes the fluid and reciprocally changes the magnetic field itself [Waskaas and Kharkats 1999]. MHD effects operate according to the action of Lorentz force ($F_L = i \times B$), which induces fluid flow in the cell and thus affects the transport rate of electroactive species towards the electrode [Monzon and Coey 2014]. In an appropriate design, this force can benefit the uniformity of flow field, which affects ion distribution between electrodes and increases the rate of electrochemical process [Gu and Fahidy 1987]. The largest effect of Lorentz force and, consequently, the largest MHD effect are achieved when the external B is applied perpendicularly to the direction of the ion flux (i.e., when B oriented parallel to the electrode surface, $\theta = 90º$). On the contrary, when B is applied parallel to the direction of the ion flux (i.e., when B oriented perpendicular to the electrode surface, $\theta = 0$), the Lorentz force is zero [Ganesh et al. 2005]. In a nutshell, the presence of an applied external B during electrolytic processes can cause induction of additional convection in the diffusive layer at the electrode surface through the MHD effect [Fahidy 1973]. This additional convection enhances creation of laminar flow at the electrode surface, and subsequently a decrease of the diffusion layer thickness [Khan and Petrikowski 2001, Bund et al. 2003]. The decrease in diffusion layer or electrical double layer thickness can increase the limiting current density (i_L), the effective c.d. inside the electrical double layer), and thereby the enhanced mass transport [Bund et al. 2003, Ganesh et al. 2005, Koza et al. 2011]. The knowledge of i_L and thickness of diffusion boundary layer is particularly important in improving *space-time yield* of electrolysis and especially of high current density electrolysis. Basically, the natural mode of convection of electrolyte is changed to a forced type under applied magnetic field. This effect leading an increase of i_L due to decrease of diffusion layer thickness can be explained as follows.

During electrolysis, cations have to be transported from bulk electrolyte to the cathode surface. In general, this mass transport occurs by diffusion, convection, and migration. Close to the electrode surface, the primary mass transport process is diffusion. Without the flow of current, the concentration of cations is constant ($c = c_0$) in the electrolyte, as shown by line 1 in Fig. 1.9). After switching the current on, the concentration of cations decreases from c_0 to c_s (curve 2 in Fig. 1.9). There is a concentration gradient in front of the cathode with a thickness of δ_N (diffusion boundary layer). Here, δ_N is defined as the diffusion layer thickness. It is the distance from the electrode surface to the point of intersection between the *tangent at the concentration profile* and concentration of bulk electrolyte (line 1) [Filzwieser et al. 2002]. With an increase of deposition time, δ_N increases until steady-state conditions are reached (curve 2a, time-independent δ_N). Current density can be calculated according to Fick's law of diffusion (Equation 1.12) [Filzwieser et al. 2002]:

$$i = nFD\left(\frac{\partial c}{\partial x}\right)_{x \to 0} = nFD\left(\frac{c_0 - c_s}{\partial_N}\right) \tag{1.12}$$

Where, n is the valency of the metal ions, F is the Faraday constant (96,500 C), and D is the diffusion coefficient of the ionic species. When the surface concentration of depositing cations decreases to zero ($\lim c_s \to 0$), the current density reaches a maximum value (curves 3 and 3a in Fig. 1.9) [Filzwieser et al. 2002]. This value of current density is called limiting current density, i_L (Equation 1.13).

$$i_L = nFD\left(\frac{c_0}{\partial_N}\right) \tag{1.13}$$

The value of i_L increases linearly with an increase of concentration c_0, with an increasing diffusion constant, and a decreasing diffusion boundary layer δ_N. Since the diffusion constant and concentration of the solute cannot be influenced extensively, an increase of i_L can be obtained mainly by a decrease of δ_N. In the presence of applied B, the δ_N value decreases as a result of MHD operating near the electrode surface leading to increase in mass transport and enhanced i_L [Steiner and Ulrich 1989, Filzwieser et al. 2002].
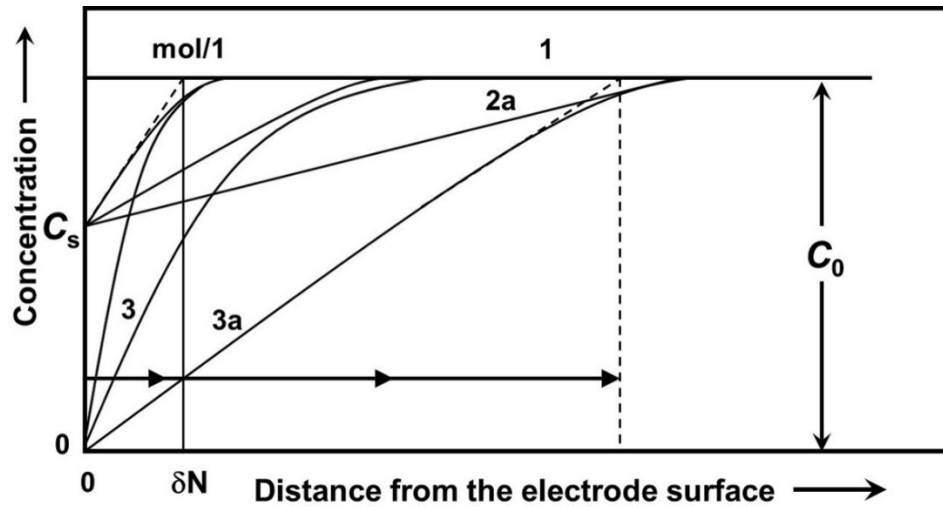
Fig. 1.9- Concentration gradient at the cathode surface and the variation in i_L value (Adopted and modified from, Filzwieser et al. 2002)

1.13.4 Effect of magnetic field on electrodeposition

The B induced during electrodeposition can change flow patterns, increase in the intensity of mixing, increase in the rate of deposition, and hence, can modify deposit structure. During MED, the enhanced convection and the strong push for deposition can be explained using the MHD effect, interacting with the structure of the convective diffusion layer at the electrodes. It is reported that the superimposition of B during electrodeposition has great influence on the deposit characteristics like nucleation, growth, texture, phase composition, macro-stresses, hardness, morphology, current efficiency, preferred orientation etc [Khan and Petrikowski 2001, Koza et al. 2008]. The MHD effect, arises mainly due to Lorentz force (force acting on charged ions moving in an electromagnetic field) can enhance the mass transport at the electrode/ electrolyte interface during deposition and can impart better coating properties [Ganesh et al. 2005, Koza et al. 2008]. MED can ensure a more uniform current distribution, leading to a more uniform deposited layer with change in the crystallization behavior. Apart from that, MED can enhance the corrosion resistance and electrocatalytic activity of the deposits. The extent of effect due to superimposition of B during MED on coating characteristics depends on the intensity and direction (parallel or perpendicular) of the applied magnetic field [Ganesh et al. 2005]. Nowadays, MED has attained more attention towards the effect on induced codeposition of the reluctant metals (elements

which cannot be deposited alone from aqueous solutions) like, molybdenum, tungsten, phosphorus, boron etc., in the presence of inducing metals (Fe, Co, Ni etc.). A number of investigators have reported the significant effect of the applied magnetic field on various aqueous electrolytic processes [Fahidy 1983, Waskaas and Kharkats 1999, Lin et al. 2012, Lin and Hourng 2014].

1.14 CHARACTERIZATION OF ELECTRODEPOSITED COATINGS

The structural, morphological and compositional characterization of the electrodeposits are mainly carried out using microscopy and diffractometry techniques. The coating morphology and composition are monitored widely using scanning electron microscopy (SEM) and energy dispersive spectroscopy (EDS), respectively. At the same time, X-ray diffraction (XRD) study can be used for the detailed structure information of the deposit in small sample processing time as compared with the other techniques.

SEM is one of the most versatile and advanced techniqueue that reveals detailed information about the morphology and the composition of test materials. Especially in the case of electrodeposits, SEM is a very useful tool for analyzing the surface appearance as compared with the optical microscope. The advantage of covering a rough topography completely in focus through the greater depth of field and better resolution making it more useful than the optical one [Li and Ebrahimi 2003, Dumelié et al. 2005]. A focused beam of high-energy electrons is used in SEM to generate a variety of signals at the sample surface due to 'electron-sample' interaction and which reveals the information about the sample [Goldstein et al. 2012]. If the emission source is a thermionic emitter, it is called SEM and if it is field emitter, it is field emission scanning electron microscopy (FESEM). A field-emission cathode in the electron gun provides narrower probing beams at low as well as high electron energy, resulting in both improved spatial resolution and minimized sample charging and damage [Taglauer and Vickerman 1997]. The selected areas of the metal/alloy/composite coatings can be examined directly using SEM without any preparation due to its conducting nature. Whereas, SEM cannot be used for determining the crystal structure and orientations of grains due to its incapability to produce electron diffraction patterns. The chemical composition of the sample can be determined through the EDS facility attached with

SEM. It is possible to focus the electron beam in a small area and to determine the chemical composition of the sample. The primary electrons undergo collision with electrons in the atom causing the ejection of core electron. The excited atom undergoes emission of characteristic X-ray photon or Auger electron and decay to ground state [Goldstein et al. 2012]. These emitted X-rays will be sorted by energy using energy dispersive detector or by wavelength with wavelength spectrometer. An output signal proportional to the number X-ray photons generated in the area under electron interaction is recorded. The EDS facility also helps in imaging the distribution of a particular chemical element called 'elemental mapping' by analyzing the characteristic X-rays [Taglauer and Vickerman 1997, Goldstein et al. 2012]. These X-rays are characteristic of each atom and serves as fingerprint and provide valuable information of the sample allowing quantitative analysis, line profiling and spatial distribution imaging [Dumelié et al. 2005]. Thus SEM with EDX is an efficient and nondestructive tool for imaging and analyzing a modified surface.

The XRD is a very useful and commonly used technique for the phase structure identification of the deposit. The metal/alloy/composite coated material can be analyzed by directing the monochromatic X-rays towards the sample, and collecting the diffracted rays. The all possible orientations of the crystal lattice can be obtained by scanning the sample through a range of 2θ angles [Goldstein et al. 2012]. It is a nondestructive technique which gives detailed information about how the atoms pack together in the crystalline state along with an idea about the inter-atomic distances and accordingly the shape and size of the unit cell for any compound can be detected. X-ray diffraction is hence considered as one of the most important characterization tools used in solid state chemistry and materials science. Since the wavelength of X-ray and inter-atomic spacing of crystal are comparable, the X-ray interacts with the material and scatter to generate diffraction patterns, satisfying Bragg's law (Equation 1.14) [Taglauer and Vickerman 1997].

$$n\lambda = 2d\sin\theta \tag{1.14}$$

Bragg's law relates the wavelength (λ) of electromagnetic radiation to the diffraction angle (θ) which in turn is related to the lattice spacing (d) in a crystalline sample. The resultant diffracted rays are detected by a detector. The peaks in the

diffraction pattern can be correlated with a set of crystal lattice planes. Since each set of planes have different *d* value, the *θ* value changes as per Bragg condition [Taglauer and Vickerman 1997]. Further, the obtained patterns can be compared with the data given in powder diffraction file collected and maintained by Joint Committee of Powder Diffraction Standards (JCPDS), created by International Commission on Diffraction Data (ICDD) database.

1.15 CORROSION

The deterioration of a metal through chemical or electrochemical reaction with its environment is called corrosion, according to Fontana (1986). The corrosion is an inter-disciplinary subject, involves all basic sciences and all disciplines of engineering. Corrosion arises basically due to the interaction of the materials with their environment and it cannot be defined without reference to the environment. Almost all environments are corrosive in one or other way to certain degree and some of the specific corrosive environments are: *i)* air and humidity *ii)* fresh, distilled, salt and marine water *iii)* natural, urban, marine and industrial atmospheres *iv)* steam and gases, like chlorine *v)* ammonia vi) hydrogen sulphide *vii)* sulfur dioxide and oxides of nitrogen *viii)* fuel gases *ix)* acids x) alkalies *xi)* soils etc [Ahmad 2006]. It may, therefore, be observed that corrosion is a potent force which destroys the economy, depletes resources and causes costly and untimely failures of plants, equipments and components.

The term corrosion was restricted only to metals and their alloys till 1960s. The ceramics, polymers, composites and semiconductors were not included in the class of corroding materials. However, now the term corrosion encompasses all types of natural and manmade materials and it is not confined to metals and alloys alone [Fontana 1986, Ahmad 2006].

1.15.1 Corrosion mechanism

A *corrosion cell* formation is necessary for a corrosion to take place. The essential components of a corrosion cell are, *anode*, *cathode*, *electrolyte* and *metallic path*, as shown in Fig. 1.10. Where, *anode*: is one of the two dissimilar metal electrodes in an electrolytic cell, at which electrons are released and it is the more reactive metal, compared with the other. *Cathode:* is another electrode in the electrolytic cell, at which

reduction is taking place, i.e., electrons are consumed. *Electrolyte:* is the electrically conductive solution (e.g. salt solution) and, the presence of such medium is necessary for corrosion to occur. *Metallic Path:* is connecting the two electrodes externally and provides a path for the current or electron flow.
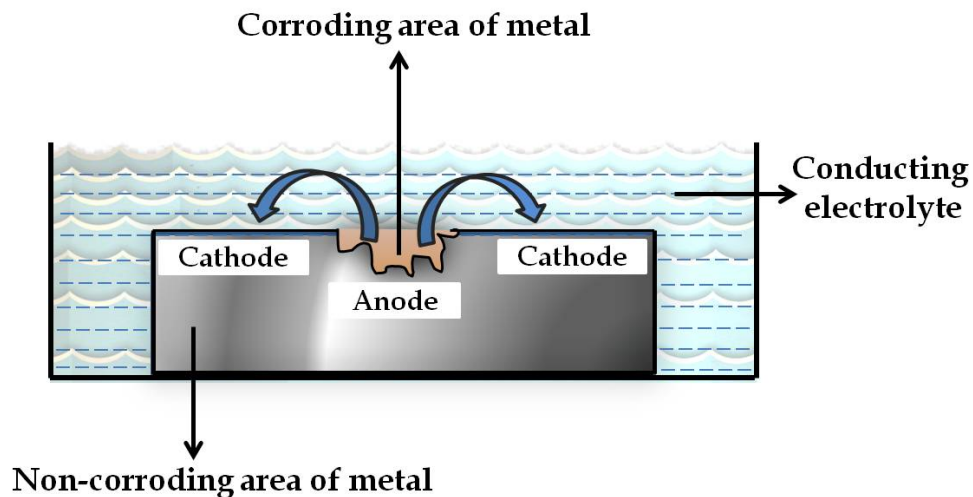
Fig. 1.10- Schematic representation of a corrosion cell (Adopted and modified from, Ahmad 2006)

The transport of atomic, molecular or ionic species at the interface of a material is the general mechanism of corrosion, and the rate of which is controlled by the slowest step. It is difficult to observe the process directly on an atomic scale, whereas, the possible mechanisms can be inferred from indirect measurements and observations like, rate of change in weight or dimensions, rate of build-up of corrosion products, change in surface appearance examined using SEM or change in mechanical, physical properties etc. However, the mechanism of electrochemical corrosion can be inferred from the electrical potential and current measurement [Fontana 1986, Revie and Uhlig 2008].

1.15.2 Importance of corrosion control

In safety and economic point of view, it is important to control the corrosion to make a compromise between the benefits generated by a certain level of corrosion control versus the costs that would result if that level of control were not maintained. The failure of damage of machines, equipments or functional products due to corrosion can lead to safety problems and thereby the cost. Since the choices of materials, enforcement of

manufacturing procedures and control of products to implement safety measures not only involves humanitarian concerns but also economics. Hence, it is important to control corrosion [Fontana 1986, Ahmad 2006, Revie and Uhlig 2008].

1.15.3 Methods of measuring the corrosion rate

In general, the determination of corrosiveness of the environment and the rate of metal loss is called corrosion rate (CR) measurement. There are several techniques for the quantitative evaluation of the effectiveness of the corrosion control and prevention methods adopted. The conventional weight loss and electrochemical methods are two evaluating techniques, among them, the electrochemical methods are the most prevalent one [Allen et al. 2001, Yang 2008].

1.15.3.1 Weight loss technique

The simplest and the practical means of evaluating CR of a material is through weight loss or chemical method. The loss in weight of a material of known mass exposed to a synthetic corrosion media is determined periodically with time, and the loss in mass with respect to unit time and unit area is taken as CR [Allen et al. 2001, Yang 2008].

1.15.3.2 Electrochemical techniques

The rapid and accurate CR determination ability of the electrochemical techniques making it more popular among corrosion engineers and researchers. The electrochemical CR determination needs only at most several hours to complete, whereas the other long term corrosion studies such as weight loss method may take days or weeks to complete. This convenience of fast analyzing capability of electrochemical measurements is especially useful for those metals or alloys that are highly corrosion resistant [Bard et al. 1980]. The electrochemical techniques for the measurement of general corrosion are classified into two types depending on the current used as: *i)* Potentiodynamic polarization or Tafel's extrapolation method (DC method) and *ii)* Electrochemical impedance spectroscopy (EIS) or Alternate Current (AC) method.

i) Potentiodynamic polarization method

The data extraction from direct current measurements essentially implies the determination of parameters which give a measurement of the corrosion rate through theoretical approaches such as the Tafel extrapolation. This method was first used by Wagner and Traud to verify the mixed potential theory [Fontana 1986]. The CR determination is carried out by supplying a cathodic current to the sample to be analyzed using an auxiliary electrode, usually platinum. The current is measured using an ammeter and the potential measurement of the working electrode is made by a potentiostat/galvanostat, with respect to a reference electrode. A potentiodynamic polarization experiment for Tafel extrapolation typically starts at a potential about 250 mV negative to the open circuit potential (OCP), and scans upward through the potential of zero current (which might be different than the original OCP) to a value that is about 250 mV positive to the original OCP. Less polarization is required if the Tafel slope is low [Allen et al. 2001]. The line describing the behavior in the Tafel region can be extrapolated to the corrosion potential to determine the corrosion rate. The rate of polarization in a potentiodynamic scan is typically between 0.1 and 1 mV s^{-1}. The intent of such tests is to determine steady state behavior, so, given practical limitations, slower scanning is preferred [Bard et al. 1980, Poursaee 2010]. To ascertain that the current/voltage relationship reflects only the interfacial corrosion process (where cathodic process is evolution of hydrogen) at every potential of the polarization scan, the effect of capacitance should be minimized. For this purpose, the capacitor should remain fully charged; otherwise, some of the current generated would reflect charging of the surface capacitance in addition to the polarization resistance and the measured current would then be greater than the current actually produced by the corrosion reactions. To reduce the effect of the capacitance, the scan rate should be slow enough in a way that the capacitance remains fully charged during the experiment. In this case, the current–potential relationship just reflects the polarization resistance (interfacial corrosion process) at every potential of the polarization scan [Allen et al. 2001, Poursaee 2010].

This method involves the determination of the Tafel slopes β_a and β_c as well as the corrosion potential (E_{corr}) and corrosion current density (i_{corr}) from a single polarization curve as shown in Fig. 1.11. The slope of the oxidation reaction that

represents the metal becoming soluble metal ion is linear, and the corresponding slope is called anodic Tafel slope, represented by *βa*. The curve shows that for an active metal, as the electrode potential is made more positive or as the solution becomes more oxidizing, the metal dissolution increases. The cathodic branch of the polarization curve is at more negative potential than the OCP; a cathodic current to the metal specimen is measured. The slope of the linear portion of the polarization curve is the cathodic Tafel slope, represented by *βc*. As the potential is made more negative, the rate of the reduction reaction increases [Allen et al. 2001, Yang 2008].
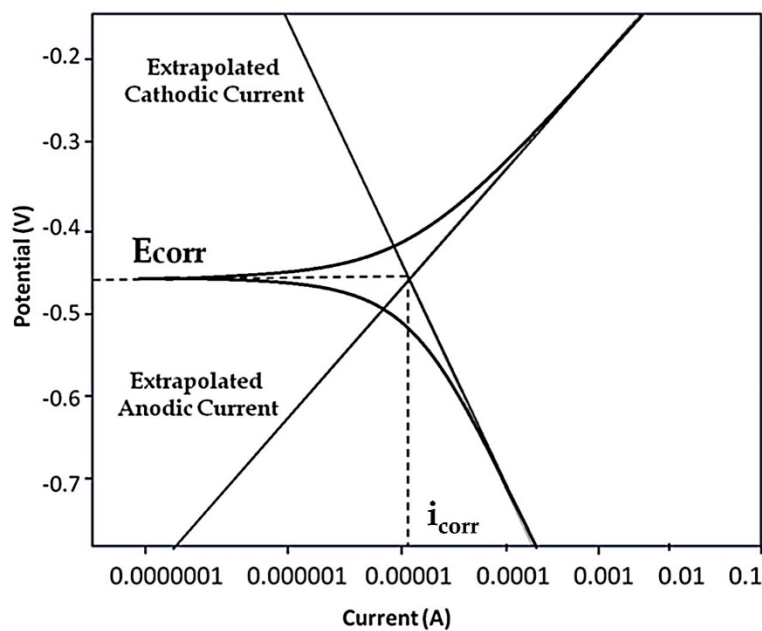
Fig. 1.11- Typical potentiodynamic polarization plot showing anodic and cathodic polarization curves with Tafel's slopes (Adopted from, Yang 2008)

The relationship for anodic and cathodic processes under activation polarization is given in Equation 1.15 and 1.16.

$$\eta_a = \alpha_a + \beta_a \log i \qquad (1.15)$$

$$\eta_c = \alpha_c + \beta_c \log i \qquad (1.16)$$

Where, η_a is anodic polarization or anodic overpotential, η_c is cathodic polarization or cathodic overpotential, α_a and α_c are anodic and cathodic Tafel constants, β_a and β_c are anodic and cathodic Tafel slopes, and log i is the logarithm of current density.

42

The linear portion of the cathodic branch or anodic branch of the polarization curve can be extrapolated back to the intersection with the OCP. The value of the current at this intersection yields i_{corr}, which is equal to the rate of the anodic or cathodic reaction under freely corroding conditions. This extrapolation method can be used to determine the corrosion rate of metals, when either the cathodic or anodic branch exhibits a well-defined linear region. The corrosion rate can be calculated from the i_{corr} value using the Equation 1.17:

$$CR \ (mm \ y^{-1}) = \frac{K \ \times \ i_{corr} \ \times \ EW}{\rho} \tag{1.17}$$

Where, K is a constant with value 0.00327 mm g (μA cm year)$^{-1}$, defines the unit of corrosion rate (mm y^{-1}), i_{corr} is the corrosion current density in μA cm^{-2}, ρ is the density of the corroding material and EW is the equivalent weight of the alloy.

Though the Tafel's extrapolation method is known to be straight approach to evaluate the corrosion rates, it also has some shortcomings like, *i)* a test electrode can be polarized only a limited number of times when making Tafel plot measurements, because some degree of electrode surface roughening occurs with each polarization. There are no hard and fast rules for determining when repeated polarizations have altered the test electrode surface to the point where a new test electrode should be used for further measurements. *ii)* Tafel plots can neither be used to determine a metal-electrolyte system is passive or not (no corrosion occurs) and, nor can be used to study or measure localized corrosion, because much larger anodic polarizations are required to obtain these types of information [Fontana 1986, Yang 2008].

ii) Electrochemical impedance spectroscopy

The EIS or AC impedance method is a very popular technique to acquire the valuable information regarding electrode processes like double layer capacitance, corrosion resistance and role of inhibitors etc [Allen et al. 2001]. This electrochemical technique measures the response of the system to an AC voltage perturbation. The polarization resistance can be measured by the application of a smaller perturbation. By applying a small varying perturbation over a range of frequency, it is possible to probe the full response of the system, and not just the resistive components. EIS voltages cycles from peak anodic to cathodic magnitudes (and vice versa) using a spectrum of AC voltage

frequencies, instead of a range of single magnitude and polarity DC voltages. Resistance and capacitance values are obtained from each frequency, and these quantities can provide information on corrosion behaviors, diffusion and coating properties [Mansfeld 1990]. The EIS method differs from DC method by using AC. In DC method Ohm's law is limited to only one circuit element, i.e., the ideal resistor. The ideal resistors have several simplifying properties like, it follows Ohm's law at all current and voltage levels, its resistance value is independent of frequency, current and voltage signals through a resistor are in phase with each other etc.

Ohm's law defines resistance R in terms of the ratio between voltage V and current I as in Equation 1.18:

$$R = \frac{E}{I} \tag{1.18}$$

But the real electrochemical systems, however, contains circuit elements that exhibit much more complex behavior, and in place of resistance one can use *impedance (Z)*, which is more general circuit parameter. Impedance is also a measure of the ability of a circuit to resist the flow of electrical current. Unlike resistance, it is not limited by the simplified properties because the impedance behavior is being studied by the application of AC signal (sinusoidal wave). In the EIS technique, a small AC signal (typically a sine wave of amplitude ±10 mV) is applied over a wide range of frequency (typically from 10^5 to 10^{-2} or 10^{-3} Hz) at a number of discrete frequencies (typically 5 to 10 frequencies per decade), and the current response is measured at each frequency, 'ω'. The form of the current-voltage relationship of impedance in an electrochemical system can also be expressed as in Equation 1.19 [Yuan et al. 2009]

$$Z_{(\omega)} = E_{(t)} / I_{(t)} \tag{1.19}$$

Where, $Z_{(\omega)}$ is the impedance in ohms (Ω) as a function of frequency *(ω)*, $E_{(t)}$ and $I_{(t)}$ are the time-dependent voltage and current. Hence, Z is the measure of the overall opposition of the circuit to current, in other words, how much the circuit impedes the flow of current. Therefore, the EIS has taken into account on the effect of capacitance and inductance apart from the resistance. Impedance is more complex than resistance because the effect of capacitance and inductance vary with the frequency of the current passing through the circuit. This means that impedance varies with frequency. However, the

effect of resistance is constant regardless of frequency. Four electrical quantities which determine the impedance (Z) of a circuit are: resistance (R), capacitance (C), inductance (L) and frequency (f). Hence, the term 'impedance' is often used (quite correctly) for simple circuits which have capacitance or inductance [Mansfeld 1990, Yuan et al. 2009].

The utility of impedance spectroscopy lies in the ability to distinguish the contribution of individual components under investigation. For example, for the determination of behavior of a coating on a metal when it is in salt water, by the appropriate use of impedance spectroscopy, a value of resistance and capacitance for the coating can be determined through modeling of the electrochemical data. The modeling procedure uses electrical circuits built from components such as *resistors* and *capacitors* to represent the electrochemical behavior of the coating and the metal substrate. Changes in the values for the individual components indicate their behavior and performance. Impedance spectroscopy is a non-destructive technique and so can provide time-dependent information about the ongoing processes. The major advantages of EIS methods are the effectiveness on high resistance materials such as paints and coatings, availability of time dependent data, nondestructive nature of analysis, quantitative availability of data etc. Whereas, the expensive and complex data analysis required for quantification are the two shortcomings of this method [Mansfeld 1990].

1.15.4 Corrosion control by electrodeposited coatings

The electrodeposited metal/alloy/composite coatings are widely used for the corrosion protection of the base material. The coatings provide a layer that changes the surface characteristics of the bulk material onto which it is deposited. They provide a barrier between the corrosive environment and the substrate. Several protective metallic coatings like Cu, Bi, Zn, Sn, Cd etc. have been reported to protect easily corrodible substrates [Brenner 1963]. Copper and Nickel are examples for cathodic coatings, which are chemically less active than steel. In salt solution, the metallic coatings provide a durable, corrosion resistant layer. Such protective coatings of a given thickness need much longer time to deteriorate than an equivalent thickness of the steel substrate, due to its less reactivity than steel [Brooman 2000]. The metallic protective

coatings can serve either as noble coatings, which provide only barrier protection, or as sacrificial coatings, in addition to barrier protection which can also provide cathodic protection. In corrosion protection point of view, not only metallic coatings but also their alloy coatings show better resistance towards corrosion. Many electrodeposited alloy coatings based on Zn, Ni, Fe etc. have been reported, in terms of their corrosion protection efficiency under different environments [Masdek and Alfantazi 2010]. The Ni and its alloy coatings are found to be the promising materials of today, and are used for wide variety of applications including aircraft gas turbines, steam turbine power plants, medical applications, nuclear power systems, and the chemical and petrochemical industries [Akiyama and Fukushima 1992, Brooman 2000].

Alloys of iron-group metals (Fe, Co, and Ni) with other metallic or nonmetallic elements such as P, Mo and W, are widely used in industries owing to their unique properties like high corrosion resistance [Akiyama and Fukushima 1992, Donten et al. 2000, Sakai et al. 2006], high hardness [Mahalingam et al. 2007], brilliant luster for decorative purposes [Brenner 1963], electrocatalytic activity for hydrogen evolution [Paseka and Velicka 1997, Burchardt 2001] and interesting magnetic properties [Donten et al. 2000]. The alloy coatings such as Ni-Co [Wang et al. 2005], Ni-W [Donten et al. 2000, Sakai et al. 2006], Ni-P [Sakai et al. 2006, Mahalingam et al. 2007], Co-W [Aravinda et al. 2000, Sakai et al. 2006] and their ternary or quaternary alloys [Saedi and Ghorbani 2005] are being considered to replace conventional hard chromium deposits [Gawne and Ma 1988], as they are remarkably hard compared to pure nickel coatings [Brenner 1963]. Among which Ni-P alloy coating is the most extensively studied system using electrodeposition and electroless deposition method. The induced type of codeposition was first introduced for Ni-P deposition by Brenner (1963). Later numerous research works were reported on Ni-P alloy and its composite coatings.

Recently, electrodeposition of Ni-based alloys with transition metals such as W or Mo has taken importance due to their enhanced surface performance properties. The hard and high melting metal, W, can impart more desirable properties to the coatings for functional applications [Tsyntsaru et al. 2012], when it is alloyed with Fe group metals (Fe, Co, Ni etc.) [Tsyntsaru et al. 2012, Wasekar and Sundararajan 2015, Lee 2013, Amadeh et al. 2009]. Among them, Ni-W alloy coatings are of considerable

interest due to their wide range of engineering applications. Apart from good mechanical, tribological and magnetic properties, the electrodeposited Ni-W coatings offer excellent corrosion resistance and electrocatalytic characters [Sziráki et al. 2012]. It has been reported that Ni-W alloy coatings can be an important alternative for hard chromium coatings [Brooman 2000] as it has to be eliminated from the manufacturing processes, e.g., in the aviation and automotive industries, due to environmentally hazardous hexavalent chromium [Kirihara et al. 2016]. The electrodeposition of Ni-W alloy was first reported by Brenner (1963), of late, Younes et al. (2001) and Sridhar et al. (2005) have reported a study on electrodeposition of Ni-W alloys, focusing on the effect of additives, applied c.d. and bath temperature on the properties like Faradaic efficiency, W content and corrosion resistance. Thereafter many reports came on the corrosion resistance behavior of Ni-W alloy and its composites [Zhu et al. 2002, Younes and Gileadi 2002, Ma et al. 2004, Slavcheva et al. 2005, Eliaz et al. 2005, Juškėnas et al. 2006, Zemanová et al. 2012, Berkh et al. 2014]. Tsyntsaru et al. (2012) made a detailed review on the modern trends in W alloy electrodeposition. At present also Ni-W is one of the most studied alloy systems due to its promising material properties [Li et al. 2017].

Apart from the Ni- based alloys, their composite coatings are also reported to be effective in terms of corrosion resistance [Spyrellis et al. 2009]. The composites of Ni and its alloys obtained through the incorporation of various nanoparticles like Al_2O_3 [Webb and Robertson 1994, Steinbach and Ferkel 2001, Lozano-Morales and Podlaha 2004], TiO_2 [Li et al. 2002, Li et al. 2005], SiO_2 [Kondo et al. 2000], SiC [Yao et al. 2007, Li et al. 2017], CNT [Ding et al. 2011], MoS_2 [Liu et al. 2016], Si_3N_4 [Li and Li 2003] etc., are found to show enhanced material properties in terms of corrosion resistance. Since the electrodeposited composite coatings can impart the combined advantages of metal/alloy and hard nanoparticle inclusions, nanocomposite coatings show properties superior to their metal/alloy counterpart [Eroglu et al. 2013, Li et al. 2017].

Further, the corrosion resistance of the alloy coatings can be enhanced through modern methods of electrodeposition such as multilayer and magnetoelectrolysis approaches. A wide variety of binary and ternary alloys have been electroplated as multiple-layer films through CMM approach, including Ni-Cu, Zn-Ni, Ag-Pd, Cu-Ni-

Fe, Cu-Ag, Cu-Co, Cu-Pb, Cu-Zn, Ni-P/Ni-Co-P, and Ni/Ni-P to name a few [Simunovich et al. 1994, Zabludovsky et al. 1996, Zabludovsky and Shtapenko 1997, Yogesha et al. 2011]. Recently, Lee et al. (2015) reported the mechanical properties and corrosion resistance of electrodeposited Ni-W multilayers. The CMMA coatings were found to have manyfold improvement in corrosion resistance compared to their monolayer counterparts [Roy 2009]. Fahidy (1983) reported the importance of magnetoelectrolysis in various applications, later many reports came on the magnetic field effects on electrodeposition. Many researchers utilized MED to improve the material properties of the electrodeposited alloy coatings [Taniguchi et al. 2000, Tabakovic et al. 2003, Tabakovic et al. 2005, Rao et al. 2013, Aaboubi and Msellak 2016]

1.16 ELECTROCATALYSIS

Electrocatalysis is the term used to indicate the catalysis of electrode reactions. This can be accomplished by the action of the electrode material or alternatively by the action of species in solution or both [Trasatti 1995]. A number of phenomena which may have little in common are grouped together under the term electrocatalysis. However, it can be distinguished into homogeneous and heterogeneous to avoid this generalization of electrocatalysis. Heterogeneous electrocatalysis is more a function of the electrode material and electrode kinetics, and it refers 'electrocatalysis' in practical fields [Pletcher 1984].

1.16.1 Electrochemical water splitting

The energy crisis and environmental concerns intensified the need for searching a clean and renewable alternate energy for the future [Chen et al. 2016]. In this regards, the global economy is looking into the possibilities of utilization of the abundant, renewable and cleanest fuel, hydrogen, as a promising alternate energy carrier in the future [Reddy et al. 2016, Pu et al. 2016]. Hydrogen has been promoted as the ideal clean energy source with zero-emission [Prather 2003, Luo et al. 2016], and having excellent energy storage density [Pu et al. 2016]. Water is the most abundant source of hydrogen, free from carbon [Turner 2004, Zeng and Zhang 2010, Reddy et al. 2016], and its splitting into H_2 and O_2 is the best choice for H_2 production. Whereas the water

electrolysis is an arduous process, suffers from practical overpotentials due to sluggish electrode kinetics [Zeng and Zhang 2010, Reddy et al. 2016].

1.16.1.1 HER and OER

An archetypal electrolysis cell for water splitting is shown in Fig. 1.12. The general process taking place at the anode (under acidic condition) is oxidation of water called oxygen evolution reaction (OER) according to the equation: $2H_2O \rightarrow O_2 + 4e^- + 4H^+$. The generated electrons travel through the external circuit, while the protons move towards the cathode to complete the electrochemical circuit. Then, the protons and electrons combine at the cathode to form H_2 gas, called hydrogen evolution reaction (HER): $4e^- + 4H^+ \rightarrow 2H_2$ (under acidic condition). Here, under acidic conditions, H^+ ions are the electrochemical charge carriers. Whereas, the reactions at the anode and cathode under basic conditions are: HER: $4H_2O + 4e^- \rightarrow 2H_2 + 4OH^-$ and OER: $4OH^- \rightarrow O_2 + 2H_2O + 4e^-$. Conventional electrolysis works best at either very high or very low pH, at which the concentration of charge carriers is greatest. The minimum theoretical voltage required as driving force for the water splitting of HER and OER is 1.23 V at room temperature [Roger et al. 2017]. However, practically it needs additional energy or activation energy for the reaction to proceed at appreciable rates, called overvoltage.
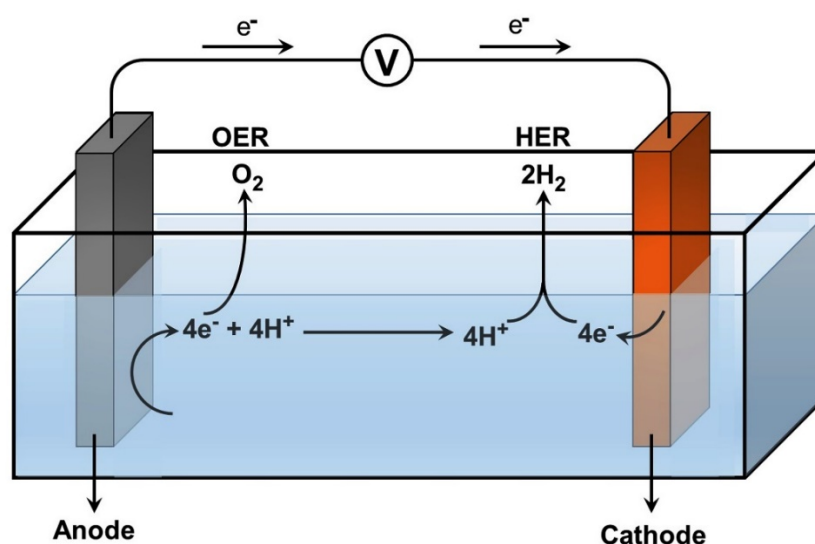
Fig. 1.12- Schematic of electrolysis cell for water splitting under acidic conditions

1.16.2 Electrode materials for electrocatalytic water splitting

The role of electrocatalysts is to reduce the overpotential as far as possible. Under acidic conditions, the best electrocatalysts are precious metals, platinum at the cathode and IrO_2 or RuO_2 at the anode [Roger et al. 2017]. However, the wide applications of these noble metals have been hindered due to their scarcity and high costs. Hence, extensive research has already been devoted to this area for the development of non-Pt materials as electrocatalysts [Zou and Zhang 2015, Cardoso et al. 2015]. At the same time, under basic conditions, the first-row transition metals (and their alloys) and oxides make excellent HER and OER catalysts, respectively. In general, the HER catalysts fall into three categories: *i)* noble metal (Pt) catalyst, *ii)* transition metal (mainly including Fe, Co, Ni, Cu, Mo and W) based electrodes and *iii)* nonmetals (mainly including B, C, N, P, S and Se) based materials [Zou and Zhang 2015, Safizadeh et al. 2015]. Most of the non-precious HER electrocatalysts reported to date are based on these twelve transition elements and nonmetals. An ideal HER electrocatalyst should have some essential requirements like; *i)* low hydrogen overvoltage at industrial current density, *ii)* no potential drift with time, *iii)* good chemical and electrochemical stability: long lifetime and no release of process-deleterious products, *iv)* high adhesion to the support, *v)* low sensitivity to poisoning by impurities, *vi)* low sensitivity to current shut down (short-circuit) or modulation, *vii)* no safety or environmental problems in the manufacture process, *vii)* easy to prepare at a low cost/lifetime ratio [Jaccaud et al. 1989, Safizadeh et al. 2015, Roger et al. 2017]. The highest abundance and the lowest price of Ni and Fe making them more desirable to make economically viable electrocatalysts [Gong et al. 2016].

As per the literature, at present, Ni is one of the active non-precious metal as HER catalysts, but it's HER activity is limited so far and hence it is necessary to enhance the catalytic activity of Ni, either through proper alloying or through other methods to increase its surface area [Domínguez-Crespo et al. 2011, Cardoso et al. 2015]. From the volcano plots reported by Trasatti (1972), as shown in Fig. 1.13, and Nørskov et al. (2005), after studying the activity of various catalysts for HER on the basis of exchange current density (a measure of the effectiveness of a catalyst for the HER) as a function of the calculated hydrogen adsorption energies, it is revealed that the efficiency of Ni catalyst towards HER can be greatly improved by weakening the

Ni–H bond [Trasatti 1972], as it is much stronger than Pt–H bond [Li et al. 2015]. In this direction many reports came on Ni-based alloys like Ni-P [Shervedani and Lasia 1997, Burchardt 2000], Ni-Co [Correia et al. 1999, Wu et al. 2004], Ni-Mo [Jakšić et al. 2000, Kedzierzawski et al. 2001, Wang et al. 2015], Ni-S [Han et al. 2003] etc., in different electrolytes.
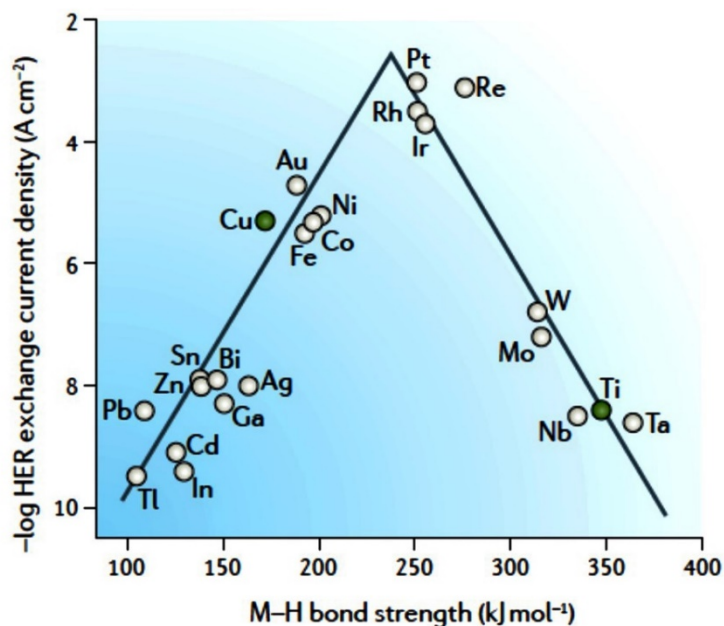
Fig. 1.13- Trasatti's HER volcano plot: the exchange current densities for HER versus the energy of the intermediate M–H bond formed between absorbed H and the electrode surface (Adopted from, Roger et al. 2017)

The detailed cross-examination of volcano plot allows the design of new HER catalysts by combining elements on opposite slopes of the volcano to produce new materials with intermediate hydrogen binding energy, and hence improved catalytic performance [Roger et al. 2017]. As guided by this facts, it is clear that the combination of Ni with alloying elements like W and Mo can offer enhanced catalytic performance. Along with Ni, more abundant and cheap materials such as Co and Fe, and their alloys have been a subject of intense research, due to their promising electrocatalytic properties.

In principle, the materials with intrinsic catalytic activity and high surface area can show low overvoltage and hence high electrocatalytic activity for HER [Zhou et al. 2016]. In this regards, compared to Ni-based alloys, the Ni-based composite materials

containing active solid particles have been received more and more attention as new electrocatalytic candidates [Williams 1966, Aal and Hassan 2009, Krstajić et al. 2011a]. The enhanced properties of this Ni-based composites are attributed to the synergistic effect of Ni with the incorporated nanomaterials according to Brewer-Engel theory [Krstajić et al. 2011a]. On the other hand, the incorporated particles can also decrease Ni grain size and result in a high electrode specific surface area [Zheng et al. 2012]. In this direction, several metal/alloy composites are reported as efficient electrode materials for electrocatalytic HER [Krstajić et al. 2011b, Zhou et al. 2016]. Some of the nanomaterials like TiO_2 [Thiemig and Bund 2008, Chen et al. 2010a], CeO_2 [Zheng et al. 2012], CNT [Chen et al. 2002] etc. has been already attracted considerable attraction and impact as the best inclusions to enhance the electrocatalytic activity of the metal/alloy, when it forms a composite with them [Williams 1966, Aal and Hassan 2009, Krstajić et al. 2011a].

1.16.3 Electrodeposition as a tool for electrode material synthesis

Numerous research works on the HER activity of various elements like Cu, Au, Mo, Pd, Rh, Fe [Pentland et al. 1957], Ni [Lasia and Rami 1990], RuO_2 [Kötz and Stucki 1987], Ti [Thiemig and Bund 2008] etc. were reported during the last decades. Whereas, the prepared cathodes either in the form of pure metal or in alloyed form are not found to be necessarily better than steel cathodes (using commercially for alkaline HER). Whereas, compared with the bulk materials, the alloy/composite coatings were found to show improved electrocatalytic activity and decrease in overvoltage, due to increase in effective surface area of the cathode. Although there are several methods available for the fabrication of coatings, the cost effectiveness and simplicity of electrodeposition making it more attractive and reliable [Mirkova et al. 2011, Luo et al. 2016]. A variety of coatings such as metal, alloy or composite can be developed with high precision through electrodeposition, and also it allows to have a close control over the desired properties of the deposits. It also allows the convenience of producing the deposits of desired composition, porosity (large area surfaces), low-temperature growth and the possibility to control film thickness, morphology and phase structure by adjusting the electrical parameters and the composition of electrolytes [Correia et al. 1999, Zheng et al. 2012]. The interesting advantages of electrodeposition over other

coating techniques (like, plasma or thermal spraying, thermal decomposition, in-situ activation etc.) are: *i)* simple setup, *ii)* easy to develop non-crystalline phases, *iii)* control over composition of the coating, *iv)* suitable for scalability and *v)* low cost [Aal and Hassan 2009, Krstajić et al. 2011a]. Moreover, it can improve the adherence of the deposits on the substrate surface and enhance the electrocatalytic activity and stability. Many literature reports are there on the electrodeposited metal/alloy/composite electrocatalysts [Aal and Hassan 2009, Krstajić et al. 2011b, Zheng et al. 2012].

Many reports are there on the efficiency and cost effectiveness of electrodeposited coatings (metal/alloy/composite) as electrode materials for electrocatalytic water splitting reactions. Arul Raj accompanied with Vasu reported many electrodeposited Ni- based binary and ternary alloys as cathode materials for alkaline HER [Raj and Vasu 1990, Raj and Vasu 1992]. They observed the electrodeposited Ni-Mo alloy coating as the best towards alkaline HER with low overpotential [Raj and Vasu 1990, Raj 1992a, Raj 1992b, Raj 1993]. The same research group also reported the codeposited Ni- based ternary alloys such as Ni-Mo-Fe, Ni-Mo-Cu, Ni-Mo-Zn, Ni-Mo-Co, Ni-Mo-W, Ni-Mo-Cr as electrode material for alkaline HER [Raj 1992a, Raj 1993]. Thereafter many alloy and composite electrodes developed using electrodeposition technique were reported as efficient materials for HER [Low et al. 2006, Shervedani et al. 2008, Lupi et al. 2009, Kaninski et al. 2009]. Then, Herraiz-Cardona et al. (2013) developed porous electrodes through galvanic codeposition to enhance the HER efficiency through increasing the effective surface area, and they succeeded in depositing porous Ni-Co alloy electrode. Later, numerous number of publications came on the electrodeposited Ni- based alloys [Ullal and Hegde 2014a, Ngamlerdpokin and Tantavichet 2014, Cardoso et al. 2015, You et al. 2015, Pérez-Alonso et al. 2015, Tang et al. 2015, Vargas-Uscategui et al. 2015, Bachvarov et al. 2016, Shetty and Hegde 2017], composites [Kuang et al. 2013, Subramanya et al. 2015, Badrayyana et al. 2015, Danilov et al. 2016], oxides/hydroxides [Danilovic et al. 2012, Trotochaud et al. 2014], heterostructures [Gong et al. 2013, Feng et al. 2015, Zhang et al. 2016] etc., as efficient electrode materials for alkaline HER.

1.16.4 Magnetic field effects on electrocatalysis

The major factors which contribute towards the electrocatalytic cell overvoltage are activation polarization, concentration polarization and ohmic polarization [Balat 2008, Schlögl 2012, Huggins 2010]. The sluggish kinetics due the nature of the electrode is leading to the formation activation polarization and it can be controlled to a certain extent by modifying the electrode material [Wang et al. 2014]. Concentration polarization arises due to the limitations in mass transport resulting from the formation of electrical double layer. Whereas, the ohmic polarization arising from various factors also plays a major role in the high energy consumption during water electrolysis [Balat 2008, Wang et al. 2014]. The overall contribution of circuit resistance (R_c), solution resistance (R_s), material resistance (R_m) and bubble resistance (R_b) leading to ohmic voltage drop during electrolysis [Wassef and Fahidy 1976]. Where, the resistance due to electrode material can be compromised by the selection, design or synthesis of the material [Tilak et al. 1986, Keita and Nadjo 1985]. The electric resistance also can be nullified through proper connections, and hence in an electrolytic cell, the contributions from R_m and R_c can be considered as constant. Then, the solution resistance depends on the conductivity of the electrolyte and also on the distance between the electrodes. This effect also can be minimized to a certain extent by the use of electrolytes of high electrical conductivity and maintaining a minimum distance between the electrodes [Wang et al. 2014]. However, the resistance developing on the electrode surface due to the formation of bubbles remains as a major contributing factor towards ohmic voltage drop during electrolysis [Kiuchi et al. 2006, Shen et al. 2011, Cong 2013]. The interference of the gas bubbles, developed on the electrode surface as well as the evolved gas bubbles got dispersed within the electrolyte, with the applied electric field in the form of a shield can lead to large ohmic voltage drop due to high bubble resistance [Fahidy 1983, Kiuchi et al. 2006]. To overcome this effect, the bubbles formed on the electrode surface should be removed faster as it is formed.

In this regards, inducing an external magnetic field can offer better results through MHD effect arising from Lorentz force [Fahidy 1983, Ragsdale et al. 1998]. Many reports are there on the magnetic field induced convection due to Lorentz force operating on moving charged species in an electromagnetic field [Tacken and Janssen 1995, Ganesh et al. 2005, Lin et al. 2012, Monzon and Coey 2014]. The magnitude of

Lorentz force ($F_L = qvB \sin\theta$) is maximum when it is applied perpendicular ($\theta = 90°$) to the applied current density or velocity of the moving charged species [Monzon and Coey 2014]. This enhanced mass transport due to MHD convection can reduce the polarization resistance as well as the ohmic drop due to bubble resistance through the easy detachment of generated gas bubbles from the electrode surface [Kiuchi et al. 2006, Lin and Hourng 2014]. The reduction in cell overvoltage by superimposing external magnetic field is irrespective of the nature of the electrode material, provided all other conditions maintained as the same. Therefore by proper design of the electrode material and superimposition of an external magnetic field of optimal strength can offer efficient electrolysis of water by minimizing the polarization effects. Wassef and Fahidy (1976) reported a detailed study on the magnetic field effects on water electrolysis. Thereafter many researchers have succeeded in using the magnetic field as a tool to improve the electrochemical reaction kinetics [Steiner and Ulrich 1989, Devos et al. 2000, Hinds et al. 2001, Matsushima et al. 2009, Aaboubi 2011].

1.16.5 Electrochemical techniques for electrocatalytic study

1.16.5.1 Cyclic voltammetry

Cyclic voltammetry (CV) is a method for investigating the electrochemical behavior of a system. This most widely used technique for obtaining qualitative information about the electrochemical reactions was first reported, and theoretically explained by Randles (1948). The wide acceptability of this technique was resulted from its ability to provide considerable amount of information rapidly on thermodynamics of redox processes, on the kinetics of heterogeneous charge-transfer reactions and on coupled chemical reactions or adsorption processes [Hibbert 1993].

In the case of electrocatalytic study, the stability and activity of the electrode material towards chemical reactions can be established from this sweep reversal method. The electrode-ion interaction at the electrode/electrolyte interface can be obtained from the exceptionally potent and the most widely used CV technique [Bard et al. 1980, Wieckowski 1999]. The current response of the CV can give a direct measure of the surface adsorbed ionic species of the electrolyte and hence its efficiency towards the catalytic reduction of adsorbed H^+ ions i.e., for HER [Bockris and Khan 2013]. CV gives useful information about the behavior of electroactive species and

mechanism of electrochemical reactions. In this technique, potential of working electrode is scanned from an initial point to a final point and then switched back to other side of potential and then swept to initial point. The excitation signal for CV is a linear potential scan with a triangular waveform as shown in Fig. 1.14(a). This triangular potential excitation signal sweeps the potential of the electrode between two values, sometimes called the switching potentials. During this process, the response or current is monitored by a potentiostat, which is measured between working and counter electrodes with respect to the standard reference electrode. The cycling of potential at working electrode with respect to time is carried out at a particular rate called sweep or scan rate with units as volts per second (V s^{-1}). The voltammogram thus recorded as current (Y-axis) *vs* potential applied (X-axis) is called cyclic voltammogram (Fig. 1.14(b)). The potential axis is also a time axis that is related to scan rate [Wieckowski 1999, Zhao et al. 2009]. The current measured during the analysis is often referred as current density by normalizing with respect to the surface area of the electrode, and then plotted against the potential in cyclic voltammogram. The width and height of the peak obtained at the scanned region, characteristic of the electrode reactions, depends on various factors like the nature of the electrode material, concentration of the electrolyte, scan rate etc [Brett and Brett 1993, Zhao et al. 2009].
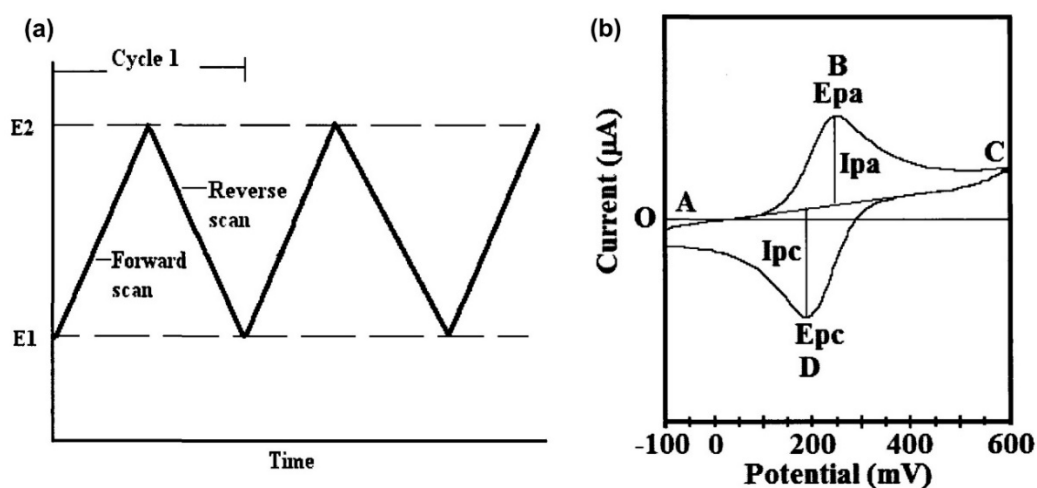
Fig. 1.14- a) Variation of the applied potential as a function of time in a cyclic voltammetry experiment, and b) a typical cyclic voltammogram of current versus potential (Adopted from, Bard and Zoski 2013)

56

In a typical CV experiment, thus the potential of working electrode is continuously scanned at a specific scan rate from initial to the final value. The scan starts at a potential where no electrochemical reaction occurs and scanned to a region where the electrochemical reaction of interest (oxidation/reduction) takes place. A positive potential ramp can be applied to carry out an oxidation process, where the electroactive species loses an electron at the electrode to give an anodic peak current (i_{pa}) at a given potential (E_{pa}). Whereas, the cathodic peak current (i_{pc}) are observed as a result of reduction process, when potential is applied in the negative direction, leading to a reduction peak at a given potential (E_{pc}) [Zhao et al. 2009].

1.16.5.2 Chronopotentiometry

Chronopotentiometry (CP) is an electrochemical characterisation method that measures the electric potential response of a system to an imposed current. CP is the most basic constant current technique, in which current is applied across an electrochemical cell, without stirring. Compared to other dynamic characterisation methods like electric impedance spectroscopy, cyclic amperometry or voltammetry, it allows to correlate significant transient states with the measured electric potential [Wilhelm et al. 2001]. The differences of the transport conditions can be inferred from the variation in potential responses. Since it is possible to analyze the dynamic voltage response in time, CP can give more detailed information compared to steady-state voltage or current sweeps. CP is widely used as an important analytical tool in electrochemistry to study the transport process and reactions in the electrolytes, electrodes and membranes. Mechanism of chemical reactions and the formation of activated complex at the electrode surface can be obtained from the CP analysis [O'M and Reddy 1970, Gileadi 1993, Zhao et al. 2009].

The constant current CP is a valuable tool to study the electrocatalytic efficiency of the electrode materials under working conditions. In the case of HER, the applied constant current leads to the continuous reduction of the H^+ ions at the cathode surface leading to the continuous evolution of H_2. The potential responses vary according to the nature of the electrode material and also with respect to the availability of the redox couple within the medium [Gileadi 1993]. The 'potential-time' (E-t) curve show deviation either due to the instability of the electrode material under working conditions

or due to the unavailability or decrease in concentration of the H^+ ions in the electrolyte with time [Wilhelm et al. 2001]. At the same time, as the efficiency of the electrode material is increasing towards HER, the potential value may move close to zero. Therefore, from the obtained 'E-t' response at a particular electrode potential, it is possible to establish the robustness of the electrode material under HER working conditions [Ullal and Hegde 2014a]. In the electron transfer reaction, $2H^+ + 2e^- \rightarrow H_2$, before applying the current the concentration of the H^+ species at the electrode surface is the same as in the bulk of the solution. Whereas, once the reducing current is applied, H^+ is reduced to form H_2 at the electrode surface in order to support the applied current. Therefore, the concentration of H^+ at the electrode surface decreases, leading to the formation of a concentration gradient of H^+ between the bulk solution and the electrode surface [Bard et al. 1980, Wilhelm et al. 2001]. The concentration of H^+ vary with time, and hence the potential. As the concentration of H^+ becomes zero at the electrode surface and hence, the current can no longer be supported by this electron transfer reaction leading to large variation in potential [Gileadi 1993, Wieckowski 1999, Zhao et al. 2009]. The current excitation and potential response of CP are shown in Fig.1.15. The variation in potential response at a very low concentration of the electroactive species after a certain time (t_1) of analysis is shown in Fig. 1.15 (b).
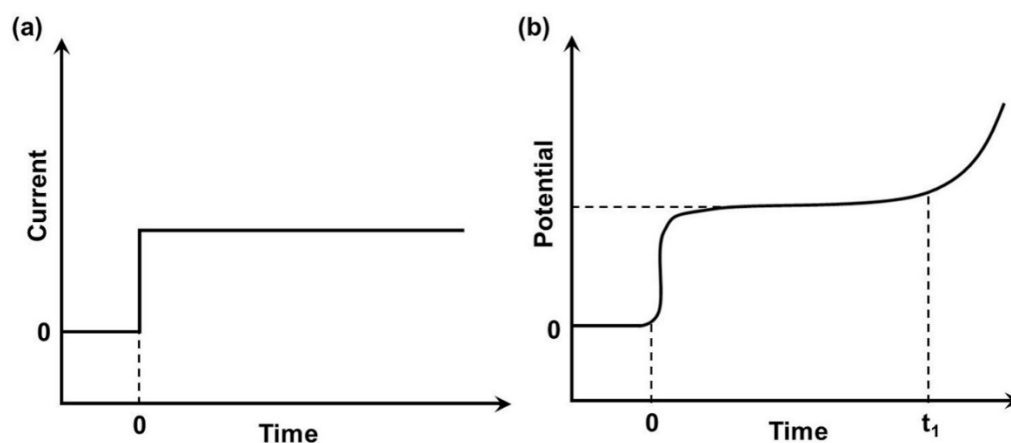
Fig.1.15- a) Current excitation and b) potential response for CP analysis (Adopted from, Bard et al. 1980)

58

1.17 SCOPE AND OBJECTIVES

The literature review on Ni- based alloy coatings, focusing on their corrosion resistance and electrocatalytic efficiency for alkaline water electrolysis revealed that the alloying of Ni with the hard and high melting transition metal, W and a nonmetal, P can impart many promising material properties. The optimization of a new electrolytic bath for the development of Ni-W alloy coating with desirable properties can ensure better results in terms of corrosion resistance and electrocatalytic activity. Being less studied system, due to the induced codeposition behavior of Ni-W alloy, the detailed study by altering the mass transport mechanisms during deposition can help in tailoring the coating characteristics. Though Ni-P alloys are the most studied systems, the deposition of such coatings from alkaline baths is seen to be less reported. Thus, guided by the literature review on electrodeposition and properties of alloy coatings, it was found that:

i) The corrosion resistance of metal/alloy coatings can be increased substantially by tailoring the composition, phase structure and morphology of the coatings by controlling the deposition c.d.

ii) Periodic modulation in mass transport process at cathode brings a periodic modulation in composition of the coatings.

iii) The HER activity of the alloy coatings can be improved by the incorporation nanomaterials through composite electrodeposition.

iv) Superimposition of a magnetic field during deposition can offer better material properties in terms of corrosion resistance and electrocatalytic activity.

Many properties including corrosion behavior of monolayer alloy coatings can be increased to several folds by multilayer coating approach. Accordingly, CMM Ni-W and Ni-P alloy coatings can be developed from their respective baths for the better corrosion protection of MS. Coating configuration can be optimized for their peak performance against corrosion, in comparison with their monolayer alloy coatings. The electrocatalytic performance of the alloy coatings can be examined, and it can be further enhanced through the development of their nanocomposite coatings. The effect of inducing B during deposition and electrocatalytic activity can be studied and compared with the conventional processes. Hence, this work is planned to carry out in two ways,

depending on the type of mass transport at the electrode/electrolyte interface, i.e., by modulating: *i)* c.d. and *ii)* magnetic field in both direction and intensity. The following experimental procedures has been adopted in the study:

1) Optimization of new electrolytic baths for the deposition of alloy coatings using DC.

2) Development of multilayered alloy coatings by pulsing the cathode c.d. using same bath.

3) Analysis of the electrocatalytic activity of alloy coatings and its further enhancement through the development of nanocomposite coatings.

4) Examination of the effect of magnetolysis on production and properties of alloy coatings, in terms of corrosion resistance, hardness and electrocatalytic activity.

5) Analysis of the magnetic field superimposition effects on mass transfer for enhanced HER on alloy surface.

The corrosion character of electrodeposited alloy coatings was evaluated by electrochemical DC and AC techniques. The process and product of electrodeposition were analyzed using different electro-analytical methods. The surface morphology, elemental composition and crystallite texture of electrodeposited coatings were analyzed, and correlated to their properties. Thus, from available literature on corrosion protection efficacy and electrocatalytic behavior of Ni-based alloy coatings developed by electrodeposition method, the following objectives have been proposed to be accomplished in the present study.

1.17.1 Objectives

1. To optimize electrolytic baths of Ni-W and Ni-P alloy for the deposition of bright, uniform, protective monolayer coatings on MS using glycerol as an additive.

2. To enhance the corrosion protection efficacy of monolayer alloy coatings (Ni-W and Ni-P) through multilayer technique by pulsing the DC, and to optimize their coating configurations in terms of number of layers and cyclic cathode c.d.'s.

3. To study the electrocatalytic behavior of electrodeposited Ni-W and Ni-P alloy coatings towards HER and OER in 1.0 M KOH medium.

60

4. To improve the HER efficacy of Ni-P alloy coatings by electrochemical dissolution and the incorporation nanoparticles such as Ag and TiO_2.

5. To enhance the HER activity of Ni-W alloy coatings through the development of Ni-W-MWCNT and Ni-W-rGO nanocomposite coatings.

6. To study the effect of applied magnetic field (in terms of intensity and direction), on the surface morphology, crystallographic orientation, and consequently on the corrosion behavior of Ni-W alloy coatings.

7. To study the electrocatalytic behavior of MED Ni-W alloy coatings developed under different applied magnetic field strengths from the same bath.

8. To study the effect of inducing magnetic field (B) of varying intensity during electrolysis, and thereby to understand the effect of B on the HER efficiency of Ni-W alloy coating.

9. To understand the structure - property relation of electrodeposited coatings, i.e., how deposition conditions (like composition of the bath, c.d., temperature, pH, direction and intensity of B) are related to the composition, surface morphology, thickness, hardness, phase structure and electrocatalytic behavior of the coatings.

10. To identify the most effective mode of mass transport, controlled by various methods, namely, cathode c.d. and induced B for better material property of the coatings namely, corrosion resistance and electrocatalytic behavior.

CHAPTER 2

MATERIALS AND METHODS

This chapter discusses the details of materials and methods used for the synthesis and characterization of electrodeposited Ni-based alloys and their nanocomposite coatings. The procedures adopted for the optimization of electrolytic baths and deposition of alloys and their nanocomposite coatings are discussed, followed by a concise description of the characterization techniques used. The setup and the methods used to test the efficacy of the developed coatings for different applications such as corrosion resistance and electrocatalytic activity are also described.

Electroplating is an exceptionally important and attractive technology, due to its economic feasibility and simple operation. It is concerned with covering inexpensive and widely available base materials with plated layers of different metals/ alloys/composites with superior properties to extend their use to the applications which otherwise would be prohibitively expensive. In principle, electroplating of a metal/ alloy/composite is not a simple dip and dunk process. It is probably one of the most complex processes known because of the unusually large number of critical elementary phenomena, or process steps involved. Generally, a practicable method for electrodepositing any metal/alloy/composite involves three steps. The first step is concerned with the surface preparation of the substrate to be plated. Second and the most important step involves the optimization of a suitable plating bath. This requires a practical knowledge of the electrochemistry of elements, the solubility of their salts, and the chemistry of their complexes. Finally, the third step involves direct deposition of the metal/alloy/composite coating from the optimal bath.

2.1 MATERIALS

2.1.1 Chemicals and materials

Nickel sulfate hexahydrate ($NiSO_4 \cdot 6H_2O$), dihydrated sodium tungstate ($Na_2WO_4 \cdot 2H_2O$), sodium hypophosphite ($NaPO_2H_2 \cdot H_2O$), tri-sodium citrate dihydrate ($C_6H_5Na_3O_7 \cdot 2H_2O$), ammonium chloride ($NH_4Cl$), boric acid ($H_3BO_3$), glycerol

($C_3H_8O_3$), trichloroethylene (TCE), potassium hydroxide (KOH), sodium chloride (NaCl), ammonium hydroxide (NH_4OH), potassium permanganate ($KMnO_4$), hydrogen peroxide (H_2O_2), hydrochloric acid (HCl), nitric acid (HNO_3), sulfuric acid (H_2SO_4) and graphite powder are the basic chemicals used for present study. This chemicals used for bath preparation, surface cleaning and other synthesis are of Analar grade, procured from Merck, Mumbai, India. Distilled water was used for all electrolytic bath preparations and synthesis. The other chemicals and nanoparticles such as, silver nitrate (>99% $AgNO_3$), sodium borohydride (>99% $NaBH_4$), titanium dioxide (TiO_2, P<25, anatase) and multi-walled carbon nanotubes (MWCNT, 98% purity, outer diameter × length = 7-15 nm × 0.5-10 µm) were obtained from Sigma-Aldrich Company, St. Louis, MO, United States of America. Mild steel (MS) panels, copper rod and copper plates were used as the substrates for experimental investigation.

2.2 EXPERIMENTAL METHODS

The research work unfolds the fabrication and characterization of electrodeposited Ni-based alloys (such as Ni-W and Ni-P) and their nanocomposite coatings. The complete details of the research work are given in the form of a flow chart in Fig. 2.1.
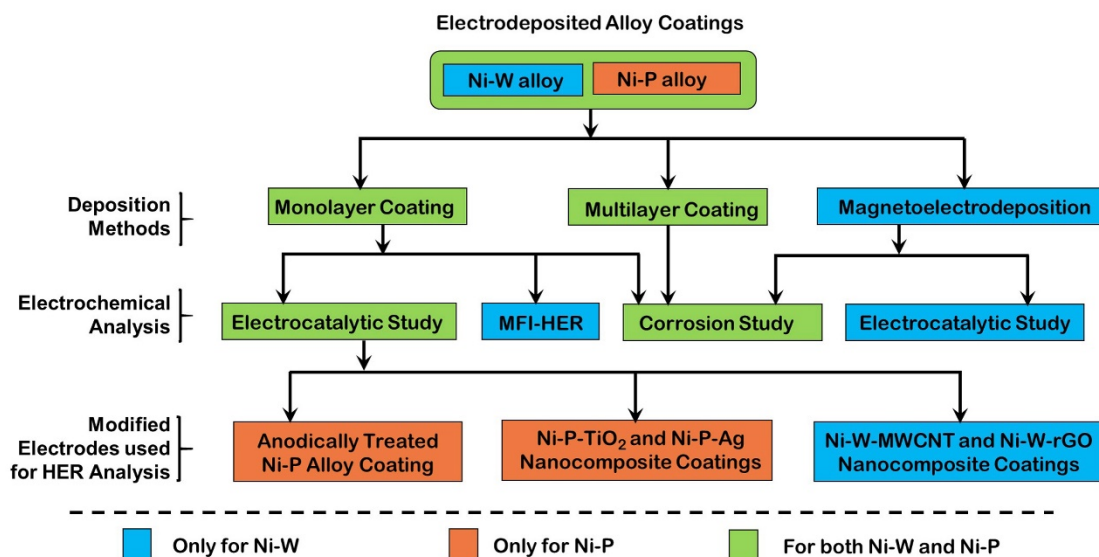
Fig. 2.1- The flow chart of the complete research work

The step wise description of the methods adopted in the present study are discussed in the following sections.

2.2.1 Surface cleaning

All substrates (MS panels, copper plates and copper rod) of various sizes (10.0×5.0 cm^2, 5.0×5.0 cm^2 and 2.5×3.0 cm^2) were pretreated by mechanical polishing, using emery coated mops of gradually decreasing grit sizes. Then the mirror polished specimens were degreased with TCE, electrocleaned cathodically for 2 minutes and then anodically for 30 seconds. Later the specimens were washed in running water, rinsed in distilled water, followed by a dip for 10 seconds in 10% HCl (for MS substrate) or 10% HNO_3 (for copper substrate) [Cramer and Covino Jr 2005]. Finally, washed and rinsed with distilled water, and then immediately taken for deposition.

2.2.2 Optimization of plating baths

The Hull cell is a specially designed cell for carrying out practical plating tests on electroplating solutions. The optimal conditions necessary to obtain good quality electrodeposits of Ni-W and Ni-P alloy were achieved using Hull cell method [Parthasaradhy 1989, Nasser 2004]. The various steps adopted for Hull cell optimization of the electrolytic plating baths are schematically represented in Fig. 2.2.
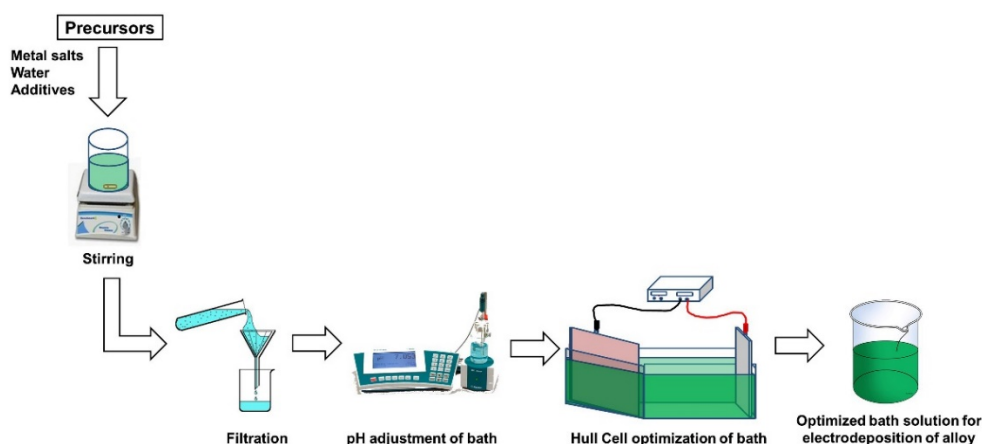
Fig. 2.2- Schematic of Hull cell optimization process

Because a Hull cell produces a deposit that is a true reproduction of the electroplate obtained at various current densities (c.d.'s) within the operating range of a particular system, it allows experienced operators to determine multiple process parameters, such as brightness, concentration of primary bath components and additives, presence of metallic and organic impurities, effects of temperature and pH

etc. [Brenner 1963, Nasser 2004]. Hence, the Ni-W and Ni-P alloy baths were primarily optimized by conventional Hull cell method. When a voltage is applied across the anode and cathode, the resulting c.d. will vary along the length of the cathode, being highest at the point it is closest to the anode. In this way, one can, within a single test run, assess the effect of varying c.d. Accordingly, after such a run, the cathode was removed and inspected. Based on the visual observation of plated panels the *operating window* of the c.d. required for the proposed bath was determined, using the Hull cell scale. It was used to assess any factor that produces a change in the property of the electrodeposits over a wide range of c.d.'s, and it is an invaluable analytical tool for determining the influence of any parameter on the appearance of the deposit [Nasser 2004].

2.2.3 Development monolayer alloy coatings

The plating was carried out on MS substrate (having an active surface area of 6. 25 cm^2), after surface preparation through mechanical polishing, degreasing, electropolishing and pickling in 10% HCl. All depositions were carried out in a rectangular PVC vessel of 250 mL capacity by keeping pure Ni anode and substrate parallel, at 5 cm distance. The pH of the bath was maintained at an optimal value by tuning with NH_4OH/H_2SO_4, whenever required. The deposition was performed with continuous agitation near the cathode to overcome the limitation in mass transfer due to concentration polarization. For comparison purpose, all depositions were performed for 600 s (10 min) duration at room temperature (298 K) from the optimal bath by using computer-controlled DC Power Analyzer (Agilent Technologies, Model: N6705) as a power source. A schematic of the deposition setup is shown in Fig. 2.3.
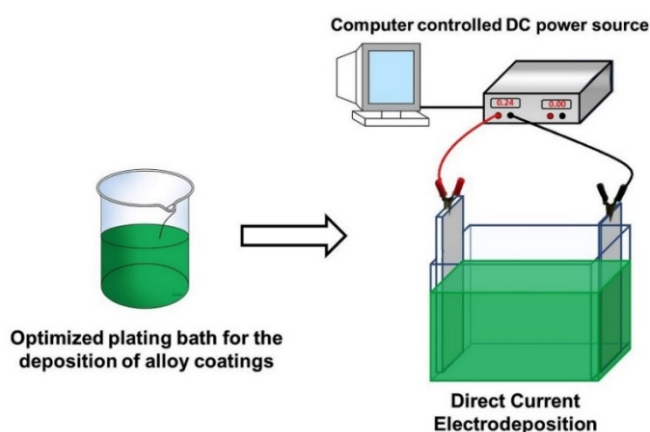
Fig. 2.3- Schematic of DC electrodeposition

2.2.4 Development of multilayered alloy coatings

Development of multilayer coatings by electrolytic methods for increased material properties was carried out by passing DC of different current strength in a pulsed manner, which enables the development of coatings having a periodic modulation in composition [Leisner et al. 1996, Roy 2009]. Driven by the fact that periodic modulation in mass transport process at cathode film (by periodic change in the c.d.) leads to the development of multilayer coatings (with periodic modulation in composition) on the surface of cathode, CMMA coatings were developed. Accordingly, the current is made to cycle between different c.d.'s, called cyclic cathode current densities (CCCD's). The power pattern used for deposition of monolayer and multilayer alloy coatings along with their corresponding coatings obtained are shown schematically in Fig. 2.4.
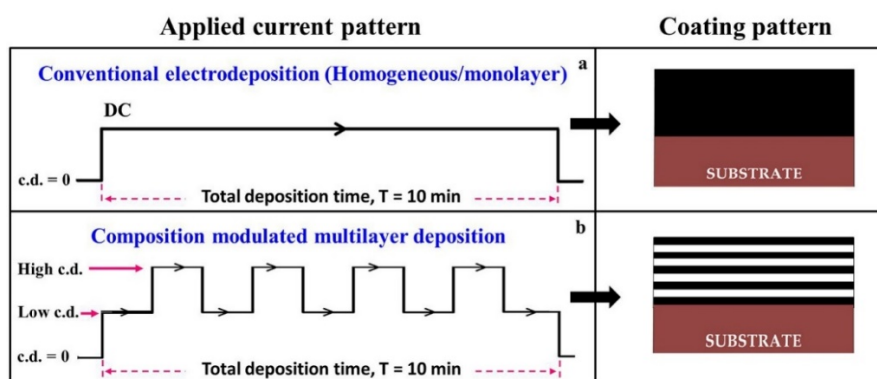
Fig. 2.4- Schematic of power patterns used for deposition (left) of Ni-W and Ni-P alloy, and the corresponding coatings developed (right): a) monolayer, and b) multilayer

Conveniently, CMMA coating having alternatively different compositions are represented as: $(Ni-M)_{1/2/n}$. Where, M = W and P, 1 and 2 indicate the first and second cathode c.d. which were selected to be applied for the deposition of alloys of different composition and 'n' represents the number of layers formed during total plating time, i.e., 10 min. Hence, CMMA Ni-M coatings with different coating configuration, i.e., under different sets of CCCD's and with different number of layers were developed, and are subjected to characterization. By proper setting-up of the power source, the CCCD's were set to change alternatively, during deposition of multilayer coatings. The

coated surfaces were rinsed with distilled water several times, dried in hot air and desiccated under vacuum till further analysis.

2.2.5 Magnetoelectrodeposition

The electrodeposition in the presence of induced B, called MED is a promising technique to overcome the mass transfer limitations during deposition to achieve coatings with tailor-made properties [Fahidy 1983, Waskaas and Kharkats 1999, Mohanta and Fahidy 1978]. The MED Ni-W alloy coatings were accomplished at desired c.d. in conjunction with induced B, using DC power source (DC Power Analyzer, Agilent Technologies, Model: N6705) and an Electromagnet (Polytronics, Model: EM 100), respectively. MEDs were carried out under different conditions of induced B, both in terms of intensity (from 0.1 T to 0.4 T) and direction (parallel and perpendicular to the direction of flow of ions). The deposition c.d. was kept constant (4.0 A dm^{-2}, which was obtained as optimal for conventional alloy coatings) for MEDs to study the effect of applied magnetic field on coating characteristics. The coatings deposited under normal electrodeposition (ED), i.e., under natural convection and MED, i.e., under forced convection are conveniently represented, respectively as (Ni-W)$_{B=0 \text{ T}}$ and (Ni-W)$_{B=0.1 \text{ T/per, or par,}}$ depending on intensity and direction of B with respect to the direction of flow of ions. All depositions were carried out on MS substrate (having an active surface area of 6.25 cm^2), after surface preparation through mechanical polishing, degreasing, electropolishing and pickling in 10% HCl. A PVC vessel of 250 mL capacity was used for plating process, by keeping pure Nickel anode and substrate parallel, 5 cm apart. All depositions were performed for 10 min duration at room temperature from the optimal bath, for comparison purpose. The schematic of the setup used for MED, in terms of the direction of B (parallel or perpendicular), is shown in Fig. 2.5.
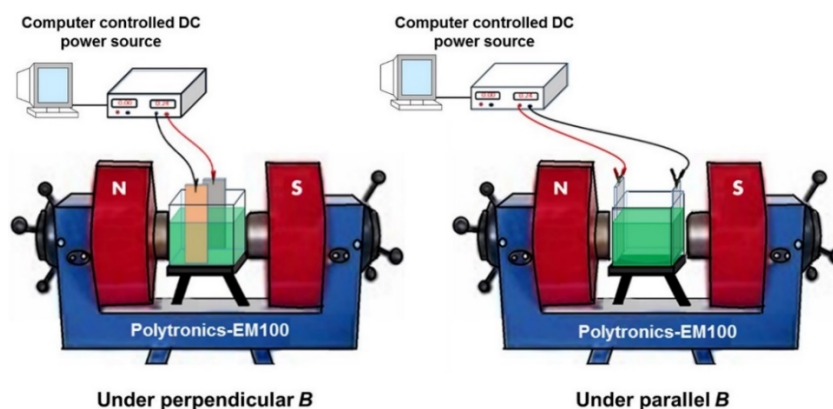
Fig. 2.5- Schematic of experimental setup used for MED under conditions of perpendicular and parallel magnetic field

2.2.6 Development of alloy coatings for electrocatalytic study

Electrocatalytic characterization of Ni-W and Ni-P alloy coatings (test electrodes) were made by depositing the coatings on a copper rod having $1cm^2$ cross-sectional area, using a homemade electrodeposition setup as shown in Fig. 2.6. The developed test electrodes were used for the electrocatalytic activity study towards alkaline HER and OER in 1.0 M KOH medium.
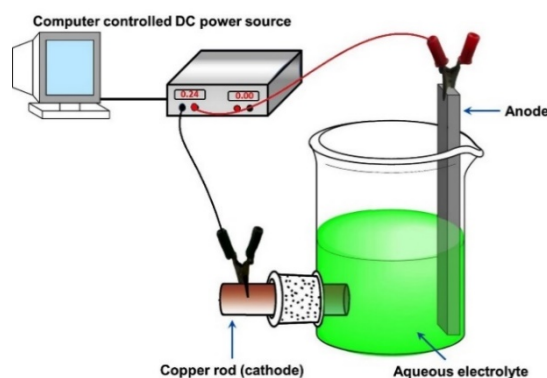
Fig. 2.6- Schematic of the experimental setup used for electrodeposition of alloy coatings on copper rod

2.2.7 Electrochemical dissolution

Electrochemical anodic dissolution or electrochemical leaching was used to prepare porous test electrodes with large effective surface area to enhance the electrocatalytic activity of conventional alloy electrodes. The porous Ni-P alloy test electrode was prepared by electrochemical dissolution of the as-deposited Ni-P alloy coating. The

electrochemical dissolution was carried out in the same vessel used for electrodeposition (Fig. 2.6), with the as-deposited Ni-P alloy as the anode and Ni as the cathode, in 0.1 M H_2SO_4 as dissolution medium. The required c.d. and the duration of electrochemical dissolution were optimized for the peak performance of alkaline HER. A c.d. of 1 A dm^{-2} for a duration 3 min was found to be the optimal condition for dissolution. The surface morphology of the coatings after dissolution was studied using SEM analysis and the developed porous electrode was tested for its electrocatalytic activity towards HER.

2.2.8 Synthesis of Ni-P-TiO$_2$ nanocomposite coating

The Ni-P-TiO$_2$ nanocomposite test electrode was prepared on the copper rod by composite electrodeposition technique from an optimal Ni-P plating bath containing TiO$_2$ nanoparticles (0.5 g L^{-1}). Electroplating was performed using the same plating setup (Fig. 2.6) of 400 mL capacity, consisting of a copper rod and nickel plate as cathode and anode, respectively. The TiO$_2$, used in this work (P<25, anatase) was obtained from Sigma-Aldrich Company, St. Louis, MO, United States of America. Since its solubility is very less in the plating bath, the solution was stirred overnight for particle dispersion using a magnetic stirrer. The composite coating was developed at an applied c.d. of 4.0 A dm^{-2} (obtained as optimal for alloy coatings towards alkaline HER) for the same deposition time of 600 s. The stepwise illustration of the composite electrodeposition process is shown in Fig. 2.7.

TiO$_2$

Optimal Bath + TiO$_2$ (0.5 g L^{-1})

Overnight stirring

Composite electrodeposition
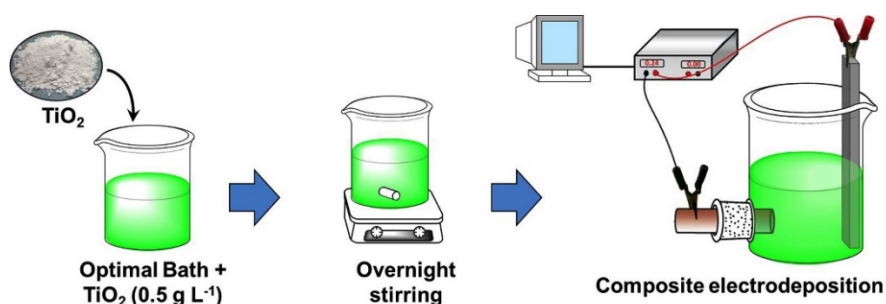
Fig. 2.7- The schematic of composite electrodeposition for the development of Ni-P-TiO$_2$ nanocomposite coating

2.2.9 Synthesis of Ag nanoparticles

A stable yellow colloidal dispersion of silver nanoparticles or silver nanoparticle sol (SNS) was prepared through the procedure reported by Mulfinger et al. (2007), using $AgNO_3$ (>99%), $NaBH_4$ (99%) and distilled water. The possibility of aggregation was controlled by the use of glycerol (as capping agent) in the present study, other than the usual polyvinylpyrrolidone (PVP) as reported [Huang et al. 1996, DongVan et al. 2012]. Glycerol adsorption has a major role in the formation of the particle surface charge and thereby the stabilization of growing silver nanoparticles as shown in the Fig. 2.8.
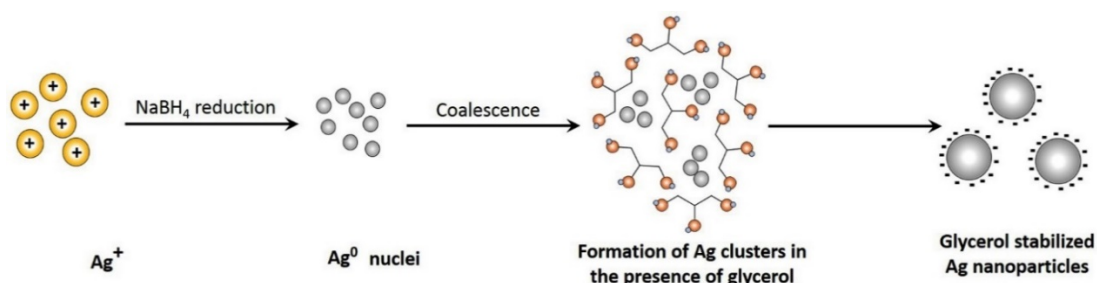
Fig. 2.8- The scheme showing the formation of glycerol stabilized Ag-nanoparticles through $NaBH_4$ reduction

2.2.9.1 Development of Ni-P-Ag nanocomposite coating

The Ni-P-Ag nanocomposite coating was prepared by using the synthesized SNS through sol-enhanced electrodeposition method [Chen et al. 2010]. The obtained stable yellow transparent SNS was added into the as optimized Ni-P alloy plating bath (in varying quantities such as10, 20, 30, 40 and 50 mL L^{-1}) for the deposition of Ni-P-Ag coating through sol-enhanced composite electrodeposition. Composite coatings were deposited on copper substrate, immediately after the addition of SNS into the plating solution with constant stirring. The amount of SNS required to achieve a highly dispersed Ag nanoparticles within the Ni-P alloy matrix was also optimized. A schematic of the sol-enhanced electrodeposition is shown in Fig. 2.9.
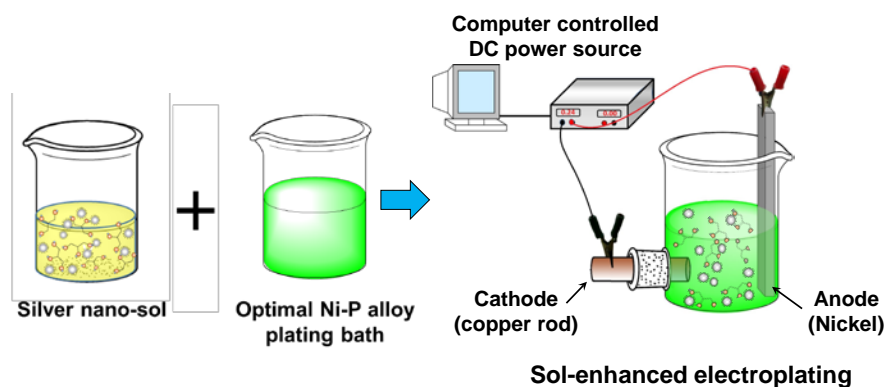
Fig. 2.9- Schematic of sol-enhanced electrodeposition of Ni-P-Ag nanocomposite coating

2.2.10 Functionalization of MWCNT

The MWCNT (98% purity, outer diameter × length = 7-15 nm × 0.5-10 μm) used in the present study was sourced from Sigma-Aldrich, St. Louis, Missouri, United States and functionalized using chemical method as reported by Yang et al. (2012). The oxidation process was carried out through acid treatment method, by refluxing in a two-necked round-bottomed flask containing 1:3 molar ratio of HNO_3 and H_2SO_4, with continuous magnetic stirring at 140 ºC for 3 hours. After that, the reaction mixture was washed several times with distilled water on a sintered glass filter until the pH reaches 7, and then dried in vacuum oven for 24 hours, at 70 ºC.

2.2.10.1 Synthesis of Ni-W-MWCNT nanocomposite coating

The nanocomposite coating was obtained through the codeposition of MWCNTs along with metal ions from the optimal alloy plating bath containing homogeneously dispersed acid treated MWCNTs. The homogeneous dispersion of the MWCNTs in the plating bath was effected by overnight stirring of the bath loaded with functionalized MWCNTs (0.5 g L^{-1}). The nanocomposite coating was developed at a deposition c.d. of 4.0 A dm^{-2}, which was obtained as the optimal c.d. for alloy coating from the same bath. A schematic of the deposition of Ni-W-MWCNT nanocomposite coating is shown in Fig. 2.10(a).

2.2.11 Synthesis of graphene oxide

Graphene oxide (GO) was synthesized using modified Hummer's method as reported by Su et al. (2013). Graphite powder was mixed properly with acid mixture of HNO_3

and H_2SO_4 through magnetic stirring at 0–5 ºC for 15 min in a 500 mL reaction flask. Then $KMnO_4$ was added slowly to the above solution and it was stirred continuously for 2 hours under 10–15 ºC and then under 35 ºC for half an hour. Subsequently, 138 mL distilled water was added slowly to the suspension within 10 min and then the temperature was kept at 95–98 ºC for 30 min. Immediately, the suspension was diluted by 210 mL warm distilled water (40 ºC) and treated with 18 mL of H_2O_2 (30 %) to reduce residual permanganate to soluble manganese ions. Finally, the resulting suspension was filtered, washed with distilled water and dried in a vacuum oven at 60 ºC for 24 hours to obtain GO.

2.2.11.1 Ni-W-rGO nanocomposite coating

The GO synthesized through chemical method was used for the development of Ni-W-rGO nanocomposite test electrode. The Ni-W alloy plating bath containing homogeneously dispersed GO (0.5 g L^{-1}) was used to develop the Ni-W-rGO coating through composite electrodeposition. The homogeneous dispersion of GO in the plating bath was achieved through overnight stirring of the bath loaded with GO. The added GO was found to be deposited as reduced graphene oxide (rGO) from the characterization results. The Ni-W-rGO composite coating was also developed at the optimal deposition c.d. 4.0 A dm^{-2}. A schematic of the Ni-W-rGO composite electrodeposition is shown in Fig. 2.10(b).
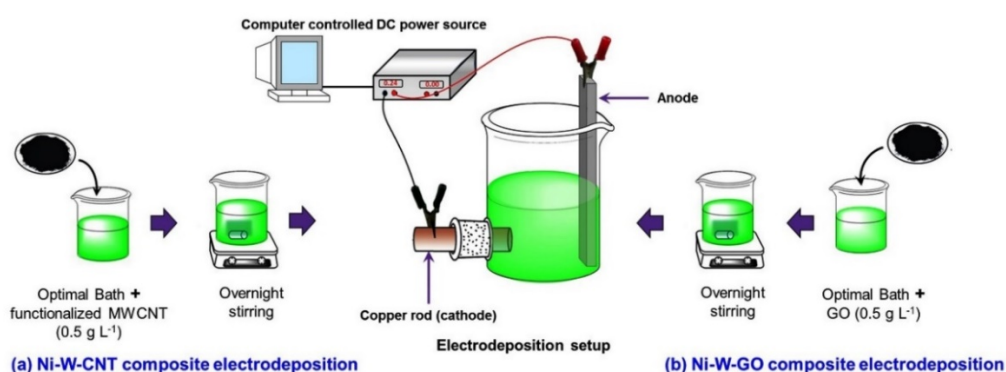
Fig. 2.10- Schematic of the composite electrodeposition for the development of: a) Ni-W-MWCNT and, b) Ni-W-rGO nanocomposite coatings

2.2.12 Development of MED Ni-W alloy coatings for HER

The MED technique was utilized for enhancing the HER activity of the Ni-W alloy coatings. A schematic of the electrodeposition setup used for the development of MED Ni-W alloy coatings for HER is shown in Fig. 2.11.
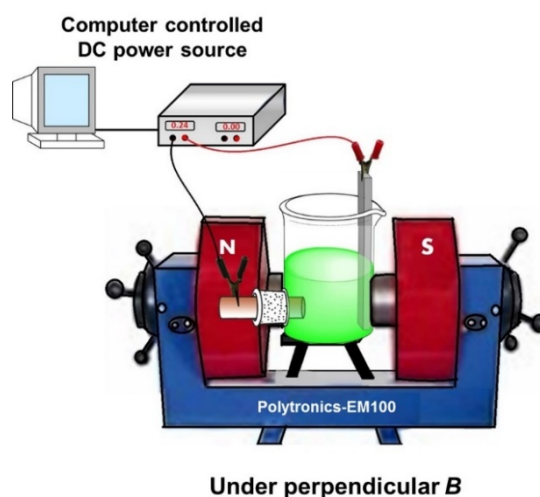
Fig. 2.11- Schematic of the electrodeposition setup used for the development of MED Ni-W alloy coatings for HER

The MED Ni-W alloy coatings were deposited on copper rod of 1 cm^2 exposed surface area from the optimal bath under applied magnetic field (in perpendicular to the direction of movement of ions) of varying intensity (from 0.1 to 0.4 T), at an applied c.d. of 4.0 A dm^{-2}, obtained as optimal for ED coatings. An electromagnet (Polytronics, Model: EM 100) and a power source (DC Power Analyzer, Agilent Technologies, Model: N6705) were used as magnetic and electric source for the development of MED coatings. All the depositions were carried out in a custom made glass set up of 400 mL capacity (Fig. 2.11) using copper rod as cathode and Ni as anode, for same duration of 600 s, at room temperature. The obtained coatings were rinsed several times with distilled water, dried and desiccated till further analysis.

2.3 CHARACTERIZATION METHODS

The developed alloys and their nanocomposite coatings were characterized using various instrumental methods of analyses. The surface morphology and composition of electrodeposited alloy coatings were examined using SEM (Model: JSM–7610F from

74

JEOL, USA) and EDS (Link ISIS-300 Micro-analytical System, Oxford Instruments, UK, interfaced with SEM) analysis, respectively. The coatings developed on the substrate (MS or copper plate having same specification of copper rod) with a dimension of 1.0×1.0 cm^2 was mounted directly on sample holder using carbon tape for analysis. Whereas, the surface morphology and composition of some nanocomposite coatings were obtained using FESEM (Model: Neon 40 Crossbeam, Carl Zeiss, Oberkochen, Germany) and EDS (Oxford) analysis tool. The phase structure analysis of the alloy coatings was carried out using XRD (Model: JDX–8P, JEOL, Japan, with CuK$_\lambda$ radiation (λ = 1.5418 Å) as the X–ray source) technique. The phase structure of the MED coatings and the incorporation of GO into the composite matrix as rGO were also confirmed through XRD analysis (Model: Rigaku Miniflex 600, with CuK$_\lambda$ radiation as the X–ray source). The thickness of the alloy and composite coatings were measured using Digital Thickness Tester (Model: Coatmeasure M&C, ISO–17025), and verified through theoretical calculations from Faraday's law and SEM cross-sectional analysis. The microhardness of the deposits was measured by Vickers method, using Microhardness Tester (Model: CLEMEX, CMT. HD, Canada). The synthesized Ag nanoparticles were characterized using UV-Vis spectroscopy and transmission electron microscope (TEM) analyses. The optical properties of the clear yellow colloidal SNS (diluted with distilled water) was studied using UV-Vis spectroscopy (Model: Analytik Jena Specord S 600, Spectrophotometer, Germany). The size and morphology of the Ag nanoparticles were obtained from TEM (Model: JEM-2100, JEOL, Japan) analysis. The TEM analysis was carried out by drying a drop of the freshly prepared SNS on a copper grid. The functionalized MWCNTs were characterized using Fourier transform infrared (FTIR, Model: Bruker Alpha FTIR Spectrometer, Bruker Optic GmbH, Ettlingen, Germany) spectroscopy analysis in ATR mode by scanning from wave number $500 - 4000$ cm^{-1}. The GO nanosheets synthesized through chemical method was characterized using different instrumental methods of analyses such as Raman spectroscopy (Model: Bruker Senterra R200, USA), XRD (Model: Rigaku Miniflex 600, with CuK$_\lambda$ radiation as the X–ray source) and TEM (Model: JEOL, JEM-2100).

2.3.1 Instruments/equipments used for the present study

The various instruments/equipments used for the present investigation along with their model number and purpose of use are tabulated in Table 2.1.

Table 2.1- The list of various instruments/equipments used for the present investigation

Name of the instrument/equipment	Model No. and manufacturer/supplier	Purpose used for
Electronic Weighing Balance	SC-391, Scientech, India	For weighing the salts for bath preparation, and also for weighing the plated samples
pH Meter	EQ-611, Equiptronics, India	To adjust the plating bath pH
Magnetic stirrer	EQ-771, Equiptronics, India	To attain homogeneous mixing of the plating bath before plating
Bench Polisher	BPP/A, Sugama Machine Tool, India	Primary mechanical polishing of the substrates
DC Power source	Aplab-LD3202, India	Conventional electrodeposition
DC Power Analyzer	Agilent-N6705, Agilent Technologies, USA	Development CMMA coatings
Electromagnet	EM 100, Polytronics, India	For the development of MED coatings
SEM	JSM–7610F from JEOL, USA	Surface morphology analysis
EDS	Link ISIS-300 Micro-analytical System, Oxford Instruments, UK	Elemental composition analysis
FESEM	Neon 40 Crossbeam, Carl Zeiss, Oberkochen, Germany	Surface morphology analysis
XRD	JDX–8P, JEOL, Japan	Phase structure analysis
XRD	Rigaku Miniflex 600, USA	Phase structure analysis
Digital Thickness Tester	Coatmeasure M&C, ISO–17025, India	Coating thickness measurement

Vickers Microhardness Tester	CLEMEX, CMT. HD, Canada	Testing microhardness of the coatings
TEM	Model: JEM-2100, JEOL, Japan	To study the microstructure of Ag nanoparticles and GO
UV-Vis Spectrophotometer	Analytik Jena Specord S 600, Spectrophotometer, Germany	To study the optical properties of SNS
FTIR	Bruker Alpha FTIR Spectrometer, Bruker Optic GmbH, Ettlingen, Germany	To characterize the functionalized MWCNTs
Raman Spectrometer	Bruker Senterra R200, USA	To characterize GO
Potentiostat/galvanostat	Biologic SP- 150, Biologic Science Instruments, France	Electrochemical characterization of the coatings

2.4 EVALUATION OF PROPERTIES OF ELECTRODEPOSITED COATINGS

The behaviors of electrodeposited alloy and composite coatings towards corrosion resistance and electrocatalytic activity were evaluated using various electrochemical methods of analysis.

2.4.1 Corrosion study

Corrosion study was carried out to assess the relative performance of different alloy coatings (both Ni-W and Ni-P), and also to understand how a multilayer coating (developed by modulating c.d.) and MED coatings are advantageous over monolayer alloy coatings deposited from same bath for same duration. Both electrochemical DC, Potentiodynamic polarization and AC, EIS methods were used for evaluating the corrosion behaviors of the coatings [Bard and Faulkner 2000, Barsoukov and Macdonald 2005], in 5% NaCl as the representative corrosion medium. A corrosion cell of 250 mL capacity with a three electrode configuration, having working electrode, counter electrode and reference electrode as shown in Fig. 2.12 was used for the study. During corrosion study, the electroplated substrate was used as working electrode, saturated calomel electrode (SCE) as a reference electrode, connected through agar-agar salt bridge, and platinized platinum as counter electrode. The OCP was recorded

after 600 s equilibration time, followed by corrosion test at OCP, by both EIS and Tafel's polarization methods. The EIS responses were recorded in the frequency range from 100 kHz to 10 mHz with the voltage perturbation amplitude of 10 mV. Further, the Tafel's polarization measurements were made within a scan range of ±250 mV from OCP, at a scan rate of 1.0 mV s^{-1} [Shaw 2003]. All electrochemical measurements were made using computer controlled potentiostat/galvanostat, Biologic SP- 150 (Biologic Science Instruments, France).

Electrochemical Workstation

Saturated Calomel Electrode
(Connected through Luggin capillary)

Platinum counter electrode

Alloy coated substrate as working electrode
(having exposed surface area of 1.0 cm^2)
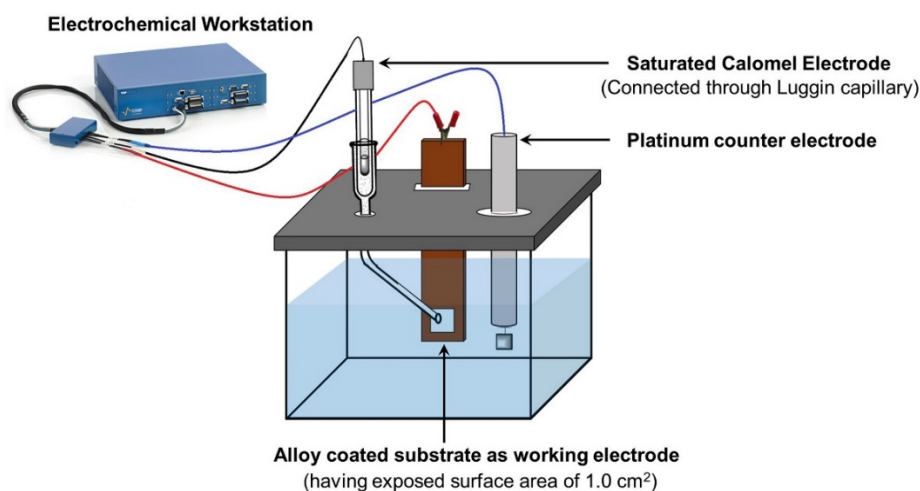
Fig. 2.12- The schematic of the home made three electrode corrosion study setup

2.4.2 Electrocatalytic activity study

Electrocatalytic characterization of the alloy and composite test electrodes developed on copper rod was carried out using a customized three-electrode tubular glass cell as shown in Fig. 2.13. Electrodeposited copper rod was used as working electrode, platinized platinum of same surface area (1.0 cm^2) as counter electrode, and SCE as reference. Electrocatalytic efficacy of the coatings was evaluated by measuring the amount of H$_2$ and O$_2$ gases liberated, respectively at cathode and anode, using graduated gas collectors. All potentials reported in the present study are with reference to SCE. Luggin's capillary with Agar-KCl salt bridge was used to minimize the error due to Ohmic drop. Electrocatalytic behavior of the coatings was evaluated in 1.0 M KOH medium because of its capability to give better reaction rate through high dissociation, compared with other electrolytes. Electrochemical techniques such as CV and CP were used to assess the stability and robustness of the test electrodes towards alkaline water

electrolysis [Bard and Faulkner 2000]. The CV measurements were made by cycling the potential within a potential ramp of 0.0 to -1.6 V for HER and 0.0 to 0.75 V for OER, under electrocatalytic test conditions at a scan rate of 50 mV s^{-1}, for 50 cycles. The CP analysis was carried out by applying a constant c.d. of -300 mA cm^{-2} (cathodic) for HER and +300 mA cm^{-2} (anodic) for OER, for a duration of 1800 s. Computer controlled potentiostat/galvanostat Biologic SP- 150 (Biologic Science Instruments, France) was used for all electrochemical analysis. The practical activity of the test electrodes towards HER and OER were estimated by measuring the amount of H_2 and O_2 gas liberated during the analysis.
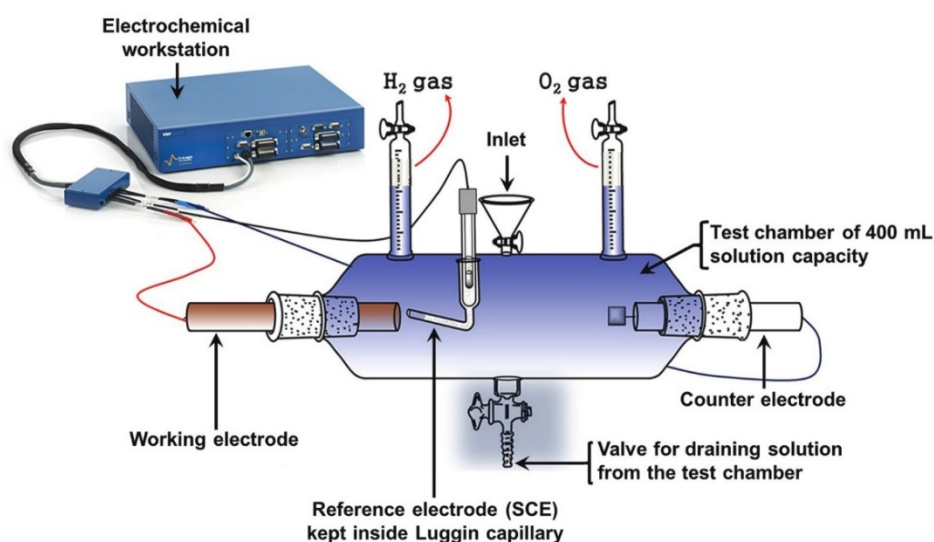
Fig. 2.13- Tubular three-electrode glass cell used for the quantification of electrocatalytic activity of alloy/composite test electrodes, in terms of H_2/O_2 gases liberated during the analysis

2.4.3 Magnetic field induced HER

The effect of applied magnetic field on water electrolysis was studied by inducing *B* of varying intensity (0.1 to 0.4 T), in the perpendicular direction during electrolysis [Koza et al. 2011]. The magnetic field induced HER (MFI-HER) was studied using optimal Ni-W alloy coating (deposited at 4.0 A dm^{-2}) as the test electrode. The optimal coating configuration studied under different conditions of applied *B* and in the absence of *B* can be represented as (Ni-W)$_{B=0.1\ T}$ and (Ni-W)$_{B=0\ T}$, respectively. Since the MFI-HER was studied only under perpendicular *B*, the direction is not specified in the coating

configuration. The schematic of the experimental setup used for the MFI-HER is shown in Fig. 2.14. The external magnetic field was applied using an electromagnet (Polytronics, Model: EM 100) during the electrocatalytic study. The distance between the working electrode and counter electrode was optimized for the peak performance of MFI-HER without affecting the quantification of evolved H_2, through intermixing of the gases evolved from the cathode and anode. The stability and performance of the test electrode for the MFI-HER at different applied magnetic field strengths (0.1 to 0.4 T) were tested using electrochemical methods of analysis.
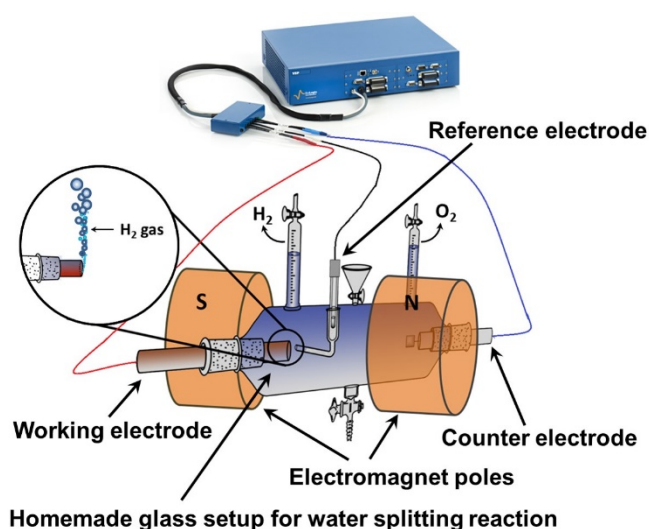
Fig. 2.14- The schematic of the experimental setup used for MFI-HER on Ni-W alloy coating

CHAPTER 3

OPTIMIZATION OF Ni-W AND Ni-P ALLOY PLATING BATHS
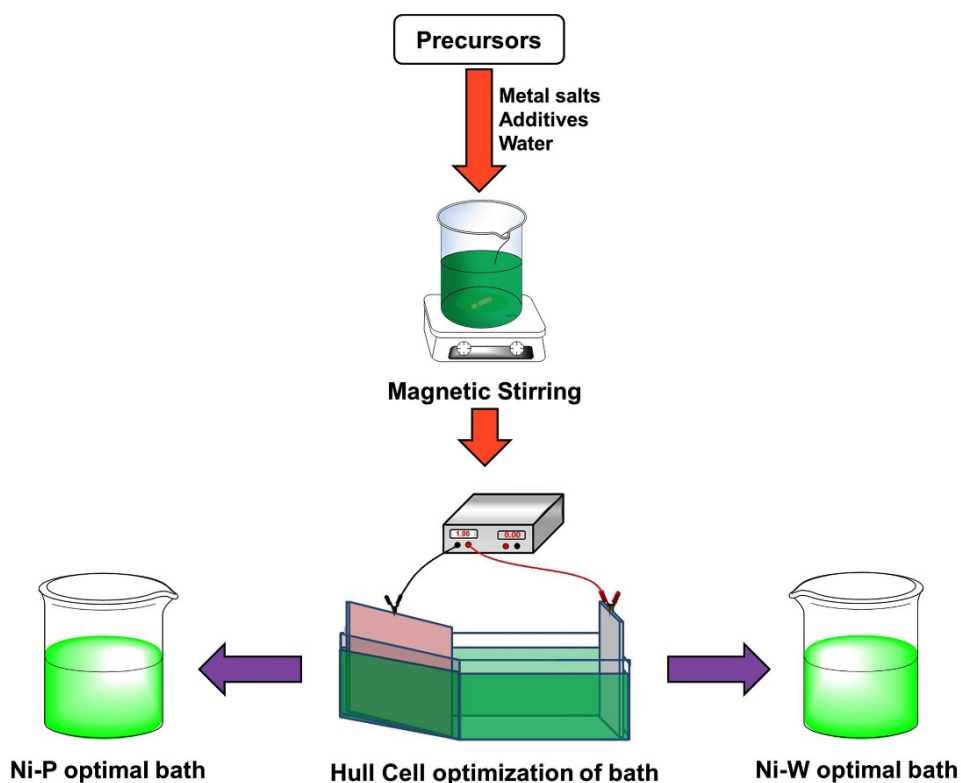
This chapter discusses the optimization of Ni-W and Ni-P alloy plating baths using standard Hull cell method. The effect of bath constituents and operating parameters on the coating characteristics were studied, and arrived at an optimal condition for the development of bright alloy coatings, using glycerol as additive. The induced codeposition behavior of the reluctant metals (W and P) in the presence of inducing metal (Ni) was studied using cyclic voltammetry analysis and a plausible mechanism for alloy deposition was proposed.

3.1 RESULTS AND DISCUSSION

The experimental results of the plating bath optimization of Ni-W and Ni-P alloys are discussed below.

3.2 OPTIMIZATION OF Ni-W ALLOY PLATING BATH

Ni-W alloy plating bath optimization was achieved through standard Hull cell method [Parthasaradhy 1989]. The basic electrolyte used for the optimization process was prepared using $NiSO_4 \cdot 6H_2O$ and $Na_2WO_4 \cdot H_2O$ as metal sources, $Na_3C_6H_5O_7 \cdot 2H_2O$ as complexing agent, NH_4Cl as conducting salt, H_3BO_3 as buffer and $C_3H_8O_3$ as additive, in distilled water. Hull cell experiment indicated that the c.d. plays an important role in the plating process [Kanani 2004]. The effect of composition and operating parameters on the deposit character was assessed from the Hull cell code as shown in Fig. 3.1. Based on the visual observation of plated Hull cell panels the *operating window* of the c.d. required for the proposed bath was determined, using the Hull cell scale.
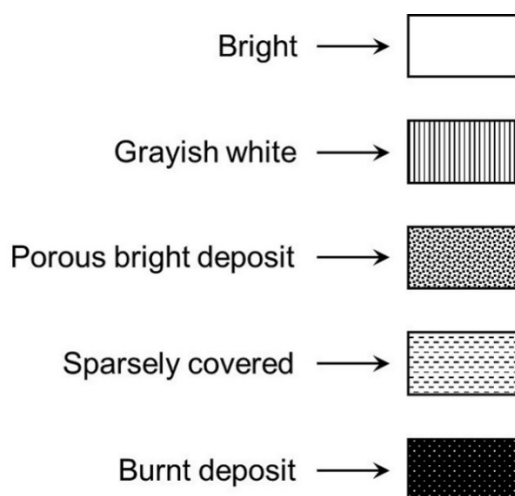
Fig. 3.1- Hull cell code

3.2.1 Effect of bath constituents on deposit character

3.2.1.1 Effect of $NiSO_4 \cdot 6H_2O$

The variation in appearance of Hull cell panel at different compositions of $NiSO_4 \cdot 6H_2O$ in the plating bath is shown in Fig. 3.2. The concentration of $NiSO_4 \cdot 6H_2O$ was varied from 12.2 - 80.6 g L^{-1} i.e., from 0.04 to 0.30 M. At lower concentrations of $NiSO_4 \cdot 6H_2O$, bright and uniform deposit was observed (Fig. 3.2(b)). However, with

further increase of $NiSO_4 \cdot 6H_2O$ in the bath, the deposit was found to become dull in appearance (Fig. 3.2(d)). Hence, 22.4 g L^{-1} was obtained as the optimal concentration of $NiSO_4 \cdot 6H_2O$.

3.2.1.2 Effect of $Na_2WO_4 \cdot 2H_2O$

The obtained variation in the deposit spectrum of Hull cell panel with the concentration of $Na_2WO_4 \cdot 2H_2O$ in the plating bath is shown in Fig. 3.3. The concentration of $Na_2WO_4 \cdot 2H_2O$ was varied from 20.4 to 115.6 g L^{-1}, i.e. from 0.06 to 0.35 M. Initially the brightness of the coating was observed to be increased uniformly up to 46.07 g L^{-1} with the reduced black region of burnt deposit as shown in Fig. 3.3(b). But, further increase of $Na_2WO_4 \cdot 2H_2O$ content decreased the bright region as shown in Fig. 3.3(c) and 3.3(d). Hence, 46.07 g L^{-1} was selected as the optimal concentration.

3.2.1.3 Effect of $Na_3C_6H_5O_7 \cdot 2H_2O$

$Na_3C_6H_5O_7 \cdot 2H_2O$ was used as a complexing agent to enhance the solubility of the bath constituents and thereby to facilitate the induced codeposition of the alloy coating. The concentration of $Na_3C_6H_5O_7 \cdot 2H_2O$ in the electrolyte was varied from 56.2 to 142.8 g L^{-1}, i.e., from (0.19 M to 0.49 M). The bright deposit with low burnt deposit region was obtained at 102.06 g L^{-1} (Fig. 3.4(c)) and it was taken as optimal concentration.

3.2.1.4 Effect of NH_4Cl

NH_4Cl was used as conducting salt to increase the conductivity of plating bath. The concentration of NH_4Cl was varied from 8.34 to 53.49 g L^{-1} (from 0.16 to 1.0 M). The appearance of the deposit was improved up to 36.15 g L^{-1} and its further addition led to a decrease in the bright deposit region as shown in Fig. 3.5(d). Hence, NH_4Cl concentration was maintained as 36.15 g L^{-1} throughout the study. Further, it was also observed that the addition of conducting salts drastically decreased the cell voltage, during electroplating.

3.2.1.5 Effect of H_3BO_3

H_3BO_3 was used as a buffer, to prevent the large pH fluctuations of electrolyte during deposition. It was observed that the addition of H_3BO_3 into the plating bath improved the homogeneity of the deposit without imparting a mirror-finish to the coatings. The

effect of H_3BO_3 concentration on the deposit characteristics of Hull cell panel is as shown in Fig. 3.6. The concentration of H_3BO_3 was varied from 10.2 to 61.8 g L^{-1} (from 0.16 M to 1.0 M). A bright deposit, over a wide range of c.d. was observed at 20.0 g L^{-1}. Further, the high amount of H_3BO_3 was found to have no effect on the brightness of the deposit (Fig. 3.6(d)).

3.2.1.6 Effect of $C_3H_8O_3$

$C_3H_8O_3$ was used as the brightener, and added into the bath in required quantity to get a smooth mirror-finish. The effect of varying $C_3H_8O_3$ content (10-25 mL L^{-1}) on Hull cell panel appearance is given in Fig. 3.7. The coating was found to be bright and uniform up to 20 mL L^{-1} of $C_3H_8O_3$ (Fig. 3.7(b)) and the further addition of $C_3H_8O_3$ was found to show no improvement in deposit character. Therefore 20 mL L^{-1} was selected as the optimal concentration of additive.
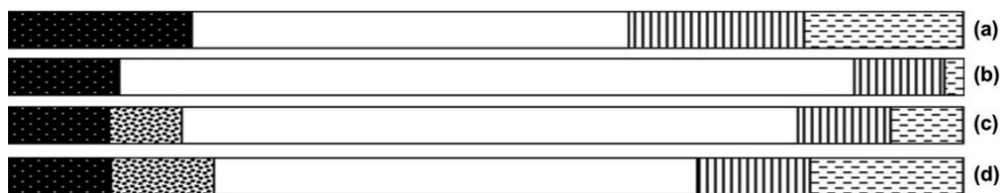
Fig. 3.2- Effect of $NiSO_4 \cdot 6H_2O$ on test panel at 1.0 A cell current for 5 minutes duration (a) 12.2 g L^{-1} (b) 22.4 g L^{-1}, (c) 48.2 g L^{-1}, and (d) 80.6 g L^{-1}
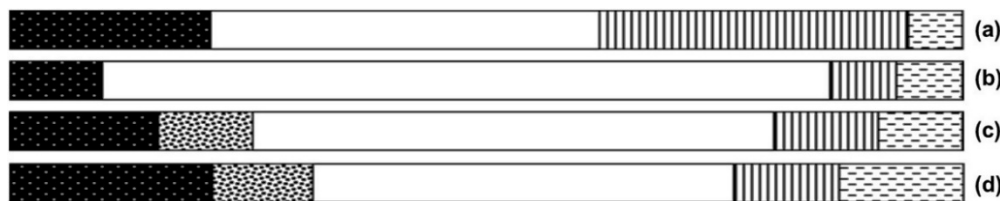
Fig. 3.3- Effect of $Na_2WO_4 \cdot 2H_2O$ on test panel at 1.0 A cell current for 5 minutes duration (a) 20.4 g L^{-1}, (b) 46.07 g L^{-1}, (c) 82.1 g L^{-1}, and (d) 190 gL^{-1}
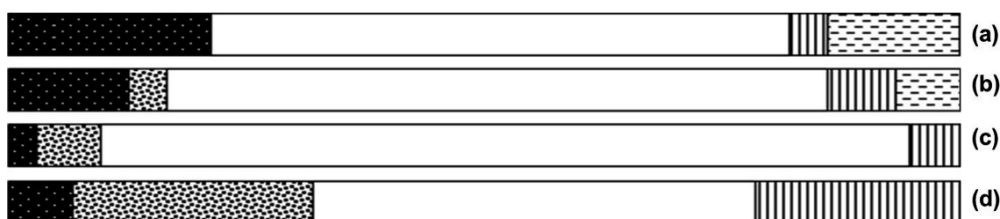
Fig. 3.4- Effect of $Na_3C_6H_5O_7 \cdot 2H_2O$ on test panel at 1.0 A cell current for 5 minutes duration (a) 56.2 g L^{-1}, (b) 86.4 g L^{-1}, (c) 102.06 g L^{-1}, and (d) 142.8 g L^{-1}
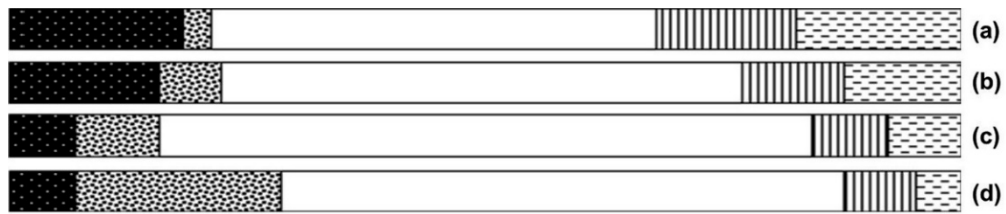
Fig. 3.5- Effect of NH₄Cl on test panel at 1.0 A cell current for 5 minutes duration (a) 8.34 g L^{-1}, (b) 18.2 g L^{-1}, (c) 36.15 g L^{-1}, and (d) 53.49 g L^{-1}
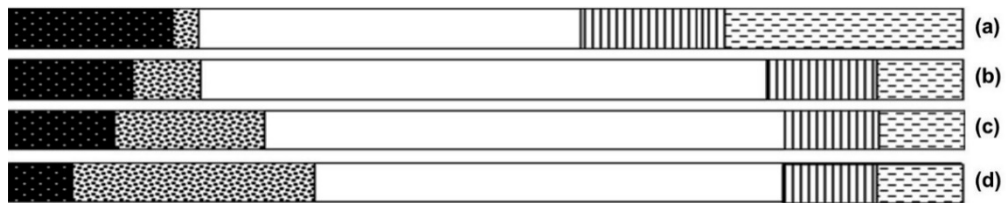
Fig. 3.6- Effect of H₃BO₃ on test panel at 1.0 A cell current for 5 minutes duration (a) 6.18 g L^{-1}, (b) 20.0 g L^{-1}, (c) 48.4 g L^{-1}, and (d) 61.8 g L^{-1}
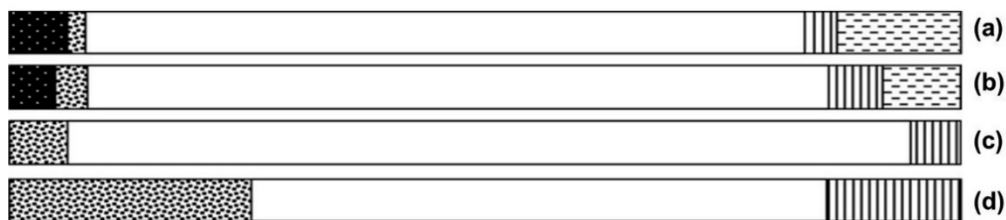
Fig. 3.7- Effect of C₃H₈O₃ on test panel at 1.0 A cell current for 5 minutes duration (a) 10.0 mL L^{-1}, (b) 15.0 mL L^{-1}, (c) 20.0 mL L^{-1}, and (d) 25.0 mL L^{-1}

Thus each bath constituents have been varied over a wide range of their concentrations, keeping the composition of other constituents in the bath constant. The concentration at which wide bright deposit obtained on Hull cell panel was considered as optimal concentration and the optimal composition of each constituent are given in Table 3.1. The operating conditions, for the development of coatings at room temperature, such as deposition c.d. and pH was also optimized. The optimal operating c.d. range was obtained as 1.0 to 4.0 A dm^{-2}. The bath was maintained under alkaline pH conditions to ensure the complete solubility of the bath constituents and also to avoid the precipitation during deposition. The pH = 8.5 was obtained as the optimal one for quality deposit and long term stability of the plating solution. The fine tuning of the pH was carried out using NH₄OH and H₂SO₄. The bath was optimized to give equal effectiveness towards MS and copper substrates, under the same set of conditions.

Table 3.1- Bath composition and operating parameters of the optimal Ni-W alloy plating bath

Bath constituents	Composition (per Liter)	Operating parameters
$NiSO_4 \cdot 6H_2O$	22.4 g	Anode: Pure Ni
$Na_2WO_4 \cdot 2H_2O$	46.07 g	Cathode: MS or Copper
$Na_3C_6H_5O_7 \cdot 2H_2O$	102.06 g	pH = 8.5
H_3BO_3	20.0 g	Temp: 303 K (30 °C)
NH_4Cl	36.15 g	c.d. range: 1.0 - 4.0 A dm^{-2}
$C_3H_8O_3$	20.0 mL	

3.2.2 Chemistry of glycerol

Glycerol is a non-toxic, biodegradable, and recyclable liquid that is highly inert, stable and compatible with many other non-toxic and non-irritating chemicals [Wolfson and Dlugy 2009]. Further, it facilitates the dissolution of inorganic salts, acids, bases and transition metal complexes, hence can be used as a green additive for electroplating. In the case of aqueous plating bath; it is highly miscible with the formation of hydrogen bonds with water molecules and also with free metal ions present in the solution. As the electrode surface is charged, it can get adsorbed on the surface through the electron rich hydroxyl groups, hence, can enhance the adhesion of the coating. Glycerol can interact with the metal surface, metal oxide and deposited metal atoms through its electron-rich hydroxyl groups. The interaction of glycerol at the electrode surface is schematically represented in Fig. 3.8.
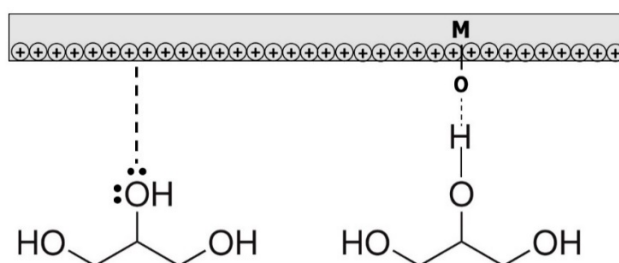
Fig. 3.8- The plausible mechanism of adsorption of additive onto the alloy surface

In fact, glycerol molecules can interact with the alloy coatings through the empty d-orbitals of the transition metal deposits [Kumar et al. 2015], and this property can be exploited to use it as an additive in electrodeposition, for grain size refinement and formation of smooth and bright coatings.

3.2.3 Cyclic voltammetry study

The chemical composition of bath plays an important role in process and product of electrolysis. A specific chemical species in the bath can induce changes in the thermodynamic and the kinetic parameters during the electrodeposition since they can even modify the electronic structure of the substrate [Crousier et al. 1993]. Hence, CV study was carried out to understand the effect of complexing agent ($Na_3C_6H_5O_7 \cdot 2H_2O$) and additive ($C_3H_8O_3$) on the process of alloy deposition. Cyclic voltammograms (CV's), obtained under different conditions of bath A, B, C and D are shown by curves a, b, c and d, respectively in Fig. 3.9. Here, it should be noted that curves correspond to A is for bath in the absence of any additive, i.e. ($NiSO_4 \cdot 6H_2O + NH_4Cl + H_3BO_3$), B is ($A + Na_3C_6H_5O_7 \cdot 2H_2O$), C is ($B + Na_2WO_4 \cdot 2H_2O$) and D is ($C + C_3H_8O_3$). The CV experiments were carried out at a scan rate of 100 mV s^{-1} in a potential window of -2.0 to +2.0 V.

The CV's, shown in Fig. 3.9 clearly indicate the variation in Ni-W alloy deposition process after the addition of complexing agent and additive, evident from the shape and size of CV's recorded under different conditions. The i_{pa} values of the CV's were found to be decreased from conditions A to D, and contrarily E_{pa} valued were increasing i.e., shifting towards the more positive side (from curve *a* to curve *d* in Fig. 3.9). Hence, it may be inferred that both complexing agent and additive are responsible for increased electrochemical stability of the deposited coatings.
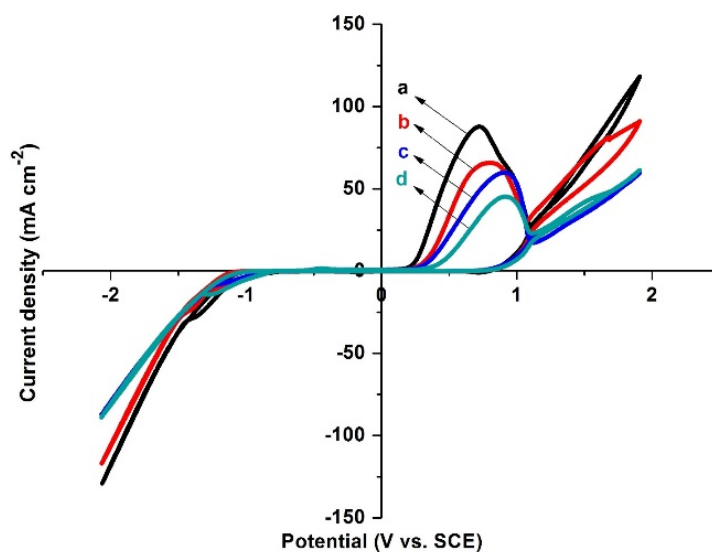
Fig. 3.9- Cyclic voltammograms for Ni-W bath at different conditions: a) A = with no additives (i.e., $NiSO_4 \cdot 6H_2O$ + NH_4Cl + H_3BO_3, b) B = A + complexing agent ($Na_3C_6H_5O_7 \cdot 2H_2O$), c) C = B + $Na_2WO_4 \cdot 2H_2O$, and d) D = C + $C_3H_8O_3$, at a scan rate of 100 mV s^{-1}

Further, to identify the role of bath constituents on the mode of mass transport of ions towards cathode during deposition, CV study was carried out at different scan rates, i.e., 20, 40, 60 and 80 mV s^{-1}. Firstly, the CV study was carried out under bath condition corresponding to A at different scan rates, and their i_{pa} for stripping of Ni deposition was determined. Similarly, the CV study was made by adding $Na_3C_6H_5O_7 \cdot 2H_2O$, $Na_2WO_4 \cdot 2H_2O$ and $C_3H_8O_3$ one after another, i.e., under conditions corresponding to B, C, and D. The i_{pa} values obtained at different scan rates for different conditions of the bath were determined from the respective CV's. The scan rate dependence on $i_{pa,}$ under different conditions of Ni-W bath is shown in Fig. 3.10. From Fig. 3.10, it is important to note that the slopes of plots corresponding to condition A, C and D remains almost unchanged. Hence the chemical constituents corresponding to A, C and D are responsible for migration and convection mode of mass transfer process, i.e., adsorption controlled. But high slope corresponding to B (on addition of $Na_3C_6H_5O_7 \cdot 2H_2O$) indicates that the complexing agent is responsible for diffusion controlled deposition of Ni-W alloy, due to complexation of metal ions. Almost parallel linear plots, observed in Fig. 3.10 for conditions referring to A, C and D indicates that

the Ni-W alloy deposition is more an adsorption-controlled process than a diffusion controlled one.
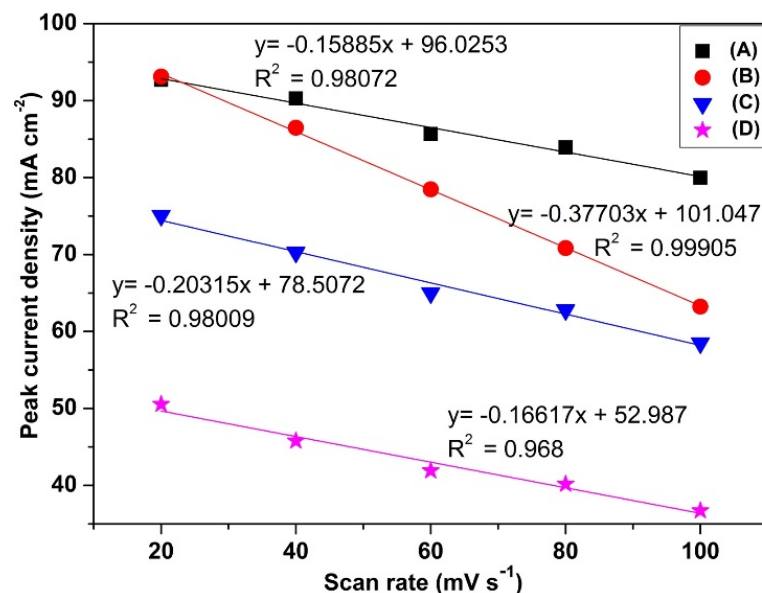
Fig. 3.10- Scan rate dependency on i_{pa} values of Ni-W bath under different conditions of A, B, C and D, at 303 K

3.2.4 Induced codeposition

The most striking feature of induced codeposition is the deposition of otherwise non-depositable metals, like tungsten, molybdenum, germanium, phosphorous etc., the phenomenon involves some additional peculiarities which are different from ordinary alloy deposition. There are few unusual, and quite surprising features are likely to be observed in induced codeposition, as reported by Brenner (1963). They are: *i).* Higher the content of the reluctant metal (here it is W) in the deposit, the lower is the cathode current efficiency at which the alloy can be deposited. *ii).* The reluctant metal deposits preferentially under some circumstances, this is quite unexpected in view of the inability of the metal to deposit by itself. *iii).* The current density - potential curves of alloy deposition are often situated at nobler (more positive) potentials than those of the inducing metal itself. In a broader sense, electrodeposition may be defined as the process of depositing a substance upon an electrode by electrolysis. The essence of electrode kinetics is charge transfer across the interface. A profound understanding of the structure of the electrical double layer is needed for understanding the mechanism of charge transfer. There are other important factors, such as catalysis, adsorption,

mass-transfer limitations and so on, all of which may influence the rate and mechanism of charge transfer to some extent, but it is the very act of charge transfer that matters. It is the vehicle that allows the conversion of chemical to electrical energy, as in a fuel cell or a battery during discharge.

Accordingly, it has been stated by several noted authors in electrochemistry that, in the case of metal deposition, charge is carried across the interface by ions rather than by electrons. Actually, there exists a huge difference in the mechanisms, when the charge is transferred across the interface by the metal ions, and when the electrons are transferred. The electron and ion transfer process are two physically different phenomena. In this regard, the mechanism of charge transfer during metal deposition and dissolution was treated recently by Gileadi (1993). In the light of above proposal, a mechanism for induced codeposition for the bath under study has been proposed, and is shown schematically in Fig. 3.11. Accordingly, the first step in the overall mechanism is the deposition of inducing metal (any iron-group metal). Here it is Ni in the diagram, followed by the deposition of the reluctant metal. Since the induced codeposition depends on several factors, like bath composition, complexing agent, additive, pH etc. Even though iron-group metals can induce the deposition of reluctant metals like W, Mo, P etc., the simple electrolytic baths with only iron-group metal salts and reluctant metal salts, without complexing agents is limited due to the possibility for precipitation of hydroxides and tungstates of corresponding iron-group metals [Younes and Gileadi 2000, Younes and Gileadi 2002]. Tungstates can form different types of polynuclear species in water depending on the pH. At pH greater than 7.8, WO_4^{2-} species in the bath is considered to be predominant [Holt and Vaaler 1948, Vasko 1977, Tsyntsaru et al. 2012]. Hence on adjusting the chemistry of bath, in terms of pH (using NH_4OH), and complexing agent ($Na_3C_6H_5O_7 \cdot 2H_2O$), it is possible to reduce the deposition potential of metal ions by reducing the free Ni^{2+} ions, and thereby to increase the solubility of Ni salts in the bath containing WO_4^{2-} and OH^- ions. Hence it has been proposed that the first step in the induced codeposition is the deposition of inducing metal ions (Ni^{2+} ions) from the electrolyte to the metal surface (shown as I in Fig. 3.11), and second step is deposition of reluctant metal (W) on the substrate through reduction of WO_4^{2-} species by adsorbed hydrogen atoms (shown as II, in Fig. 3.11) [Tsyntsaru et al. 2012, Holt and

Vaaler 1948]. Since the composition of the alloy greatly depends on the pH of the bath, the possibility of increasing pH near the cathode film, due to electro-reduction of tungstate ions has been compensated time to time.
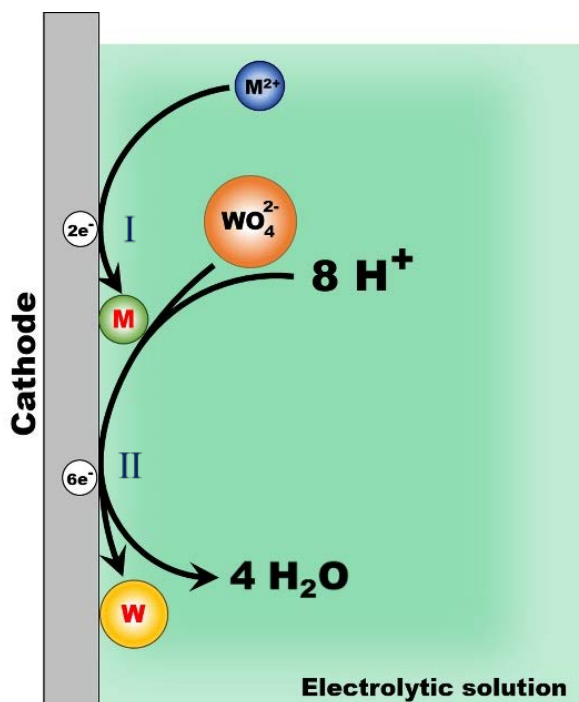
Fig. 3.11- Scheme showing the mechanism of induced codeposition in Ni-W alloy by Ni^{2+} ions

3.3 OPTIMIZATION OF Ni-P ALLOY PLATING BATH

The Ni-P alloy plating bath was also optimized using standard Hull cell method as explained in Section 3.1.1. An alkaline plating bath with $NiSO_4 \cdot 6H_2O$, $NaPO_2H_2 \cdot H_2O$, $Na_3C_6H_5O_7 \cdot 2H_2O$, NH_4Cl, H_3BO_3 and $C_3H_8O_3$ was optimized. The bath constituents were kept as the same that used for Ni-W alloy except the metal source $NaPO_2H_2 \cdot H_2O$ instead of $Na_2WO_4 \cdot 2H_2O$. The composition of each constituent and operating parameters were optimized using Hull cell experiment.

Whereas, electroplating of metals/alloys is one of the most complex processes because of the unusually large number of critical elementary phenomena involved during deposition [Kanani 2004, Jack 1993]. Due to lack of quantitative guiding principles to develop a coating of desired property, it is very difficult and time-consuming to optimize the bath composition. Even though Hull Cell method is an

established method to optimize a bath, in terms of its constituents and operating parameters, its application is limited to know only the effect of c.d. on deposit patterns; and is incapable of predicting the desired properties of the coating, like hardness, reflectivity, thickness etc [Kanani 2004]. Since the Ni-P alloy is one of the most studied systems both in electroless and electrodeposition methods, it is required to develop a Ni-P alloy of more desired characteristics. In this direction, Taguchi's statistical method was used for the optimization of deposition conditions of Ni-P alloy [Rosa et al. 2009]. *Minitab 16, Statistical software* was used for designing the experiment by reducing the number of trials to a practical level. The bath variables, i.e., [glycerol], c.d. and pH of the bath were taken as *chosen parameters* and micro-hardness and thickness of the coatings as parameters for *characteristic performance.* Experimental conditions were optimized to maximize the coating properties. Taguchi's method demonstrated that the basic Ni-P bath, having [glycerol] = 20 mL L^{-1}, c.d.= 4.0 A dm^{-2} and pH = 8.0 as ideal for developing coatings of highest microhardness and thickness. Experimental data revealed that both [glycerol] and c.d. have a close dependency on thickness and microhardness of coating, compared to pH of the solution. The obtained optimal bath and operating parameters are given in Table 3.2.

Table 3.2- The composition and operating parameters of the optimal Ni-P plating bath

Bath constituents	Composition (per Liter)	Operating parameters
$NiSO_4 \cdot 6H_2O$	28.2 g	Anode: Pure Ni
$NaPO_2H_2 \cdot H_2O$	51.0 g	Cathode: MS or Copper
$Na_3C_6H_5O_7 \cdot 2H_2O$	56.2 g	pH = 8.0
H_3BO_3	20.5 g	Temp: 303 K (30 °C)
NH_4Cl	10.2 g	c.d. range: 1.0 – 6.0 A dm^{-2}
$C_3H_8O_3$	20.0 mL	

3.3.1 Cyclic voltammetry study

CV study of the Ni-P electrolytic bath was carried out to understand the effect of added additives on the process and thereby the mechanism of deposition. CV's obtained at different bath conditions, like: in the absence of any additives, i.e. only with

$(NiSO_4 \cdot 6H_2O + NH_4Cl + H_3BO_3) = A$, $(A + NaPO_2H_2 \cdot H_2O) = B$, $(B + Na_3C_6H_5O_7 \cdot 2H_2O) = C$ and with $(C + C_3H_8O_3) = D$, at scan rate of 100 mV s^{-1} in a potential window of -2.0 to +2.0 V are shown by curves a, b, c and d, respectively in Fig. 3.12. It may be observed that the CV curve 'a' in Fig. 3.12 displays a maximum i_{pa} value in the absence of any added additive into the bath. It indicates that the Ni coating has lesser stability. However, after the addition of phosphorous salt ($NaPO_2H_2 \cdot H_2O$), i.e., a condition corresponding to B, it was found to show two anodic dissolution peaks represented as b$_1$ and b$_2$ in the curve 'b' of Fig. 3.12. It indicates that two anodic peaks are not corresponding to the dissolution of Ni-P alloy of different composition, but of those formed by two different kinetic processes [Yu et al. 2015, Crousier et al. 1994]. In other words, two peaks are attributed to the formation of Ni-P alloy of different intermetallic phases due to both electroless and electrolytic deposition [Yu et al. 2015, Lu and Zangari 2002, Gaskell 2008, Pillai et al. 2012]. Thus, multiple anodic peaks in curve 'b' of Fig. 3.12 is associated with the dissolution of nickel and phosphorous from various intermetallic phases or solid solutions. Under condition C, i.e., in the presence of complexing agent, $Na_3C_6H_5O_7 \cdot 2H_2O$ a single dissolution peak of decreased i_{pa} was observed, as shown by curve 'c' in Fig. 3.12. It indicates the formation of a single phase Ni-P alloy. Finally, on the addition of glycerol, i.e., condition corresponding to D, the further decrease in i_{pa} value (shown by curve 'd' in Fig. 3.12) indicates the increased stability of coating after the addition of glycerol. Further, it may be noted that the anodic E_{pa} values were shifted towards more noble side as electrolytic bath condition is changing from A to D. Hence, the successive decrease in i_{pa} and the successive increase in E_{pa} from the conditions of bath A to D demonstrates the role of additives in imparting brightness, homogeneity and electrochemical stability to Ni-P alloy coatings.
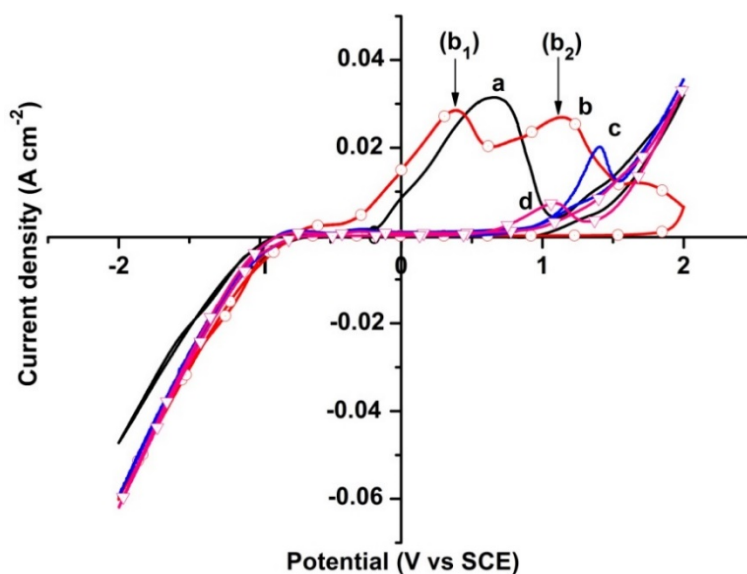
Fig. 3.12- CV study of Ni-P electrolytic bath under different conditions: a) with no additives, i.e., $NiSO_4 \cdot 6H_2O + NH_4Cl + H_3BO_3$ = A, b) A + $NaPO_2H_2 \cdot H_2O$ = B, c) B + $Na_3C_6H_5O_7 \cdot 2H_2O$ = C, and d) C + $C_3H_8O_3$ = D, recorded at a scan rate of 100 mV s^{-1}

Further, to identify the role of constituents on mode of mass transport, responsible for Ni-P coating characters, the CV study was carried out at different lower scan rates, i.e., 20, 40, 60 and 80 mV s^{-1} corresponding to conditions A, B, C and D. The i_{pa} values corresponding to A, B, C and D were determined from their respective CV responses [Allen et al. 2001]. The scan rate dependence on i_{pa} under different conditions of the bath is shown in Fig. 3.13. It is important to note from Fig. 3.13 that the slopes of plots corresponding to conditions A and D remain almost unchanged. Hence, the chemical constituents corresponding to A and D are responsible for migration and convection mode of the mass transfer process, i.e., adsorption controlled. But greater slope corresponding to B indicates that the complexing agent ($NaPO_2H_2 \cdot H_2O$) brings about the diffusion controlled deposition, which is responsible for the formation of various intermetallic phases, affected by increased diffusion of Ni ions towards the cathode. Again under conditions of C, the slope is almost same due to the interaction of additive, leading to a bright, stable and adherent Ni-P alloy coating.

94
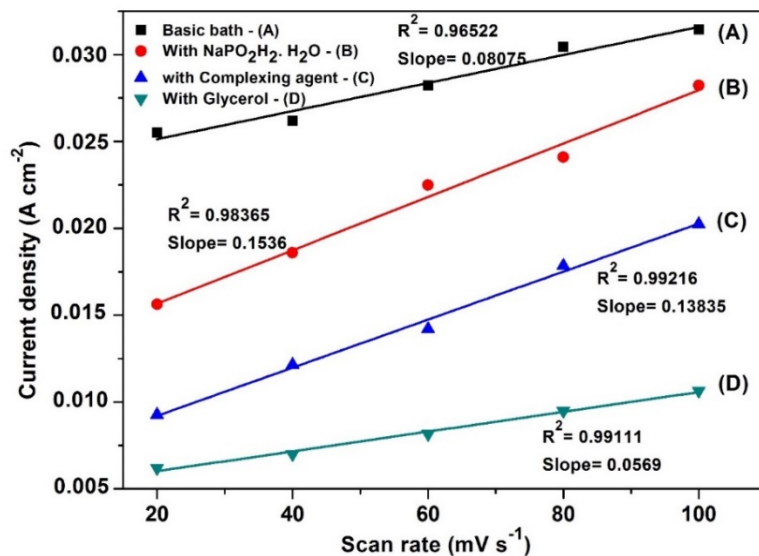
Fig. 3.13- Scan rate dependency on i_{pa} values of Ni-P bath under different conditions of A, B, C and D, recorded at 303 K

3.3.2 Mechanism of induced codeposition

It is well known that P cannot be electrodeposited as a pure phase, but can be readily codeposited with iron group metals such as Ni, from solutions containing both Ni and P ions [Sakai et al. 2006, Mahalingam et al. 2007, Brenner 1963]. It is believed that the strong atomic interaction between Ni and P makes the induced codeposition of Ni-P alloy with stoichiometric composition possible [Crousier et al. 1994]. Even though extensive studies have already been reported on electrodeposition and electroless deposition of Ni-P alloy, most of the depositions were carried out from acid bath, and deposition from alkaline bath are relatively less reported. In this direction, the present study is focused on the deposition of Ni-P alloy from an alkaline citrate bath (pH = 8.0) containing $NiSO_4 \cdot 6H_2O$, $NaPO_2H_2 \cdot H_2O$ as the source for Ni and P ions. The complexing agent, $Na_3C_6H_5O_7 \cdot 2H_2O$, along with the conducting salt NH_4Cl can prevent the precipitation of basic salts at higher pH. H_3BO_3 was used as a buffer to maintain the pH, and $C_3H_8O_3$ as the additive.

From the CV study of proposed bath (Table 3.2), it is clear that the formation of Ni-P alloy coating resulted from the synergistic effect of both electroless and electrodeposition process. The characteristic two anodic peaks found in curve '*b*' of Fig. 3. 12 indicates that, in the presence of $NaPO_2H_2 \cdot H_2O$ (reducing agent), the bath

follows both autocatalytic (electroless) and electrolytic deposition of Ni-P alloy [Sankara Narayanan and Seshadri 2008]. Since the bath can also show deposition of metal onto the substrate through chemical reduction of metal ions, i.e., by electroless deposition, the obtained alloy coating is resulted from the synergistic effect of electroless and electrodeposition [Yu et al. 2015].
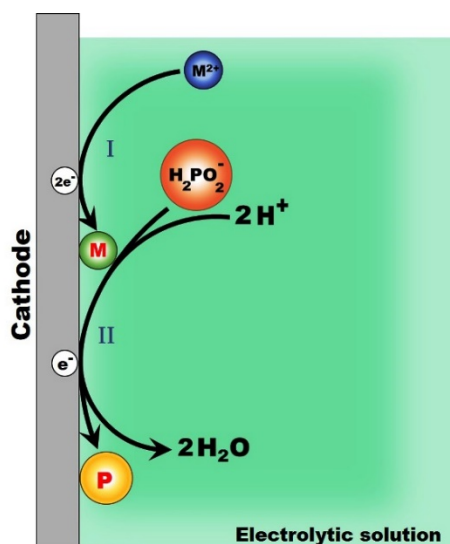
Fig. 3.14- Mechanism of induced codeposition of Ni-P alloy in the presence of additive

The CV study supports the fact that the proposed Ni-P bath exhibits induced type of codeposition, following the mechanism as shown in Fig. 3.14. According to which, reduction of Ni^{2+} ion at an active center on the cathode surface takes place (represented as step I in Fig. 3.14), followed by the surface diffusion of the adsorbed Ni atom to a suitable crystal lattice site [Narayan and Mungole 1985]. The deposited Ni can induce the reduction and codeposition of P (step II) as shown in Fig. 3.14. The codeposition of P inhibits the further surface diffusion of Ni atoms and hence the growth of crystal nuclei [Brenner 1963]. With increasing P content in the deposit, the rate of fresh nucleus formation becomes higher than the rate of growth of existing crystal nucleus leading to the grain size refining [Pillai et al. 2012]. It is already been reported that the ammoniacal alkaline Ni-P bath can give crystalline codeposited alloy coatings with varying P content; and at the same time, amorphous coatings from acid bath [Narayan and Mungole 1985]. Crystallographic structures or orientations of the Ni-P alloy coatings are also found to be influenced by the amount of P present in the

alloy coatings and undergoes transitions from crystalline to nanocrystalline and eventually to an amorphous type with increasing P content [Elsener et al. 2008].

3.4 CONCLUSIONS

1. New alkaline citrate baths have been optimized for the development of Ni-W and Ni-P alloy coatings using standard Hull cell optimization method.

2. The effect of bath constituents and operating parameters on the coating characteristics were studied using Hull cell code by comparing the deposit spectrum on Hull cell scale.

3. The nature of induced codeposition of the alloy coatings and the scan rate dependence on the mass transport were studied under different conditions of the bath using CV study.

4. The CV study demonstrated that the addition of both complexing agent and glycerol contributes to the enhanced electrochemical stability of the deposited Ni-W and Ni-P alloy coatings.

5. A plausible mechanism for the induced codeposition of Ni-W and Ni-P alloy coatings were established on the basis of CV study of the alloy plating baths.

CHAPTER 4

CMMA COATINGS OF Ni-W AND Ni-P ALLOYS FOR BETTER CORROSION PROTECTION
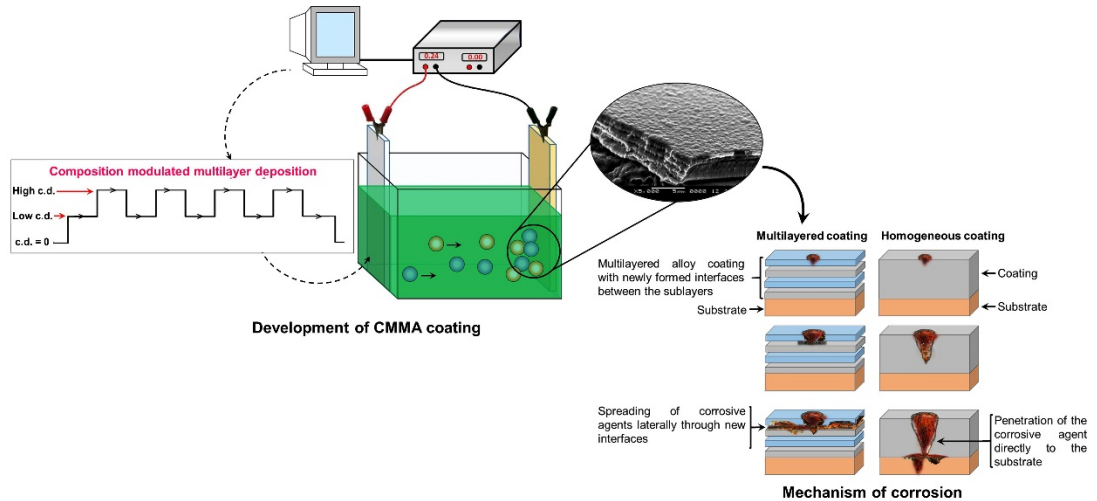
The chapter deals with the theme of tailoring the properties of alloy coatings by modulating the mass transfer process at cathode for the development of a new class of coatings; called CMM or in short laminar coatings. The work embodied in this chapter is to demonstrate how the corrosion resistance of monolayer Ni-W and Ni-P alloy coatings can be increased to many folds of its magnitude by multilayer deposition. The Ni-W and Ni-P coatings were deposited on MS in laminar multilayer pattern, having alternate layers of alloys with different compositions from their respective optimal citrate baths using SBT by modulating the DC. CMMA coating configurations were optimized in terms of current pulse height and thickness of each layer to maximize its corrosion protection ability than the monolayer coatings, developed from the same bath. The better corrosion resistance of CMMA coatings were explained with plausible mechanisms.

4.1 RESULTS AND DISCUSSION

The experimental results obtained for the structural, morphological and electrochemical characterization of the monolayer and multilayer Ni-W and Ni-P alloy coatings are discussed below.

4.2 DEVELOPMENT OF CORROSION RESISTANT Ni-W ALLOY COATINGS

Hull cell study revealed that the optimal c.d. for newly formulated electrolyte, for deposition of bright, uniform and corrosion resistant monolayer Ni-W alloy coating, is in the range of c.d. 1.0 A dm^{-2} to 4.0 A dm^{-2} as discussed in Chapter 3. Then by using optimal bath, monolayer Ni-W coatings were deposited at different c.d.'s, using a known quantity of DC, with no modulation in the current pulse. All the coatings were observed to be bright in visual appearance. The electrodeposited coatings were tested for their W content, CCE or Faradaic efficiency, microhardness, thickness and corrosion behaviors, and the corresponding data are reported in Table 4.1.

4.2.1 Characteristics of monolayer Ni-W alloy coatings

4.2.1.1 Effect of current density on coating properties

The effect of c.d. on W content in the deposit and CCE are shown in Fig. 4.1, supported by the data given in Table 4.1. It may be noted that W content of the alloy increases with c.d., in compliance with citrate baths of Ni-W alloy. The binary alloy of Ni-W is expected to form a solid solution in Ni matrix even up to 12.5 at. % of W [Bakar 1992]. Hence there is a probability of coexistence of non-equilibrium solid solution with a metastable solid solution in the alloys having W content beyond threshold limit. But, W content in present Ni-W samples is within expected solubility limit, indicating that the bath produced a solid solution of Ni-W alloy, and are confirmed by XRD and EDS analysis.
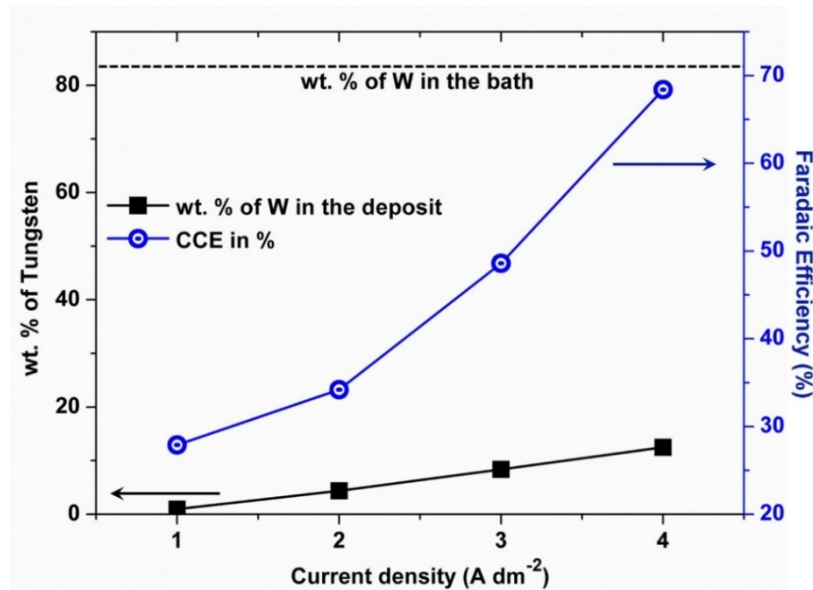
Fig. 4.1- Variation of Faradaic efficiency and W content of the deposit with deposition c.d.

The dependency of W and CCE on the deposition c.d. can be attributed to the reduction in the static potential of the alloy compared to the parent metals, explained by Ma et al. (2004). According to which, a larger difference between the static potentials of Ni and W is responsible for less CCE at lower c.d. Consequently, minimum CCE (27.9%) was observed at lower c.d. side as may be seen in Table 4.1. At high c.d., the CCE of bath increased linearly with c.d. and reached its maximum up to 68.4% as shown in Fig. 4.1. It may be noted that, under no conditions of c.d. studied, the W content in the deposit reached to that in the bath (shown by the horizontal line in Fig. 4.1), confirming the anomalous type of codeposition. However, at very high c.d., coatings are found to be very brittle, confirmed from the SEM images, shown in Fig. 4.2. Further, as W content increased, its hardness and thickness were also found to be increased as shown in Table 4.1. The microhardness of the coatings was examined using Vickers indentation method, and it was found that hardness of the coating increased with c.d., i.e., due to increased W content in the deposit. The thickness of the coatings was also found to be increased with c.d. Thus, increase in the thickness, hardness and W content of the coatings with c.d. were attributed to the improved corrosion resistance of the monolayer alloy coatings with deposition c.d. as given in Table 4.1.

Table 4.1- Effect of deposition c.d. on the coating characters of monolithic Ni-W alloy coatings deposited from optimized bath at 303 K

c.d. (A dm^{-2})	Wt.% of W in deposit	CCE (%)	Vickers micro hardness (V$_{100}$) (GPa)	Thickness (μm)	-E$_{corr}$ (mV *vs* SCE)	i_{corr} (μA cm^{-2})	CR × 10^{-2} (mm y^{-1})
1.0	0.9	27.9	2.60	8.3	524	9.5	7.6
2.0	4.3	34.2	2.75	10.5	451	8.7	7.0
3.0	8.3	48.6	2.80	12.4	431	7.6	6.2
4.0	12.4	68.4	3.22	15.9	487	6.5	5.3

4.2.1.2 SEM study

The SEM images of Ni-W alloy coatings deposited at different c.d.'s are shown in Fig. 4.2. As may be seen, the morphology of the coatings was changed significantly with c.d., indicating that corrosion performance of the coating bears close relation with its composition and surface structure. The coatings displayed micro-cracks at high c.d. due to inherent brittle nature of the W and also due to hydrogen embrittlement [Zhu et al. 2002]. Further, the cracks on surface increased with W content in the deposit (Table 4.1). According to the conclusion made by Zhu et al. (2002), it was assumed that the formation of a layer of mixed tungsten oxides which prevents nickel deposition, and catalyzes hydrogen evolution. It may further explained by the fact that during alloy deposition, hydrogen gas remain adsorbed on the surface due to low hydrogen overvoltage of W. The adsorbed hydrogen leads to the development of strain in the deposit, which subsequently leads to the formation of micro-cracks on the surface. Thus micro-cracks on the surface of the coatings may be attributed to low hydrogen overvoltage of W, which was observed to be more at high c.d.'s. It is evident from the SEM images of coatings deposited at different c.d.'s as shown from Fig. 4.2(a) through Fig. 4.2(d).
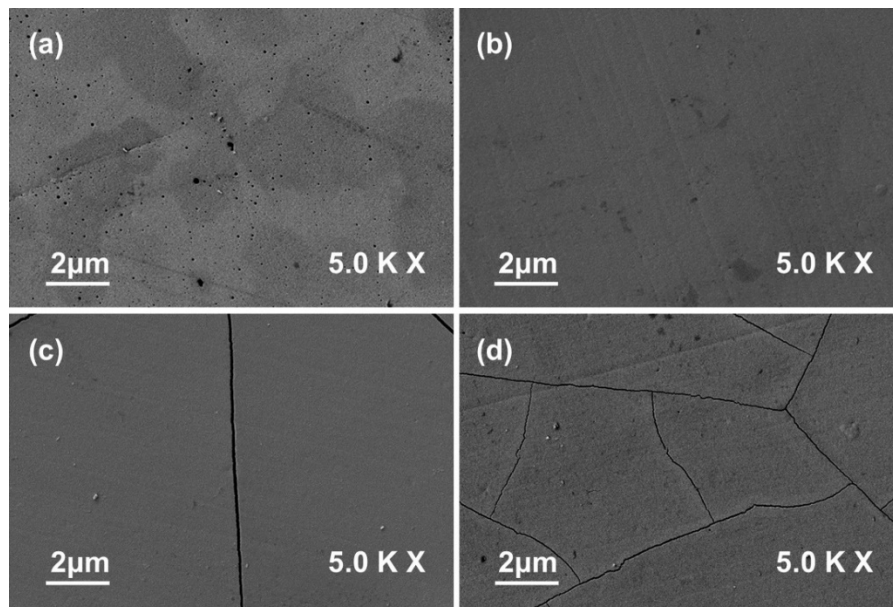
Fig. 4.2- SEM images of Ni-W alloy coatings deposited at: a) 1.0 A dm^{-2}, b) 2.0 A dm^{-2}, c) 3.0 A dm^{-2}, and d) 4.0 A dm^{-2}

4.2.1.3 XRD Study

XRD analysis was used to determine the phase composition of the Ni-W alloy coatings, and identification of the phases corresponding to different c.d.'s was obtained from the signals of peak profiles of the X-ray reflection plotted as a function of 2θ. The XRD spectra of the coatings, deposited at different c.d.'s are labelled by their Miller indices, are shown in Fig. 4.3. The intensity of prominent peak corresponding to (111) phase was found to be increased with c.d. as shown in Fig. 4.3, without any noticeable changes corresponding to other phases. From the intensity and position of the XRD signals, it may be seen that c.d. plays an important role in composition, and hence phase structure of Ni-W alloy coatings. The diffractograms having characteristic peaks corresponding to (111), (200) and (311) are attributed to Ni$_{17}$W$_3$ phases along with a Ni (222) phase [Zemanová et al. 2012].

An approximation of Ni and W content of the alloy deposit was made using EDS analysis. At higher c.d.'s, peak corresponds to a new phase with higher W content in comparison to the Ni$_{17}$W$_3$ phase as in lower c.d.'s are also visible. The phase corresponds to Ni-W alloy with (402), (530) and (092) are also found to be present at higher c.d.'s with fcc crystal lattice. The lattice growth from cubic to face-centered cubic increased its crystalline nature and microhardness as supported by the obtained

results. Further, at low c.d. limit the XRD peak corresponding to dissolved nickel and iron was observed at $2\theta = 37°$ as shown in Fig. 4.3. This is due to formation intermetallic compound of Ni and Fe on MS (substrate). However, it is not visible in the case of coatings deposited at high c.d., due to increase in thickness with deposition c.d.
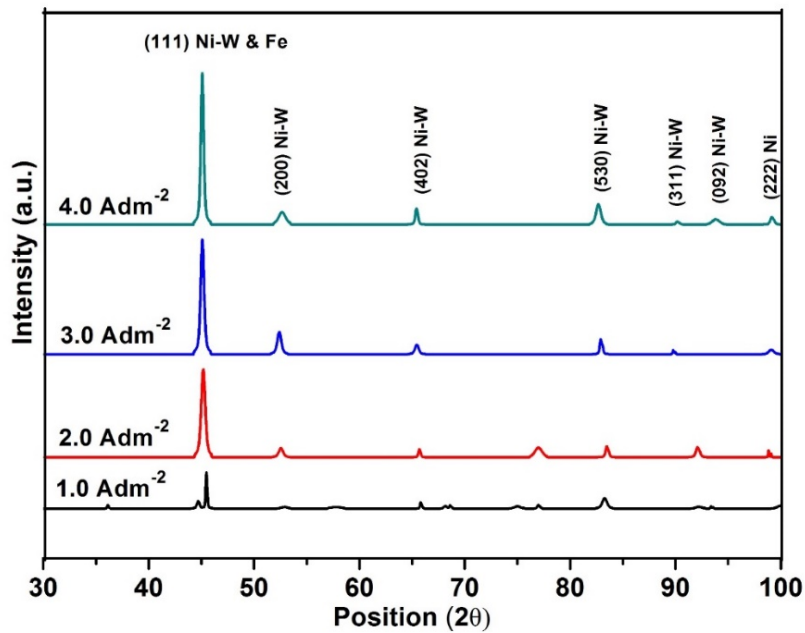
Fig. 4.3- X-ray diffraction patterns of Ni-W alloy coatings deposited at different c.d.'s from the same bath

The grain size of the electrodeposited Ni-W alloy coatings was determined using Scherrer formula as given in Eq. 4.1.

$$D_p = \frac{0.94\lambda}{\beta_{\frac{1}{2}}\cos\theta} \tag{4.1}$$

Where, D_p is the average crystallite size, λ is the wavelength of the x-rays used for the analysis, β is the line broadening in radius, θ is the Bragg angle. The grain size of the coatings was found to be decreased with increase in deposition c.d. from 33 to 24 nm. The coating developed at 4.0 A dm^{-2} was found to have the minimum grain size (24 nm). Further, the coatings were found to be more and more nanocrystalline in nature with increasing W content in the coating [Indyka et al. 2014, Ma et al. 2004].

4.2.1.4 Corrosion behavior of the homogeneous/monolithic Ni-W alloy coatings

The corrosion resistance of the monolithic Ni-W alloy coatings (tested in 5% NaCl as the representative corrosion medium) was found to be increased with deposition c.d. as given in Table 4.1. The coating developed at 4.0 A dm^{-2} was found to be the optimal coating with least CR (5.3×10^{-2} mm y^{-1}). The decrease in CR of the coatings at high c.d. is attributed to the increased W content. Both the crystalline phases Ni$_{17}$W$_3$ and Ni-W (W- rich), observed in the XRD pattern (Fig. 4.3) are responsible for the decreased CR of the coatings obtained at high deposition c.d.

4.2.2 Electrodeposition of laminar coatings

4.2.2.1 Optimization of cyclic cathode current densities

Many properties including corrosion resistance of monolayer alloy coatings can be increased to many folds by multilayer coating, despite of having same coating thickness. It is reasoned by increased surface area due to layering, i.e., periodic modulation in mass transport process at cathode brings periodic modulation in the composition of the coating; which leads to increase in the number of interfaces, and hence increased surface area. Thus multilayer Ni-W alloy coatings were accomplished by making the cathode c.d. to cycle between two values. Consequently, alternate layers of alloys with different compositions and properties were achieved by precise control over the cathode c.d.'s, called CCCD's.

To find the corrosion resistance of CMM Ni-W alloy coatings, initially coatings were developed at different sets of CCCDs with 10 layers (arbitrarily chosen), and their corrosion data are reported in Table 4.2. Based on the composition of monolayer Ni-W alloy coatings, developed at different c.d.'s, CMMA coatings were deposited on MS using square current pulses of different pulse height. The multilayered Ni-W alloy coatings having different coating configurations were developed and their corrosion performances were evaluated. It may be noted that CR was decreased substantially, when CMMA coatings were carried out at different sets of c.d.'s as given in Table 4.2. This observation confirms the fact that composition of alternating layer is not the deciding parameter for improved property of the coatings (here, it is corrosion resistance), but the number of intervening layers involved, responsible for increased

surface area. The less CR observed in the case of a combination of CCCD's 1.0 A dm^{-2} and 4.0 A dm^{-2}, and this set was selected to study the effect of further layering.

Table 4.2- Corrosion behaviors of CMM Ni-W alloy coatings having 10 layers at different set of CCCD's

CCCD's (A dm^{-2})	-E$_{corr}$ (mV vs SCE)	i_{corr} (μA cm^{-2})	CR ($\times$ 10^{-2} mm y^{-1})
CMMA coatings developed using dual pulses having a difference of 3.0 A dm^{-2}			
(Ni-W)$_{1.0/4.0/10}$	439	5.0	4.1
CMMA coatings developed using dual pulses having a difference of 2.0 A dm^{-2}			
(Ni-W)$_{2.0/4.0/10}$	431	12.7	10.2
CMMA coatings developed using dual pulses having a difference of 1.0 A dm^{-2}			
(Ni-W)$_{2.0/3.0/10}$	424	15.2	12.1

4.2.2.2 Optimization of total number of layers

The changed intrinsic properties of electrodeposits as a result of reduced grain size, and large number of interfaces can lead to a substantial improvement in corrosion resistance of multilayered coatings, usually up to an optimal limit. Therefore by selecting the combination of 1.0 and 4.0 A dm^{-2} as CCCD's for dual square current pulses, CMM Ni-W alloy coatings with 10, 60, 120, 300 and 600 layers were developed, and their CR's were monitored (Table 4.3). It is interesting to note that CR's of the multilayered coatings were decreased with the number of layers up to 300 layers, and then started increasing as reported in Table 4.3.

Table 4.3- Corrosion data of multilayered Ni-W alloy coatings with different number of layers deposited from optimal bath at optimal CCCD's

Coating configuration	Time for each layer deposition (s)	$-E_{corr}$ (mV vs SCE)	i_{corr} ($\mu A\ cm^{-2}$)	CR ($\times 10^{-2}\ mm\ y^{-1}$)
(Ni-W)$_{1.0/4.0/10}$	60	439	5.0	4.1
(Ni-W)$_{1.0/4.0/60}$	10	436	4.1	3.3
(Ni-W)$_{1.0/4.0/120}$	5	415	3.6	2.9
(Ni-W)$_{1.0/4.0/300}$	2	359	1.0	0.8
(Ni-W)$_{1.0/4.0/600}$	1	542	7.6	6.1

The increase in CR at high degree of layering, i.e., at 600 layers is attributed to the interlayer diffusion of CMMA deposit to become monolithic, caused by the lack of sufficient time for metal ions to relax (against diffusion under applied c.d.) and to deposit on the cathode with distinct interface [Leisner et al. 1996, Ullal and Hegde 2014, Venkatakrishna and Hegde 2010]. As more numbers of layers are allowed to form in same time duration, the time for the deposition of each layer, say (Ni-W)$_{1.0}$ is small (as the total time for deposition remains same, 10 min). Hence at a high degree of layering no modulation in the composition is likely to take place, and hence no improvement in corrosion resistance observed. Consequently, multilayered coatings tend to become monolayer/homogeneous coatings. The CR obtained for multilayered coating with 600 layers was found to be almost close to that of the CR of the optimal monolayer coating (developed at 4.0 A dm^{-2}), and it is in agreement with the possibility for interlayer diffusion at higher degree of layering.

Finally, experimental results revealed that CMM Ni-W coating deposited at optimal CCCD's, having 300 layers, represented by (Ni-W)$_{1.0/4.0/300}$ showed the least CR (0.8 $\times$ 10^{-2} mm y^{-1}) in 5 % NaCl medium, compared to its monolayer coating (5.3 $\times$ 10^{-2} mm y^{-1}), deposited from the same bath for the same duration of time. Hence, the coating configuration (Ni-W)$_{1.0/4.0/300}$ can be proposed as optimal for the deposition of multilayered coating.

4.2.2.3 Corrosion behavior of CMMA coatings

i) Tafel's polarization study

Due to a large surface area to volume ratio of thin films in the multilayered coating, as compared to that of bulk materials or monolayer coatings, the properties of thin films, as a rule, significantly differ from the bulk (macro-scaled) materials behavior [Tsyntsaru et al. 2012]. Hence as a whole, the corrosion resistance of the coating was found to be increasing to an extent of 300 layers and decreasing with further layering due to inter-layer diffusion. The potentiodynamic polarization behaviors of the CMM Ni-W alloy coatings with different number of layers (Fig. 4.4) are in agreement with this observation. The variation in i_{corr} and E_{corr} values of the CMMA coatings with layering suggests the trend in corrosion resistance with layering. The i_{corr} value of the CMMA coatings was found to be decreased up to 300 layers and then increased with further layering. The E_{corr} value was also found to be shifted towards the nobler side only up to 300 layers. Finally, the corresponding data obtained from the Tafel's extrapolation method (Table 4.3) also suggests the coating with 300 layers as the optimal with least CR. The improved corrosion resistance of the CMMA coatings may be attributed to the presence of alternate layers of alloys having different degree of pores and crevices, which makes the corrosion process to get hindered [Dobrzanski et al. 2007]. Hence, as the number of layers increased, the corrosive agent needs more time to penetrate through the coating, and then into the substrate material than in the case of monolayer coating.
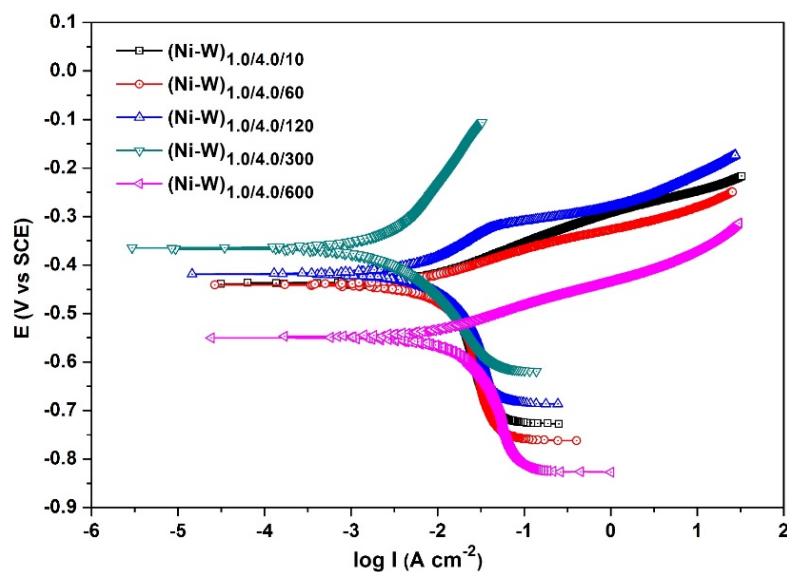
Fig. 4.4- Potentiodynamic polarization behavior of multilayer Ni-W alloy coatings having varying degree of layering, at a scan rate of 1.0 mV s^{-1}

ii) Electrochemical impedance spectroscopy study

The corrosion behaviors of the CMMA coatings were also evaluated using EIS method, and the impedance responses of the coatings with different number layers are shown in Fig. 4.5. The obtained Nyquist plots with only one depressive loop over the whole frequency range indicate the capacitance of the electrical double layer (EDL) as the reason for the improved corrosion resistance of the deposits. The decrease in CR of the CMMA coatings with layering is due to the increase in charge transfer resistance (R_{ct}) between metal and medium, as evidenced by the nature of Nyquist responses. The anomalous flattening behavior of the Nyquist plot is generally ascribed to the inhomogeneity of the metal surface arising from the surface roughness or interfacial phenomena occurring at the time of deposition [Dobrzanski et al. 2007, Barsoukov and Macdonald 2005].
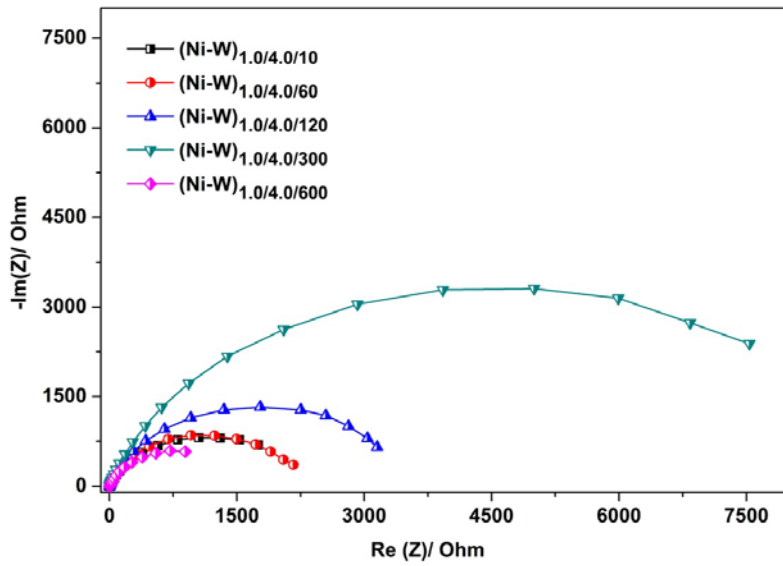
Fig. 4.5- Nyquist responses of the CMM (Ni-W)$_{1.0/4.0}$ alloy coatings with different degrees of layering, showing variation of R_{ct} values with number of layers

An electrical equivalent circuit (EEC) was used for modelling the interface behavior of the coating at optimal configuration in solution environment as shown in Fig. 4.6. An excellent agreement was found between impedance response of the coating under optimal condition and the simulated EEC, the corresponding circuit is also shown in the inset of Fig. 4.6. The equivalent circuit shows the presence of porous nature of the deposit due to the presence of micro-cracks on the surface, where, R_s - solution resistance, R_{po} - resistance of the porous layer, C_c - capacitance of the coating and C_{dl} - double layer capacitance involved in the equivalent circuit.
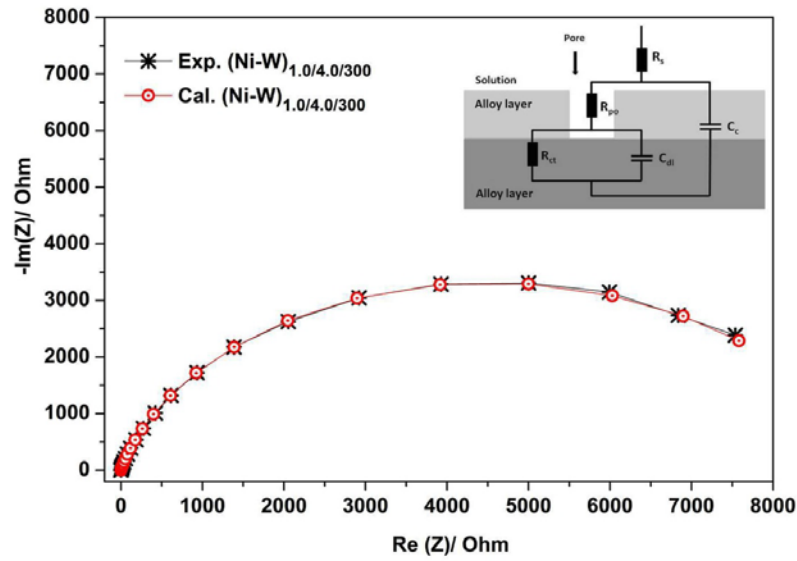
Fig. 4.6- EEC fitment for the Nyquist responses of the optimal (Ni-W)$_{1.0/4.0/300}$ coating, using Z$_{simpwin}$ software

The C_c of an intact coating can be much smaller than a typical C_{dl} value i.e., in the range of pF or nF [Barsoukov and Macdonald 2005, Mansfeld 1990]. R_{po} is the resistance of ion conducting paths developed in the coating due to the presence of micro-cracks or due to the deformation of the upper layer of the CMMA coating. These paths are physical pores filled with electrolyte, i.e., corrosion medium. Since in multilayered coating, the pore or the cracks in the upper layer is not reaching up to the substrate (MS) side, confirmed from the SEM cross-sectional analysis, due to the presence of several other layers of different composition below the upper layer. The pore will reach only up to the next layer just below the defected layer and then it can be assumed as a delaminated area of the exposed layer and as a pocket filled with an electrolyte solution. This electrolyte solution inside the cracks or pores is very different than the bulk solution outside the coating [Mansfeld 1990]. The interface between this pocket of solution and the next layer of the alloy coating is modelled as C_{dl} in parallel with a kinetically controlled charge-transfer reaction. Since only the upper few layers of the coatings are undergoing corrosion, the coating as a whole is providing protection to the substrate. Therefore, the EIS data obtained is not for a failed coating and hence there is only one time constant in the plot, as against the expected two [Barsoukov and Macdonald 2005, Mansfeld 1990].

iii) Microstructure of multilayer coating

Formation of alternate layers of alloys having distinct composition and surface morphology of the corroded CMMA coating were confirmed using SEM analyses. A cross-sectional view of CMM (Ni-W)$_{1.0/4.0/10}$ is shown in Fig. 4.7(a), and it is clearly showing the formation of 10 distinct layers along with the new interfaces in between the sublayers. The SEM image of (Ni-W)$_{1.0/4.0/10}$ coating after corrosion, marked as 4.7(b), shows the destruction of only the top layer even after corrosion study. The inspection of microscopic appearance of the surface of multilayer coating after corrosion test clearly confirms the fact that, multilayered Ni-W alloy coatings were formed in laminar fashion during deposition; and deteriorated layer by layer during corrosion. This explains why CMMA coatings offer extended protection of MS against corrosion, compared to its monolayer counterpart.
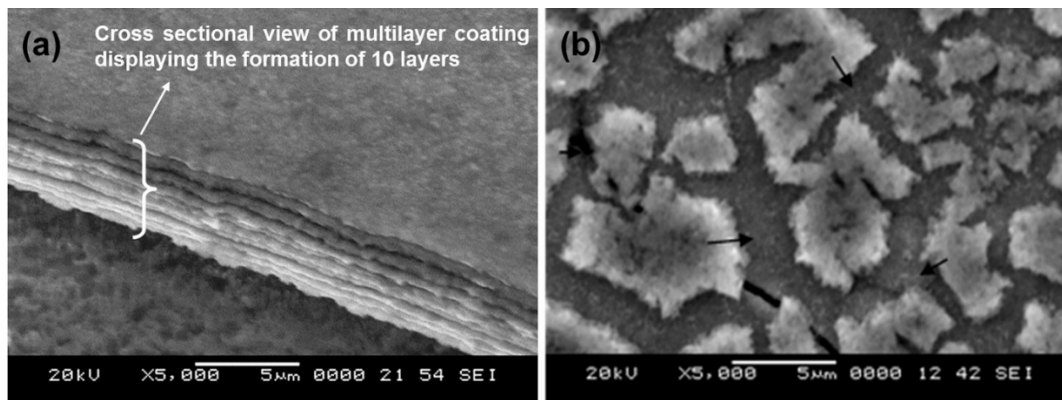
Fig. 4.7- SEM images of CMMA (Ni-W)$_{1.0/4.0/10}$ coating: a) cross-sectional view showing the formation of layered coatings, and b) top surface view after corrosion test

4.3 DEVELOPMENT OF CORROSION RESISTANT Ni-P ALLOY COATINGS

4.3.1 Properties of electrodeposited Ni-P alloy coatings

Bright, hard and adherent monolayer Ni-P alloy coatings were developed on MS at known c.d.'s using DC i.e., without modulation in the current pulse. The electrodeposited coatings were tested for their composition, hardness, thickness and corrosion behaviors, and the corresponding data are reported in Table 4.4. The experimental results showed that the P content in the deposit increases with deposition c.d. as reported in Table 4.4. Further, the CCE was also found to be increased with c.d.

The variation in CCE and P content in the deposit with deposition c.d. are shown diagrammatically in Fig. 4.8. The thickness and Vickers microhardness of the deposits were also found to be increased with c.d., as reported in Table 4.4.
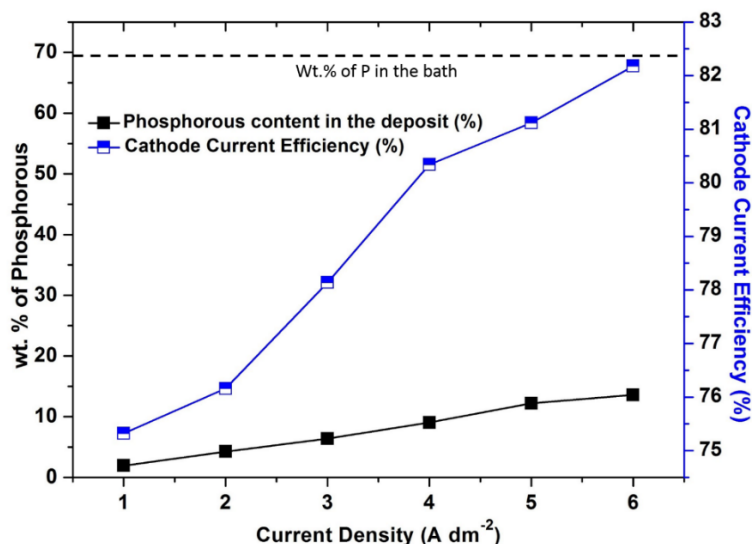
Fig. 4.8- Effect of c.d. on P content in the deposit and CCE of the bath

The corrosion data, in 5% NaCl medium, showed that the Ni-P alloy coating deposited at 4.0 A dm^{-2} as the most protective with the least CR (14.2×10^{-2} mm y^{-1}), compared to those at other c.d.'s. Hence, Ni-P alloy at 4.0 A dm^{-2} was selected as the optimal coating from the proposed bath, and is represented as (Ni-P)$_{4.0}$.

Table 4.4- Effect of deposition c.d. on the coating characteristics of Ni-P alloy coatings deposited from the optimized bath at 303 K

c.d. (A dm^{-2})	Wt.% of P in deposit	CCE (%)	Vickers micro hardness (V$_{100}$) (GPa)	Thickness (μm)	-E$_{corr}$ (mV vs SCE)	i_{corr} (μA cm^{-2})	CR × 10^{-2} (mm y^{-1})
1.0	1.9	75.3	2.34	7.9	551	38.5	40.6
2.0	4.2	76.1	2.43	11.4	532	29.4	32.8
3.0	6.3	78.1	2.47	14.1	496	25.3	26.8
4.0	9.0	80.3	2.67	18.3	513	12.0	14.2
5.0	12.1	81.1	2.59	19.4	456	17.4	18.7
6.0	13.5	82.1	2.53	19.8	505	23.0	24.1

4.3.2 SEM study

The surface appearance of each electrodeposited coatings was initially inspected visually and checked for satisfactory surface appearance with no pinhole and irregularities. Then surface micrographs of the coatings were examined under SEM. Fig. 4.9 shows the SEM images of Ni-P alloy coatings deposited at different c.d.'s, ranging from 1.0 to 6.0 A dm^{-2}. It may be observed that the roughness of coatings increased with c.d., which ended up with the formation of micro-cracks at high c.d. The formation of micro-cracks in the deposit, characterized by high P content, is due to the inherent brittle nature of P and internal stress in the deposits originated from the codeposition of hydrogen [Shervedani and Lasia 1997]. Further, the coatings were found to be more compact and nodular in structure with rough surface, towards high c.d.
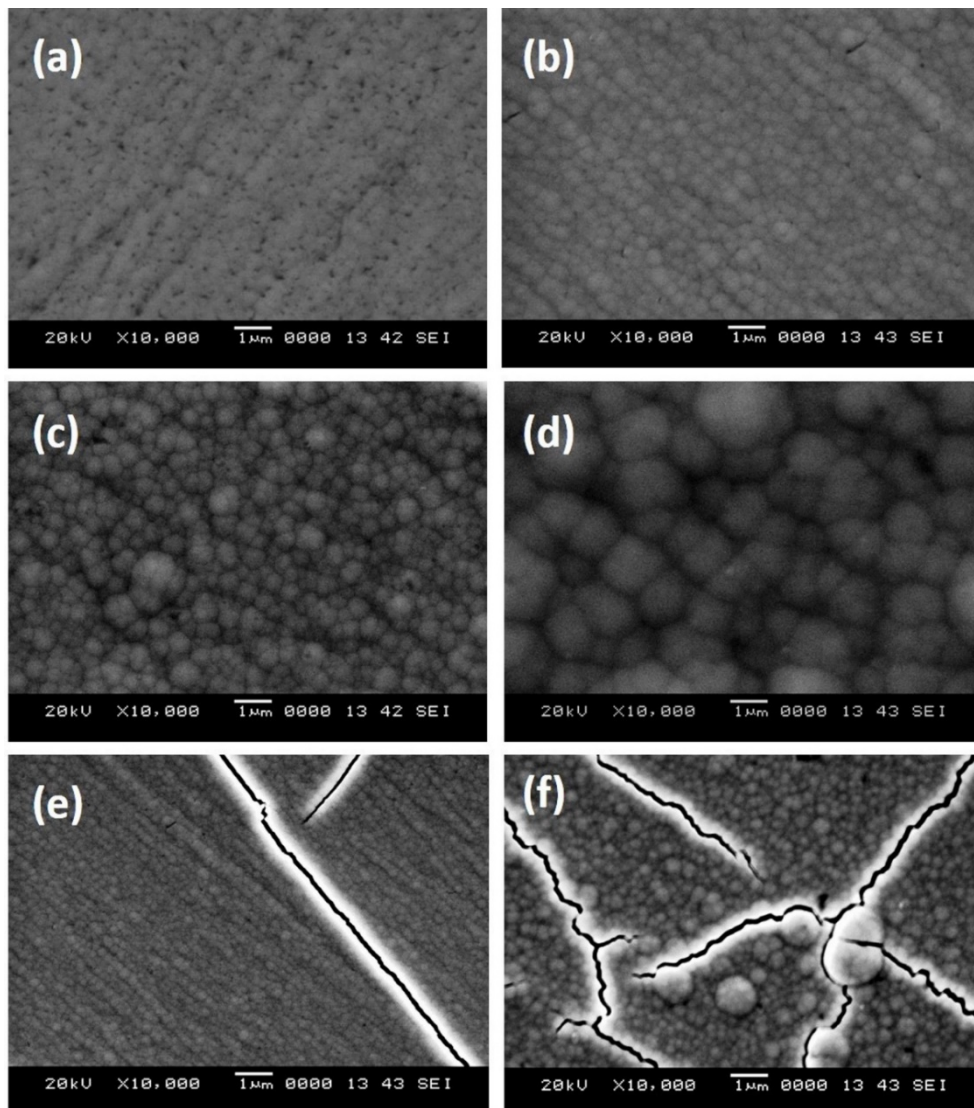
Fig. 4.9- Surface morphology of the Ni-P alloy coatings deposited at: a) 1.0 A dm^{-2}, b) 2.0 A dm^{-2}, c) 3.0 A dm^{-2}, d) 4.0 A dm^{-2}, d) 5.0 A dm^{-2}, and d) 6.0 A dm^{-2}

4.3.3 XRD Study

The phase structures of Ni-P alloy coatings deposited at different c.d.'s were assessed by XRD technique. The phases corresponding to different c.d.'s were identified by means of the signals of peak profiles of the X-ray reflection plotted as a function of 2θ (Fig. 4.10). Diffraction lines corresponding to both Ni and Ni$_3$P are observed in the diffractogram, indicating the equilibrium existence of Ni and Ni$_3$P phases in the deposits [Mahalingam et al. 2007, Narayan and Mungole 1985]. It may be seen that as the concentration of P in the deposit increased (in proportion of c.d.), the intensity of prominent Ni (111) peak in the diffraction patterns decreased gradually. The intensity

115

of Ni (200) and Ni (220) planes, observed at low c.d. (2.0 A dm^{-2}) were found to be reduced vanishingly as c.d. increased, as seen in Fig. 4.10. Further, the peak corresponding to MS (substrate) was found to be disappeared as the c.d. increased, due to increased thickness of the coatings. On the other hand, as the c.d. increased, more Ni$_3$P peaks were found and their intensity increased with c.d. and the Ni (111) peak intensity diminishes vanishingly. This is attributed to increased stress during deposition, which resulted in the precipitation of Ni$_3$P phase, caused by increased P content [Narayan and Mungole 1985, Pillai et al. 2012].
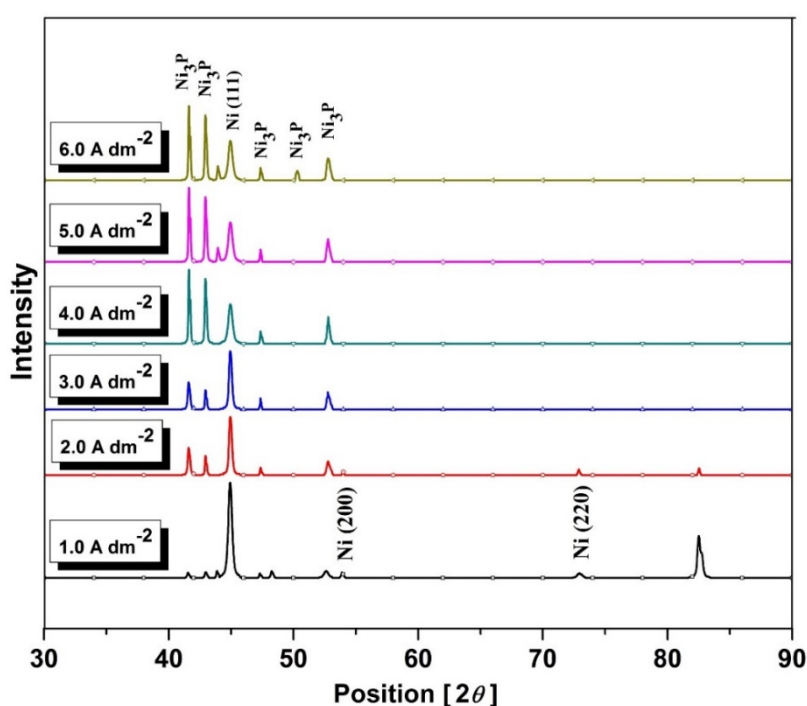
Fig. 4.10- X-ray diffraction pattern of the Ni-P alloy coatings deposited at different c.d.'s from the optimal bath

4.3.4 Electrodeposition of multilayered Ni-P alloy coatings

It is possible to control the composition and thickness of the coatings in nano/micrometric level by regulating the c.d. and it's duration. The pulsed current favour the formation of nano-laminated multilayered alloy coatings, having different composition and grain size layer by layer. It should be noted that in the present study only pulsed DC is used (Fig. 2.3), with a suitable combination of CCCD's, and it should

not be confused with regular pulse plating where current reduces to zero for every cycle, explained in the literature [Chandrasekar and Pushpavanam 2008].

4.3.4.1 Optimization of CCCD's

The electrodeposition and characterization of Ni-P alloy coatings revealed that the proposed alloy plating bath could develop coatings of different morphology, composition (62–86 wt.% of Ni) and phase structure over a wide range of deposition c.d.(1.0 – 6.0 A dm^{-2}). On the other hand, it is well known that many properties including corrosion resistance of monolayer alloy coatings can be increased to many folds of its magnitude by multilayer technique, despite of having same total coating thickness [Thangaraj et al. 2009]. It is due to increased interfacial surface area affected by layering. The periodic modulation in mass transport at cathode film (due to periodic change of current density) allows the growth of coating in layers, having different composition and grain size. This leads to the formation of coatings with number of layers separated by interfaces.

Thus, guided by above facts, multilayered Ni-P alloy coatings were deposited at different sets of pulsed c.d.'s. To optimize CCCD's for the development of the most corrosion resistant coatings, they are developed at different sets of CCCD's with 10 layers (chosen arbitrarily), and their corrosion characters were evaluated (Table 4.5). It was found that CR's of multilayered Ni-P alloy coatings decreased substantially, when the coatings were developed at different sets of c.d.'s as may be seen in Table 4.5. Among the many sets of CCCD's tried, the least CR was observed in two sets of CCCD's, i.e., a combination of 1.0 and 4.0 A dm^{-2}, and another combination of 2.0 and 5.0 A dm^{-2}. Hence, these two sets of CCCD's have been selected for further study, to see the effect of nanolaminated coatings on corrosion behavior.

Table 4.5- Corrosion data of CMM Ni-P alloy coatings having 10 layers, developed at different sets of CCCD's

CCCD's (A dm^{-2})	-E_{corr} (mV *vs* SCE)	i_{corr} (μA cm^{-2})	CR ($\times 10^{-2}$ mm y^{-1})
(Ni-P)$_{4.0}$	513	12.0	14.2
CMM Ni-P coatings developed using dual pulses having difference of 3.0 A dm^{-2}			
(Ni-P)$_{1.0/4.0/10}$	502	8.1	10.3
(Ni-P)$_{2.0/5.0/10}$	542	11.2	12.6

4.3.4.2 Optimization of total number layers

The properties of the electrodeposited coatings, due to reduced grain size and large number of interfaces can lead to a substantial improvement in their corrosion resistance character. The number of interfaces can be infinite in principle, however, they are usually up to an optimal limit [Kanani 2004]. Therefore, by selecting 1.0 & 4.0 A dm^{-2} and 2.0 & 5.0 A dm^{-2}, as two square current pulses, CMM Ni-P alloy coatings having 10, 60, 120, 300 and 600 layers were developed. The corrosion behaviors of the multilayered Ni-P alloy coatings at different coating configurations were studied, and the obtained data are reported in Table 4.6.

It is important to note that corrosion rates of multilayered coatings, having (Ni-P)$_{1.0/4.0/300}$ and (Ni-P)$_{2.0/5.0/300}$ configurations are least compared to the monolayer (Ni-P)$_{4.0}$ coating (Table 4.6). This clearly indicates the effect of layered coatings on reducing the CR of the conventional alloy coatings. On the other hand, despite of having the same degree of layering (300 layers), (Ni-P)$_{1.0/4.0/300}$ coating was found to show lesser CR compared to the (Ni-P)$_{2.0/5.0/300}$ coating (Table 4.6). It evidences the fact that not only the number of layers, but also their composition determines the performance of the coatings. Thus, better corrosion protection of multilayer Ni-P alloy coating is a combined effect of both thickness and composition of individual layers.

It is interesting to note that the CR's of multilayered Ni-P alloy coatings decreased with the number of layers up to 300 layers in both sets of CCCD's, and then started increasing as reported in Table 4.6. The increase in CR at high degree of layering, i.e., at 600 layers for (Ni-P)$_{1.0/4.0/600}$ and (Ni-P)$_{2.0/5.0/600}$ is attributed to the

diffusion of nanolayer coatings. It may be explained as follows: As more numbers of layers are allowed to form in same time duration, the time for the deposition of each layer, say $(Ni-P)_{1.0}$ is small (as the total time for deposition remains same, 10 min). Due to short pulse duration (1 second), there is no sufficient time for metal ions to relax (against diffusion under applied c.d.) and to deposit on cathode with distinct interface [Leisner et al. 1996]. Therefore at high degree of layering, no modulation in composition is likely to happen, and it is to state that at higher degree of layering multilayered Ni-P alloy coatings tends to become a monolayer. Hence, CR's of multilayered coatings having 600 layers were found to be very high, and is almost same as that of monolithic coating developed at 4.0 A dm^{-2}.

Table 4.6- Corrosion data of nanolaminated multilayer Ni-P coatings developed using different combinations of current pulses, having different number of layers

Coating configuration	Time for each layer deposition (s)	$-E_{corr}$ (mV vs SCE)	i_{corr} (μA cm^{-2})	CR ($\times 10^{-2}$ mm y^{-1})
CMM Ni-P coatings developed using a combination of 1.0 and 4.0 A dm^{-2}				
$(Ni-P)_{1.0/4.0/10}$	60	502	8.1	10.3
$(Ni-P)_{1.0/4.0/60}$	10	401	4.3	6.9
$(Ni-P)_{1.0/4.0/120}$	5	548	2.8	4.2
$(Ni-P)_{1.0/4.0/300}$	2	496	1.0	1.9
$(Ni-P)_{1.0/4.0/600}$	1	537	12.9	13.9
CMM Ni-P coatings developed using a combination of 2.0 and 5.0 A dm^{-2}				
$(Ni-P)_{2.0/5.0/10}$	60	542	11.2	12.6
$(Ni-P)_{2.0/5.0/60}$	10	560	9.1	10.8
$(Ni-P)_{2.0/5.0/120}$	5	538	5.8	8.9
$(Ni-P)_{2.0/5.0/300}$	2	419	2.1	4.4
$(Ni-P)_{2.0/5.0/600}$	1	412	13.1	14.1

The experimental results demonstrated that the CMM Ni-P alloy coating deposited at 1.0 & 4.0 A dm^{-2} combination, having 300 layers, represented by $(Ni-P)_{1.0/4.0/300}$ showed the least CR (1.92×10^{-2} mm y^{-1}) in 5% NaCl medium, in comparison to its monolayer $(Ni-P)_{4.0}$ alloy coating (14.2×10^{-2} mm y^{-1}), deposited from the same bath for the same duration of time. Hence, the optimal coating configuration proposed

for the deposition of multilayered coating from the proposed bath is CMMA (Ni-P)$_{1.0/4.0/300}$. The total thickness of the coating under optimal configuration, i.e., for (Ni-P)$_{1.0/4.0/300}$ was found to be about 16 μm. Hence, the average thickness of individual layers is estimated to be in the range of 53 nm.

4.3.5 Corrosion study

4.3.5.1 Tafel's polarization study
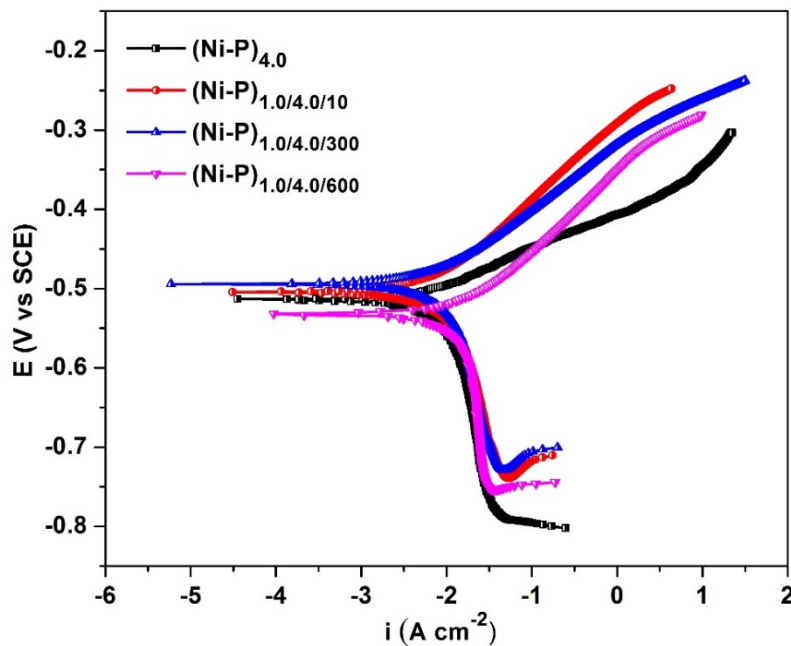
Fig. 4.11- The representative potentiodynamic polarization behaviors of the CMM Ni-P alloy coatings having different degree of layering in 5% NaCl medium

Tafel's extrapolation method was employed for determining the i_{corr} values, and thereby the corrosion rates of the coatings. Potentiodynamic polarization behaviors of CMM (Ni-P)$_{1.0/4.0}$ coatings at different degree of layering are shown in Fig. 4.11 (only representative), and their corrosion data are given in Table 4.6.

4.3.5.2 Electrochemical impedance study

The Nyquist plots obtained for CMMA coatings with different number of layers are shown in Fig. 4.12. The EIS responses were found to be depressed semicircles with one capacitive loop, attributed to the frequency dispersion of interfacial impedance, and this anomalous flattening behavior is due to the inhomogeneity of the sample surface [Fei

and Wilcox 2005]. The nature of Nyquist response indicates that the same corrosion protection mechanism is followed in the coatings of all configurations. High R_{ct} value for $(Ni-P)_{1.0/4.0/300}$ coating, with large capacitive loop indicates it as the most corrosion resistant coating.
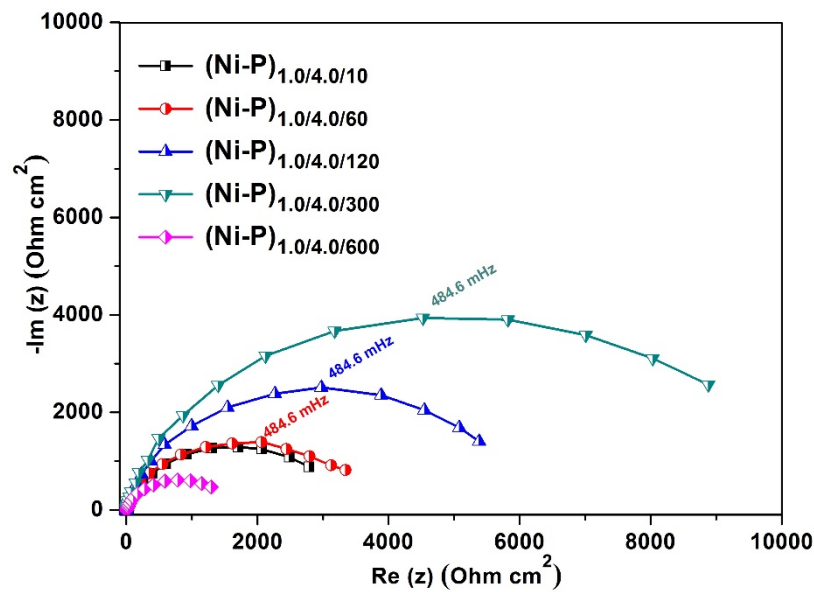
Fig. 4.12- Nyquist plots of CMM $(Ni-P)_{1.0/4.0}$ coating with different degrees of layering

The electrical interface between the electrodeposit and corrosion medium, corresponding to the optimal coating $(Ni-P)_{1.0/4.0/300}$ was modelled with an EEC, using $Z_{simpwin}$ software. A good agreement between the experimental and simulated electrochemical responses was found, as shown in Fig. 4.13. The simulated EEC with Q and R_{ct} are parallel to each is shown in the inset of Fig. 4.13. The obtained values for circuit elements, namely R_s, R_{ct} and Q are given in Table 4.7. The value of R_s was found to be almost constant as given in Table 4.7, due to the same medium and cell configurations used for the corrosion study. The variation in R_{ct} values indicates that the corrosion protection efficacy of $(Ni-P)_{1.0/4.0}$ coatings show a progressive increase with the number of layers only up to 300 layers, and then decreased. Further, the decrease in Q value with layering was also found to show the trend only up to a maximum of 300 layers.
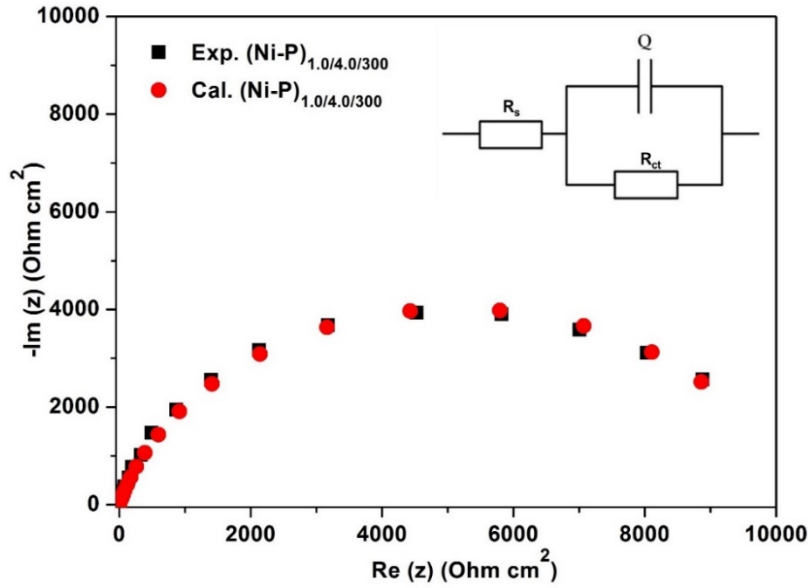
Fig. 4.13- EEC fitment of the Nyquist response corresponds to $(Ni-P)_{1.0/4.0/300}$ coating along with the obtained circuit in the inset

Table 4.7- EEC parameters of the CCMA coatings with different number of layers

Coating configuration	R_s (Ohm cm^2)	R_{ct} (Ohm cm^2)	Q (μF cm^{-2})
$(Ni-P)_{1.0/4.0/10}$	0.924	2786.4	75.5
$(Ni-P)_{1.0/4.0/60}$	0.912	3356.2	35.2
$(Ni-P)_{1.0/4.0/120}$	0.895	5432.0	32.1
$(Ni-P)_{1.0/4.0/300}$	0.943	8864.1	23.7
$(Ni-P)_{1.0/4.0/600}$	0.895	1431.0	178.2

4.3.6 SEM analysis of multilayered coating

The formation of laminar coatings having successive layers of alloys with different composition was confirmed by SEM analysis. The cross-sectional view of multilayered coating having $(Ni-P)_{1.0/4.0/6}$ configuration is shown in Fig. 4.14. Inspection of the microscopic appearance of the coating confirmed the formation 6 layers of alloys having alternatively different composition, as shown in Fig. 4.14.
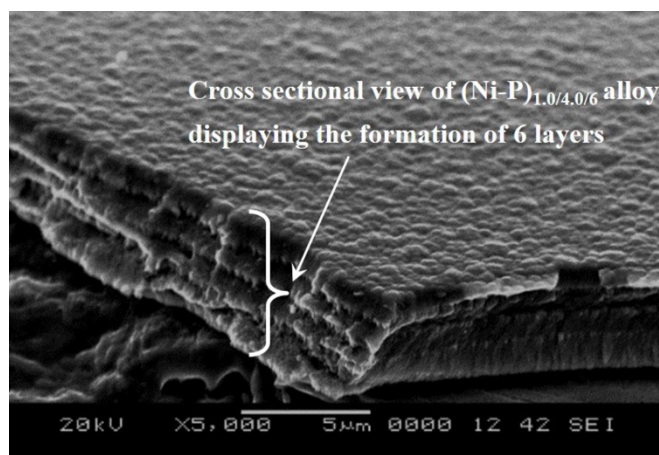
Fig. 4.14- Cross-sectional SEM image of (Ni-P)$_{1.0/4.0/6}$ coating shows the formation of laminar coating having 6 layers of different composition

4.4 MECHANISM OF CORROSION PROTECTION IN CMMA COATINGS

The increased corrosion protection of CMMA (Ni-W)$_{1.0/4.0/300}$ and (Ni-P)$_{1.0/4.0/300}$ coatings in relation to its monolayer alloy coating is attributed by the selective dissolution of layers of different composition as envisaged by Fei and Wilcox (2005). The mechanism of increased corrosion protection of multilayered coatings, in relation to its monolayer coating can be explained through a pictorial representation, shown in Fig. 4.15. Here, the multilayered coating having 4 layers and its monolayer coating, represented respectively as (Ni-M)$_{1.0/4.0/4}$ and (Ni-M)$_{4.0}$ are considered (where, M = W and P).

In the schematic diagram, it may be seen that multilayered (Ni-M)$_{1.0/4.0/4}$ coating having 2 layers of alloys with one composition (sky blue colour) alternated by 2 layers of alloys with a different composition (grey colour), gives better protection to the substrate than its monolayer alloy coating of same thickness. The enhanced corrosion protection mechanism of CMMA coatings can be explained as - when the coating is carried out in multilayers, the number of interfaces separating the alloys of two different compositions also increases. In CMMA (Ni-M)$_{1.0/4.0}$ coating, the (Ni-M)$_{4.0}$ top layer corrodes slowly, than the beneath layer (Ni-M)$_{1.0}$. Variation in the composition of successive layers results in a significant change in the phase structures; and hence when the top layer is exposed directly to corrosion medium it gets corroded first while protecting the beneath layer. The lower layers are safe until the breakdown of top most

layers occur. This leads to the spreading of corrosion product laterally at the interface. Once the breakdown of top layer takes place, the second layer is exposed to corrosive medium and this repeats layers after layers. As the number of layers increased, the corrosive agent needs more time to penetrate through the coating and then into the substrate. Due to this process, the corrosive agent path is extended or blocked [Leisner et al. 1996, Venkatakrishna and Hegde 2010]. But in the case of the monolayer, or non-nanostructured/bulk coating, the corrosion takes place unabatedly, and corrosive agent reaches the substrate very fast as shown in the schematic illustration. Thus it may be summarized that increased corrosion protection of multilayered alloy coating is due to increase in the number of interfaces, formed due to layering, compared to its monolayer coating. The interfaces allow the spreading of corrosive medium laterally, and delays attacking of the substrate [Thangaraj et al. 2009, Gu et al. 2005a, Gu et al. 2005b], and is shown diagrammatically in Fig. 4.15. It may also be concluded from the figure (Fig. 4.15) that the time required for the corroding medium to reach the substrate by penetrating through the multilayered coating (T_1) is much greater than that through the monolayer coating (T_2), i.e. $T_1 \gg T_2$.
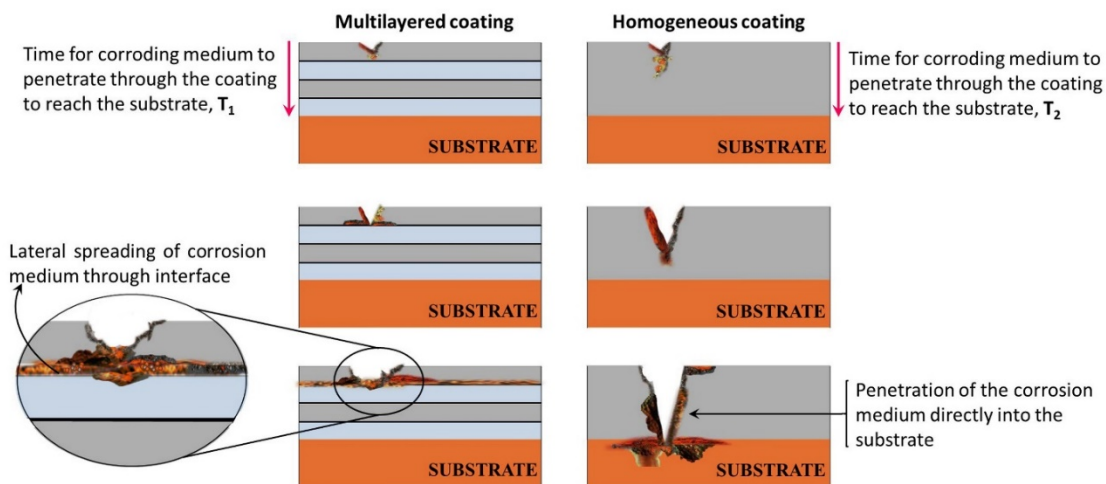
Fig. 4.15- Diagram showing the mechanism for increased corrosion protection of multilayered (Ni-M)$_{1.0/4.0/4}$ coating (left), compared to the monolayer (Ni-M)$_{4.0}$ coating (right), deposited from the same bath for same duration. It demonstrates that the time required for the corroding medium to reach the substrate by penetrating through the multilayered coating (T_1) is much greater than that through the monolayer coating (T_2)

4.4 CONCLUSIONS

Based on the experimental results of investigation on the deposition of multilayered Ni-W and Ni-P alloy coatings on MS for better corrosion protection, the following observations were made as conclusions:

1. The corrosion resistance of monolayer Ni-W and Ni-P alloy coatings were increased to many folds by nanolaminated multilayered alloy coating approach using pulsed DC.

2. Electrochemical corrosion study demonstrated that the multilayered Ni-W and Ni-P alloy coatings with 300 layers, represented generally as $(Ni-M)_{1.0/4.0/300}$ is showing the least CR compared to their monolayer (monolithic or homogenous) coatings, developed from the same bath using non-pulsed DC.

3. Better corrosion protection of multilayered Ni-W and Ni-P alloy coatings, compared to their monolayer counterpart is ascribed to the combined effect of both thickness and composition of individual layers.

4. Drastic improvement in the corrosion protection efficacy of multilayered alloy coatings is attributed to the increase in number of interfaces separating the layers of alloys having different composition and phase structures, responsible for lateral spreading of the corrosion medium.

5. Corrosion protection efficacy of multilayered coatings was found to increase with number of layers only up to an optimal level, and then decreased due to interlayer diffusion.

MAGNETOELECTRODEPOSITION: AS MEANS TO IMPROVE THE CORROSION RESISTANCE OF Ni-W ALLOY COATINGS
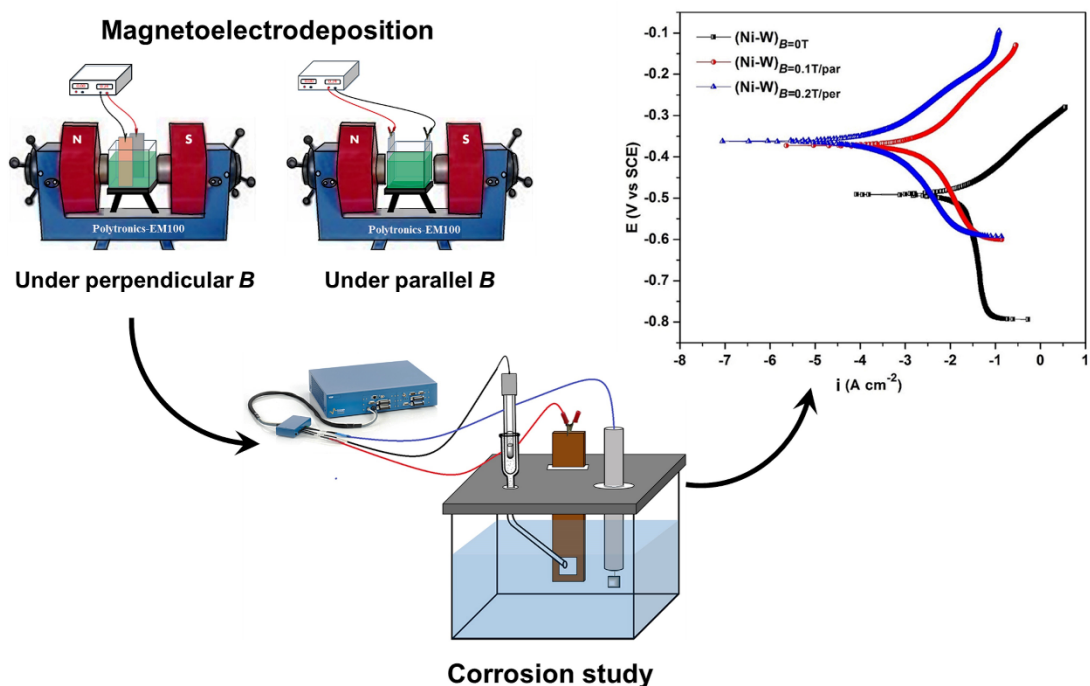
This chapter discusses the development high corrosion resistant Ni-W alloy coatings using MED approach for the protection of MS. The conditions for the deposition of more corrosion resistant MED Ni-W alloy coatings were optimized by inducing a magnetic field during deposition, in terms of varying intensity and direction, from the same bath. The applied magnetic field was used as a tool to alter the crystallinity, composition and thereby the corrosion resistance of the coatings. It was demonstrated that the corrosion resistance of Ni-W alloy coatings can be improved to many folds of its magnitude by MED approach. Significant increase in corrosion resistance exhibited by MED coatings (under both parallel and perpendicular B) is attributed to the increased W content of the alloy affected by an increase in i_L value. The high corrosion resistance of the MED Ni-W alloy coatings was explained in the light of MHD effect, responsible for the increased W content, brought about by the enhanced mass transport. The inherent limitations of the bath like, low i_L and induced

type of codeposition which impedes the development of W-rich alloy coatings were successfully resolved by MED method. Drastic improvement in corrosion resistance is ascribed to the basic difference in the process of electrocrystallization and phases formed during MED, confirmed by SEM and XRD study.

5.1 RESULTS AND DISCUSSION

5.1.1 Electrodeposited Ni-W alloy coatings

The corrosion behavior of the ED Ni-W alloy coatings at different c.d.'s from the optimal bath was discussed in Chapter-4. From the detailed study on the effect of c.d. on the coating characteristics revealed that the coating obtained at a deposition c.d. of 4.0 A dm^{-2} as the optimal coating with maximum W content and least CR. It is important to notice that the better corrosion protection efficacy of the coatings was characterized by high W content in the alloy as reported in Chapter-4. Whereas, it was very difficult to attain a coating with W content more than 12.4 wt.% through conventional galvanostatic methods of deposition. In this connection, to overcome the limitations of natural convection during conventional deposition, MED technique was adopted. The development of MED coatings under different conditions of applied B, in terms of direction and intensity were described in Chapter-2.

5.1.2 Characterization of the MED Ni-W alloy coatings

5.1.2.1 Surface appearance of the MED coatings

The surface topography of the MED coatings developed at different strengths of B, applied in parallel and perpendicular directions was observed through SEM. The elemental composition of the coatings was also examined using EDS analysis. A significant change in surface morphology was observed with change in direction of B. The surface appearance of the optimal ED and MED coatings (in terms of W content as observed in the EDS data given in Table 5.1) represented as, $(Ni-W)_{B=0\,T}$, $(Ni-W)_{B=0.1\,T/par}$ and $(Ni-W)_{B=0.2\,T/per}$, are shown in Fig. 5.1, for comparison. It is interesting to note that the morphology of the coating at $B= 0$ T is almost flat without any features and covered with full of micro-cracks. The presence of micro-cracks on the coating surface is attributed to the inherent brittle nature of W and also due to codeposition of H_2 gas during deposition [Brenner 1963]. But in the presence of induced B, in a parallel

direction, the formation of nodular growths were observed along with the micro-cracks as observed in Fig. 5.1(b). Whereas, in the presence of B, applied in a perpendicular direction, the coating was found to be cracks-free and covered homogeneously with nodular growths (Fig. 5.1(c)). This variation in surface morphology with a change in the direction of B, applied during deposition, confirms the effect of B on deposit characteristics. Further, the influence of intensity of B applied under a particular direction, parallel or perpendicular was also studied (Fig. 5.2 and 5.3). A remarkable change in surface morphology was also observed with variation in the intensity of B, in the case of both parallel and perpendicular directions. Under parallel B, the nodular growth was found to be diminished and becomes uneven with an increase in the intensity of B from 0.1 T to 0.4 T as observed in Fig. 5.2. The coating was observed to become more porous and flat at a higher strength of B (Fig. 5.2(d)), and looks almost similar to ED coating. This variation in surface appearance can be related to the EDS results as given in Table 5.1. The coating with maximum W content, developed under parallel B, was found to show nodular growth and the coating with least W content shows the appearance similar to a conventional coating. Similarly, under perpendicular B, all the coatings were found to be cracks free with surface morphologies varying from granular structure to nodular growths and then to porous grains as shown in Fig. 5.3. In this case also the coating with maximum W content (at $B = 0.2$ T) was found to be covered with homogeneous nodular growths, and it was found to be changed to porous grains at higher strengths of B (Fig. 5.3(d)).
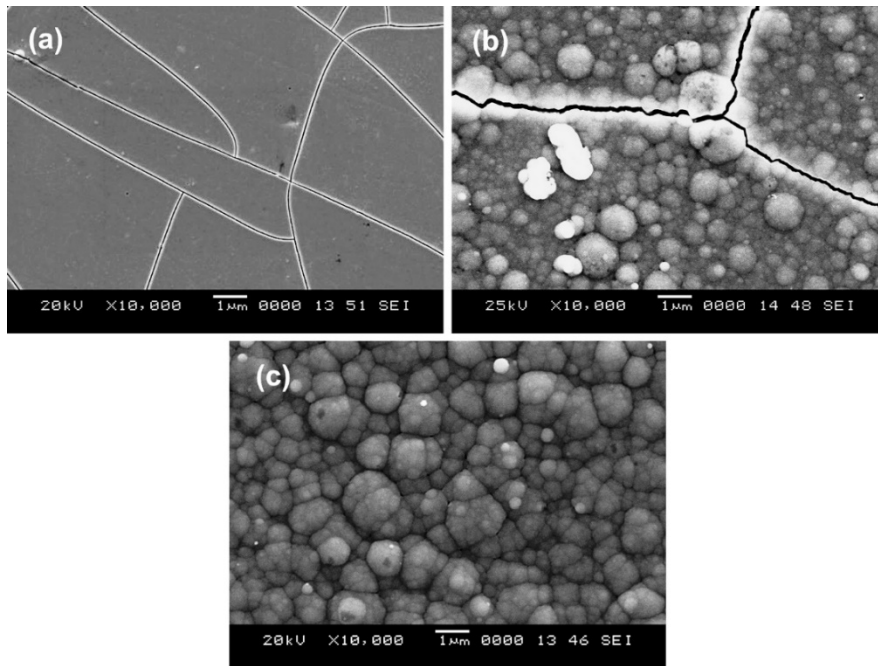
Fig. 5.1- SEM images of the optimal ED Ni-W alloy coating in comparison with MED coatings deposited under applied magnetic field in parallel and perpendicular direction: a) (Ni-W)$_{B=0\ T}$, b) (Ni-W)$_{B=0.1\ T/par}$, and c) (Ni-W)$_{B=0.2\ T/per}$
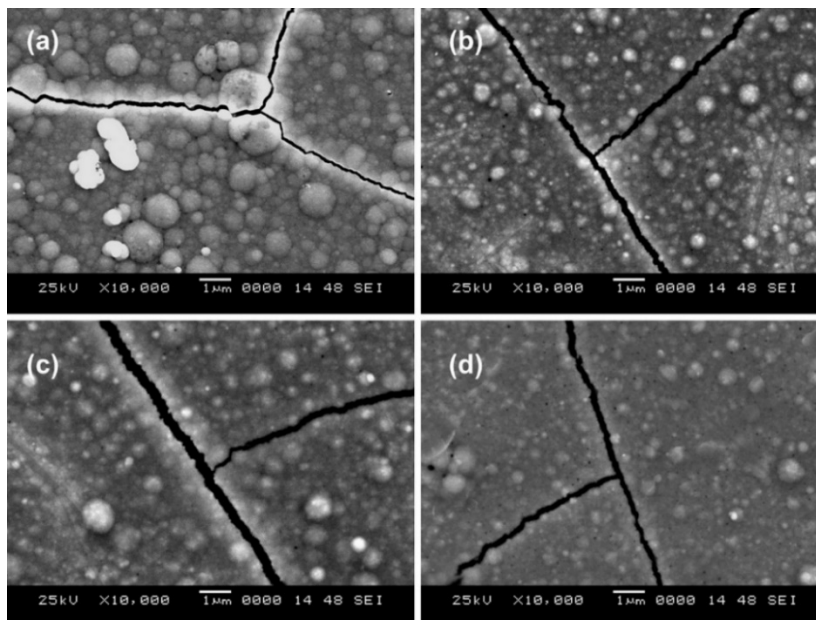
Fig. 5.2- SEM images showing the variation in surface morphology of MED Ni-W alloy coatings developed under parallel B: a) (Ni-W)$_{B=0.1\ T/par}$, b) (Ni-W)$_{B=0.2\ T/par}$, c) (Ni-W)$_{B=0.3\ T/par}$, and d) (Ni-W)$_{B=0.4\ T/par}$
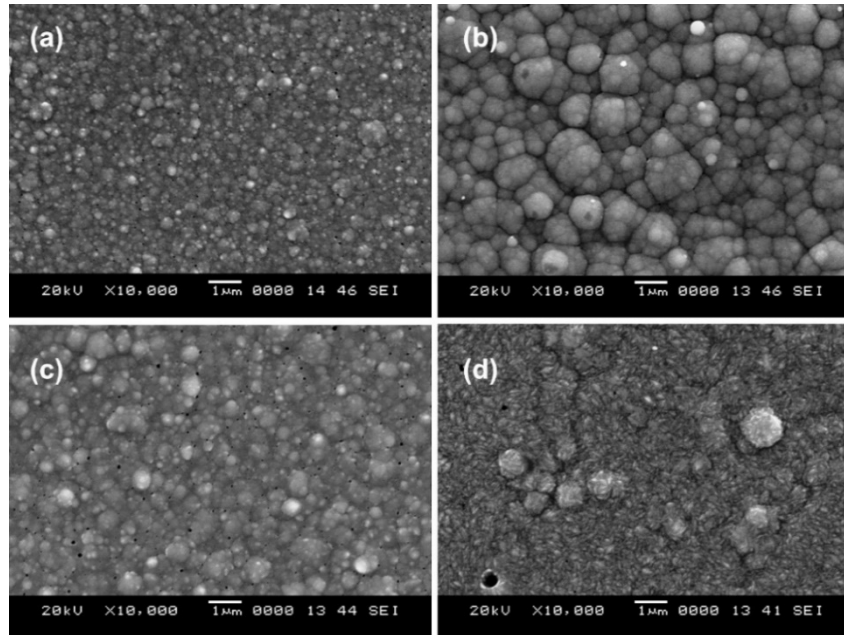
Fig. 5.3- SEM images showing the variation in surface morphology of Ni-W alloy coatings with intensity of B, applied in perpendicular direction: a) (Ni-W)$_{B=0.1\ T/per}$, b) (Ni-W)$_{B=0.2\ T/per}$, c) (Ni-W)$_{B=0.3\ T/per}$, and d) (Ni-W)$_{B=0.4\ T/per}$

5.1.2.2 Phase structure of the MED coatings

The variation in phase structure of the MED coatings developed under different conditions of B was studied using XRD analysis. The variation in XRD pattern obtained for optimal MED coatings, in terms of W content, under parallel and perpendicular B in comparison with the ED coating are shown in Fig. 5.4. The obtained results show the presence of new reflections corresponding to W-rich phases in the MED coatings, developed under different conditions of applied B. It may be noted that the XRD results show variation in the direction of crystal growth, evident from the change in intensity of the main peak, with change in direction of the applied magnetic field. The crystal growth in ED coating was in the (111) plane, and it was found to be changed into (530) and (220) under parallel and perpendicular B, respectively. The change in intensity of the main peaks are attributed to the formation of W-rich phases under different conditions of applied B. The change in peak intensity with variation in strength of applied B, in a particular direction (either parallel or perpendicular), was also studied and it was found to show a remarkable variation in the intensity of individual peaks as shown in Fig. 5.5 and 5.6).
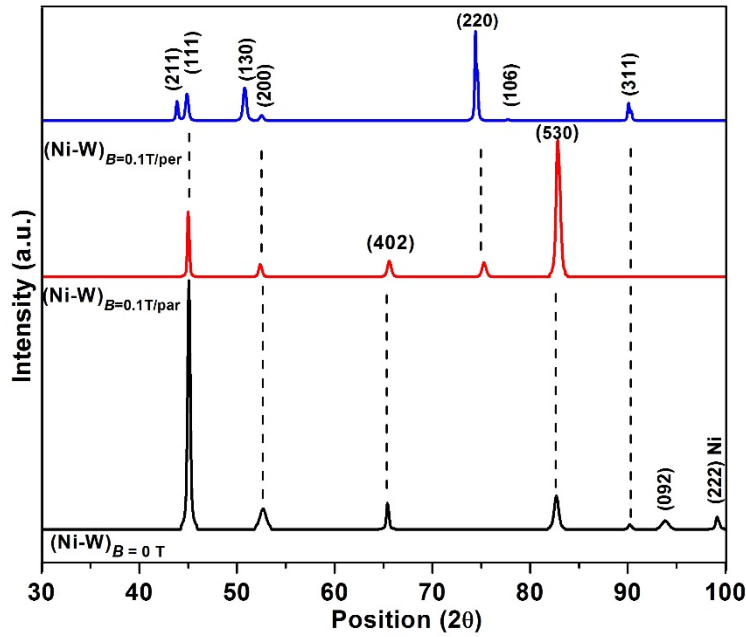
Fig. 5.4- The variation in XRD pattern of the MED Ni-W alloy coatings achieved under parallel and perpendicular directions of *B* in comparison with the conventional ED coating
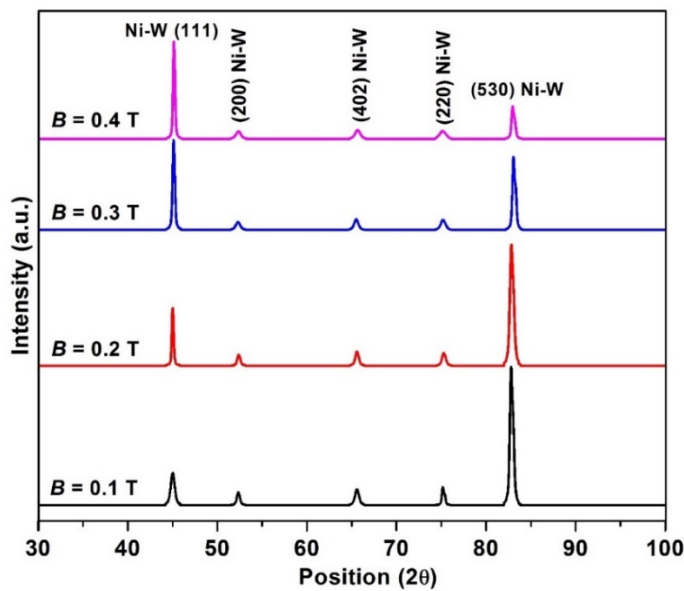
Fig. 5.5- XRD pattern showing the variation in phase structure of the Ni-W alloy coatings with intensity of *B*, applied in parallel direction: a) (Ni-W)$_{B=0.1\ T/par}$, b) (Ni-W)$_{B=0.2\ T/par}$, c) (Ni-W)$_{B=0.3\ T/par}$ and d) (Ni-W)$_{B=0.4\ T/par}$
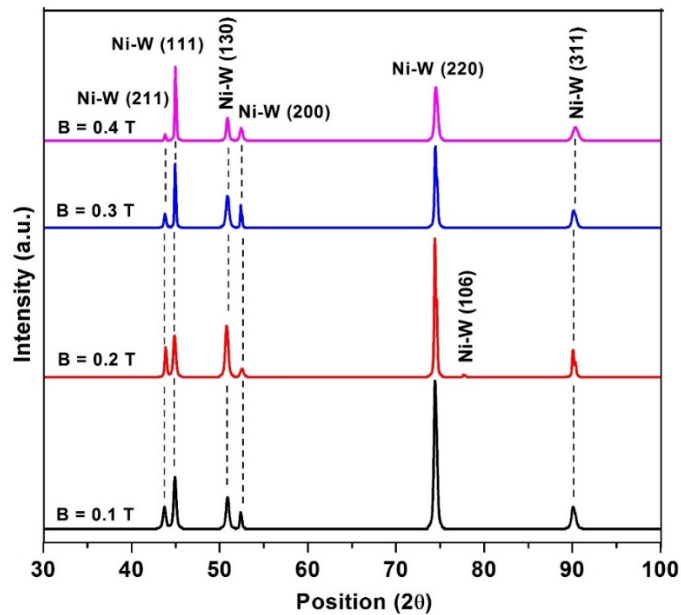
Fig. 5.6- XRD pattern showing the variation in phase structure of the Ni-W alloy coatings with intensity of *B*, applied in perpendicular direction: a) (Ni-W)$_{B=0.1\ T/per}$, b) (Ni-W)$_{B=0.2\ T/per}$, c) (Ni-W)$_{B=0.3\ T/per}$ and d) (Ni-W)$_{B=0.4\ T/per}$

5.1.3 Corrosion study

The effect of *B* on coating characteristics such as appearance, elemental composition, thickness, microhardness and corrosion resistance are given in Table 5.1. All the coating characteristics were found to have a close relationship with the amount of W content present in the coatings and hence, on the direction and intensity of *B* applied during deposition. The coatings developed under perpendicular *B* was found to have the maximum W content and thereby the optimal characteristics. The coating configuration (Ni-W)$_{B=0.2\ T/per}$ was obtained as the optimal coating in terms of W content, and also with maximum thickness, hardness and corrosion resistance (least CR). Overall, the coatings developed under perpendicular *B* was found to show superior characteristics over the coatings under parallel *B*.

133

Table 5.1- Effect of B on the deposit characteristics of Ni-W alloy electrodeposited from optimized bath at 303 K

Coating configuration	Wt.% of W	Thickness (µm)	Vicker's microhardness V_{100} (GPa)	$-E_{corr}$ (mV *vs.* SCE)	i_{corr} (µA cm^{-2})	CR ($\times 10^{-2}$ mm y^{-1})
(Ni-W)$_{B=0.1\ T/par}$	21.6	16.2	3.85	373	3.1	2.41
(Ni-W)$_{B=0.2\ T/par}$	18.4	15.8	3.62	395	4.3	3.85
(Ni-W)$_{B=0.3\ T/par}$	15.1	15.7	3.40	428	5.2	4.81
(Ni-W)$_{B=0.4\ T/par}$	13.7	15.2	3.31	442	6.1	5.11
(Ni-W)$_{B=0.1\ T/per}$	27.1	16.4	4.16	401	2.9	2.10
(Ni-W)$_{B=0.2\ T/per}$	32.4	16.8	4.32	361	1.1	0.14
(Ni-W)$_{B=0.3\ T/\ per}$	20.3	15.6	3.74	344	4.2	3.11
(Ni-W)$_{B=0.4\ T/\ per}$	18.1	15.2	3.51	325	4.8	4.13
(Ni-W)$_{B=0\ T}$	12.4	15.9	3.22	487	6.5	5.35

From the data, it may be noted that the corrosion resistance of MED coatings, deposited under applied B has increased drastically, compared to the one under natural convection ($B = 0$ T). Further, it is evident that the effect is more pronounced when B is applied perpendicular to the direction of flow of ions. The potentiodynamic polarization and EIS behaviors of MED Ni-W alloy coatings, developed under applied B of varying intensities (from 0.1 T to 0.4 T) in parallel direction are shown in Fig. 5.7, and the corresponding data are given in Table 5.1.
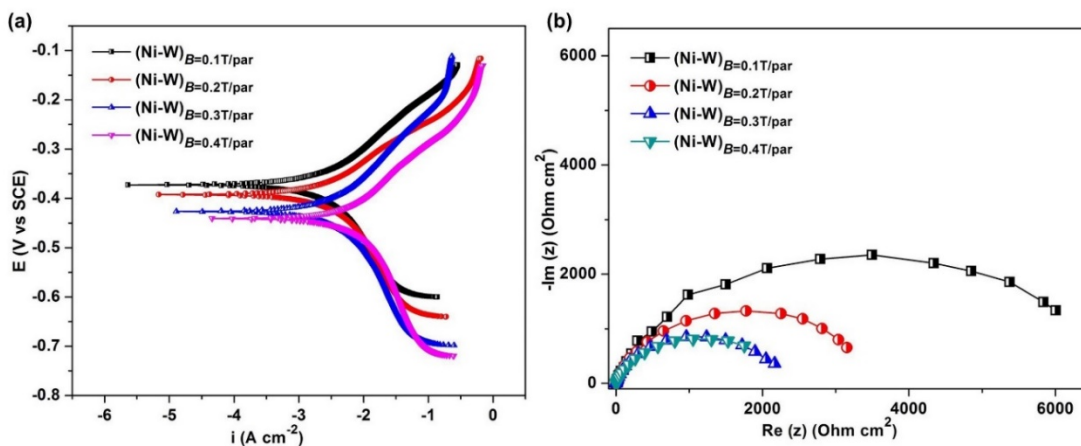
Fig. 5.7- The potentiodynamic polarization and EIS responses of MED Ni-W alloy coatings developed from optimal bath under varying intensities of *B*, applied in parallel direction

The Tafel curves of the MED Ni-W alloy coatings achieved under parallel *B* of varying intensities show a gradual increase in CR, and also the E_{corr} values were found to be shifted towards the more negative side as shown in Fig. 5.7(a). The Tafel curve fitting results given in Table 5.1 confirms the decrease in corrosion resistance of the coatings with an increase in strength of applied *B*, in parallel direction. The EIS responses also support the same observations as obtained from Tafel polarization study. The depressed semicircles of decreased diameter with an increase in the intensity of *B*, in parallel direction, again confirms the trend in corrosion resistance of MED coatings (Fig. 5.7(b)). Among the MED coatings obtained under parallel field, the coating configuration (Ni-W)$_{B=0.1 T/par}$ was found to be the best with least CR, nobler E_{corr} value and maximum diameter for the EIS response. Further, the Tafel polarization and EIS responses of the MED coatings developed under varying intensities of *B*, applied in perpendicular direction, was also recorded and shown in Fig. 5.8.
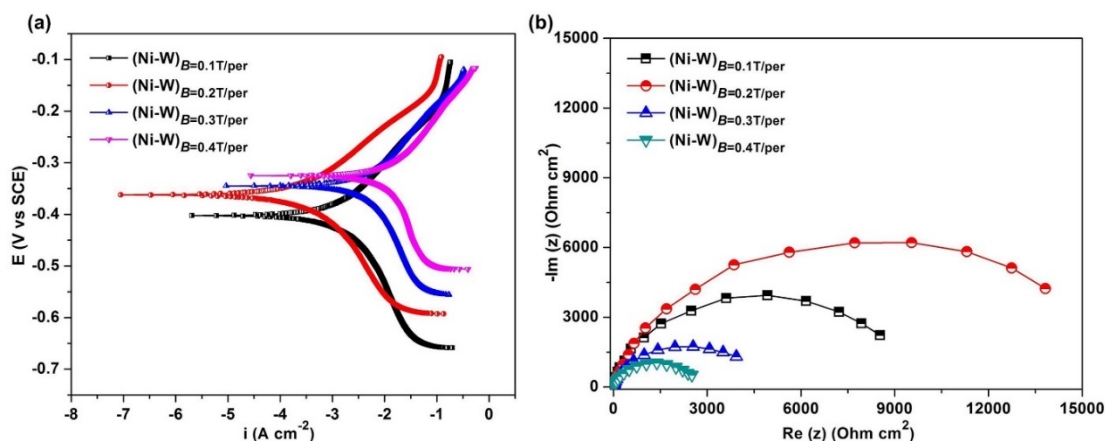
Fig. 5.8- Potentiodynamic polarization and EIS responses of MED Ni-W alloy coatings, developed from optimal bath under varying intensities of B, applied in perpendicular direction

It may be noted that, Fig. 5.8 and the corresponding data in Table 5.1 shows the experimental evidence for the trend in corrosion resistance behavior of MED coatings developed under perpendicular B. The CR of MED coatings was found to be decreased only up to an optimal intensity of B (0.2 T), and then increased (Table 5.1). The EIS responses also support the same observation with the largest diameter of the Nyquist plot for coating configuration $(Ni-W)_{B=0.2\ T/per}$. Further, an EEC fitment of the Nyquist responses was also made to simulate the behavior at the electrode/electrolyte interface. A representative fitment result and the obtained EEC are shown in Fig. 5.9.

The simulated circuit was found to be similar to a simple Randles circuit with R_s, R_{ct} and Q as the circuit elements [Barsoukov and Macdonald 2005]. The data pertaining to the fitment of MED coatings developed under different conditions of applied B are given in Table 5.2. The fitment results again support the corrosion behavior of the coatings in terms of CR values as tabulated in Table 5.1. The R_{ct} values of the coatings were observed to be large for those developed under perpendicular B than parallel, under same intensities of B. Moreover, the variation in R_{ct} and CR values show a close relationship with the W content in the coating developed under different conditions of B. The coating configurations, $(Ni-W)_{B=0.1\ T/Par}$ and $(Ni-W)_{B=0.2\ T/Per}$ were found to be the optimal coatings with large R_{ct} values and least capacitance values, under parallel and perpendicular directions of B.
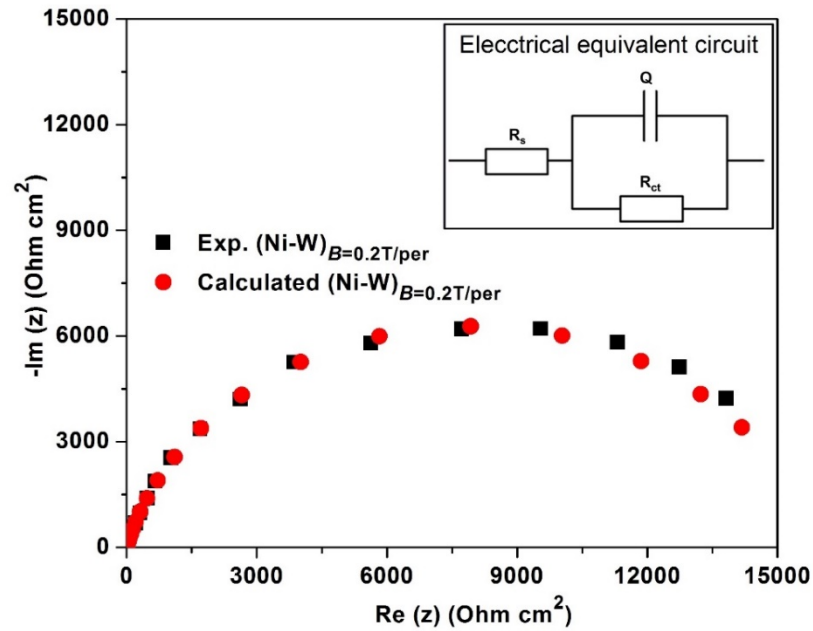
Fig. 5.9- A representative EEC fitment of the Nyquist responses and the obtained circuit (in the inset)

The obtained experimental results show a strong dependence of the coating characteristics such as composition, structure, morphology, physical properties and corrosion resistance on the intensity and direction of the applied magnetic field. The effect of applied B on the process of electrodeposition or the mechanism of MED responsible for the improved properties are attributed to the enhanced mass transport resulted from the MHD effect, due to Lorentz force [Monzon and Coey 2014, Fahidy 1983, Waskaas and Kharkats 1999, Tacken and Janssen 1995, Koza et al. 2008, Bund et al. 2003].

Table 5.2- The EEC parameters of the MED Ni-W alloy coatings developed under different conditions of *B*

Ni-W coating configuration	R_s (Ohm cm^2)	R_{ct} (Ohm cm^2)	Q (µF cm^{-2})
(Ni-W)$_{B=0.1\ T/par}$	0.91	5816	68.5
(Ni-W)$_{B=0.2\ T/par}$	1.0	3214	118.1
(Ni-W)$_{B=0.3\ T/par}$	1.5	2216	162.6
(Ni-W)$_{B=0.4\ T/par}$	1.6	1824	171.7
(Ni-W)$_{B=0.1\ T/per}$	1.0	8316	44.8
(Ni-W)$_{B=0.2\ T/per}$	1.0	14809	23.5
(Ni-W)$_{B=0.3\ T/per}$	1.2	4252	96.4
(Ni-W)$_{B=0.4\ T/per}$	1.4	2684	141.3
(Ni-W) $_{B=0\ T}$	1.0	1497	178.4

5.1.4 Effect of magnetic field

The improved corrosion resistance of MED coatings is mainly attributed to change in composition, structure and morphology of the deposits compared with the ED coatings. As W content in the deposit was almost impossible to increase further by tuning the applied c.d. (above 4.0 A dm^{-2}) in a normal deposition, MED technique was found to be effective in enhancing the convective effect [Mohanta and Fahidy 1978, Fahidy 1983], through magnetic field induced or forced convection at the cathodic diffusion layer [Krause et al. 2007, Devos et al. 2000, Monzon and Coey 2014, Fahidy 1973], and thereby to enhance the W content in the coating. The W content was found to be maximum in MED coating developed by applying *B* in perpendicular direction than in parallel direction. This can be explained by the MHD effect, arises mainly due to Lorentz force (given by the equation $F_L = qvB\ \sin\theta$), is maximum under the perpendicular magnetic field, i.e., when the angle between the magnetic field and c.d. is 90˚ ($\theta = 90$˚) [Fahidy 1983, Koza et al. 2008, Aaboubi and Msellak 2016]. Whereas, under parallel magnetic field it will be zero ($\theta = 0$). A schematic showing the

mechanism of MED under an applied magnetic field in the perpendicular direction is given in Fig. 5.10.

In conventional deposition, ions move in the direction of applied c.d. [Dini 1993], whereas in the presence of applied B, in perpendicular direction, the ions can move in circular path influenced by the Lorentz force acting on them under electromagnetic conditions of deposition (Fig. 5.10(a)) [Waskaas and Kharkats 1999, Koza et al. 2010, Fahidy 1973]. This movement of ions in circular path leading to an enhanced mass transport near the cathode surface and thereby reduces the double layer thickness as shown in Fig. 5.10(b) [Krause et al. 2007, Jha and Aina 2016, Ebadi et al. 2012]. The forced convection and reduction in double layer thickness leading to increase in i_L value of the reluctant metal (W) and thereby its preferential deposition [Fahidy 1983]. Whereas, in the case of applied B in parallel direction, the Lorentz force is zero and hence the extent of magnetically stimulated convective effect is less as compared with that under perpendicular direction [Koza et al. 2008, Fahidy 1973, Matsushima et al. 2008]. Even though the Lorentz force is zero, some other forces like paramagnetic forces and magnetic susceptibility of the solution in the presence of applied B (in parallel direction) can impart changes in the composition, structure and morphology of the coatings [Aaboubi and Msellak 2016, Li et al. 2013]. However, the variation in such effects with a slight difference in intensity of applied B may be negligible. Overall, though the parallel B is less effective in inducing the mass transport process compared with perpendicular B, the applied magnetic field in parallel direction can make a distinction in coating properties from the coating developed without any applied magnetic field and the coatings developed at different intensities of B.

Magnetoelectrodeposition

B_{in}

ΔV

F

v

v

F

v

q

$\leftarrow i$

Enlarged view of the process taking place during
magnetoelectrodeposition under perpendicular magnetic field

(b)

Enhanced mass
transport of charged
electroactive species
under an applied
magnetic field, B

δ_{MED} δ_{ED}

$\odot$ **B**

i_L **MED**

i_L **ED**

Electrode

Variation in diffusion layer
thickness given by the relation

$$i_L = \frac{nFDC_B}{\partial}$$

i

Natural convection

Distance from the cathode

Reduction in double layer thickness due to
magnetohydrodynamic effect, induced by applied magnetic

Fig. 5.10- The schematic of mechanism of MED, under an applied *B* in perpendicular direction; a) the movement of charged species near the cathode surface, and b) the reduction in double layer thickness and thereby the enhanced mass transport due to MHD effect

The observed improvement in properties of the MED coatings is attributed to the increased W content in the coating, effected from the magnetic field stimulated mass transport. Whereas, in the case of both parallel and perpendicular magnetic field, a

saturation point is observed in the applied intensity of B. In parallel, $B = 0.1$ T was observed as the optimal field intensity and any further increase in the intensity of B was found to have no impact on enhancing the coating characteristics. This lowest intensity of B applied in parallel direction brings a distinction in coating characteristics from the ED coating, than the coatings developed at other higher intensities. This is attributed to the increase in hydrogen evolution during deposition, at higher intensities of B, and which leads to the deformation of the nodular growths at the coating surface along with the formation of micro-cracks (Fig. 5.2). In the case of perpendicular B, an applied magnetic field intensity of 0.2 T was found to be the optimal. Initially, the coating characteristics were found to be enhanced with the intensity of B and then decreased after the optimal value. This decrease in coating characteristics in terms of corrosion resistance is also attributed to the increased evolution of hydrogen during deposition leading to the formation of porous deposits (Fig. 5.3). Further, the coatings achieved under conventional conditions and parallel B were found to have micro-cracks on the surface, but those obtained under perpendicular B was observed to be cracks-free. The micro-cracks on the coatings are attributed to the hydrogen embrittlement, resulted from the codeposition of H_2 gas during deposition [Brenner 1963]. In the case of deposition at perpendicular B, the MHD effect enhances the fast discharge of the gas bubbles from the surface of the coating immediately after its formation [Koza et al. 2009, Balzer and Vogt 2003] and prevents the development of strain in the coatings. This mechanism of fast disentanglement of the H_2 gas bubbles from the surface through the combined effect of Lorentz force [Monzon and Coey 2014] and hydrogen buoyancy force [Lin and Hourng 2014] inhibits the formation of micro-cracks in the coatings developed under perpendicular B. Whereas, this effect also attains a saturation point at $B = 0.2$ T and then decreases due to the large increase in H_2 evolution with increase in W content, which is having low hydrogen overvoltage [Tsyntsaru et al. 2012] leading to the formation of porous deposits at higher strengths of B.
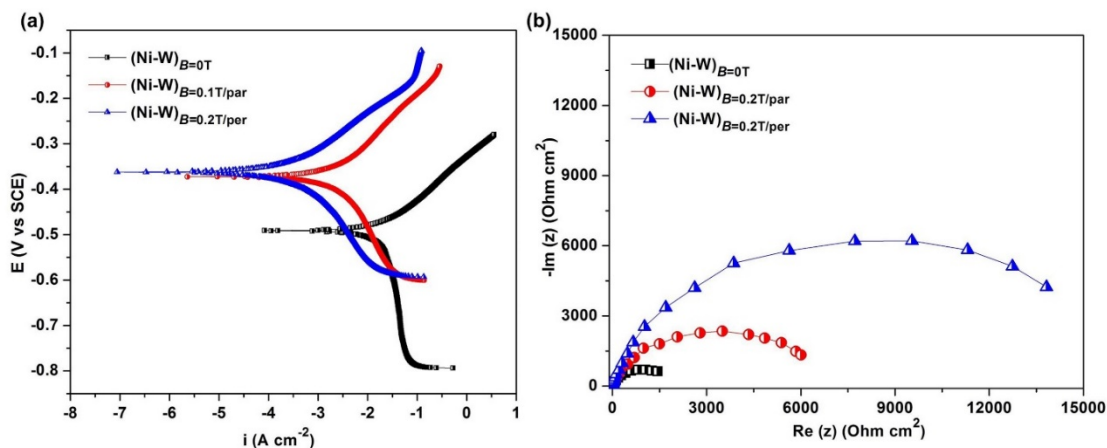
Fig. 5.11- Comparison of corrosion behaviors of the ED and MED coatings through: a) potentiodynamic polarization method, and b) EIS method

A comparison of the potentiodynamic polarization and EIS responses of the ED and MED coatings are given in Fig. 5.11. The enhanced corrosion resistance of the MED coatings is mainly due to the increased W content. Among the MED coatings developed by applying B in parallel and perpendicular directions, the corrosion resistance was found to be increased with W content irrespective of the direction of B. The coating with maximum W content (32.4%), $(Ni-W)_{B=0.2\ T/per}$, was obtained as the optimal coating in terms of corrosion resistance. The Tafel and Nyquist responses of the optimal Ni-W alloy coatings developed under conditions of conventional, parallel and perpendicular B supports the enhancement in corrosion resistance with W content in the coating. The lower CR and more noble E_{corr} value along with the largest R_{ct} value confirm $(Ni-W)_{B=0.2\ T/per}$ as the best coating. The cracks free surface with more compact spherical grains is ascribed to the high corrosion resistance character of $(Ni-W)_{B=0.2\ T/per}$ (Fig. 5.1(c)). Further, the drastic improvement in the corrosion protection efficacy of MED coatings are attributed to the W-rich unique phase structures formed, namely Ni_4W (211), Ni_4W (130), $Ni_{17}W_3$ (220) and NiW (106) which do not correspond to any known phases in ED Ni-W alloy coatings, evidenced by XRD analyses (Fig. 5.4).

5.2 CONCLUSIONS

The following observations were made as conclusions after analyzing the experimental results obtained from the corrosion study of ED and MED Ni-W alloy coatings:

1. Under optimal conditions, MED coatings exhibit many fold increase in corrosion resistance compared to conventional ED coatings, achieved from the same bath.

2. The limitations, like low i_L value and induced type of codeposition towards the development of more corrosion resistant coatings from the proposed bath has been successfully resolved through the development of cracks free W- rich coatings through MED approach.

3. The enhanced corrosion resistance of the MED coatings (both parallel and perpendicular) is ascribed to the increase in W content of the alloy due to increased i_L.

4. The decrease of diffusion layer thickness due to applied magnetic field is attributed to the better crystallographic orientation, and hence the corrosion resistance of the MED coatings.

5. Drastic improvement in the corrosion protection efficacy of MED coatings is attributed to the W-rich unique phases, namely Ni_4W (211), Ni_4W (130), $Ni_{17}W_3$ (220) and NiW (106) which do not correspond to any known phases in ED Ni-W alloy coatings.

6. Changed crystallographic orientation and surface morphology of MED coatings, responsible for better corrosion protection efficacy were explained in the light of MHD effect.

7. The surface morphology and corrosion performance of MED coatings were found to be the function of MHD effect, in both direction and intensity of applied magnetic field.

CHAPTER 6

ELECTROCATALYTIC ACTIVITY OF ELECTRODEPOSITED

Ni-W AND Ni-P ALLOY COATINGS

Alloy electrodeposition   **Water splitting**
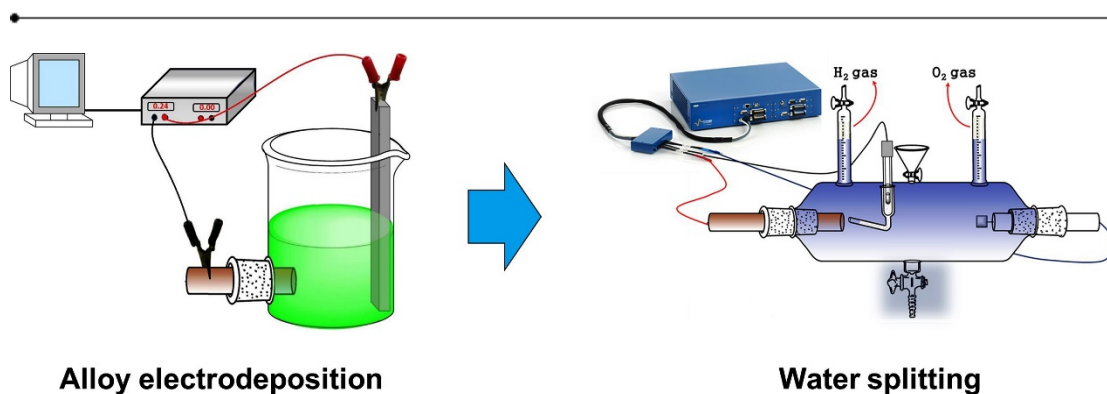
The chapter discusses the development of electroactive Ni-W and Ni-P alloy coatings for alkaline water splitting reaction. The electrocatalytic activity of Ni-W and Ni-P alloy coatings, deposited at different c.d.'s were tested in 1.0 M KOH medium. The alkaline water splitting efficiency of the coatings towards HER and OER were examined using electrochemical methods such as CV and CP. The practical effectiveness of the test electrodes were ascertained by quantifying the amount of H_2 and O_2 gases evolved from the respective electrodes during analysis. Further, the long-term stability of coatings under electrocatalytic working conditions was confirmed in terms of corrosion resistance using electrochemical methods. A dependency of the electrocatalytic activity for HER and OER with c.d., and hence to the relative amount of the alloying elements was found. The composition of the alloy showing maximum activity towards HER was found to have an adverse effect on OER and vice versa. The variation in electrocatalytic activities of the coatings developed at different c.d.'s were explained in the light of their phase structure, surface morphology and chemical composition, with plausible mechanisms and illustrations.

6.1 RESULTS AND DISCUSSION

The experimental results obtained for the electrocatalytic activity study for HER and OER on Ni-W and Ni-P alloy coatings are reported below.

6.2 ELECTROCATALYTIC ACTIVITY OF Ni-W ALLOY COATINGS

The Ni-W alloy coatings were deposited at different c.d.'s (1.0 – 4.0 A dm^{-2}) from the optimal bath for electrocatalytic study as explained in Chapter-2. The morphological structural and compositional characterization of the coatings developed at different c.d.'s were discussed in Chapter-4. Further, all the developed coatings were found to be corrosion resistant under electrocatalytic working conditions. The electrocatalytic activity of the test electrodes towards HER and OER were examined using CV and CP techniques, as described in Chapter-2. HER and OER are the most studied electrochemical reactions due to its widespread applications in many electrochemical technologies such as, alkaline water electrolysis and chlor-alkali production [Lupi et al. 2009, Zhu et al. 2015]. The CV technique allows determination of a set of parameters that are useful for the evaluation of the electrode performance. The hydrogen desorption peak area is one of the main parameters among the electrode characteristics. It depends on the active specific surface of the deposit: the larger the active specific surface, the higher the amount of hydrogen produced during the reduction of the hydrogen adsorbed on the electrode. Another important parameter characterizing the electrode material is the discharge potential of hydrogen; determining the interception of the voltammetric curve tangent with the x-axis. It indicates the electrocatalytic properties of the cathodic material used in the water electrolysis and thus allows evaluation of the energy consumption in hydrogen production [Lupi et al. 2009]. The CP study for a fixed time (1800 s) by applying a definite cathodic or anodic c.d. (-300 mA cm^{-2}) gives the information about the stability and robustness of the electrode material under electrocatalytic working conditions. In this method, when a constant current is flowing between two electrodes, the change in potential is monitored as a function of time with respect to a suitable reference electrode. The basis of this experiment is to find the redox (electron transfer) reactions that occurs on the surface of working electrode to support the applied current. Further, the practical effectiveness of each test electrodes was

evaluated by quantifying the amount of H_2 or O_2 gas liberated during the analysis. Accordingly, electrocatalytic behaviors of the Ni-W alloy coatings for alkaline water splitting of both HER and OER was studied.

6.2.1 Electrocatalytic activity for alkaline HER

6.2.1.1 Cyclic voltammetry study for HER

The water splitting ability of Ni-W alloy coatings for HER was obtained by CV study within a potential ramp of 0.0 V to -1.6 V at a scan rate of 50 mV s^{-1}, for 50 cycles. The scan rate of 50 mV s^{-1} was selected amongst the different scan rates, based on the better readability of data. For CV curves of 50 cycles, the cathodic current response at -1.6 V was found to be decreased sequentially with increase in the number of cycles and then becomes stable. This may be attributed to the progressive resistance induced by the H_2 bubbles formed on the catalyst surface; and the stable and reproducible CV curves obtained indicates a state of equilibrium between adsorption and desorption of H_2 gas on the electrode surface [Ullal and Hegde 2014]. The current response corresponds to the equilibrium for H_2 evolution is called, cathodic peak current density, abbreviated as i_{pc}. Accordingly, the CV responses of different Ni-W alloy deposits having variation in relative i_{pc} values are shown in Fig. 6.1, and the corresponding electrochemical data are given in Table 6.1. From Fig. 6.1, it may be noted that the Ni-W coating obtained at 4.0 A dm^{-2} exhibits the highest i_{pc} value (-0.66 A cm^{-2}), compared to the other coatings. Thus the highest i_{pc} values recorded by Ni-W coatings deposited at 4.0 A dm^{-2} may be attributed to the highest W content (12.5 wt. %), compared with all other coatings deposited from the same bath. Further, it may be noted that the corresponding data reported in Table 6.1 shows a gradual decrease in the onset potential for H_2 evolution, with increase in deposition c.d. This variation in onset potential for H_2 evolution further confirms that the Ni-W alloy coatings deposited at high c.d. are more congenial for HER. Thus the electrocatalytic behavior of Ni-W alloy deposits was found to have a close relationship with the deposition c.d., a dictating parameter of surface morphology, composition and phase structure of the deposits. An experimental study by Herraiz et al. (2011), demonstrated that the intrinsic catalytic activity for HER on Ni-based electrodeposits depend on the synergism among the catalytic properties of Ni and of its counterpart's. Hence, it may be concluded that the highest realized i_{pc} value of Ni-W

coating corresponding to 4.0 A dm^{-2} is attributed to the synergistic effect of lower Ni content (87.5 wt.%) and higher W content (12.5wt. %) of the deposit, compared with the other coatings.
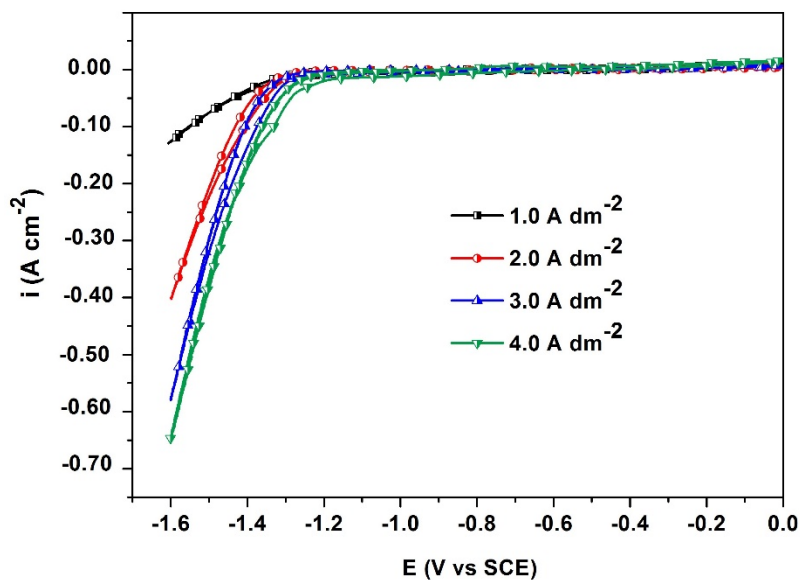
Fig. 6.1- The CV responses of Ni-W alloy coatings deposited at different c.d.'s towards HER

6.2.1.2 Chronopotentiometry study for HER

The practical effectiveness of each test electrodes was evaluated by measuring the amount of H$_2$ gas liberated during the analysis. The chronopotentiograms of Ni-W alloy coatings deposited at different c.d.'s along with the amount of hydrogen gas liberated (in the inset) are shown in Fig. 6.2. It may be noted that the maximum amount of H$_2$ gas was produced by the Ni-W alloy coating deposited at 4.0 A dm^{-2}, compared to the coatings deposited at other c.d.'s. This observation further confirms the fact that the Ni-W coating developed at 4.0 A dm^{-2} as the most electrocatalytically active coating towards HER. An initial sharp decrease of potential immediately after starting the electrolysis as observed in some coatings may be due to an increased reduction of H$^+$ to H$_2$ as the current is applied suddenly. However, the constant potential immediately after a few minutes of starting electrolysis as observed in Fig. 6.2 indicates that the HER takes place unabatedly on the electrode surface at applied c.d.
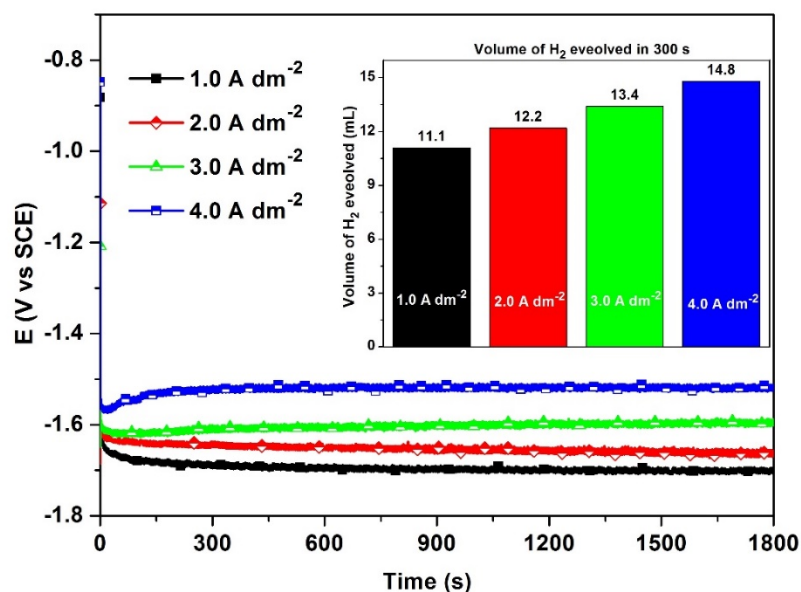
Fig. 6.2- CP responses of the Ni-W alloy coatings under impressed cathodic current of -300 mA cm^{-2} along with the volume of H$_2$ gas evolved from each test electrodes in 300 s in the inset

Table 6.1- The HER parameters of Ni-W alloy coatings developed at different c.d.'s from optimal bath

Coating configuration (A dm^{-2})	Cathodic peak c.d. at -1.6 V (A cm^{-2})	Onset potential for H$_2$ evolution (V vs SCE)	Volume of H$_2$ evolved in 300 s (mL)
1.0	-0.11	-1.39	11.1
2.0	-0.42	-1.32	12.2
3.0	-0.58	-1.26	13.4
4.0	-0.66	-1.21	14.8

6.2.2 Electrocatalytic activity for OER

6.2.2.1 Cyclic voltammetry study for OER

The Ni-W alloy coatings deposited at different c.d.'s were also tested for its electrocatalytic activity for OER in 1.0 M KOH medium, in the same line as done for HER. The CV experiments for OER on Ni-W alloy deposits were conducted in the potential range of 0.0 to +0.75 V at a scan rate of 50 mV s^{-1}, and the corresponding CV

149

responses are shown in Fig. 6.3. The onset potentials for continuous evolution of O_2 gas for each test electrodes developed at different c.d.'s are shown in the CV curves. It was observed that the Ni-W alloy coating deposited at 1.0 A dm^{-2} shows good catalytic activity towards OER with the lowest onset potential (0.51 V) and maximum i_{pa} value at 0.75 V (Fig. 6.3 and Table 6.2). The mechanism proposed for OER involves the adsorption of OH$^-$ from the medium onto the surface of the electrode followed by the formation of adsorbed oxygen through electron transfer leading to the formation of O_2 gas [Lyons and Brandon 2008, Jüttner 1984]. The detailed mechanism of OER is explained in section 6.4.2.

The cathodic and anodic peaks observed in the cyclic voltammograms (Fig. 6.3) in the applied potential range (0.0 to +0.75V) are due to the formation and reduction of a NiOOH layer. In this potential range, the substrate surface is covered with a thin p-type semiconducting layer of NiO(H$_2$O) [Peeters et al. 2001], and can enhance the OER within the potential range by enhancing the OH$^-$ adsorption. Whereas, apart from this potential range, the activity will be limited due to the lack of formation of a semiconducting layer of NiO(H$_2$O). This is in agreement with the well-established generalization on OER that, it normally takes place on a metal surface which is firstly covered with appropriate oxides [Kubisztal and Budniok 2008]. In the present study, the coating developed at 1.0 A dm^{-2} was found to show the maximum activity towards OER due to its higher Ni content leading to better adsorption of OH$^-$ through redox reaction under the applied potential.
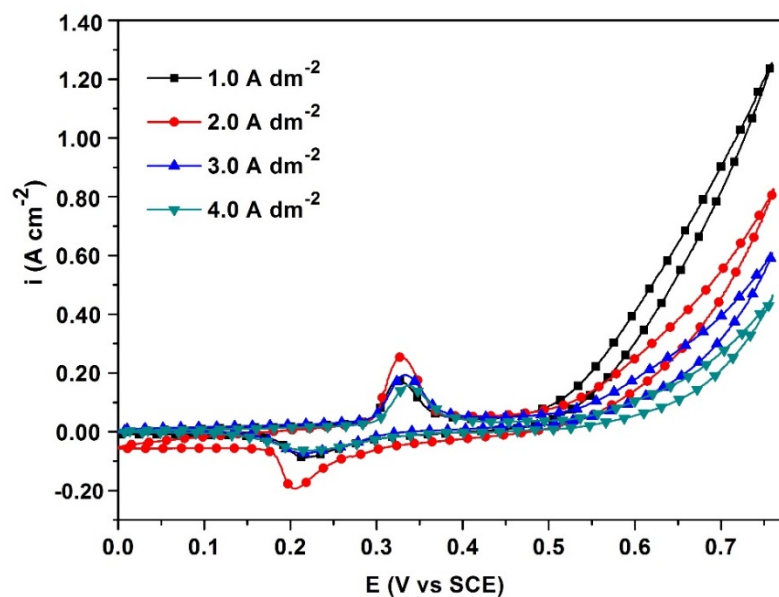
Fig. 6.3- CV responses of Ni-W alloy coatings deposited at different c.d.'s towards OER

6.2.2.2 Chronopotentiometry study for OER

The CP responses and the amount of O_2 gas evolved during the analysis from each test electrodes are shown in Fig. 6.4. As the current pulse (anodic) of +300 mA cm^{-2} was applied, a sharp increase in the potential was observed until a potential at which OH^- is oxidized to O_2 is reached. In other words, an equilibrium state is reached between the newly forming bubble and bubbles escaping from the surface of the electrode [Ullal and Hegde 2014, Herraiz-Cardona et al. 2011]. The inset of Fig. 6.4 shows the relative amount of O_2 liberated in 300 s on each Ni-W alloy coating deposited at different c.d.'s, and the corresponding volumes are given in Table 6.2. In this case, the amount of O_2 gas liberated on the surface of coating deposited at 4.0 A dm^{-2} is less compared to the other coatings. In other words, the Ni-W alloy deposited at 1.0 A dm^{-2} exhibits the lowest potential for O_2 evolution. Hence, the alloy coating deposited at 1.0 A dm^{-2} is more electroactive for OER compared to the other coatings. Thus, the experimental results from the HER and OER of electrodeposited Ni-W alloy coatings deposited at different c.d.'s, it may be inferred that the surface favoring the cathodic reaction has an adverse effect on anodic reaction and vice versa. It may be due to the unique phase structure and composition of the coatings deposited at different c.d.'s, but from the

same bath. To sum up, a variation in H_2 and O_2 evolution with c.d. was found as shown in Fig. 6.2 and Fig. 6.4, respectively. This indicates a synergism between the good catalytic property of W (due to low hydrogen overvoltage) and Ni (having increased adsorption of OH^- ions) are responsible for the better electrocatalytic activity of the Ni-W alloy coatings as cathode and anode, respectively.
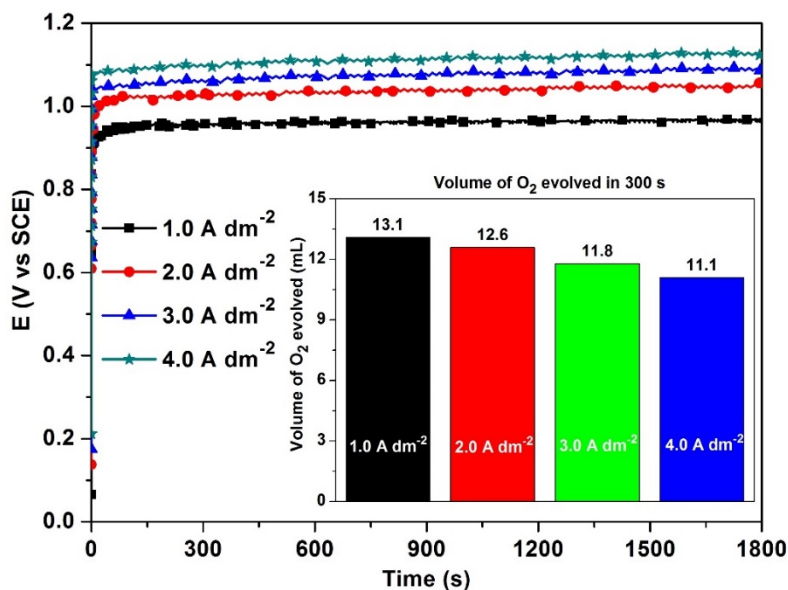
Fig. 6.4- CP responses of the Ni-W alloy coatings under an impressed anodic current of +300 mA cm^{-2} along with the volume of O_2 evolved in 300 s on each test electrodes are shown in the inset

Table 6.2- The OER parameters of Ni-W alloy coatings deposited at different c.d.'s from optimal bath

Coating configuration (A dm^{-2})	Anodic peak c.d. at 0.75 V (A cm^{-2})	Onset potential of O_2 evolution (V *vs* SCE)	Volume of O_2 evolved in 300 s (mL)
1.0	1.25	0.51	13.1
2.0	0.83	0.53	12.6
3.0	0.61	0.57	11.8
4.0	0.45	0.61	11.1

6.3 ELECTROCATALYTIC ACTIVITY OF Ni-P ALLOY COATINGS

The electrodeposition and characterization of Ni-P alloy coatings at different c.d.'s from the proposed bath were discussed in Chapter-4. The Ni-P alloy coatings developed at 2.0, 4.0 and 6.0 A dm^{-2} (only selected coatings) were tested for its electrocatalytic activity towards HER and OER in 1.0 M KOH, using electrochemical methods as discussed in Chapter-2. The obtained experimental results of investigation are reported below.

6.3.1 Hydrogen evolution reaction

6.3.1.1 Cyclic voltammetry study for HER

The electrocatalytic behavior for HER on electrodeposited Ni-P alloy test electrodes from the proposed bath at different c.d.'s were studied through CV method, in a potential window of 0.0 V to -1.6 V, at a scan rate of 50 mV s^{-1} for 50 cycles. It was observed that the initial cycles showed larger i_{pc} values, which eventually decreased with increase in number of cycles. This may be attributed to progressive resistance induced by the hydrogen bubbles formed on the catalyst surface, and a stable and reproducible CV curves were obtained at the end. This indicates a state of equilibrium for formation and detachment of hydrogen gas on electrode surface [Du et al. 2000, Ledendecker et al. 2015]. After about 30 cycles, the i_{pc} value was found to be constant, and the CV curves were observed to retrace the path of previous cycle. This situation is corresponding to the condition where, the rate of adsorption of H atom on the surface for the formation of H$_2$ gas is equal to the rate of desorption of H$_2$ gas [Du et al. 2000]. The CV curves for HER of Ni-P alloy coatings, deposited at different c.d.'s (2.0, 4.0 and 6.0 A dm^{-2}) are shown in Fig. 6.5, and the corresponding electrochemical data are given in Table 6.3. From Fig. 6.5, it may be noted that there is no much change in the i_{pc} values and onset potential for HER. Hence, the CV curves of all Ni-P alloy coatings for HER looks overlapping as may be seen in Fig. 6.5. Almost same CV patterns for coatings at different c.d.'s may be due to their lookalike morphological structures. However, the enlarged view of CV curves (shown in the inset) in Fig. 6.5 indicate that the Ni-P alloy coating at 4.0 A dm^{-2} is more favorable for hydrogen production with a

maximum current response. Hence, it was considered as the optimal c.d. for further modification of the electrode material.
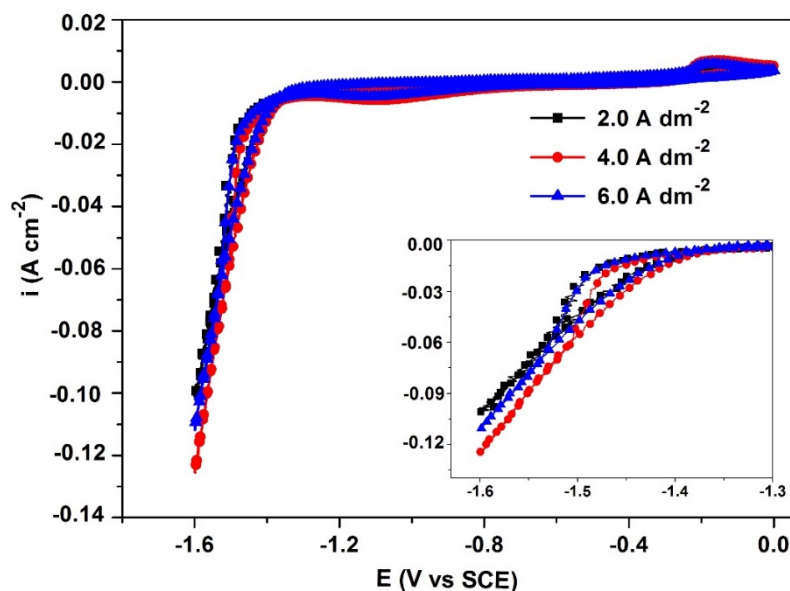
Fig. 6.5- The CV curves for HER on Ni-P alloy coatings deposited at different c.d.'s and inset shows the magnified view of CV curves displaying variation in i_{pc} values

6.3.1.2 Chronopotentiometry study

The CP study for HER on Ni-P alloy coatings achieved at selected c.d.'s were made at a constant current of -300 mA cm^{-2} for a duration of 1800 s, and the corresponding chronopotentiograms are shown in Fig. 6.6 The electrocatalytic efficiency of Ni-P alloy coatings towards HER were evaluated quantitatively by measuring the amount of H_2 liberated for first 300 s. The volume of H_2 gas evolved during the analysis are reported in Table 6.3, and shown in the inset of Fig. 6.6. It may be noted that the Ni-P alloy coating developed at 4.0 A dm^{-2} produced the maximum amount of H_2 gas, compared to the coatings at 2.0 and 6.0 A dm^{-2}. This confirmed the fact that the Ni-P coating achieved at 4.0 A dm^{-2} as the most electrocatalytically active towards alkaline HER. Further, an initial sharp decrease of potential immediately after starting of electrolysis was observed in the CP responses of all the three coatings. This is attributed to the progressive depletion of the electrolyzed species at the surface of working electrode, where the reduction of H^+ ions from the solution takes place to liberate H_2 gas, and eventually reaches a state of equilibrium between H^+ ions and H_2 [Zhu et al. 2015].

However, after few minutes of starting the electrolysis almost constant potential is reached as may be seen in Fig. 6.6. At this stage hydrogen evolution takes place uninterruptedly on electrode surface at the applied c.d. This is due to the fact that, as the current pulse is applied all H^+ is reduced to H_2.
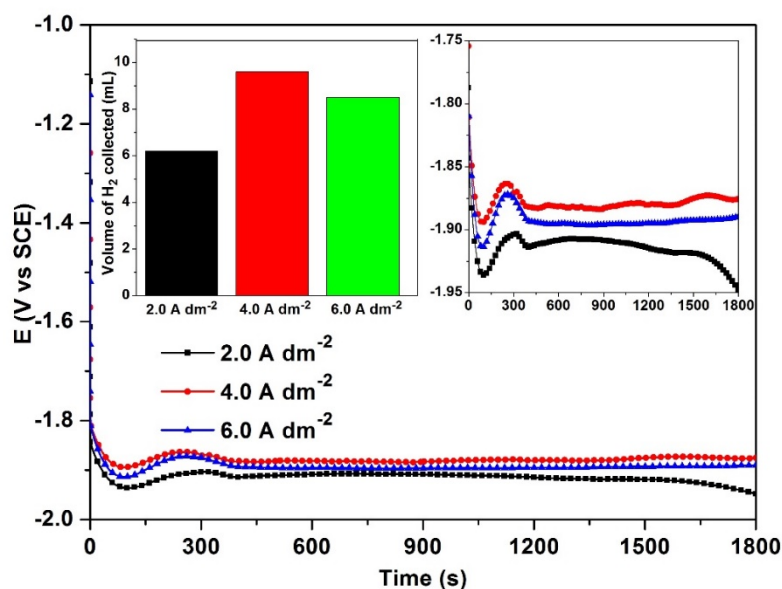
Fig. 6.6- CP curves for Ni-P alloy coatings under impressed cathodic current of -300 mA cm^{-2} along with the volume of H_2 evolved in 300 s on each test electrodes are shown in the inset

Table 6.3- The HER parameters of Ni-P alloy coatings developed at selected c.d.'s from the optimal bath

Coating configuration (A dm^{-2})	Cathodic peak c.d. at -1.6 V (A cm^{-2})	Onset potential of H$_2$ evolution (V *vs* SCE)	Volume of H$_2$ evolved in 300 s (mL)
2.0	-0.10	-1.39	6.2
4.0	-0.13	-1.30	9.6
6.0	-0.11	-1.34	8.5

155

6.3.2 Oxygen evolution reaction

6.3.2.1 Cyclic voltammetry study for OER

The CV study for Ni-P alloy coatings deposited at 2.0, 4.0 and 6.0 A dm^{-2} were conducted in the potential range of 0.0 to +0.75 V at a scan rate 50 mV s^{-1}, and the corresponding CV responses are shown in Fig. 6.7. The i_{pa} values and the corresponding onset potentials for OER on different electrode surfaces are reported in Table 6.4. From the CV curves shown in Fig. 6.7, the i_{pa} values for Ni-P alloy coating deposited at 2.0 A dm^{-2} and 6.0 A dm^{-2} was found to be more (respectively, 0.22 A cm^{-2} and 0.18 A cm^{-2}) compared to that of the coating deposited at 4.0 A dm^{-2}. Further, the Ni-P alloy coating obtained at 2.0 A dm^{-2} was found to show the highest i_{pa} value for OER, with the least onset potential. Hence, the Ni-P alloy coating deposited at 2.0 A dm^{-2} was selected as the optimal coating for OER, compared to other coatings.
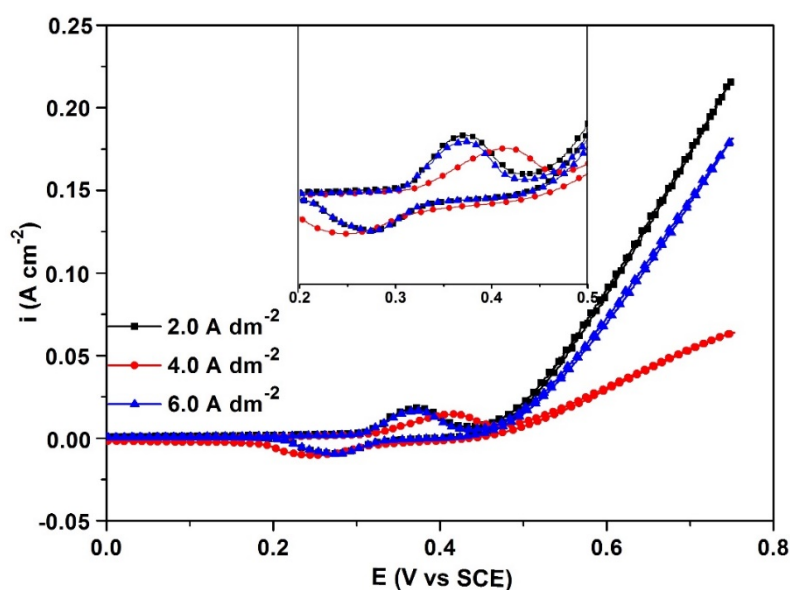
Fig. 6.7- CV responses of the Ni-P alloy coatings electrodeposited at different c.d.'s towards OER

6.3.2.2 Chronopotentiometry study

The electrocatalytic activity of Ni-P alloy coatings for OER was also tested using CP analysis and the amount of O$_2$ gas evolved during the analysis was measured in the similar way as discussed earlier, and the corresponding results are shown in Fig. 6.8. As the anodic current pulse of +300 mA cm^{-2} was applied, a sharp increase in the

potential was observed until a potential at which an equilibrium state is reached between the newly formed bubble and bubbles escaping from the surface of the electrodes [Gawad et al. 2013]. The relative amount of O_2 liberated in 300 s on each Ni-P alloy coatings deposited at different c.d.'s is shown in the inset of Fig. 6.8, and the corresponding volumes are given in Table 6.4. In this case, the coating developed at 2.0 A dm^{-2} was found to be the best for OER.
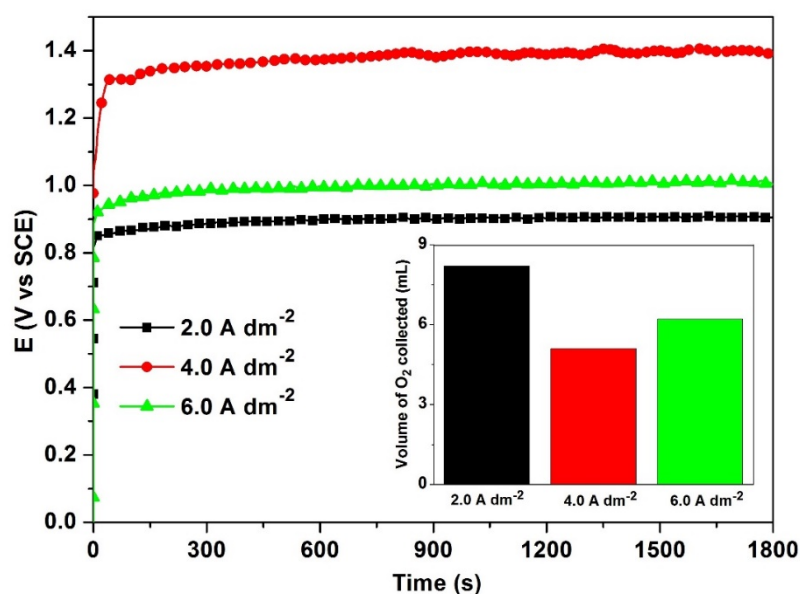
Fig. 6.8- CP responses of Ni-P alloy coatings under impressed anodic current of +300 mA cm^{-2} along with the volume of O_2 evolved in 300 s on each test electrodes are shown in the inset

Thus, from the current responses of cathodic and anodic process (i_{pc} and i_{pa}), their onset potentials, and the amount of hydrogen and oxygen gases liberated (Table 6.3 and 6.4), it may be inferred that the Ni-P alloy coating deposited at 4.0 A dm^{-2} is more suitable for HER and the coatings at 2.0 A dm^{-2} and 6.0 A dm^{-2} are more suitable for OER. In other words, the deposit characters of Ni-P alloy favorable for HER is not favorable to OER, in the same electrolyte. It may be explained by the fact that the evolution of oxygen is believed to be catalyzed by the redox transitions of interfacial oxycations between higher and lower oxidation states [Gawad et al. 2013]. Further, the oxygen evolution activity on Ni-P deposits is a function of the electrochemical properties of the redox pair prior to the onset of oxygen evolution. It is supported by

the CV of electrodeposited pure nickel in 1.0 M KOH, exhibiting anodic and cathodic peaks at 0.362 and 0.265 V respectively, corresponding to the NiOOH/Ni(OH)$_2$ transition [Omi et al. 1976]. Hence, the Ni-rich coatings show more activity towards OER than HER and vice versa.

Table 6.4- The OER parameters of Ni-P alloy coatings deposited at different c.d.'s from optimal bath

Coating configuration (A dm^{-2})	Anodic peak c.d. at 0.75 V (A cm^{-2})	Onset potential of O$_2$ evolution (V *vs* SCE)	Volume of O$_2$ evolved in 300 s (mL)
2.0	0.22	0.43	8.2
4.0	0.06	0.47	5.1
6.0	0.18	0.45	6.2

6.4 MECHANISM OF ALKALINE WATER ELECTROLYSIS

6.4.1 Synergistic effect of electrode composition on electrocatalytic activity

The experimental results of investigation on the electrocatalytic behavior of Ni-W and Ni-P alloy coatings, obtained at different c.d.'s, revealed that the composition of the coatings favorable for HER shows an adverse effect on OER, and vice versa.

In the case of Ni-W alloy coatings, a coating with 12.4 wt.% W (developed at 4.0 A dm^{-2}) and another one with 0.9 wt.% (developed at 1.0 A dm^{-2}) were found to be optimal for HER and OER, respectively. Further, the electrocatalytic activity towards HER was found to be increased with the increase in alloying element W. Whereas, in the case of Ni-P alloy coatings, a coating with 9.0 wt.% P (deposited at 4.0 A dm^{-2}) was found to be the most favorable electrode material for HER than the other coatings with lower (4.2 wt.%) and higher (13.5 wt.%) P content (deposited respectively at 2.0 A dm^{-2} and 6.0 A dm^{-2}). Contrarily, Ni-P alloy having 4.2 and 13.5 wt.% P (deposited at 2.0 A dm^{-2} and 6.0 A dm^{-2}, respectively) were found to be more favorable for OER. Unlike in the case of Ni-W alloy, the Ni-P alloy coatings were not found to show a regular increase in HER activity with P content, rather shows increase only up to an optimal composition. But still, it shows the composition dependence on HER and OER, i.e., the

HER active coating was found to show the least activity towards OER and vice versa. Hence, it may be inferred that the best electrocatalytic activity is attributed to the synergistic effect of Ni and alloying element (M), responsible for the formation of Ni-M alloy, having unique composition and phase structure [Peeters et al. 2001, Rosalbino et al. 2005].

The synergism between the good catalytic property of W (due to low hydrogen overvoltage) and Ni (having increased adsorption of OH$^-$ ions) contributed towards the better electrocatalytic activity of the Ni-W alloy coatings as cathode and anode, respectively. In the case of Ni-P alloy coatings, though there is no agreement on the reason why only certain amount of P introduced into Ni could enhance the HER, Burchardt (2000) claimed that the change in electronic structure of the alloy with the presence of P is responsible for the increase in activity. The presence of a large amount of P in the alloy causes an inhibition of the HER, on the other hand, a small amount of P catalyze the reaction. The catalytic effect towards HER is reduced when the P concentration in the alloy moves towards 0 wt.%, where the activity towards OER is found to be increased. It was also found that the adsorption strength of hydrogen on metal catalysts is closely related to the efficiency of hydrogen evolution [Nørskov et al. 2005]. If the binding between the adsorbed H and metal surface (M–H$_{ads}$) is too weak, activation of the hydrogen to the metal surface is difficult. On the other hand, strong hydrogen binding on the metal surface blocks the available reaction sites [Rosalbino et al. 2005]. It implies that the maximum rate of HER may occur only at a certain value of M–H$_{ads}$ bond strength [Nørskov et al. 2005, Narayan and Mungole 1985, Rosalbino et al. 2005]. Consequently, based on many reported works it was confirmed that Ni has the highest catalytic activity for HER among the non-noble metals due to the appropriate hydrogen adsorption energy and it is enhanced with the introduction of P [Du et al. 2000, Rosalbino et al. 2005].

Further, in general, the surface of Ni-M alloy coating with a specific composition of the alloying element M (M = W and P) as more favorable for cathodic reaction of hydrogen evolution (2H$^+$ + 2e$^-$ ↔ H$_2$), was found to be least favorable for anodic reaction of oxygen evolution (2OH$^-$ ↔ 1/2O$_2$ + H$_2$O). This behavior of the Ni-M alloy coatings is attributed to the basic difference in activation energy barrier for the kinetics of electron transfer process at the electrode/electrolyte interface for cathodic

(reduction) reaction and anodic (oxidation) reaction, responsible for H_2 and O_2 evolution, as shown schematically in Fig. 6.9.
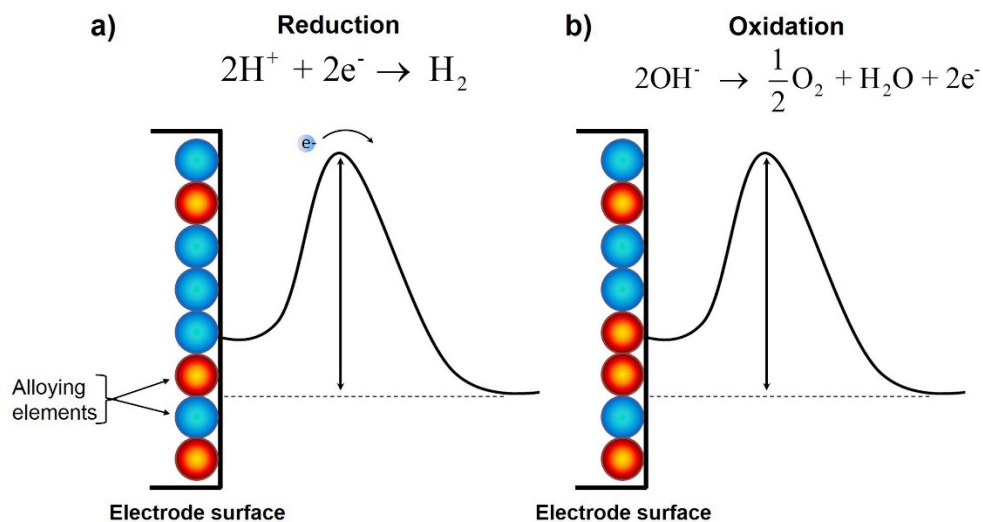
Fig. 6.9- Schematic representation of activation energy barrier favoring the kinetics of electron transfer for: a) HER on Ni-M alloy having a specific composition, and b) OER on Ni-M alloy having another specific composition

6.4.2 Mechanism of HER and OER

The factors responsible for increased HER and OER on Ni-M test electrodes under optimal conditions can be explained by a mechanism as illustrated in Fig. 6.10. The schematic representation of the steps; chemisorption, desorption and recombination leading to the evolution of H_2 gas on Ni-M electrode surface, is given in Fig. 6.10(a). The physical properties of the coatings; like size, shape, composition of the alloying element and crystallographic structure are equally responsible for their catalytic activity towards HER. In addition, properties like increased surface area, due to micro-cracks also contribute to more H^+ adsorption and hence catalytic activity.
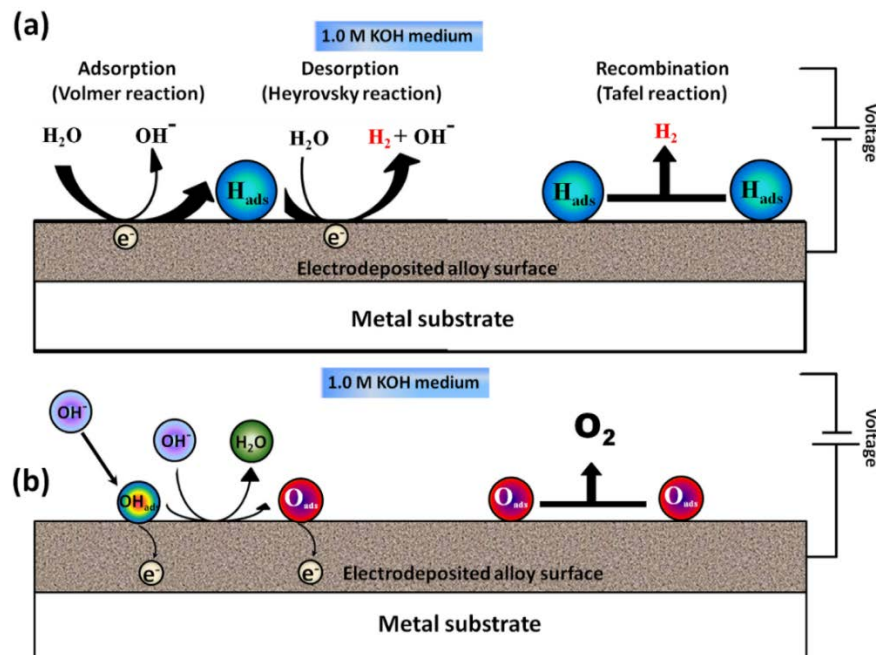
Fig. 6.10- Mechanism of alkaline water electrolysis; a) HER, and b) OER

Contrarily, the Ni-M alloy coatings (having low wt.% M) was found to be more efficient electrode material, when it is used as anode. i.e., for OER reaction. The mechanism of OER on Ni-W alloy, when used as anode is shown schematically in Fig. 6.10(b).This behavior may be explained by the adsorption of comparatively large OH⁻ ions on the electrode surface, where it overlaps with other processes like oxygen reduction at the same time. Thus enhanced OER activity of Ni-M coating may be attributed to the increased OH⁻ adsorption through the formation of a semiconducting layer in the applied potential range [Domínguez-Crespo et al. 2011]. Since the adsorption characteristics of the OH⁻ can lead to the formation of NiOOH on its surface, the increase of Ni content in the coating largely favors OER [Shibli et al. 2015]. As the Ni content in the coating decreases, the oxide layer formation becomes limited and thereby reduces OER. Therefore it may summarize that the Ni-M electrode material favoring HER has an adverse effect on OER and vice versa.

6.5 CONCLUSIONS

1. The Ni-W alloy deposited, respectively at 4.0 A dm⁻² (having about 12.4 wt.% W) and 1.0 A dm⁻² (having about 0.9 wt.% W) were obtained as the good cathode materials for HER and anode for OER, deposited from the same bath.

2. The Ni-P alloy deposited at 4.0 A dm^{-2} (9.0 wt.% P) and 2.0 A dm^{-2} (4.2 wt.% P) were found to be the best electrode materials for HER and OER, respectively.

3. The Ni-W and Ni-P alloy test electrodes having maximum activity towards HER was found to show the least activity for OER and vice versa. This behavior of the Ni-M alloy coatings is attributed to the basic difference in activation energy barrier for the kinetics of electron transfer process at the electrode/electrolyte interface for cathodic reaction and anodic reaction, responsible for H$_2$ and O$_2$ evolution, respectively.

4. The Ni-rich alloy coatings were found to show more activity towards OER and least activity towards HER in the case of both Ni-W and Ni-P alloy coatings.

CHAPTER 7

EFFECT OF MAGNETIC FIELD ON THE ELECTROCATALYTIC ACTIVITY OF Ni-W ALLOY COATINGS
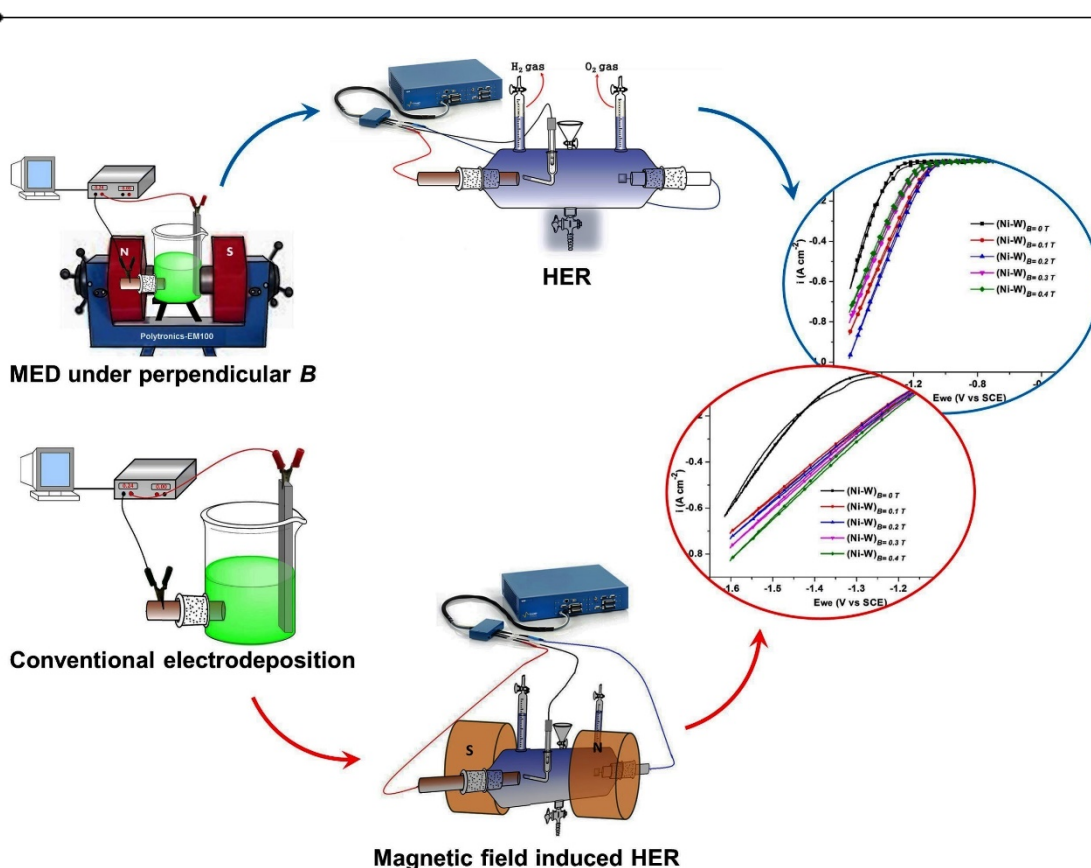
This chapter discusses the effective utilization of magnetic field as a tool to alter the electrode properties and electrocatalytic efficiencies, through MED and MFI-HER techniques. The electrocatalytic efficiency of ED Ni-W alloy coatings for HER was improved drastically through MED approach by depositing under different conditions of B, applied perpendicular in the range of 0.1 T - 0.4 T. The MED coating, (Ni-W)$_{B=0.2}$ $_T$ was obtained as the optimal alloy coating with drastic variation in HER efficiency as compared to its conventional Ni-W alloy coatings. The improvement in HER activity of MED coatings was attributed to the increased W content in the alloy, explained by MHD effect due to Lorentz force. Further, the HER efficiency of ED Ni-W alloy coating with a specific composition was enhanced by reducing the high overvoltage towards

HER at the electrode surface through an applied magnetic field during water electrolysis. The enhancement in HER efficiency of the Ni-W alloy of specific composition, without modifying the electrode material, in the presence of applied B of varying strengths (0.1 T to 0.4 T) was observed. The improvement in HER efficiency of Ni-W alloy under induced B is attributed to the increased limiting c.d. of H$_2$ through MHD force induced convection and H$_2$ bubble disentanglement.

7.1 RESULTS AND DISCUSSION

The experimental results obtained for the electrocatalytic activity study for HER on MED Ni-W alloy coatings and MFI-HER study on ED Ni-W alloy coating are discussed below.

7.2 ELECTROCATALYTIC ACTIVITY OF MED Ni-W ALLOY COATINGS FOR ALKALINE HER

The MED Ni-W coatings were deposited under applied magnetic field of varying intensity (from 01 to 0.4 T) in the perpendicular direction, at an optimal applied c.d. of 4.0 A dm^{-2}. The development of MED coatings for electrocatalytic study and its analysis was discussed in Chapter-2. The structural, morphological and compositional characterization of the coatings were discussed in Chapter-5. The obtained results for electrocatalytic activity of MED Ni-W alloy coatings towards alkaline HER is explained as below.

7.2.1 Cyclic voltammetry study for HER activity of MED coatings

The efficiency and stability in performance of the alloy electrodes can be assessed from the onset potential and cathodic current response. The obtained CV curves for MED coatings in comparison with the optimal ED coating are shown in Fig. 7.1 and the corresponding HER parameters are given in Table 7.1. From the obtained results it is clear that the W-rich MED coatings are more electrocatalytically active than the conventional ED coatings. The coating developed at an applied *B* of 0.2 T was found to be the best for HER with supreme i_{pc} value (-0.97 A cm^{-2}) and least onset potential for hydrogen evolution (-0.99 V).

164
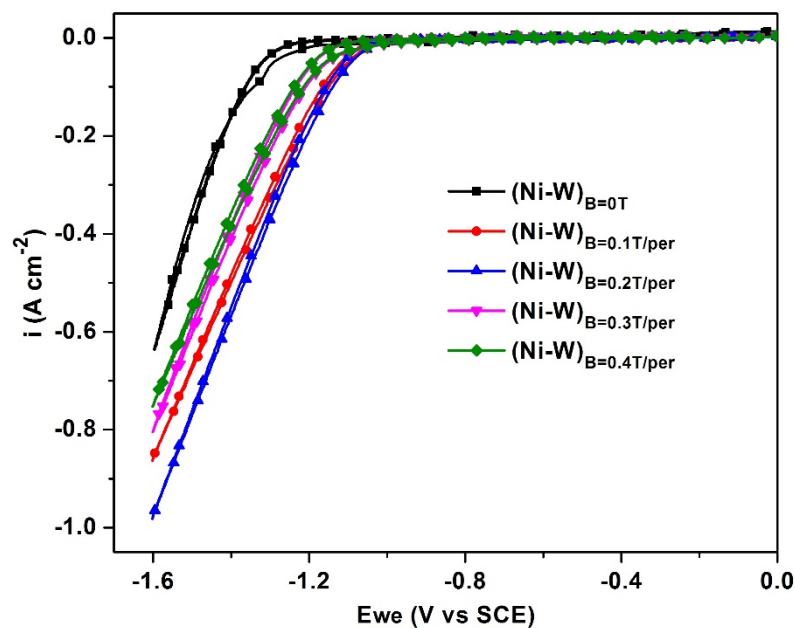
Fig. 7.1- CV responses of the MED Ni-W alloy coatings in comparison with the optimal ED coating

7.2.2 Chronopotentiometry study for HER activity of MED coatings

The catalytic stability of the MED Ni-W alloy test electrodes was established from its 'V-t' (voltage-time) characteristics under a constant applied cathodic c.d. The practical HER efficiency of the test electrodes, in alkaline KOH medium, was assessed from the quantified amount of H_2 gas evolved during the analysis. The obtained CP responses for MED Ni-W alloy coatings in comparison with optimal ED coating, along with the amount of H_2 evolved in 300 s are shown in Fig. 7.2, and the corresponding CP data are given in Table 7.1. The obtained results confirm that the coating with configuration (Ni-W)$_{B=0.2\ T}$ as the robust electrode material with maximum amount of H_2 evolved. The enhanced HER efficiency of MED coatings are ascribed to its W content, hence its changed phase structure and surface morphology.
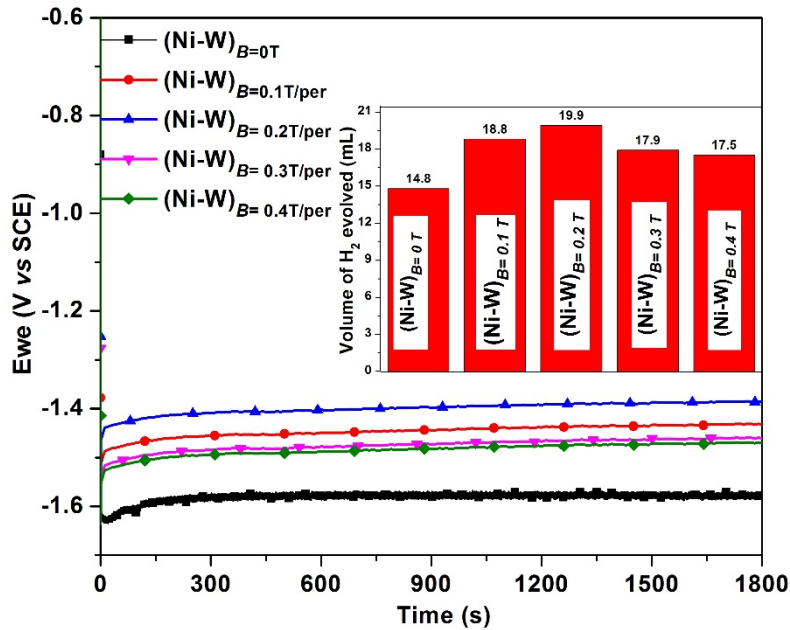
Fig. 7.2- Chronopotentiograms of the MED Ni-W alloy coatings in comparison with optimal ED coating along with the corresponding volumes of H_2 gas evolved in 300 s in the inset

Table 7.1- The HER parameters of the MED Ni-W alloy coatings

Coating configuration	Cathodic peak c.d. (A cm^{-2})	Onset potential for H_2 evolution (V *vs* SCE)	Volume of H_2 evolved in 300s (mL)
(Ni-W) $_{B=0 \text{ T/per}}$	-0.66	-1.21	14.8
(Ni-W)$_{B=0.1 \text{ T/per}}$	-0.85	-1.02	18.8
(Ni-W)$_{B=0.2 \text{ T/per}}$	-0.97	-0.99	19.9
(Ni-W)$_{B=0.3 \text{ T/per}}$	-0.80	-1.04	17.9
(Ni-W)$_{B=0.4 \text{ T/per}}$	-0.76	-1.05	17.5

Though the MED coatings developed at higher strengths of *B* were observed to be more porous, the electrocatalytic efficiency of the coatings was found to be more dependent on the W content in the coatings. The effect due to porosity in the coatings was overcome by the effect due to composition of the alloying element W, with low hydrogen overvoltage. The formation of W-rich coating resulted in vibrant H_2 bubble

disentanglement and increased catalytic c.d. (-0.97 A cm^{-2}) with low onset potential (-0.99 V) for MED (Ni-W)$_{B=0.2\ T}$, and hence confirms it as the best alloy electrode for alkaline HER.

7.3 MAGNETIC FIELD INDUCED HER ON Ni-W ALLOY

The as-deposited ED Ni-W alloy coating of a specific composition (deposited at 4.0 A dm^{-2}) was subjected to electrocatalytic study for HER under different applied magnetic field strengths (varying from 0.1 to 0.4 T), in the perpendicular direction. To exploit the maximum effect of Lorentz force developing in an electromagnetic field, on the evolution of H$_2$ gas from the electrode surface, the external magnetic field was applied perpendicular to the electrocatalytic study setup (or parallel to the electrode surface) as shown in Fig. 2.13. The CV and CP analyses were performed in the presence of applied magnetic field to assess the stability and improvement in MFI-HER.

7.3.1 Cyclic voltammetry study for MFI-HER on Ni-W alloy coating

The CV responses of the Ni-W test electrode for alkaline HER under different applied magnetic field strengths were recorded and shown in Fig. 7.3. The obtained results show a clear distinction between the CV curves obtained with and without applied magnetic field. The variation in cathodic current response and onset potential for H$_2$ evolution imply the enhancement in HER in the presence of applied magnetic field (Table 7.2). The HER efficiency of the Ni-W test electrode was found to be maximum at an induced magnetic field strength of 0.4 T, with large i_{pa} value (-0.82 A cm^{-2}) and low onset potential (-1.01 V).
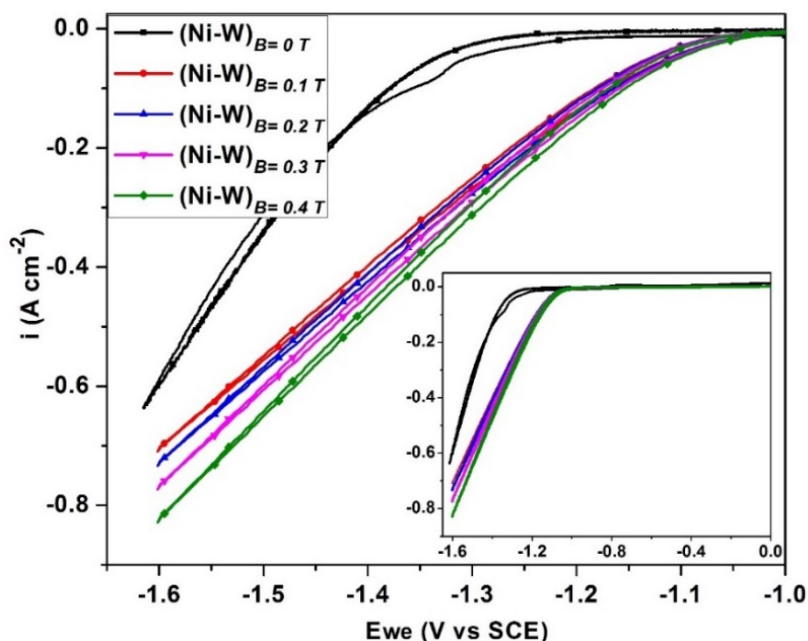
Fig. 7.3- CV responses of the MFI-HER on Ni-W alloy of a specific composition

7.3.2 Chronopotentiometry study for MFI-HER on Ni-W alloy coating

The CP responses of the Ni-W alloy test electrode for alkaline HER under different applied magnetic field strengths were recorded for 1800 s, at an applied c.d. of -300 mA cm^{-2}. The practicality of the MFI-HER was confirmed from the quantification of the evolved H$_2$ gas during analysis (for 300 s). The obtained CP curves and the corresponding amount of H$_2$ collected for MFI-HER analysis shows a remarkable difference from that obtained in the absence of *B*. The CP responses illustrate the stabilization time required for the alloy surface to attain a steady state for the continuous evolution of H$_2$ due to the large bubble resistance in the absence of applied *B* [Kiuchi et al. 2006, Waskaas and Kharkats 1999]. Whereas, in the presence of applied *B* there is no such effect of bubble resistance due to the faster detachment of H$_2$ bubbles from the electrode surface as it is formed [Wang et al. 2014, Monzon and Coey 2014]. The CP study also confirms the HER efficiency of the Ni-W alloy as maximum under an applied magnetic field strength of 0.4 T, with the maximum amount of evolved H$_2$ gas (19.1 mL).
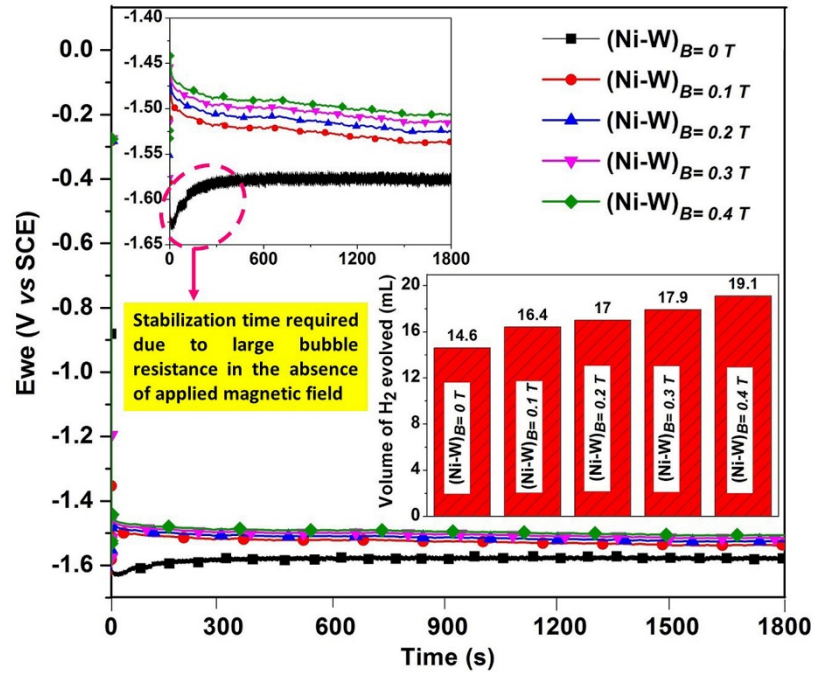
Fig. 7.4- The CP curves for MFI-HER on Ni-W alloy coating along with the quantity of H_2 evolved during the analysis (in the inset)

Table 7.2- The MFI-HER parameters of the Ni-W alloy

Operating condition	Cathodic peak c.d. ($A\ cm^{-2}$)	Onset potential for H_2 evolution (V vs SCE)	Volume of H_2 evolved in 300 s (mL)
$(Ni-W)_{B=0\ T}$	-0.66	-1.21	14.6
$(Ni-W)_{B=0.1\ T}$	-0.71	-1.07	16.4
$(Ni-W)_{B=0.2\ T}$	-0.74	-1.05	17.0
$(Ni-W)_{B=0.3\ T}$	-0.76	-1.04	17.9
$(Ni-W)_{B=0.4\ T}$	-0.82	-1.01	19.1

Though the overall results not showing that much difference between the obtained MFI-HER efficiency with increasing magnetic field strengths, the variation between the efficiency with and without applied B is significant. The small difference in MFI-HER of Ni-W alloy at different operating conditions of B may be attributed to the very small increase in applied magnetic field strength of 0.1 T each time.

7.4 EFFECT OF INDUCED MAGNETIC FIELD ON HER

The enhancement in electrocatalytic activity towards HER on Ni-W alloy in the presence of applied B is attributed to the reduction in Ohmic drop, due to bubble resistance, during electrolysis [Wang et al. 2014, Kiuchi et al. 2006, Fahidy 1983, Monzon and Coey 2014]. This can be explained by the MHD effect, arises mainly due to Lorentz force. Lorentz force is maximum under perpendicular B, i.e., when $\theta = 90^{\circ}$, $F_L = i \times B$, where i is the applied c.d. [Monzon and Coey 2014, Lin and Hourng 2014]. The ionic species in the medium moves in a circular path influenced by the Lorentz force, and can create a convective flow near the electrode surface leading to the discharge of the H_2 bubbles faster as it is formed [Wang et al. 2014, Koza et al. 2011]. This convective mass transport effect increases with applied magnetic field strength are irrespective of the nature of the electrode surface of a specific composition. Since the buoyancy force of evolved H_2 gas and MHD forces are operating in the same direction (upward), under optimal distance between the electrodes, the H_2 bubbles can escape easily from the electrode surface leading to decrease in Ohmic voltage drop. A schematic of the mechanism of MFI-HER is shown in Fig. 7.5. Where, the charged particle or ion 'q' with a velocity 'v' due to applied c.d. 'i', moves in circular path influenced by F_L, under applied B in perpendicular direction. The improvement in HER efficiency under induced B may be attributed to the enhancement in convection and H_2 bubble disentanglement.
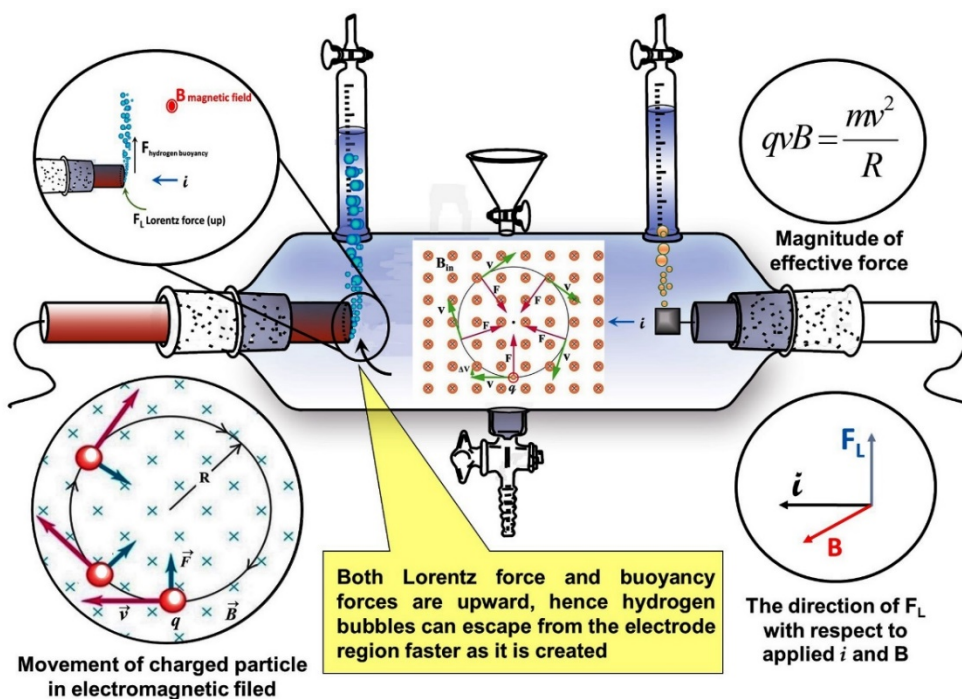
Fig. 7.5- The schematic of the mechanism of MFI-HER

Finally, it may be inferred that the formation of H_2 bubbles and their dispersal into the electrolyte is largely affected by the applied magnetic field, linked with large variation in the i_L value [Kiuchi et al. 2006, Fahidy 1983]. It is well-established fact that the i_L is proportional to the active surface area irrespective of the reaction rate-limiting step [Holze 1994]. This suggests that the current enhancement is caused by a reduced coverage of the electrode surface by the hydrogen bubbles [Lin and Hourng 2014, Bund et al. 2003]. Further, the material selection is also an important factor for increased HER activity under applied B. The test electrode used in the present study is Ni-W alloy, having 12.4% of W, i.e., Ni-rich alloy. The Ni-W alloy having still higher wt. % of W was found to exhibit still better electrocatalytic activity as described in section 7.1. Hence, the observed increase of H_2 gas on Ni-W alloy coating, with the strength of B is due to increase in the limiting current density of H_2 on its surface [Lin and Hourng 2014, Koza et al. 2011]. In other words, due to a decrease of H_2 overvoltage.

7.5 CONCLUSIONS

The following conclusions are made after analyzing the experimental results:

1. The electrocatalytic efficiency of the conventional ED coating was enhanced through the development of MED coatings from the same bath at optimal deposition c.d. of 4.0 A dm^{-2}.

2. The HER efficiency of the MED coatings was found to be increased only up to an optimal applied intensity of B (0.2 T), and then decreased.

3. The increase in HER efficiency of the MED coatings was attributed to the formation of W-rich phases and variation in surface morphology, evidenced from XRD and SEM.

4. The MED coating with coating configuration (Ni-W)$_{B=0.2\,T}$ was found to be the best electrode material with vibrant H$_2$ bubble disentanglement and increased catalytic c.d. (-0.97 A cm^{-2}) with low onset potential (-0.99 V) for HER.

5. The HER efficiency of the ED Ni-W alloy test electrode of a specific composition was improved by an external B applied in perpendicular direction during electrolysis.

6. The improvement in HER efficiency of Ni-W alloy under induced magnetic field may be attributed to increasing in the limiting current density of H$_2$ through MHD force induced convection and H$_2$ bubble disentanglement.

CHAPTER 8

MODIFICATION OF Ni-P ALLOY COATINGS FOR BETTER ELECTROCATALYTIC ACTIVITY TOWARDS ALKALINE HER
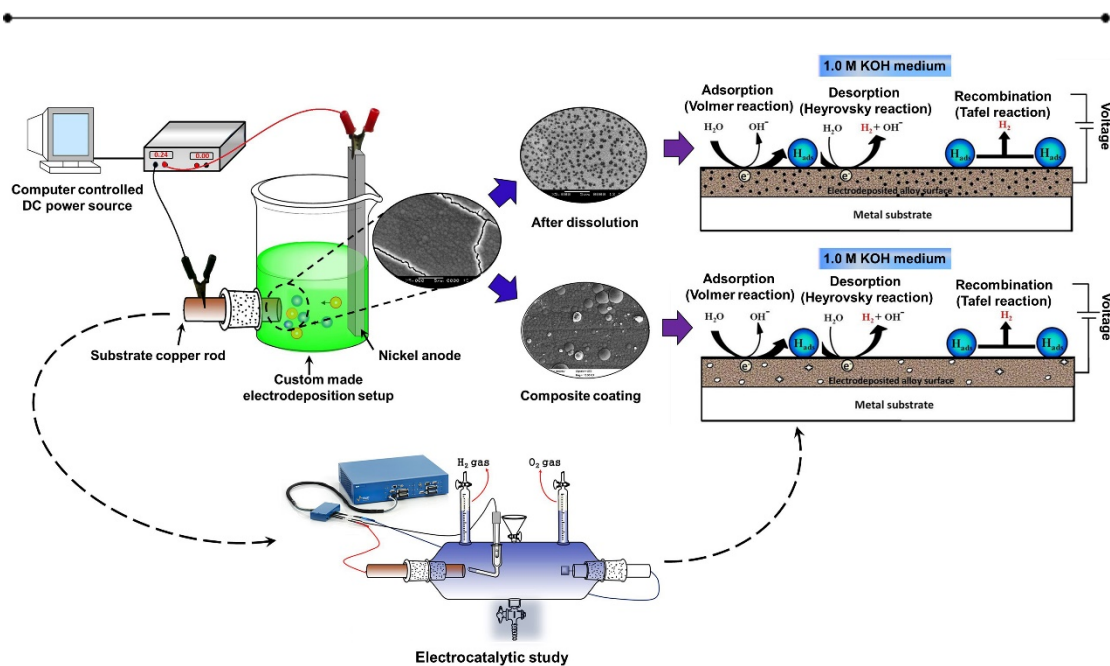
This chapter discusses the modification of Ni-P alloy coatings for better hydrogen production by electrochemical dissolution, TiO₂ and Ag nanoparticles incorporation. The electrochemical anodic dissolution or selective leaching method was adopted to develop a porous electrode, having more effective surface area to enhance the electrocatalytic efficiency. The Ni-P-TiO₂ and Ni-P-Ag nanocomposite coatings were developed through composite electrodeposition and sol-enhanced composite electrodeposition, respectively, to improve the electrocatalytic efficiency towards alkaline HER. Drastic improvement in the electrocatalytic activity for HER was found in both anodically treated and nanocomposite coatings, compared to as-coated Ni-P alloy. The large improvement in the electrocatalytic property was obtained for nano-Ag derived composite coating, and it is attributed to the increased number of electroactive sites of Ag nanoparticles.

8.1 RESULTS AND DISCUSSION

The experimental results obtained for the structural, morphological and electrochemical characterization of the Ni-P based test electrodes for alkaline HER are reported here. The detailed procedures for electrochemical dissolution and the development of Ni-P-TiO$_2$ nanocomposite coatings were discussed in Chapter-2. The morphological and compositional characterization of the modified Ni-P test electrodes and their behavior towards alkaline HER are discussed below, with plausible mechanism.

8.2 ANODICALLY TREATED Ni-P ALLOY ELECTRODE

The electrochemical (anodic) dissolution or selective leaching of the electrodeposited Ni-P alloy coating was made in order to improve its electrocatalytic ability by increasing the effective surface area. Ni-P alloy deposited at 4.0 A dm^{-2} (optimal c.d. for HER) was selected for dissolution test (at an applied c.d. of 1.0 A dm^{-2} for a duration of 3 min). The surface of the as-deposited Ni-P alloy coating was found to be silvery bright, and after dissolution treatment, the surface turned blackish bright. Fig. 8.1 depicts the surface morphology of Ni-P alloy test electrode (developed at 4.0 A dm^{-2}) before and after anodic dissolution. The enlarged view of the micro-pores of varying sizes formed after the electrochemical/selective dissolution is shown in the inset of Fig. 8.1(b).
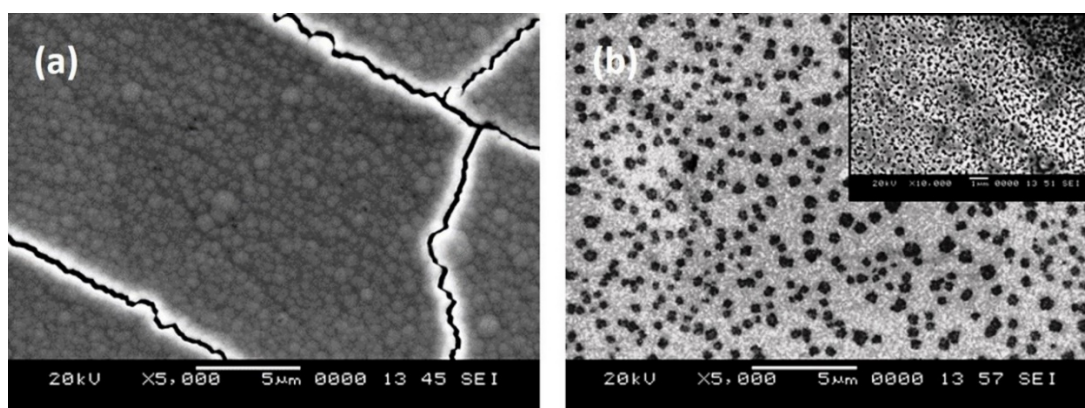
Fig. 8.1- SEM images of Ni-P alloy coatings deposited at 4.0 A dm^{-2}: a) as-deposited surface, and b) after anodic dissolution, showing the obtained microporous structure in the inset

174

8.3 Ni-P-TiO₂ NANOCOMPOSITE COATING

The Ni-P-TiO₂ nanocomposite coating was developed from the optimal bath admixed with a known quantity of TiO₂ through composite electrodeposition method, where the electrochemical codeposition or the particle incorporation occurs simultaneously with the metal ion reduction. The electrodeposited Ni-P-TiO₂ coating at an applied c.d. of 4.0 A dm^{-2} was characterized using FESEM analysis. The FESEM image of TiO₂ nanoparticles used in the present study, and the surface morphology of Ni-P-TiO₂ nanocomposite coating are shown in Fig. 8.2.
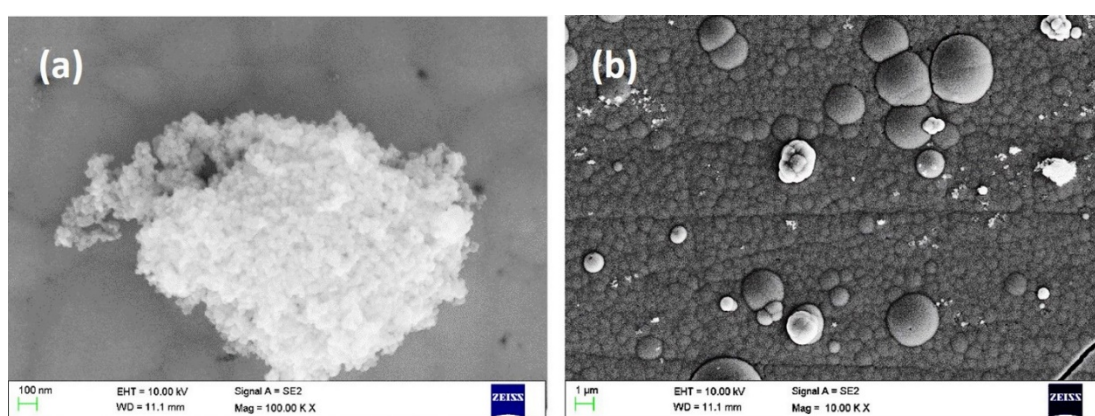
Fig. 8.2- FESEM images of (a) TiO₂ nanoparticles (b) surface morphology of TiO₂ incorporated Ni-P alloy coating developed at 4.0 A dm^{-2}

It is well known that the electrochemical composite deposition enables the production of a wide range of composite materials comparable to pure metal coatings with improved physical and electrochemical properties [Gomes et al. 2011]. The codeposition of suspended TiO₂ nanoparticles is effected from the convective and diffusive mass transfer towards the electrode surface along with metal ions after attaining surface charge through ionic clouds on the particles [Low et al. 2006, Gomes et al. 2011]. The as-deposited nanocomposite coating having TiO₂ nanoparticles within the alloy matrix, and on the surface as agglomerated particles are evidenced from the FESEM (Fig. 8.2(b)). Thus the incorporated TiO₂ nanoparticles act as catalytic centres, responsible for enhanced HER as explained by Gierlotka et al. (1997). The scheme depicting the mechanism of incorporation of nanoparticles into the alloy matrix, responsible for the improved electrocatalytic activity of Ni-P-TiO₂ coating is shown in Fig. 8.3.
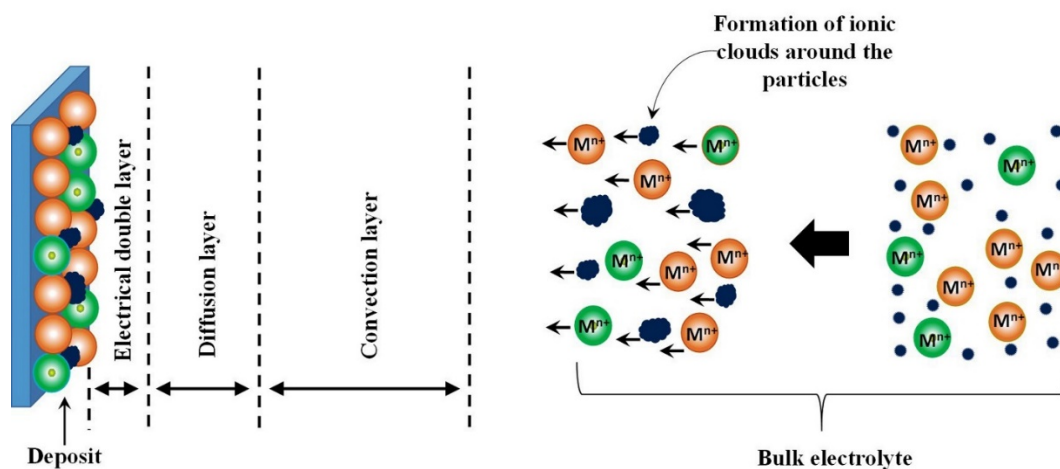
Fig. 8.3- Scheme showing the stepwise illustration for the formation of nanocomposite coating from the nanoparticle loaded optimal alloy plating bath during electrodeposition

8.4 Ni-P-Ag NANOCOMPOSITE COATING FOR BETTER HER ACTIVITY

Many reports are there on the improvement in electrocatalytic efficiency after the incorporation of colloidal particles into the metal/alloy matrix through composite electrodeposition [Yu et al. 2016, Shibli and Dilimon 2007, Danilov et al. 2016, Mirkova et al. 2011]. Whereas, in composite electrodeposition, the main limitation is to achieve a homogeneous dispersion of the colloidal particle within the metal/alloy matrix. Therefore, in continuation of adopting composite electrodeposition technique for the development of nanocomposite coating, the present study focuses on overcoming its limitation by adopting sol-enhanced electrodeposition technique for the preparation of Ni-P-Ag nanocomposite test electrode for HER. The synthesis of SNS and the electrodeposition of Ni-P-Ag nanocomposite coating are discussed in Chapter-2.

8.4.1 Characterization of Ag nanoparticles

The Ag-nanoparticles obtained through glycerol mediated $NaBH_4$ reduction of $AgNO_3$ were characterized for their size, morphology and optical properties. The TEM micrograph shows the synthesized Ag nanoparticles as spherical in shape and the average particle size as 10 nm. The obtained TEM image of a region of the sample along with the particle size distribution are shown in Fig. 8.4.
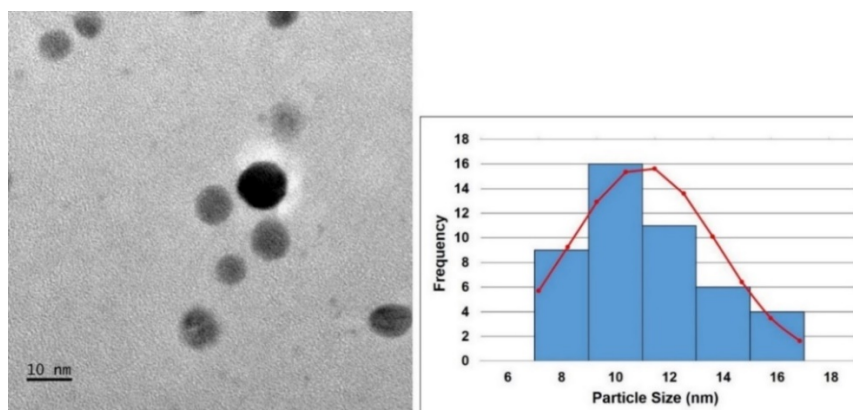
Fig. 8.4- TEM image of the Ag nanoparticles dispersed on a copper grid along with the TEM size distribution and Gaussian fitting of the Ag-nanoparticles

The optical activity of the Ag-nanoparticles in the visible region is attributed to the excitation of the d-band electrons to states above Fermi level and subsequent relaxation resulting in the photoluminescent radiative recombination [Mooradian 1969, Vasireddy et al. 2012]. The plasmon absorbance phenomenon is resulting in the yellow colour to the colloidal SNS [Abdullah and Annapoorni 2005, DongVan et al. 2012]. The UV-Vis absorption spectra of the clear yellow colloidal SNS is shown in Fig. 8.5. The average particle size was again confirmed as 10 nm from the plasmon resonance peak obtained near to 395 nm, with a full-width half maximum (FWHM) value of 56 [Mulfinger et al. 2007, Vasireddy et al. 2012, DongVan et al. 2012].
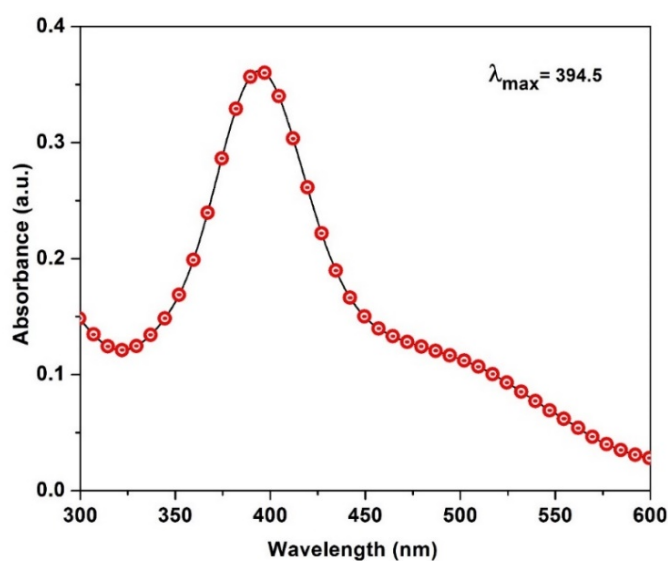
Fig. 8.5- UV-Vis absorption spectrum of the Ag nanoparticles synthesized through glycerol mediated $AgNO_3$ reduction using $NaBH_4$

8.4.2 Characterization of Ni-P-Ag nanocomposite coating

The Ni-P-Ag nanocomposite coating developed through SNS enhanced electrodeposition at optimal deposition c.d. (4.0 A dm^{-2}) was characterized using SEM and EDS analyses. The limitation over the possibility for agglomeration of the nanoparticles within the plating bath during deposition in conventional composite electrodeposition, by directly adding the nanoparticles into the plating bath, was overcome by the sol-enhanced electrodeposition. As shown in the schematic diagram (Fig. 8.6), the addition of nano-sol is allowing the homogeneous mixing and dispersion of the nanoparticles within the plating solution [Chen et al. 2010b]. Whereas, in the case of direct addition of nanoparticles into the plating bath is leading to the agglomeration of the nanoparticles by interacting with the electrolyte. In the present case, the used glycerol as nanoparticle stabilizer can also enhance the homogeneous dispersion of the Ag-nanoparticles in the plating bath. Since glycerol was used as an additive in the alloy plating bath, the same can act as the dispersed nanoparticle stabilizer in the bath and thereby to prevent its further agglomeration during the deposition.
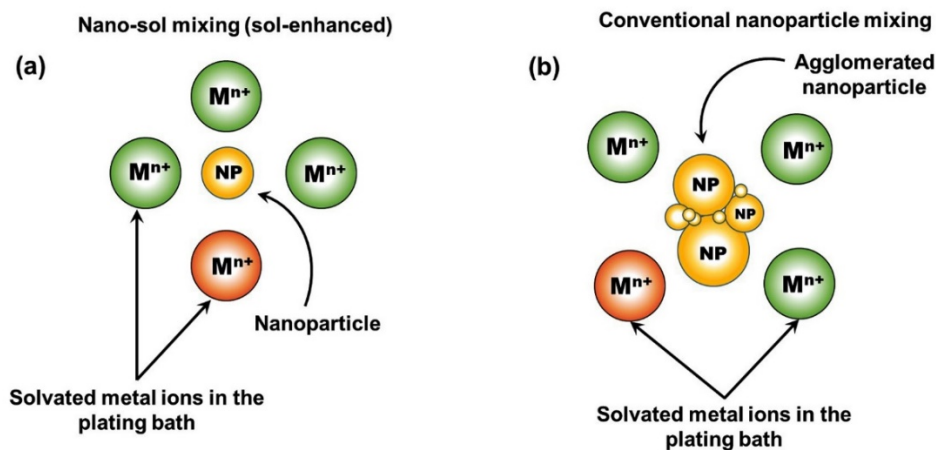
Fig. 8.6- Schematic of nanoparticle mixing in the plating bath; a) addition of the nanoparticle sol into the plating bath, and b) addition of the nanoparticles into the plating bath

The microstructure analysis of the obtained Ni-P-Ag composite coating was done using SEM. The incorporation of Ag nanoparticles within the alloy matrix and its composition in the coating were established through EDS analysis (Fig. 8.7). The

compositional analysis showed the presence of about 4.1 wt.% of Ag in the developed Ni-P-Ag nanocomposite coating.
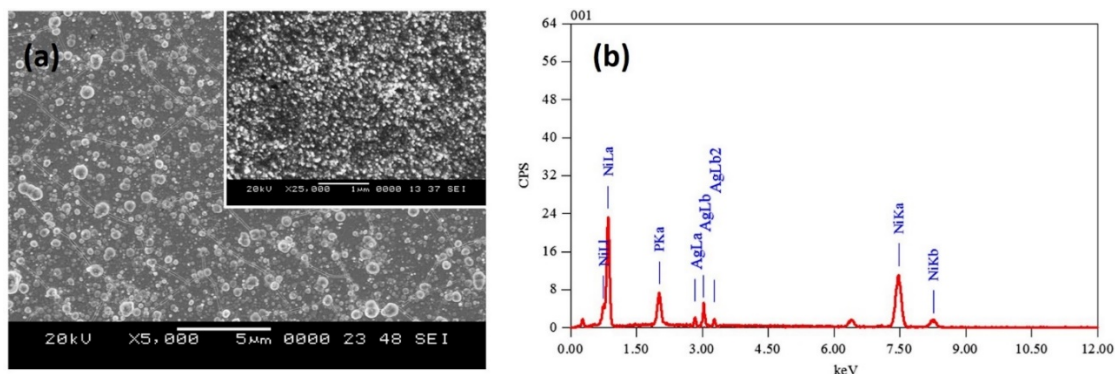
Fig. 8.7- a) SEM image, and b) EDS spectra of the Ni-P-Ag composite coating developed at an optimal c.d. of 4.0 A dm^{-2} from the alloy plating bath having homogeneously dispersed Ag nanoparticles

8.5 COMPARISON OF ELECTROCATALYTIC ACTIVITY OF MODIFIED Ni-P TEST ELECTRODES FOR ALKALINE HER

The electrocatalytic efficiency of the modified Ni-P test electrodes for alkaline HER was analyzed using CV and CP techniques in 1.0 M KOH medium. The practical effectiveness of the modified electrodes was assessed directly from the quantified amount of H$_2$ gas evolved from each test electrodes during the analysis.

8.5.1 Cyclic voltammetry analysis

The CV curves of the modified Ni-P test electrodes, developed using different methods, in comparison with the optimal as-coated Ni-P alloy coating are shown in Fig. 8.8. The obtained CV response of the Ni-P-Ag nanocomposite coating shows a remarkable variation in i_{pc} and onset potential values as compared with the other modified Ni-P test electrodes, as given in Table 8.1. The large variation in i_{pc} value for the Ni-P-Ag nanocomposite test electrode is attributed to the enhanced adsorption of the H$^+$ ions on the electrode surface, influenced by the increased surface area and the number of active sites affected from the incorporation of Ag nanoparticles into the alloy matrix [Shibli and Dilimon 2007, Danilov et al. 2016, Mirkova et al. 2011].

179
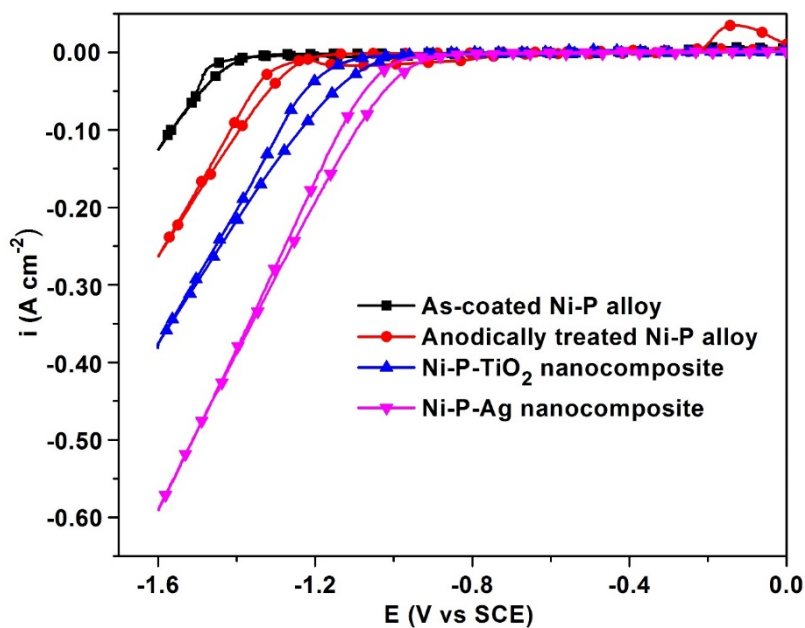
Fig. 8.8- The CV curves of the as-coated Ni-P alloy, in comparison with that of anodically treated Ni-P alloy, Ni-P-TiO₂ nanocomposite and Ni-P-Ag nanocomposite coatings

8.5.2 Chronopotentiometry analysis

The CP responses of the modified Ni-P test electrodes in comparison with the optimal as-coated Ni-P alloy (developed at 4.0 A dm^{-2}) along with the amount of H$_2$ gas evolved during the analysis (for first 300 s) are shown in Fig. 8.9. The corresponding HER parameters are listed in Table 8.1. The obtained results show the Ni-P-Ag nanocomposite test electrode as the best material for alkaline HER with good stability and maximum amount of H$_2$ gas produced during the analysis.
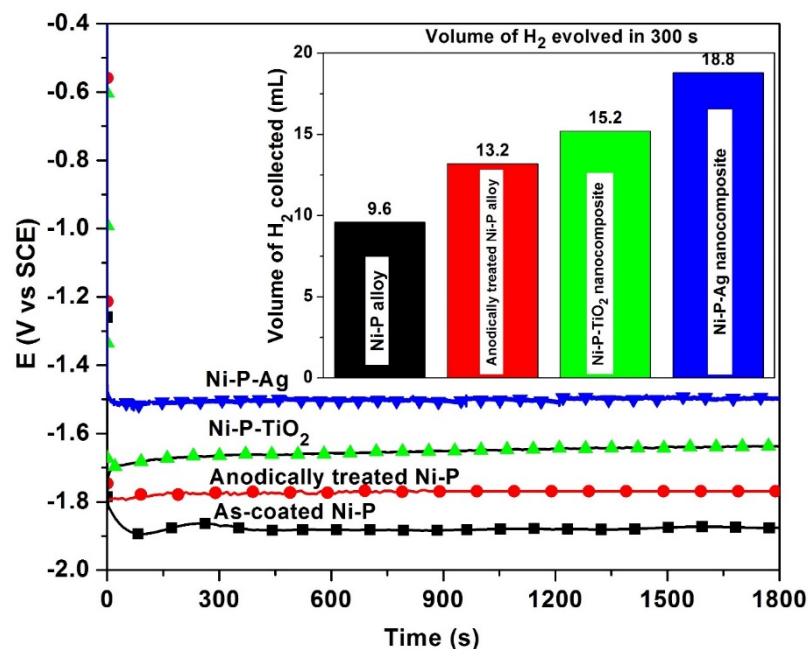
Fig. 8.9- The CP responses of the as-coated Ni-P alloy, in comparison with that of anodically treated Ni-P alloy, Ni-P-TiO$_2$ nanocomposite and Ni-P-Ag nanocomposite coatings along with the amount of H$_2$ gas evolved (in the inset)

The improvement HER activity of Ni-P alloy coating through anodic dissolution may be ascribed to the increased porosity, affected by selective leaching. Due to an increase of porosity, the metal particles resides in a pore of a similar size are more, and hence a considerable part of its surface will be in intimate contact with the pore walls and, therefore, favours hydrogen production [Wieckowski et al. 2003]. Thus improved electrocatalytic activity after anodic treatment is due to increase in the porosity of the coating; which leads to increase in the surface area and thereby making more active metal atoms to come in intimate contact with the electrolyte. Whereas, the enhanced HER activity of the nanocomposite coatings are attributed to the increased surface area and increase in the number of active sites through the incorporation of TiO$_2$ and Ag nanoparticles. Further, the improvement in electrocatalytic activity of Ni-P alloy coating after modification through dissolution treatment and nanoparticles incorporation are mainly resulted from the change in electronic structure, surface area and the increase in active sites for hydrogen adsorption [Ledendecker et al. 2015].

Table 8.1- The comparison of HER parameters of as-coated Ni-P alloy, anodically treated Ni-P alloy, Ni-P-TiO$_2$ nanocomposite and Ni-P-Ag nanocomposite test electrodes achieved through conventional electrodeposition, electrochemical dissolution, composite electrodeposition and sol-enhanced electrodeposition, respectively, from the same Ni-P alloy plating bath

Coating type	Cathodic peak c.d. at -1.6 V (A cm^{-2})	Onset potential of H$_2$ evolution (V *vs* SCE)	Volume of H$_2$ evolved in 300 s (mL)
As-coated Ni-P alloy	-0.13	-1.30	9.6
Anodically treated Ni-P alloy	-0.26	-1.22	13.2
Ni-P-TiO$_2$ nanocomposite	-0.38	-1.19	15.2
Ni-P-Ag nanocomposite	-0.59	-0.95	18.8

The HER activity of the Ni-P alloy test electrode in comparison with the modified Ni-P test electrodes such as, anodically treated, Ni-P-TiO$_2$ nanocomposite and Ni-P-Ag nanocomposite coatings (Table 8.1) suggest Ni-P-Ag as the best electrode material for alkaline HER. The observed intensification in electrocatalytic activity of the Ni-P-Ag nanocomposite test electrode for alkaline HER is accredited to the increased surface area and the increased number of active sites for hydrogen adsorption affected by the homogeneous dispersion of the Ag nanoparticles in the alloy matrix, achieved through sol-enhanced electroplating technique [Ledendecker et al. 2015, Danilov et al. 2016].

8.6 CONCLUSIONS

The following conclusions are established based on the study on synthesis, characterization and electrocatalytic study of modified Ni-P test electrodes for alkaline HER.

1. The improved electrocatalytic activity after anodic treatment is due to increase in the porosity of the coatings, leading to an increase in the surface area and thereby making active metal atoms to expose more to the electrolyte.

2. Spherical shaped silver nanoparticles with an average particle of 10 nm were successfully synthesized through glycerol mediated reduction of $AgNO_3$ using $NaBH_4$ and characterized.

3. Sol-enhanced electroplating has been successfully employed for the deposition of Ni-P-Ag nanocomposite coating with a homogeneously dispersed Ag nanoparticles to intensify the electrocatalytic efficiency of the Ni-P alloy electrodes for HER.

4. A drastic improvement in HER activity was observed for the Ni-P-TiO_2 and Ni-P-Ag nanocomposite test electrodes with low onset potential for H_2 evolution, large i_{pc} value and the maximum amount of H_2 gas evolved during the analysis, in comparison with the as-coated and anodically treated Ni-P alloy.

5. The observed high efficiency of Ni-P-Ag nanocomposite test electrode for alkaline HER is accredited to the increased surface area and the increased number of active sites for hydrogen adsorption affected by the homogeneous dispersion of the Ag-nanoparticles in the alloy matrix, achieved through sol-enhanced electroplating technique.

CHAPTER 9

MODIFICATION OF Ni-W ALLOY COATINGS FOR BETTER ELECTROCATALYTIC ACTIVITY TOWARDS ALKALINE HER
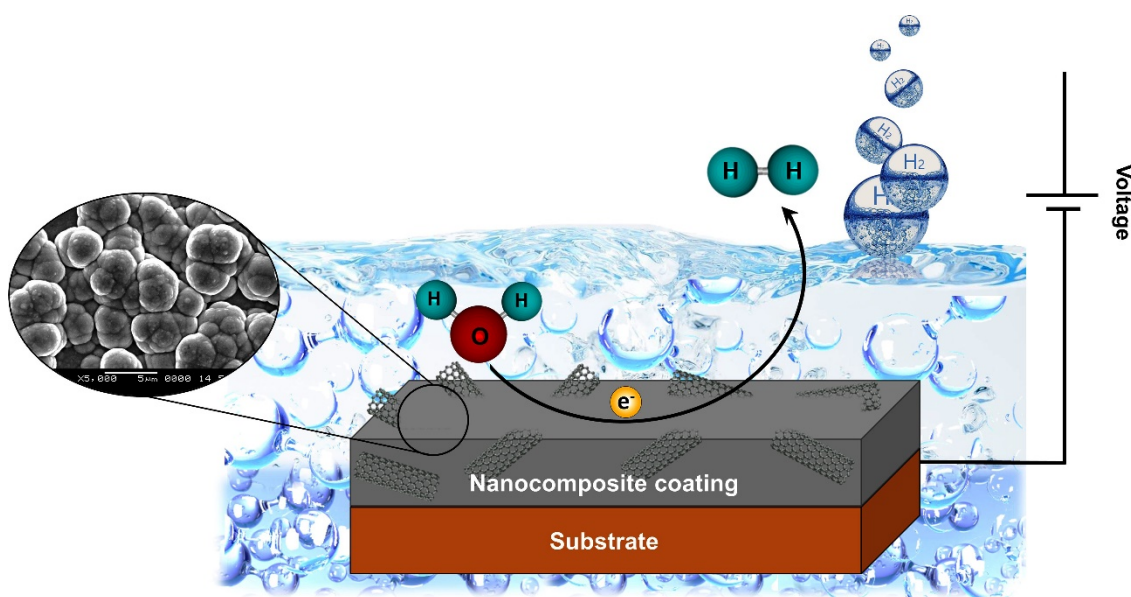
This chapter discusses the development of Ni-W-MWCNT and Ni-W-rGO nanocomposite coatings for better HER efficiency. The nanocomposite coatings were developed by exploiting the advantage of composite electrodeposition technique. The effect of CNT and GO on the induced codeposition behavior of the reluctant metal W was studied, and related to their electrocatalytic efficiency. The variation in electrocatalytic activity with composition, structure and morphology of the coatings were examined systematically using XRD, SEM and EDS analyses. Drastic improvement in the electrocatalytic activity for HER was found in both Ni-W-CNT and Ni-W-rGO composite coatings, compared to the as-coated Ni-W alloy. The obtained results showed Ni-W-MWCNT composite coating as the best electrode material for alkaline HER, attributed by both increased W content and number of electroactive centers, affected by the homogeneous distribution of MWCNT in the alloy matrix.

9.1 RESULTS AND DISCUSSION

The electrocatalytic efficiency of the Ni-W alloy coatings was discussed in Chapter-6. The HER efficiency of optimal Ni-W alloy coating (deposited at 4.0 A dm^{-2}) was enhanced by the incorporation of MWCNT and rGO, through composite electrodeposition. The procedure adopted for the development of both Ni-W-MWCNT and Ni-W-rGO nanocomposite coatings were explained in Chapter-2.

9.2 Ni-W-MWCNT NANOCOMPOSITE COATING FOR BETTER HER ACTIVITY

9.2.1 Characterization of functionalized MWCNT

The chemically modified MWCNTs, through acid treatment, were characterized using FTIR analysis (ATR mode) to identify the introduced surface functional groups (Fig. 9.1).
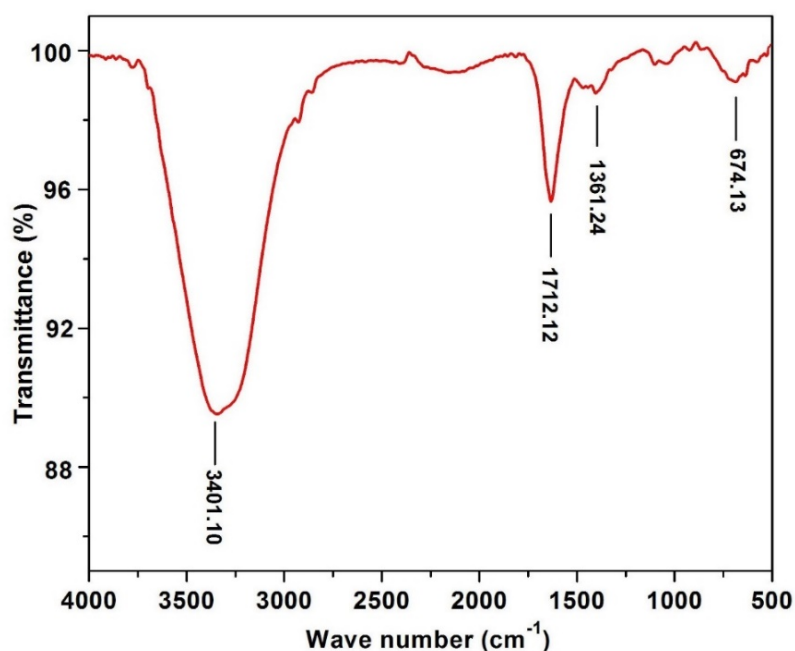
Fig. 9.1- FTIR spectrum of the acid treated MWCNTs showing characteristic peaks of generated functional groups confirm the surface modification after chemical oxidation

The presence of characteristics peaks due to generated chemical functional groups in acid treated MWCNTs compared with the as-received MWCNT, as per the reported literatures, support the surface modification after chemical oxidation [Yang et

al. 2012, Naseh et al. 2009, Wepasnick et al. 2011]. The identified peaks around 1361, 1712 and 3401 cm^{-1} are corresponding to C–O, C=O and O–H stretching, respectively. The peaks at 674, 1712 and 3401 confirm the introduction of carboxylic (-COOH) functional group into the chemically modified MWCNTs as shown in Fig. 9.2.
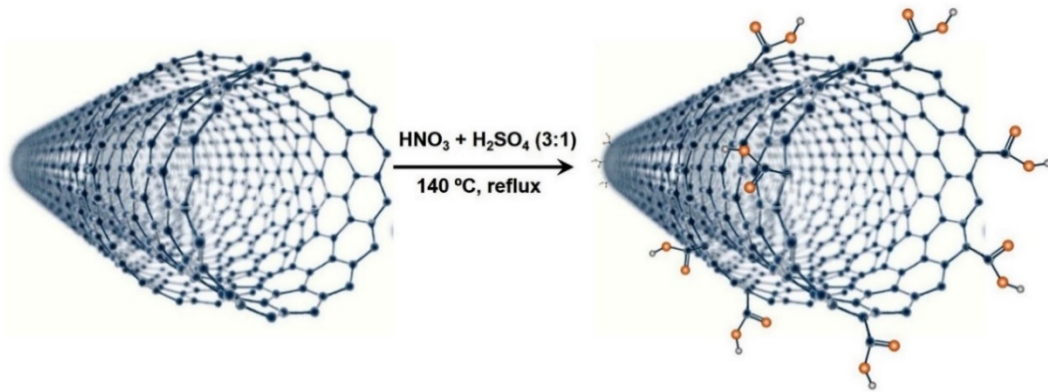
Fig. 9.2- Schematic of surface modification of MWCNTs after chemical treatment

9.2.2 Characterization of Ni-W-MWCNT nanocomposite coating

9.2.2.1 SEM study

The surface topography of the alloy and composite coatings (deposited at 4.0 A dm^{-2}) were observed using SEM analysis and the obtained images are shown in Fig. 9.3. The surface of Ni-W alloy coating was found to be flat, smooth and covered with full of micro-cracks. Whereas, the nanocomposite coating was found to be cracks-free with nodular growths. The variation in morphology of the nanocomposite coating as compared with the conventional alloy deposit itself reflects the effect of addition of functionalized MWCNTs into the plating bath [Arai et al. 2008]. The incorporation of MWCNTs into the alloy matrix was confirmed by the EDS analysis.
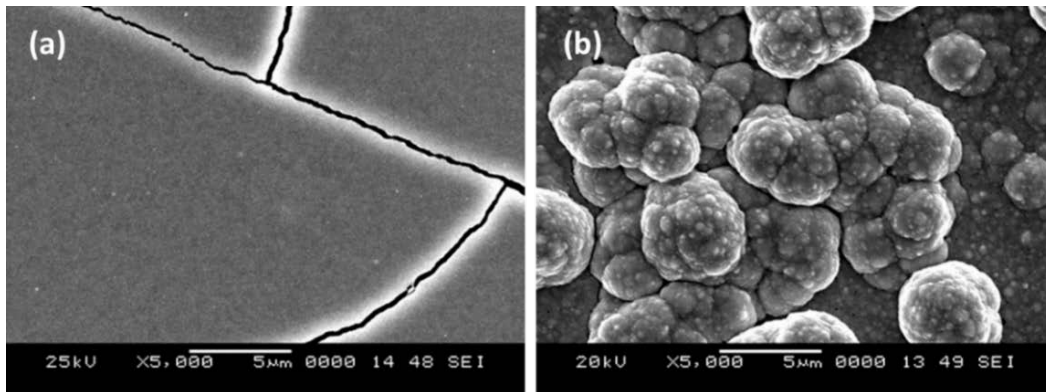
Fig. 9.3- The surface topography of the coatings developed at 4.0 A dm^{-2}: a) Ni-W alloy coating, and b) Ni-W-MWCNT nanocomposite coating

9.2.2.2 XRD analysis

The variation in phase structure due to the incorporation of MWCNTs into the alloy matrix through composite electrodeposition was studied using XRD study. The obtained XRD results are shown in Fig. 9.4, and which confirms the formation of new crystal orientation corresponds to the W-rich phases along with the peaks corresponds to carbon. The direction of crystal growth itself was found to be changed from Ni-W (111) plane to Ni-W (220) plane. This observation further suggests the role of MWCNTs in enhancing the coating properties. The incorporation of MWCNTs into the metal matrix was evidenced from the (002) and (100) peaks corresponds to carbon in the XRD pattern [Zhao and Gao 2004, Khabouri et al. 2015].
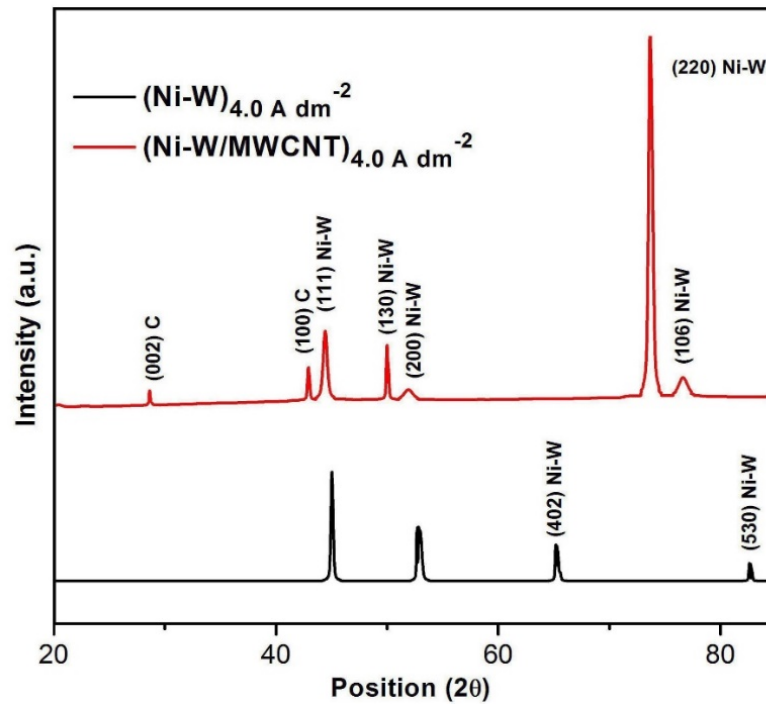
Fig. 9.4- XRD pattern of Ni-W-MWCNT nanocomposite coating in comparison with Ni-W alloy coating

9.2.3 Properties of the developed composite coating

The properties of the alloy coating were found to be influenced to a greater extent by composite electrodeposition technique as evidenced from the variation in composition (Table 9.1), morphology (Fig. 9.3) and structure (Fig. 9.4) of the coating. The composite electrodeposition was found to show an anomalous deposition behavior as compared with the usual induced codeposition of Ni-W alloy, attributed to the incorporation of MWCNTs into the alloy matrix. The schematic of MWCNT incorporation leading to the improved properties of nanocomposite coating is shown in Fig. 9.5.
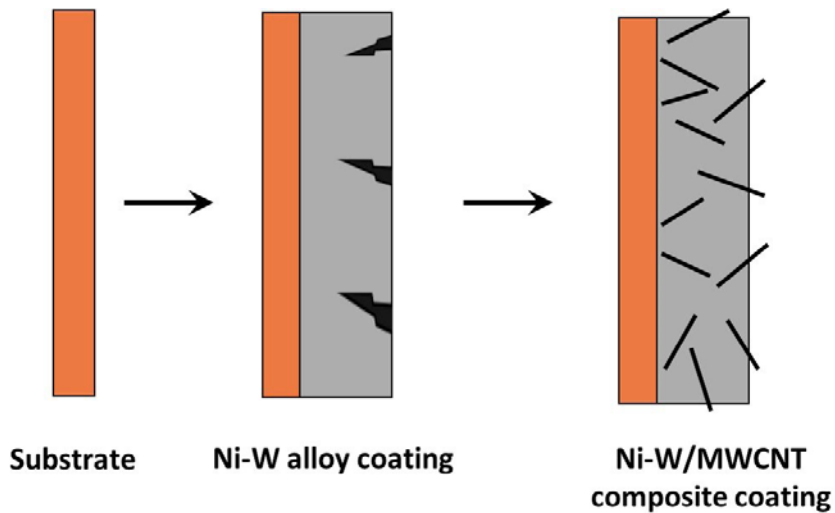
Fig. 9.5- Schematic of the variation in deposit characteristics in alloy and nanocomposite coatings

The incorporated MWCNT into the alloy matrix increased the effective surface area for deposition and further induced the preferential deposition of the reluctant metal W. The enhanced deposition of the alloy from the plating bath also onto the surface of incorporated MWCNTs led to the formation of nodular type growth on the nanocomposite coating surface, as distinct from the flat alloy surface (Fig. 9.3(a)). Moreover, the alloy coating was found to have micro-cracks on the surface due to the inherent brittle nature of W and hydrogen embrittlement. Whereas, in the case of nanocomposite coating, the incorporated MWCNTs helped in reinforcing the alloy deposit to prevent the formation of micro-cracks and thereby to enhance the microhardness of the nanocomposite coating [Arai et al. 2008, Low et al. 2006]. The variation in coating properties resulted from composite electrodeposition is evident from the obtained composition, thickness and hardness values reported in Table 9.1.

Table 9.1- The properties of the Ni-W-MWCNT nanocomposite coating in comparison with conventional alloy coating

Coatings developed at 4.0 A dm^{-2}	Wt.% of W in the deposit	Wt.% of C in the deposit	Thickness of the coating (µm)	Vicker's microhardness V_{100} (GPa)
Ni-W-MWCNT nanocomposite coating	25.6	4.2	16.2	4.64
Ni-W alloy coating	12.4	---	15.9	3.22

9.3 Ni-W-rGO NANOCOMPOSITE COATING FOR BETTER HER ACTIVITY

The effect of GO addition into the alloy plating bath on the coating properties and thereby the HER activity were studied. The synthesis of GO and its utilization in composite electrodeposition were discussed in Chapter-2.

9.3.1 Characterization of Graphene Oxide

The synthesized GO nanosheets were characterized using various instrumental methods of analysis. The obtained GO was examined using Raman spectroscopy, an invaluable technique to obtain the structure, crystallization and defects of carbon materials [Kuang et al. 2013, Su et al. 2013]. The Raman spectra of the obtained GO nanosheets are given in Fig. 9.6. The presence of two peaks at 1318 and 1610 cm^{-1}, characteristics of the D and G bands corresponds to carbon lattice defects and E$_{2g}$ phonon of sp^2 C atoms, respectively [Kuang et al. 2013, Huang et al. 2016, Su et al. 2013].
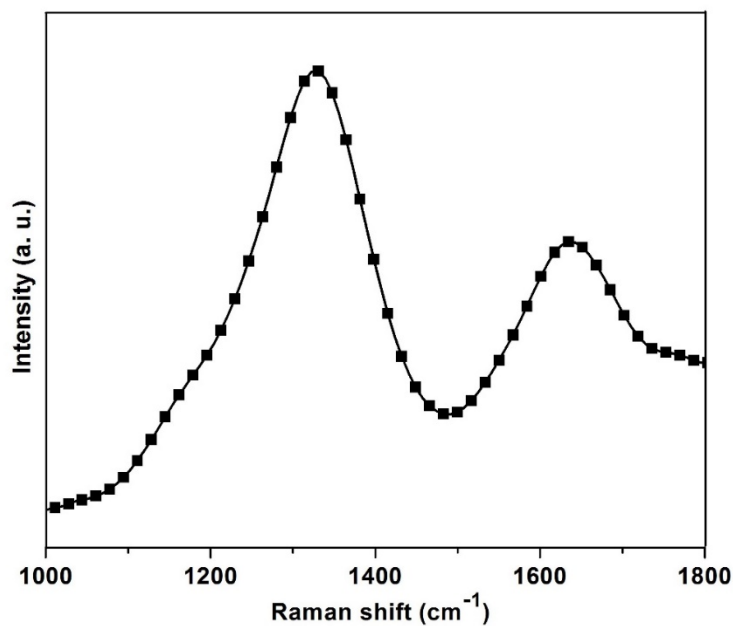
Fig. 9.6- Raman spectrum of the GO showing the D and G bands

The formation of GO is also confirmed by the XRD analysis. Fig. 9.7 shows the XRD pattern obtained for the synthesized GO nanosheets. The absence of characteristics reflection of graphite ($2\theta = 26°$) and the presence of a reflection at $2\theta = 10.4°$, with *d* spacing of 0.68 nm, due to the intercalation of oxygen confirms the formation of GO [Su et al. 2013, Allahbakhsh et al. 2014, Kumar et al. 2013].
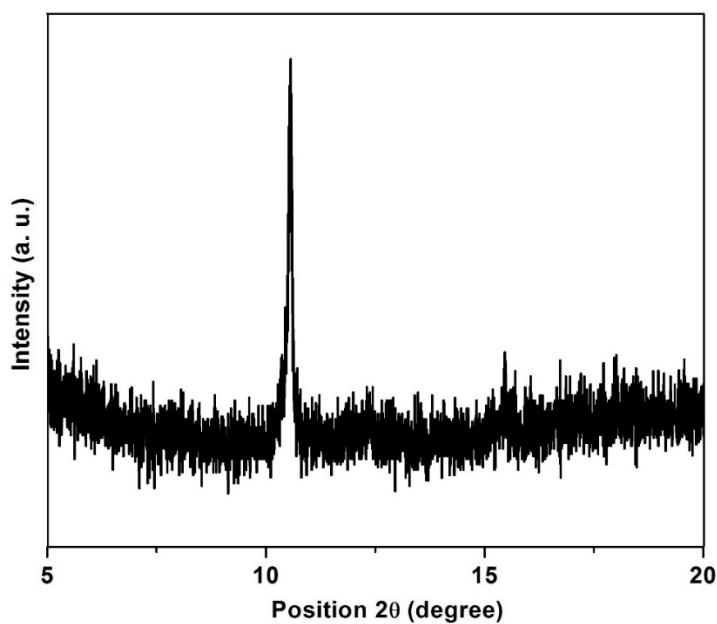
Fig. 9.7- XRD pattern of GO showing the presence of (101) reflection at $2\theta = 10.4°$

Further, the structural characterization of GO nanosheets was performed using TEM analysis (Fig. 9.8). The obtained TEM image clearly depicts the rippled and entangled GO nanosheets. The presence of single nanosheets is also evident from the TEM image as shown in Fig. 9.8. All these characterizations confirm the formation of GO after the chemical treatment of graphite, and it was used for the preparation of Ni-W-rGO nanocomposite coating.

100 nm
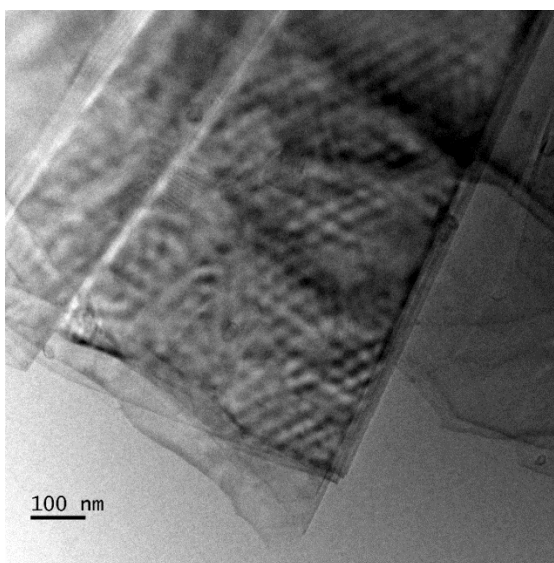
Fig. 9.8- TEM image of the synthesized graphene oxide

9.3.2 Characteristics of Ni-W-rGO nanocomposite coating

9.3.2.1 SEM study

The surface appearance of the alloy and nanocomposite coatings were examined using SEM and the obtained images are shown in Fig. 9.9. The alloy coating was found to be almost flat with full of micro-cracks on the surface. Whereas, the nanocomposite coating was observed to have homogeneous nodular growths along with the micro-cracks on the surface. The variation in surface appearance of the composite coating compared with the optimal alloy coating is attributed to the incorporation of GO nanosheets into the alloy matrix. Further, the change in surface morphology of the composite coating is ascribed to the increase in W content in the coating effected from the addition of GO into the plating bath. The increase in W content is evident from the EDS results as tabulated in Table 9.2. The micro-cracks on the alloy and nanocomposite

coatings are attributed to the hydrogen embrittlement and also due to the inherent brittle nature of W.
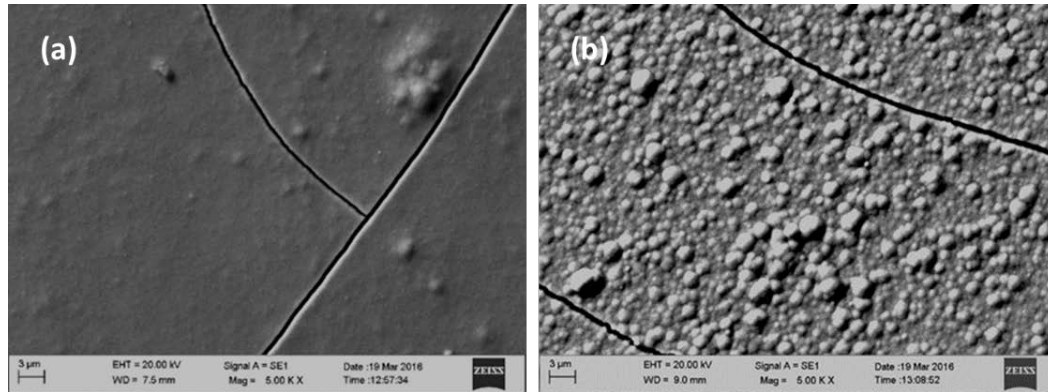
Fig. 9.9- The SEM images of the coatings developed at 4.0 A dm^{-2}: a) Ni-W alloy coating, and b) Ni-W-rGO composite coating

9.3.2.2 XRD analysis

The phase structure of the alloy and nanocomposite coatings were analyzed using XRD technique and the obtained XRD pattern are shown in Fig. 9.10. The distinct variation in the reflections of composite coating from the alloy coating confirms the variation in composition and thereby the variation in the crystal structure of the composite obtained after the incorporation of GO into the alloy matrix. The direction of crystal growth in the nanocomposite coating was observed to be changed to W-rich (220) plane than the (111) plane in the alloy. Further, there was a small shift in the positions of main peak reflections of the nanocomposite coating compared with the alloy coating. This shift in peak positions is attributed to the incorporation of GO and thereby the increased W content in the composite coating as compared with alloy coating. The refinement in grain size leading to the formation of nodular growths on the composite surface is also evident from the peak broadening effect, observed in the composite coating [Su et al. 2013, Kumar et al. 2013, Cargill III 1970]. The presence of (002) peak at $2\theta = 26.4°$ confirms that the GO is deposited as reduced graphene nanosheets into the alloy matrix [Kuang et al. 2013, Chen et al. 2011, Kumar et al. 2013], and hence, it can be called as Ni-W-rGO nanocomposite. Further, the W-rich nanocomposite coating resulted in the formation of new reflections corresponds to the W-rich phases. It may also note that

194

the intensity of the peaks present in the alloy coating was found to be decreased or disappeared in the nanocomposite coating along with the formation of new reflections.
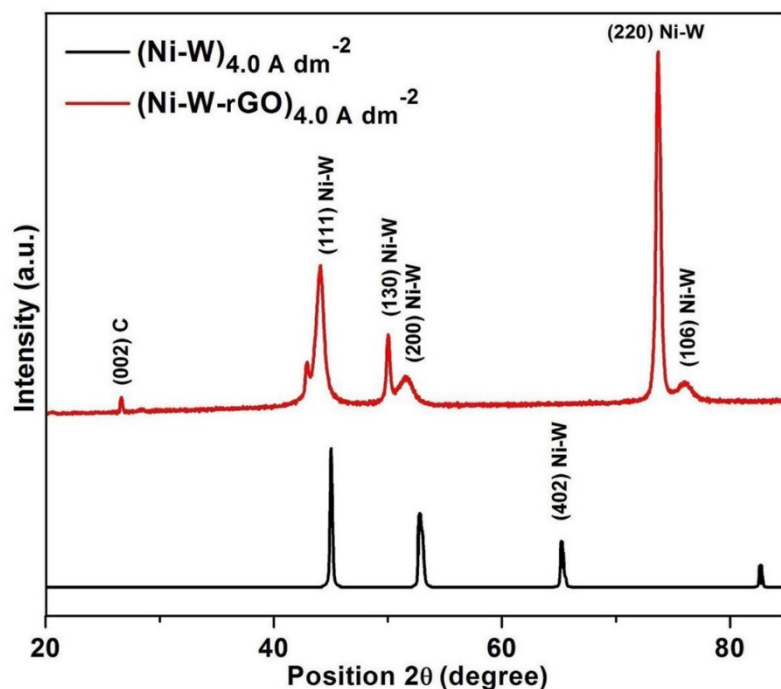
Fig. 9.10- The XRD pattern obtained for Ni-W alloy coating in comparison with the Ni-W-rGO nanocomposite coating

9.3.3 Effect of GO on coating properties

The addition of GO into the plating bath was found to influence the coating properties to a greater extent. The composite electrodeposition leading to the formation of Ni-W-rGO nanocomposite coating was found to be effective in enhancing the W content in the coating. The codeposition of the GO as rGO nanosheets along with the metal ions increased the effective surface area for deposition and thereby triggered the enhanced deposition also onto the surface of incorporated graphene nanosheets [Liu et al. 2011, Wang et al. 2014]. This type of enhanced deposition activated by the reduced graphene sheets intersticed in the alloy matrix resulted in the formation of W-rich nanocomposite coating. The effect of incorporated rGO on the coating properties such as composition, thickness and microhardness are given in Table 9.2. The alloy and composite coatings were found to be bright in visual observation. The thickness and microhardness of the

composite coating were also found to be increased in the composite coating with an increase in W content in the coating.

Table 9.2- The properties of the Ni-W alloy and Ni-W-rGO nanocomposite coating developed from the same bath under optimal conditions

Coatings developed at 4.0 A dm^{-2}	Wt.% of W in the deposit	Wt.% of C in the deposit	Thickness of the coating (µm)	Vicker's microhardness V_{100} (GPa)
Ni-W-rGO nanocomposite	22.4	3.1	16.1	3.91
Ni-W alloy	12.4	---	15.9	3.22

9.4 COMPARISON OF HER ACTIVITY OF Ni-W-MWCNT AND Ni-W-rGO NANOCOMPOSITES

The electrocatalytic activity of the Ni-W alloy coating towards alkaline HER was found to be improved in the nanocomposite coatings through the incorporation of C-nanomaterials such as MWCNT and GO. The electrochemical investigation on the enhancement in the electrocatalytic activity was carried out through CV and CP analysis, and the obtained results are discussed below.

9.4.1 Cyclic voltammetry and chronopotentiometry analysis

The activity and stability of the test electrodes towards alkaline HER was established by cycling the potential in the cathodic region. The variation in the CV curves of the alloy coating in comparison with the nanocomposite coatings are shown in Fig. 9.11. The variation in i_{pc} values of the coating with respect to onset potential for HER, obtained from the stable curves of cyclic voltammograms can give an idea about the robustness of the electrode material [Shen et al. 2011, Zeng and Zhang 2010]. The onset potential (*vs* SCE) of the nanocomposite electrodes were found to become nobler as compared with the alloy electrode and the Ni-W-MWCNT nanocomposite test electrode was found to have the least onset potential for HER (-0.97 V). The i_{pc} values

were also found to be increased for nanocomposite coatings compared with the alloy coating as given in Table 9.3. The maximum current response with respect to a minimum onset potential was observed to be present in the case of Ni-W-MWCNT nanocomposite test electrode (-1.07 A cm^{-2}). The optimal CV response of the Ni-W-MWCNT nanocomposite coating towards alkaline HER is attributed to the variation in surface morphology and composition, evidenced by SEM and EDS analysis.
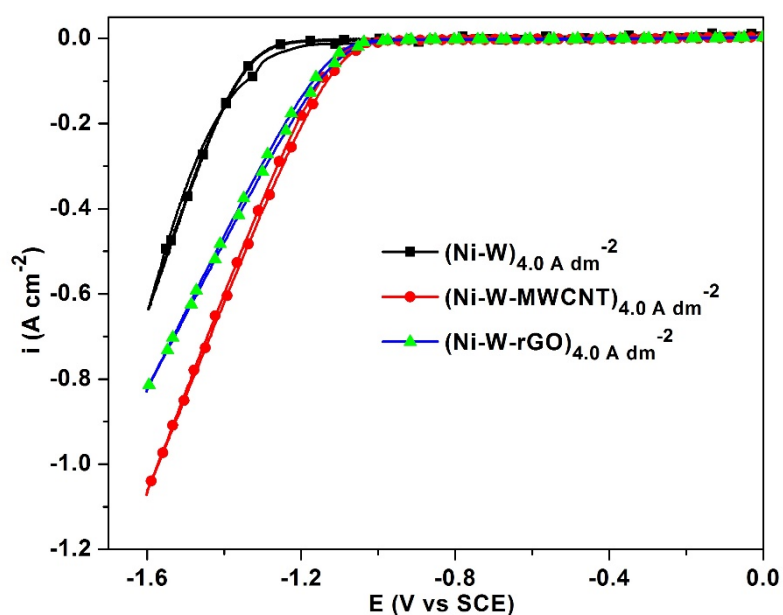
Fig. 9.11- The variation in CV responses of the Ni-W alloy coating in comparison with the Ni-W-MWCNT and Ni-W-rGO nanocomposite coatings

The CP responses of the alloy and composite coatings recorded under constant cathodic current represent the long-term stability and robustness in performance of the test electrodes under the working conditions of alkaline HER. The stable CP curves from the initial time till the end of 1800 s, obtained for all the test electrodes confirms the stability in performance of the developed coatings. Further, the practical working efficiency of the test electrodes was confirmed from the amount of H_2 gas evolved during the analysis. The obtained CP data also confirms Ni-W-MWCNT nanocomposite coating as the best coating towards alkaline HER with the maximum amount of H_2 gas evolved during the analysis (20.1 mL), as given in Table 9.3.
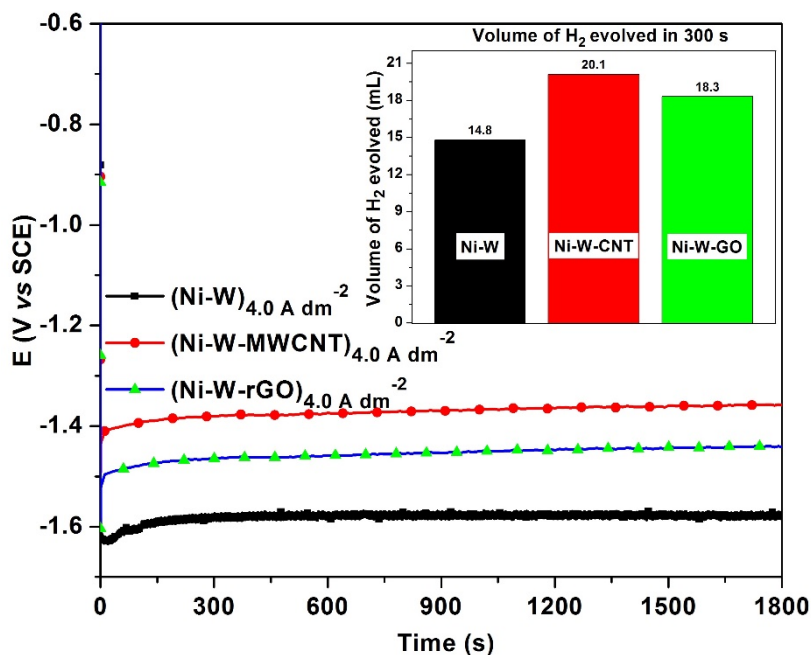
Fig. 9.12- The variation in CP responses along with the amount of H_2 evolved during the analysis (in the inset) for the Ni-W alloy coating in comparison with the Ni-W-MWCNT and Ni-W-rGO nanocomposite coatings

Table 9.3- The alkaline HER parameters of the Ni-W alloy in comparison with the Ni-W-MWCNT and Ni-W-rGO nanocomposite coatings

Coatings developed at 4.0 A dm^{-2}	Cathodic peak c.d. (A cm^{-2})	Onset potential for H_2 evolution (V vs SCE)	Volume of H_2 evolved in 300 s (mL)
Ni-W alloy	-0.66	-1.21	14.8
Ni-W-MWCNT nanocomposite	-1.07	-0.97	20.1
Ni-W-rGO nanocomposite	-0.83	-1.03	18.3

The increase in electrocatalytic efficiency of the nanocomposite coatings towards alkaline HER compared with the conventional Ni-W alloy coating is ascribed to the variation in surface morphology, phase structure and chemical composition resulted from the incorporation of C- nanomaterials such as MWCNT and GO. The influence of such nanomaterial additives on the induced codeposition of the reluctant

198

metal W in the plating bath resulted in the formation of low hydrogen overvoltage W-rich coatings, and thereby the enhanced electrocatalytic activity towards alkaline HER.

9.5 CONCLUSIONS

The following conclusions were made after analyzing the effect of C- nanomaterials on the coating properties and electrocatalytic activity towards alkaline HER:

1. The enhanced electrocatalytic activity of the Ni-W-MWCNT and Ni-W-rGO nanocomposite coatings compared with the conventional Ni-W alloy coating towards alkaline HER is attributed to the variation in surface morphology and composition, evidenced by SEM and EDS analysis.

2. The influence of nanomaterial additives (MWCNT and GO) on the induced codeposition of the reluctant metal W in the plating bath resulted in the formation of low hydrogen overvoltage W- rich coatings, and thereby the enhanced electrocatalytic activity towards alkaline HER

3. The Ni-W-MWCNT nanocomposite coating was obtained as the optimal electrode material for alkaline HER with a maximum cathodic current response (i_{pc} = -1.07 A cm^{-2}) at a minimum onset potential (-0.97 V) for HER.

CHAPTER 10

SUMMARY AND CONCLUSIONS

This chapter summarizes the experimental results of investigation on the corrosion resistance and electrocatalytic activity of electrodeposited Ni-based alloys (Ni-W and Ni-P) and their nanocomposite coatings. The improvement in corrosion resistance of alloy coatings through multilayer approach is presented and a comparison is made among the Ni-W and Ni-P multilayered alloy coatings along with their monolayer counterparts. The effect of deposition c.d. and applied B on the coating properties towards corrosion resistance and HER activity are presented here. The comparative study on the HER activity of alloys and their nanocomposite coatings have been reported comparatively here. The corrosion resistance and electrocatalytic efficiency of all alloy and nanocomposite coatings developed through different electrodeposition techniques have been reported, and the results are compared.

10.1 SUMMARY

Electroplating is an extremely important technology, and is concerned with covering inexpensive and widely available base materials with plated layers of different metals/alloys having superior properties to extend their use to applications which otherwise would be prohibitively expensive. Generally, electrodeposited alloys have a better appearance than the parent metals, being smoother, brighter, and finer grained. It is further asserted that relative to the single metals involved, alloy deposits can have different properties in certain composition ranges. They can be denser, harder, more corrosion resistant, more protective of the underlying base metal, tougher and stronger, more wear resistant, superior with respect to magnetic properties, more suitable for subsequent electroplate overlays and conversion chemical treatment, and superior in antifriction applications etc. Nowadays, the subject of alloy electroplating is being dealt with an ever increasing number of scientific publications. The reason for this is due to the vastness of the number of possible alloy combinations and the concomitant possible practical applications. Hence, the corrosion resistance of the electrodeposited Ni-W and

Ni-P alloy coatings have been studied and their corrosion resistance character was further enhanced through CMM and MED approach. The corrosion resistance of the coatings was analyzed in 5% NaCl, as representative corrosion medium, using electrochemical methods such as potentiodynamic polarization and EIS methods. The effectiveness of the electrodeposited alloy coatings as electrode material for water splitting reaction was studied in 1.0 M KOH medium using electrochemical methods. The HER efficiency of the alloy coatings was further enhanced using different methods such as MED, MFI-HER, electrochemical anodic dissolution and nanoparticles incorporation.

10.1.1 Optimization of Ni-W and Ni-P alloy plating baths

The Ni-W and Ni-P plating baths were optimized through Hull cell method, and the obtained optimal composition of the alloy plating baths are given in Table 10.1. Apart from the metal sources, all other constituents were maintained as the same in both Ni-W and Ni-P alloy plating baths, with slight variation in composition. The reluctant metals W and P were found to follow induced codeposition in the presence of inducing metal Ni and hence, the amount of reluctant metal salts were kept more compared to the inducing metal salt in both the alloy plating baths. The composition of the other constituents like complexing agent, buffer, conducting salt and brightener were optimized accordingly to epitomize the coating characteristics. The amount of the additive required in both the plating baths were found to be the same as shown in Table 10.1.

The operating parameters like c.d., pH, temperature etc. are also crucial factors affecting the coating properties. Accordingly, the operating parameters were optimized for better performance of the plating bath, and the optimal operating conditions are given in Table 10.1. The pH of the solutions was maintained as alkaline to ensure the complete solubility of the bath constituents and long-term stability of the bath. All the depositions were made at room temperature within the optimal c.d. range for each plating bath as given in Table 10.1.

Table 10.1- The composition and operating conditions of optimal Ni-W and Ni-P alloy plating baths

Bath constituents	Composition (per Liter)	
	Ni-W	Ni-P
NiSO$_4$·6H$_2$O	22.4 g	28.2 g
Na$_2$WO$_4$·2H$_2$O	46.07 g	-
NaPO$_2$H$_2$·H$_2$O	-	51.0 g
Na$_3$C$_6$H$_5$O$_7$·2H$_2$O	102.06 g	56.2 g
H$_3$BO$_3$	20.0 g	20.5 g
NH$_4$Cl	36.15 g	10.2 g
C$_3$H$_8$O$_3$	20.0 mL	20.0 mL
Operating parameters	Ni-W	Ni-P
pH	8.5	8.0
Temperature	303 K (30 °C)	303 K (30 °C)
c.d. range	1.0 – 4.0 A dm^{-2}	1.0 – 6.0 A dm^{-2}
Anode	Pure Ni	Pure Ni
Cathode	MS or Copper	MS or Copper

10.1.2 Characteristics of monolayer Ni-W and Ni-P alloy coatings

Ni-W and Ni-P monolayer alloy coating were developed on MS substrate and characterized for their thickness, hardness and corrosion resistance. All the coatings were deposited for same duration of time, 600 s (10 min), for comparison purpose. The comparison of the coating characteristics along with the CR's of the optimal Ni-W and Ni-P alloy coatings are given Table 10.2. From the data given in Table 10.2, it may be noticed that the Ni-W alloy coating shows superior properties compared with the Ni-P alloy coating. The improved coating characteristics of the Ni-W alloy compared with the Ni-P alloy coating is attributed to the superior characteristics of the alloying element W.

Table 10.2- Comparison of CR's and deposit characters of the optimal monolayer Ni-W and Ni-P alloy coatings developed from their respective baths

Monolayer alloy coatings	Ni-W	Ni-P
Optimal c.d. (A dm^{-2})	4.0	4.0
pH	8.5	8.0
Bath temperature (K)	303	303
Wt.% of the alloying elements in the deposit	W = 12.4 Ni = 87.6	P = 9.0 Ni = 91.0
CCE (%)	68.4	80.3
Coating thickness (µm)	15.9	18.3
Vickers microhardness (V$_{100}$) (GPa)	3.22	2.67
CR ($\times 10^{-2}$ mm y^{-1})	5.3	14.2
Nature of the deposit	Bright	Bright
Anode	Pure Ni	Pure Ni
Cathode	MS or Copper	MS or Copper

10.1.3 Electrodeposition of multilayered Ni-W and Ni-P alloy coatings

Nanolaminated multilayered Ni-W and Ni-P alloy coatings were developed on MS from their respective plating baths to enhance the corrosion protection efficacy of their monolayer counterparts. The CMMA coatings having nanolaminated layers of alternatively different composition have been achieved using pulsed DC, by cyclic modulation of cathode c.d. The composition and number of layers (hence thickness) were tailored by periodic modulation of c.d. and time, using a programmable power source. The deposition conditions were optimized for both composition and thickness of individual layers for best performance of the coatings against corrosion. The comparison of CR's of the optimal monolayer and multilayered Ni-W and Ni-P alloy coatings are shown in Fig. 10.1. The CMMA coatings were found to show many fold increase in corrosion resistance as compared to its monolayer counterpart developed from the same electrolytic bath. Drastic improvement in the corrosion protection

efficacy of nanolaminated multilayered Ni-W and Ni-P alloy coatings were attributed to increase in number of interfaces, separating layers of alloys having different morphology, composition and phase structures. Whereas, the corrosion resistance of the multilayered alloy coatings was found to be improved with increase in number of layers, only up to an optimal level and then decreased. The decrease of corrosion resistance at higher degree of layering is attributed to the interlayer diffusion of the multilayers to become monolayer, due to very short deposition time of each layer. The CMM N-W alloy coating was found to be superior in corrosion resistance than the CMM Ni-P alloy with very low CR as given in Table 10.3 and Fig. 10.1.
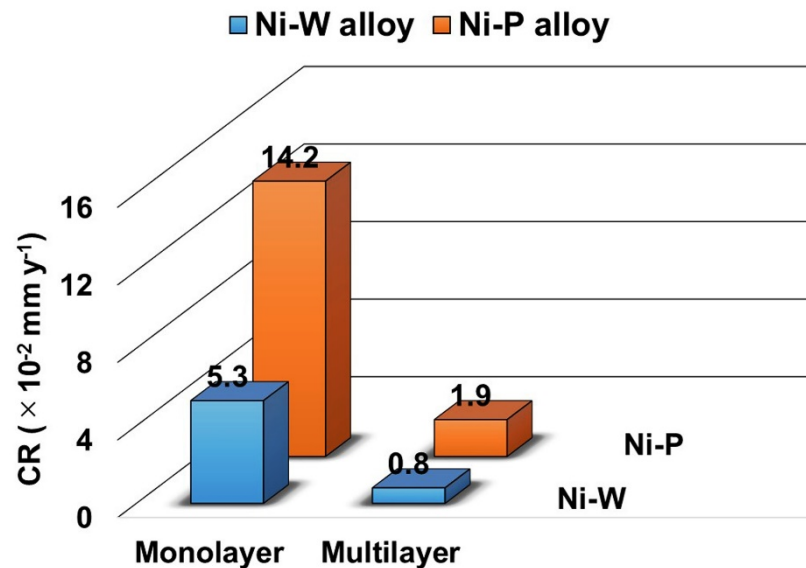
Fig. 10.1- Comparison of the corrosion rates of monolayer and multilayered Ni-W and Ni-P alloy coatings under optimal conditions

10.1.4 MED Ni-W alloy coatings for improved corrosion resistance

High corrosion resistant Ni-W alloy coatings were developed using MED approach for the protection of MS substrates. The conditions for the development of more corrosion resistant MED Ni-W alloy coatings were optimized by inducing *B* during deposition, in terms of intensity and direction, from the same bath. The applied *B* was used as a tool to alter the crystallinity, composition and thereby the corrosion resistance of the coatings. Significant increase in corrosion resistance exhibited by MED coatings (under both parallel and perpendicular *B*) is attributed to the increased W content of the alloy

affected by an increase in i_L value. The enhanced mass transport and thereby the increase in i_L was resulted from the MHD effect, in the presence of applied B. The MED coatings developed under perpendicular B was found to show superior properties over the coatings developed under parallel. The enhanced characteristics of MED coatings developed under perpendicular B are attributed to the maximum MHD effect, arises mainly due to Lorentz force. The Lorentz force (given by the equation $F_L = qvB \sin\theta$) is maximum under perpendicular B (where, $\theta = 90°$), and is zero under parallel B (where, $\theta = 0$). The comparison of CR's of the optimal Ni-W alloy coatings developed using different approaches from the same bath are shown in Fig. 10.2. From the comparison given in Fig. 10.2 and Table 10.3, it is clear that the MED is the best method to develop a high corrosion resistant Ni-W alloy coating.
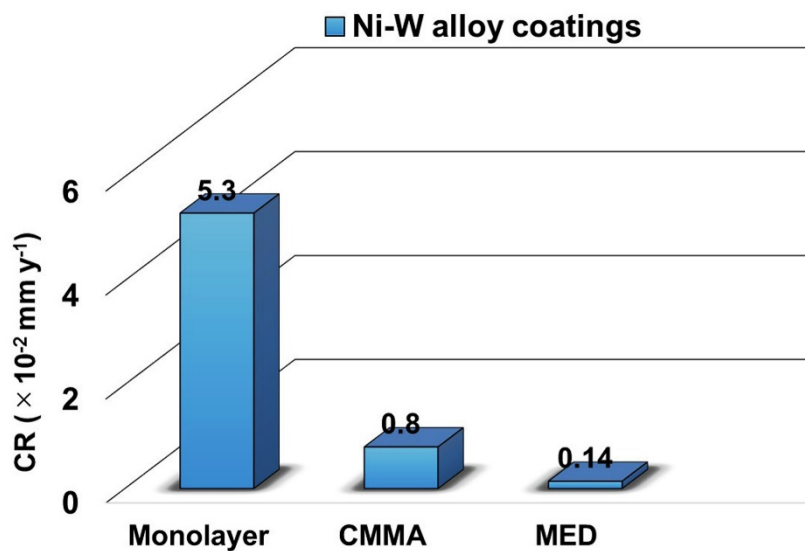
Fig. 10.2- Comparison of CR's of the optimal Ni-W alloy coatings developed using different approaches

The comparison of overall corrosion study results of the optimal Ni-W and Ni-P alloy coatings developed using different techniques are given in Table 10.3. The data shown in Table 10.3 suggests the multilayer and MED approaches as promising methods for enhancing the corrosion resistance of the conventional alloy coatings. Among all the coatings developed, the MED coating with configuration (Ni-W)$_{B=0.2 \text{ T/per}}$ was observed as the best coating with least CR.

Table 10.3- Comparison of CR's of binary Ni-W and Ni-P alloy coatings, developed through different approaches under optimal conditions

Coating type	Optimal coating configuration	$-E_{corr}$ (mV vs SCE)	i_{corr} ($\mu A\ cm^{-2}$)	CR ($\times 10^{-2}$ mm y^{-1})
Ni-W	Monolayer (Ni-W)$_{4.0}$	487	6.5	5.3
	CMMA (Ni-W)$_{1.0/4.0/300}$	359	1.0	0.8
	MED (Ni-W)$_{B=0.2\ T/per}$	361	1.1	0.14
Ni-P	Monolayer (Ni-P)$_{4.0}$	513	12.0	14.2
	CMMA (Ni-P)$_{1.0/4.0/300}$	496	1.0	1.9

10.1.5 Electrocatalytic activity study

The electrocatalytic activity of the Ni-W and Ni-P alloy coatings towards HER and OER were analyzed in alkaline 1.0 M KOH medium. The electrochemical methods such as CV and CP techniques were used to testify the robustness of the test electrodes under the electrocatalytic working conditions. Further, the practical utility of the electrode materials was evaluated by quantifying the amount of H_2 and O_2 gases evolved during the analysis. The optimal conditions used for the electrocatalytic study are tabulated in Table 10.5.

Table 10.4- The optimal conditions used for the electrocatalytic study of Ni-W and Ni-P alloy coatings, and their nanocomposite coatings

Operating parameters	Optimal condition
Medium	1.0 M KOH
Temperature	303 K (30 °C)
Working electrode	Electrodeposited Ni-W and Ni-P alloys or their nanocomposite coatings achieved on copper substrate
Counter electrode	Platinized platinum
Reference electrode	SCE
Cathodic cyclic potential sweep applied for HER	0.0 to -1.6 V
Anodic cyclic potential sweep applied for OER	0.0 to +0.75 V
Scan rate for CV	50 mV s^{-1}
Constant cathodic c.d. applied for HER CP	-300 mA cm^{-2}
Constant anodic c.d. applied for OER CP	+300 mA cm^{-2}
Time for CP analysis	1800 s

10.1.5.1 Electrocatalytic activity of Ni-W and Ni-P alloy coatings

The effect of alloying elements, W and P, on the electrocatalytic activity of Ni was studied, based on their induced codeposition behavior, and related to the composition, structure and surface morphology of the developed coatings. A dependency of the electrocatalytic activity for HER and OER with relative amount of the alloying elements in the deposit was found in both Ni-W and Ni-P alloy coatings. The variation of electrocatalytic activity with W or P content in the alloy coatings showed the existence of a synergism between Ni and the alloying elements. In both the cases, the

coating with optimal characteristics towards HER was found to show very low activity towards OER and vice versa. A comparison of the electrocatalytic efficiencies of the optimal Ni-W and Ni-P alloy coatings towards HER and OER, in terms of the H_2 and O_2 gases evolved (in 300 s) during the analysis are shown in Fig. 10.3. The corresponding HER and OER parameters of both the alloys are given in Table 10.5. The obtained results showed that the alloying of Ni with W gives superior properties towards HER, attributed by its better hydrogen adsorption energy than in Ni-P alloy.
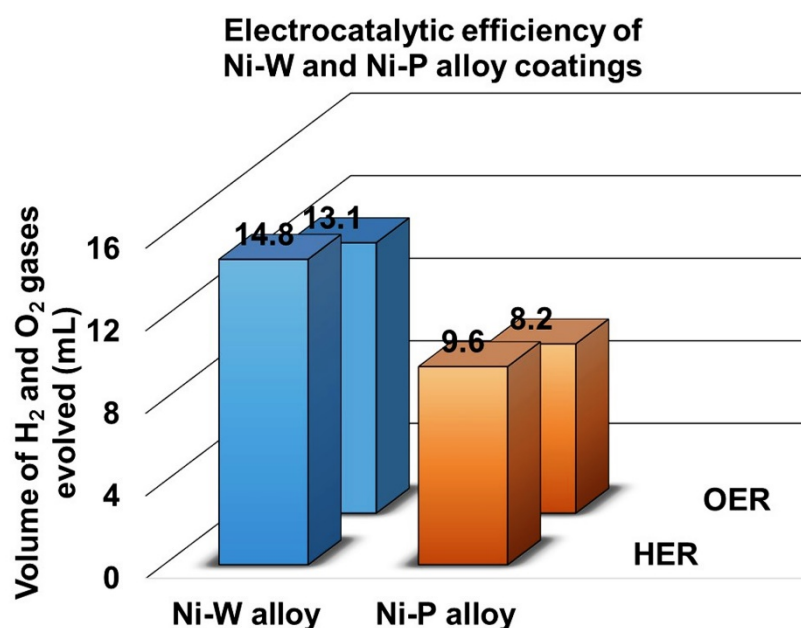
Fig. 10.3- Comparison of the electrocatalytic activity of the optimal Ni-W and Ni-P alloy coatings towards HER and OER, in terms of the amount of H_2 and O_2 gases evolved in 300 s from the corresponding test electrodes

10.1.5.2 Methods for enhancing the HER efficiency of alloy coatings

The HER efficiency of the Ni-W and Ni-P alloy test electrodes were further enhanced by modifying the electrode material through MED approach, electrochemical dissolution method and nanoparticles incorporation. Moreover, the HER efficiency was tried to enhance through MFI-HER approach, by altering the working conditions of electrolysis rather than modifying the electrode material. The HER activity of the optimal Ni-P alloy coating (developed at 4.0 A dm^{-2}) was enhanced by modifying the alloy test electrode through electrochemical anodic dissolution, to increase the effective surface area, and nanocomposite coating development. Accordingly, Ni-P-TiO$_2$ and Ni-

P-Ag nanocomposite coatings were developed through composite electrodeposition and sol-enhanced electrodeposition, respectively. Similarly, the HER activity of the optimal Ni-W alloy coating (deposited at 4.0 A dm^{-2}) was further enhanced by modifying the alloy test electrode through MED approach, to enhance the W content in the deposit, and nanocomposite coating development. In this regard, Ni-W-MWCNT and Ni-W-rGO nanocomposite coatings were developed to improve the HER efficiency of Ni-W alloy. Further, the HER efficiency of optimal Ni-W alloy test electrode was enhanced by inducing *B* of varying intensities during electrolysis (in the perpendicular direction), without making any modifications to the test electrode.

10.1.5.3 HER efficiency of the modified Ni-P test electrodes

The HER activity of the modified Ni-P coatings achieved through different methods in comparison with the optimal alloy coating is shown in Fig. 10.4, and the corresponding HER parameters are given in Table 10.5. The HER activity of the optimal Ni-P alloy electrode was found to show improvement after each modification such as electrochemical dissolution, TiO_2 incorporation and Ag nanoparticle incorporation. The Ni-P-Ag nanocomposite coating was found to show the optimal HER characteristics among the modified Ni-P alloy test electrodes. The observed intensification in electrocatalytic activity of the Ni-P-Ag nanocomposite electrode for alkaline HER is accredited to the increased surface area and the increased number of active sites for hydrogen adsorption affected by the homogeneous dispersion of the Ag nanoparticles in the alloy matrix, achieved through sol-enhanced electroplating technique.

HER efficiency of Ni-P alloy and its nanocomposite coatings

Values shown on bars: 9.6 (Ni-P), 13.2 (Anodically treated Ni-P), 15.2 (Ni-P-TiO$_2$), 18.8 (Ni-P-Ag)

Y-axis: Volume of H$_2$ evolved (mL); X-axis categories: Ni-P, Anodically treated Ni-P, Ni-P-TiO$_2$, Ni-P-Ag
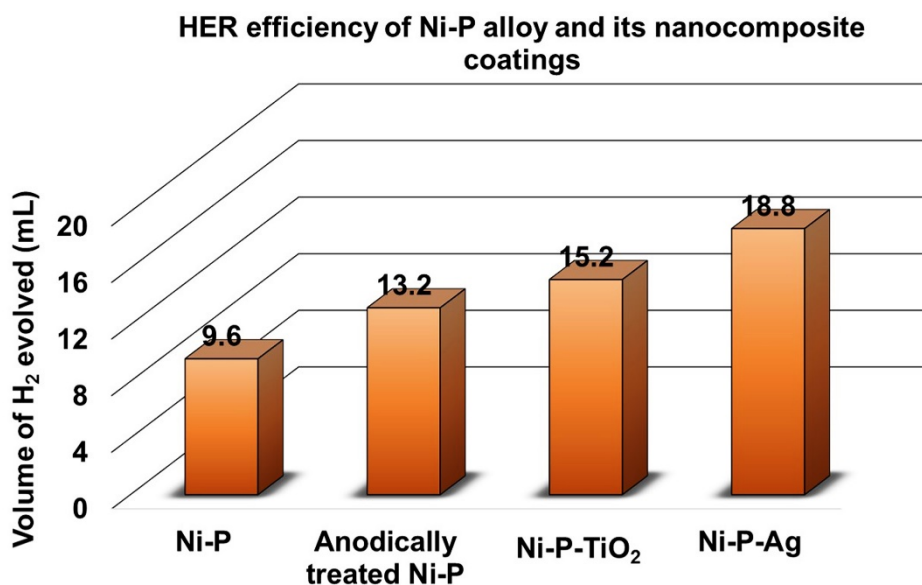
Fig. 10.4- Comparison of the HER activity of Ni-P alloy and its nanocomposite coatings developed using different methods, in terms of the amount of H$_2$ gas evolved in 300 s

10.1.5.4 Magnetic field effect on electrocatalytic activity of Ni-W alloy

The effect of applied magnetic field was utilized in two directions to enhance the HER activity of Ni-W alloy. Magnetic field effect during electrodeposition (MED) was utilized to modify the electrode material in one way and in another way, the effect of induced magnetic field during electrocatalytic study (MFI-HER) was utilized to reduce the overvoltage due to bubble resistance. In the case of modified Ni-W alloy coatings through MED approach, the improvement in HER activity is attributed to the increased W content. Whereas, in the case of MFI-HER, the enhancement is due to the MHD force induced convection and H$_2$ bubble disentanglement. The comparison of HER activity on Ni-W alloy under different conditions are shown in Fig. 10.5, and the corresponding data are given in Table 10.5.

10.1.5.5 Effect of MWCNT and GO on the HER efficiency of Ni-W alloy

Ni-W-MWCNT and Ni-W-rGO coatings were developed by exploiting the advantage of composite electrodeposition technique. The nanocomposite coatings were deposited from the optimal bath containing homogeneously dispersed functionalized MWCNTs and GO (synthesized using chemical method). The added GO was found to be deposited as rGO, as evidenced from the characterization techniques. Interestingly, the MWCNT

and GO added into the plating bath was found to influence the induced codeposition of the reluctant metal W, and thereby the electrocatalytic efficiency. Drastic improvement in the electrocatalytic activity for HER was found in both Ni-W-MWCNT and Ni-W-rGO nanocomposite coatings, compared to the as-coated Ni-W alloy. The obtained results showed that the Ni-W-MWCNT nanocomposite coating as the best electrode material for alkaline HER, attributed by both increased W content and number of electroactive centers, affected by the homogeneous distribution of MWCNT in the alloy matrix. The HER activity of the Ni-W alloy coatings of different composition and under a different operating condition in comparison with its nanocomposite coatings are shown in Fig. 10.5. The corresponding HER parameters are tabulated in Table 10.5.
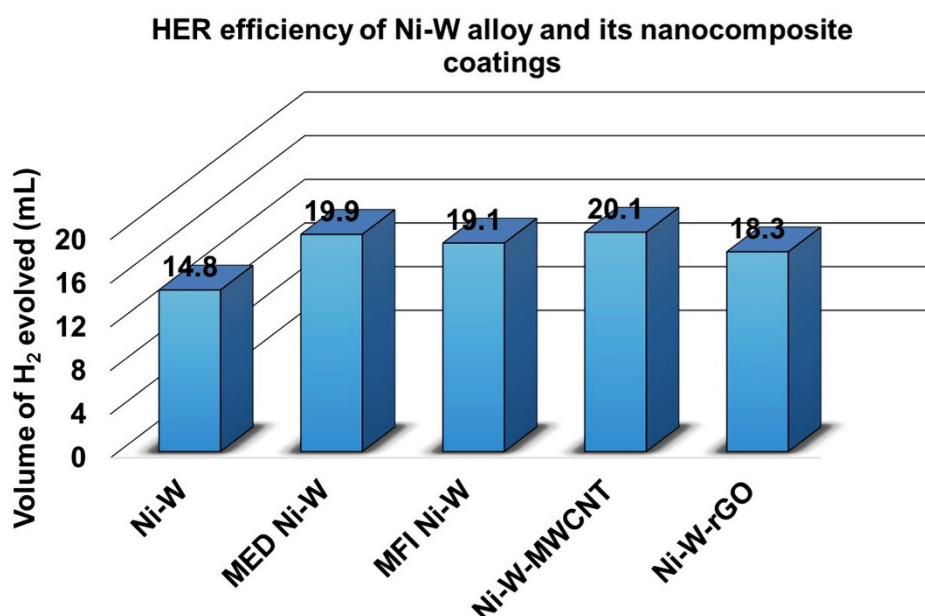
Fig. 10.5- Comparison of the HER activity of Ni-W alloy and its nanocomposite coatings developed using different methods, in terms of the amount of H_2 gas evolved in 300 s

The overall electrocatalytic study results of the optimal Ni-W and Ni-P alloy coatings and their nanocomposite coatings are tabulated in Table 10.5. The obtained results confirm that the nanoparticles incorporation and the utilization of magnetic field effects as promising techniques to enhance the HER activity of conventional alloy coatings. Among all the alloy and nanocomposite test electrodes tested for HER

efficiency, the Ni-W-MWCNT nanocomposite coating was observed as the best electrode material for alkaline HER.

Table 10.5- The comparison of electrocatalytic activity study results of the optimal Ni-W and Ni-P alloy coatings, and their nanocomposite coatings

Activity for	Alloy coating type	Optimal coating configuration	Cathodic peak c.d. at -1.6 V (A cm^{-2})	Onset potential for H$_2$ evolution (V *vs* SCE)	Volume of H$_2$ evolved in 300 s (mL)
HER	Ni-W	(Ni-W)$_{4.0}$	-0.66	-1.21	14.8
		MED (Ni-W)$_{B=0.2 \text{ T/per}}$	-0.97	-0.99	19.9
		MFI (Ni-W)$_{B=0.4 \text{ T}}$	-0.82	-1.01	19.1
		(Ni-W-MWCNT)$_{4.0}$	-1.07	-0.97	20.1
		(Ni-W-rGO)$_{4.0}$	-0.83	-1.03	18.3
	Ni-P	(Ni-P)$_{4.0}$	-0.13	-1.30	9.6
		Anodically treated (Ni-P)$_{4.0}$	-0.26	-1.22	13.2
		(Ni-P-TiO$_2$)$_{4.0}$	-0.38	-1.19	15.2
		(Ni-P-Ag)$_{4.0}$	-0.59	-0.95	18.8

Activity for	Coating type	Optimal coating configuration	Anodic peak c.d. at 0.75 V (A cm^{-2})	Onset potential of O$_2$ evolution (V *vs* SCE)	Volume of O$_2$ evolved in 300 s (mL)
OER	Ni-W	(Ni-W)$_{1.0}$	1.25	0.51	13.1
	Ni-P	(Ni-P)$_{2.0}$	0.22	0.43	8.2

10.2 CONCLUSIONS

1. New alkaline citrate baths were optimized for the development of Ni-W and Ni-P alloy coatings using standard Hull cell method.

2. The coating developed at 4.0 A dm^{-2} was obtained as the optimal coating with least CR in case of both Ni-W and Ni-P alloy coatings deposited from their respective baths.

3. The corrosion resistance of monolayer Ni-W and Ni-P alloy coatings were increased to many folds of its magnitude by the development of nanolaminated multilayer alloy coatings using pulsed DC.

4. Electrochemical corrosion study demonstrated that the multilayered Ni-W and Ni-P alloy coatings with 300 layers, represented as (Ni-M)$_{1.0/4.0/300}$ is showing the least CR compared to their monolayer coatings, developed from the same bath using non-pulsed DC.

5. The MED Ni-W alloy coating with configuration (Ni-W)$_{B=0.2\ T/per}$ was obtained as the best alloy coating with least CR among all Ni-W and Ni-P alloy coatings developed using different techniques.

6. The Ni-W and Ni-P alloy coatings obtained at 4.0 A dm^{-2} (having about 12.4 wt.% W and 9.0 wt.% P, respectively) were obtained as the optimal cathode materials for HER, deposited from their respective baths.

7. The HER efficiency of the optimal Ni-W alloy test electrode was enhanced through MED and MFI-HER approach.

8. The Ni-P-Ag nanocomposite coating was obtained as the best electrode material for alkaline HER among all the other Ni-P alloy based test electrodes developed by different methods.

9. The Ni-W-MWCNT nanocomposite coating was obtained as the best electrode material for alkaline HER among all the other Ni-W and Ni-P alloys and their nanocomposite coatings studied.

10. The experimental results of corrosion and electrocatalytic study of electrodeposited Ni-based alloys and their nanocomposite coatings showed that there exist a strong dependence of the coating properties on the composition, structure and surface morphology.

11. The magnetic field induced mass transfer was confirmed as the most effective mode of mass transport to impart better coating properties in terms of corrosion resistance and electrocatalytic activity.

SCOPE FOR FURTHER WORK

❖ Use of other additives or alloying elements (to form ternary alloy) can further improve the coating characteristics of binary Ni-W and Ni-P alloy coatings.

❖ Doping of other nanoparticles to improve the performance of coatings.

❖ Magnetic field effects on coating characters of Ni-P alloy can be explored.

❖ Magnetoelectrodeposition may give better coating properties to nanocomposite coatings through the homogeneous dispersion of the nanoparticles in the alloy matrix, which is otherwise difficult to achieve.

❖ Multilayered coatings of these alloys can be prepared by bringing modulation in mass transport at the cathode through ultrasonic and magnetic field effects.

❖ The approach can be extended for the development of many other alloy/nanocomposite coatings for exploring their photocatalytic and sensor applications.

REFERENCES

Aaboubi, O. and Msellak, K. (2016). "Magnetic field effects on the electrodeposition of Co-Ni-Mo alloys." *Appl. Surf. Sci.*, *396* 375–383.

Aaboubi, O., Omar, A. Y. Ali, Franczak, A. and Msellak, K. (2015). "Investigation of the electrodeposition kinetics of Ni–Mo alloys in the presence of magnetic field." *J. Electroanal. Chem.*, *737* 226–234.

Aal, A. A. and Hassan, H. B. (2009). "Electrodeposited nanocomposite coatings for fuel cell application." *J. Alloys Compd.*, *477* (1), 652–656.

Abdullah, A. and Annapoorni, S. (2005). "Fluorescent silver nanoparticles via exploding wire technique." *Pramana*, *65* (5), 815–819.

Ahmad, Z. (2006). *Principles of corrosion engineering and corrosion control*, Butterworth-Heinemann, Elsevier, USA.

Akiyama, T. and Fukushima, H. (1992). "Recent Study on the Mechanism of the Electrodeposition of Iron-group Metal Alloys." *ISIJ Int.*, *32* (7), 787–798.

Allahbakhsh, A., Sharif, F., Mazinani, S. and Kalaee, M. R. (2014). "Synthesis and characterization of Graphene Oxide in suspension and powder forms by chemical exfoliation method." *Int. J. Nano Dimension*, *5* (1), 11.

Allen, J. B., Larry, R. F. and others (2001). *Electrochemical methods: fundamentals and applications*, Department of Chemistry and Biochemistry University of Texas at Austin, John Wiley & Sons, USA.

Amadeh, A., Moradi, H. and others (2009). "Wear behavior of carbon steel electrodeposited by nanocrystalline Ni–W coating." *Int. J. Iron & Steel Soc. Iran*, *6* (2), 14–19.

Arai, S., Fujimori, A., Murai, M. and Endo, M. (2008). "Excellent solid lubrication of electrodeposited nickel-multiwalled carbon nanotube composite films." *Mater. Lett.*, *62* (20), 3545–3548.

Aravinda, C. L., Muralidharan, V. S. and Mayanna, S. M. (2000). "Electrodeposition and dissolution of Co–W alloy films." *J. Appl. Electrochem.*, *30* (5), 601–606.

Aruna, S. T., Grips, V. W. and Rajam, K. S. (2009). "Ni-based electrodeposited composite coating exhibiting improved microhardness, corrosion and wear resistance properties." *J. Alloys Compd.*, *468* (1), 546–552.

Bachvarov, V., Lefterova, E. and Rashkov, R. (2016). "Electrodeposited Ni-Fe-Co and Ni-Fe-Co-P alloy cathodes for hydrogen evolution reaction in alkaline medium." *Int. J. Hydrogen Energy*, *41* (30), 12762–12771.

Badrayyana, S., Bhat, D. K., Shenoy, S., Ullal, Y. and Hegde, A. C. (2015). "Novel Fe–Ni-graphene composite electrode for hydrogen production." *Int. J. Hydrogen Energy*, *40* (33), 10453–10462.

Bakar, H. (1992). *ASM Handbook Volume 3 Alloy Phase Diagrams*, ASM International, Materials Park, Ohio, USA.

Balat, M. (2008). "Potential importance of hydrogen as a future solution to environmental and transportation problems." *Int. J. Hydrogen Energy*, *33* (15), 4013–4029.

Balzer, R. J. and Vogt, H. (2003). "Effect of electrolyte flow on the bubble coverage of vertical gas-evolving electrodes." *J. Electrochem. Soc.*, *150* (1), E11–E16.

Bard, A. J. and Faulkner, L. R. (2000). *Electrochemical Methods: Fundamentals and Applications*, Wiley, New York.

Bard, A. J. and Zoski, C.G. (2013). *Electroanalytical Chemistry: A Series of Advances: Volume 25*, CRC Press, USA.

Bard, A. J., Faulkner, L. R., Leddy, J. and Zoski, C. G. (1980). *Electrochemical methods: fundamentals and applications*, Wiley, New York.

Barsoukov, E. and Macdonald, J. R. (2005). *Impedance spectroscopy: theory, experiment, and applications*, John Wiley & Sons, New York.

Berkh, O., Eliaz, N. and Gileadi, E. (2014). "The Initial Stages of Electrodeposition of Re-Ni Alloys." *J. Electrochem. Soc.*, *161* (5), D219–D226.

Blum, W. (1921). "The structure and properties of alternately deposited metals." *Trans. Am. Electrochem. Soc.*, *40* 307–320.

Bockris, J. O. and Khan, S. U. (2013). *Surface electrochemistry: a molecular level approach*, Springer Science & Business Media, Germany.

Brenner, A. (1963). *Electrodeposition of alloys: principles and practice*, Academic Press, USA.

Brett, C. M. and Brett, A. M. O. (1993). *Electrochemistry: principles, methods, and applications*, Oxford university press, UK.

Brooks, I., Lin, P., Palumbo, G., Hibbard, G. D. and Erb, U. (2008). "Analysis of hardness–tensile strength relationships for electroformed nanocrystalline materials." *Mater. Sci. Eng. A*, *491* (1), 412–419.

Brooman, E. W. (2000). "Corrosion performance of environmentally acceptable alternatives to cadmium and chromium coatings: Chromium—Part II." *Metal Finishing*, *98* (8), 39–45.

Bund, A., Koehler, S., Kuehnlein, H. H. and Plieth, W. (2003). "Magnetic field effects in electrochemical reactions." *Electrochim. Acta*, *49* (1), 147–152.

Burchardt, T. (2000). "The hydrogen evolution reaction on $Ni-P_x$ alloys." *Int. J. Hydrogen Energy*, *25* (7), 627–634.

Cardoso, D. S. P., Amaral, L., Santos, D. M. F., Šljukić, B., Sequeira, C. A. C., Macciò, D. and Saccone, A. (2015). "Enhancement of hydrogen evolution in alkaline water electrolysis by using nickel-rare earth alloys." *Int. J. Hydrogen Energy*, *40* (12), 4295–4302.

Cargill III, G.S. (1970). "Structural Investigation of Noncrystalline Nickel-Phosphorus Alloys." *J. Appl. Phys.*, *41* (1), 12–29.

Chandrasekar, M. S. and Pushpavanam, M. (2008). "Pulse and pulse reverse plating—Conceptual, advantages and applications." *Electrochim. Acta*, *53* (8), 3313–3322.

Chen, L., Tang, Y., Wang, K., Liu, C. and Luo, S. (2011). "Direct electrodeposition of reduced graphene oxide on glassy carbon electrode and its electrochemical application." *Electrochem. Commun.*, *13* (2), 133–137.

Chen, W., He, Y. and Gao, W. (2010a). "Electrodeposition of sol-enhanced nanostructured $Ni-TiO_2$ composite coatings." *Surf. Coat. Technol.*, *204* (15), 2487–2492.

Chen, W., He, Y. and Gao, W. (2010b). "Synthesis of Nanostructured Ni–TiO$_2$ Composite Coatings by Sol-Enhanced Electroplating." *J. Electrochem. Soc.*, *157* (8), E122–E128.

Chen, X. H., Cheng, F. Q., Li, S. L., Zhou, L. P. and Li, D. Y. (2002). "Electrodeposited nickel composites containing carbon nanotubes." *Surf. Coat. Technol.*, *155* (2), 274–278.

Chen, Z., Ma, Z., Song, J., Wang, L. and Shao, G. (2016). "Novel one-step synthesis of wool-ball-like Ni-carbon nanotubes composite cathodes with favorable electrocatalytic activity for hydrogen evolution reaction in alkaline solution." *J. Power Sources*, *324* 86–96.

Cong, R. G. (2013). "An optimization model for renewable energy generation and its application in China: a perspective of maximum utilization." *Renewable Sustainable Energy Rev.*, *17* 94–103.

Correia, A. N., Machado, S. A. and Avaca, L. A. (1999). "Studies of the hydrogen evolution reaction on smooth Co and electrodeposited Ni–Co ultramicroelectrodes." *Electrochem. Commun.*, *1* (12), 600–604.

Cramer, S. D. and Covino Jr, B. S. (2005). *ASM Handbook Volume 13b: Corrosion: Materials*, ASM international, Ohio, USA.

Crousier, J., Hanane, Z. and Crousier, J. P. (1993). "A cyclic voltammetry study of the Ni-P electrodeposition." *Electrochim. Acta*, *38* (2), 261–266.

Crousier, J., Hanane, Z. and Crousier, J. P. (1994). "Electrodeposition of Ni-P amorphous alloys. A multilayer structure." *Thin Solid Films*, *248* (1), 51–56.

Danilov, F. I., Tsurkan, A. V., Vasil'eva, E. A. and Protsenko, V. S. (2016). "Electrocatalytic activity of composite Fe/TiO$_2$ electrodeposits for hydrogen evolution reaction in alkaline solutions." *Int. J. Hydrogen Energy*, *41* (18), 7363–7372.

Danilovic, N., Subbaraman, R., Strmcnik, D., Chang, K. C., Paulikas, A. P., Stamenkovic, V. R. and Markovic, N. M. (2012). "Enhancing the alkaline hydrogen evolution reaction activity through the bifunctionality of Ni(OH)$_2$/metal catalysts." *Angew. Chem.*, *124* (50), 12663–12666.

Devos, O., Aaboubi, O., Chopart, J. P., Olivier, A., Gabrielli, C. and Tribollet, B. (2000). "Is there a magnetic field effect on electrochemical kinetics?" *J. Phys. Chem. A*, *104* (7), 1544–1548.

Ding, G., Wang, Y., Deng, M., Cui, X., Wu, H. and Zhu, L. (2011). *Research and Application of CNT Composite Electroplating*, InTech Publications, Croatia.

Dini, J. (1993). *Electrodeposition: The Materials Science of Coatings and Substrates*, Noyes Publications, New Jersey.

Dini, J. W. (1993). *Electrodeposition*, Noyes Publications, New Jersey.

Dobrzanski, L. A., Lukaszkowicz, K., Pakula, D. and Mikula, J. (2007). "Corrosion resistance of multilayer and gradient coatings deposited by PVD and CVD techniques." *Arch. Mater. Sci. Eng.*, *28* (1), 12–18.

Domínguez-Crespo, M. A., Torres-Huerta, A. M., Brachetti-Sibaja, B. and Flores-Vela, A. (2011). "Electrochemical performance of Ni–RE (RE= rare earth) as electrode material for hydrogen evolution reaction in alkaline medium." *Int. J. Hydrogen Energy*, *36* (1), 135–151.

Dong, P. Van, Ha, C. H., Kasbohm, J. and others (2012). "Chemical synthesis and antibacterial activity of novel-shaped silver nanoparticles." *Int. Nano Lett.*, *2* (1), 1–9.

Donten, M., Cesiulis, H. and Stojek, Z. (2000). "Electrodeposition and properties of Ni-W, Fe-W and Fe-Ni-W amorphous alloys. A comparative study." *Electrochim. Acta*, *45* (20), 3389–3396.

Du, J., Xie, S., Li, N. and Xu, L. (2000). "Preparation of Ni–Mo–Co Alloy Electrodes and Their Electrocatalytic Activities for Hydrogen Evolution." *Nanosci. Nanotechnol. Lett.*, *8* (5), 382–386.

Dukovic, J. O. and Tobias, C. W. (1990). "Simulation of leveling in electrodeposition." *J. Electrochem. Soc.*, *137* (12), 3748–3755.

Dumelié, N., Benhayoune, H., Rousse-Bertrand, C., Bouthors, S., Perchet, A., Wortham, L., Douglade, J., Laurent-Maquin, D. and Balossier, G. (2005). "Characterization of electrodeposited calcium phosphate coatings by complementary scanning electron microscopy and scanning-transmission electron microscopy associated to X-ray microanalysis." *Thin Solid Films*, *492* (1), 131–139.

Ebadi, M., Basirun, W. J., Alias, Y., Mahmoudian, M. R. and Leng, S. Y. (2012). "Investigation of electrodeposition of Ni–Co–Fe–Zn alloys in DMSO with MHD effect." *Mater. Charact.*, *66* 46–55.

Eliaz, N. and Gileadi, E. (2008). *Induced codeposition of alloys of tungsten, molybdenum and rhenium with transition metals.* In: Modern Aspects of Electrochemistry, Springer, New York, pp 191–301.

Eliaz, N., Sridhar, T. M. and Gileadi, E. (2005). "Synthesis and characterization of nickel tungsten alloys by electrodeposition." *Electrochim. Acta*, *50* (14), 2893–2904.

Elsener, B., Atzei, D., Krolikowski, A. and Rossi, A. (2008). "Effect of phosphorus concentration on the electronic structure of nanocrystalline electrodeposited Ni–P alloys: an XPS and XAES investigation." *Surf. Interface Anal.*, *40* (5), 919–926.

Eroglu, D., Vilinska, A., Somasundaran, P. and West, A. C. (2013). "Use of dispersants to enhance incorporation rate of nano-particles into electrodeposited films." *Electrochim. Acta*, *113* 628–634.

Fahidy, T. Z. (1973). "Hydrodynamic models in magnetoelectrolysis." *Electrochim. Acta*, *18* (8), 607–614.

Fahidy, T. Z. (1983). "Magnetoelectrolysis." *J. Appl. Electrochem.*, *13* (5), 553–563.

Fei, J. Y. and Wilcox, G. D. (2005). "Electrodeposition of Zn–Co alloys with pulse containing reverse current." *Electrochim. Acta*, *50* (13), 2693–2698.

Feng, J., Gong, M., Kenney, M. J., Wu, J. Z., Zhang, B., Li, Y. and Dai, H. (2015). "Nickel-coated silicon photocathode for water splitting in alkaline electrolytes." *Nano Res.*, *8* (5), 1577–1583.

Filzwieser, A., Hein, K. and Mori, G. (2002). "Current density limitation and diffusion boundary layer calculation using CFD method." *JOM*, *54* (4), 28–31.

Fontana, M. G. (2005). *Corrosion engineering*, McGraw-Hill Education, USA.

Gan, Y. X. (2012). "Structural assessment of nanocomposites." *Micron*, *43* (7), 782–817.

Ganesh, V., Vijayaraghavan, D. and Lakshminarayanan, V. (2005). "Fine grain growth of nickel electrodeposit: effect of applied magnetic field during deposition." *Appl. Surf. Sci.*, *240* (1), 286–295.

Gaskell, D.R. (2008). *Introduction to the Thermodynamics of Materials*, CRC Press, USA.

Gawad, S. A., Baraka, A. M., Morsi, M. S. and Eltoum, M. A. (2013). "Development of Electroless Ni–P–Al$_2$O$_3$ and Ni–P–TiO$_2$ Composite Coatings from Alkaline Hypophosphite Gluconate Baths and their Properties." *Int. J. Electrochem. Sci.*, *8* 1722–1734.

Gawne, D. T. and Ma, U. (1988). "Engineering properties of chromium plating and electroless and electroplated nickel." *Surf. Eng.*, *4* (3), 239–249.

Gierlotka, D., RO' Winski, E., Budniok, A. and Lagiewka, E. (1997). "Production and properties of electrolytic Ni–P–TiO$_2$ composite layers." *J. Appl. Electrochem.*, *27* (12), 1349–1354.

Gileadi, E. (1993). *Electrode kinetics for chemists, chemical engineers, and materials scientists*, Capstone, USA.

Goldstein, J., Newbury, D. E., Echlin, P., Joy, D. C., Romig Jr, A. D., Lyman, C. E., Fiori, C. and Lifshin, E. (2012). *Scanning electron microscopy and X-ray microanalysis: a text for biologists, materials scientists, and geologists*, Springer Science & Business Media, Germany.

Gomes, A., Fernández, B., Pereira, I. and Pereiro, R. (2011). *Electrodeposition of metal matrix nanocomposites: improvement of the chemical characterization techniques*, InTech Open Access Publisher, Croatia.

Gong, M., Li, Y., Wang, H., Liang, Y., Wu, J. Z., Zhou, J., Wang, J., Regier, T., Wei, F. and Dai, H. (2013). "An advanced Ni–Fe layered double hydroxide electrocatalyst for water oxidation." *J. Am. Chem. Soc.*, *135* (23), 8452–8455.

Gong, M., Wang, D. Y., Chen, C. C., Hwang, B. J. and Dai, H. (2016). "A mini review on nickel-based electrocatalysts for alkaline hydrogen evolution reaction." *Nano Res.*, *9* (1), 28–46.

Gu, C., Lian, J. and Jiang, Z. (2005a). "Multilayer Ni-P Coating for Improving the Corrosion Resistance of AZ91D Magnesium Alloy." *Adv. Eng. Mat.*, *7* (11), 1032–1036.

Gu, C., Lian, J., Li, G., Niu, L. and Jiang, Z. (2005b). "High corrosion-resistant Ni–P/Ni/Ni–P multilayer coatings on steel." *Surf. Coat. Technol.*, *197* (1), 61–67.

Gu, Z. H. and Fahidy, T. Z. (1987). "The Effect of Magnetic Fields on Electrolytic Convection Generated at Inclined Cylindrical Cathodes." *J. Electrochem. Soc.*, *134* (9), 2241–2248.

Han, Q., Liu, K., Chen, J. and Wei, X. (2003). "A study on the electrodeposited Ni–S alloys as hydrogen evolution reaction cathodes." *Int. J. Hydrogen Energy*, *28* (11), 1207–1212.

Herraiz-Cardona, I., González-Buch, C., Valero-Vidal, C., Ortega, E. and Pérez-Herranz, V. (2013). "Co-modification of Ni-based type Raney electrodeposits for hydrogen evolution reaction in alkaline media." *J. Power Sources*, *240* 698–704.

Herraiz-Cardona, I., Ortega, E., Antón, J. G. and Pérez-Herranz, V. (2011). "Assessment of the roughness factor effect and the intrinsic catalytic activity for hydrogen evolution reaction on Ni-based electrodeposits." *Int. J. Hydrogen Energy*, *36* (16), 9428–9438.

Hibbert, D. B. (1993). *Introduction to electrochemistry*. In: Introduction to Electrochemistry, Springer, New York, pp 1–10.

Hinds, G., Spada, F. E., Coey, J. M. D., Ní Mhíocháin, T. R. and Lyons, M. E. G. (2001). "Magnetic Field Effects on Copper Electrolysis." *J. Phys. Chem. B*, *105* (39), 9487–9502.

Holt, M. L. and Vaaler, L. E. (1948). "Electrolytic Reduction of Aqueous Tungstate Solutions." *J. Electrochem. Soc.*, *94* (2), 50–58.

Holze, R. (1994). *Electrochemistry—Principles, methods and applications*, Oxford University Press, UK.

Huang, H. H., Ni, X. P., Loy, G. L., Chew, C. H., Tan, K. L., Loh, F. C., Deng, J. F. and Xu, G. Q. (1996). "Photochemical formation of silver nanoparticles in poly(N-vinylpyrrolidone)." *Langmuir*, *12* (4), 909–912.

Huang, Y., Fan, H., Chen, Z., Gu, C., Sun, M., Wang, H. and Li, Q. (2016). "The effect of graphene for the hydrogen evolution reaction in alkaline medium." *Int. J. Hydrogen Energy*, *41* (6), 3786–3793.

Huggins, R. A. (2010). *Energy storage*, Springer, New York.

Idrissi, H., Millet, J. P., Audisio, S. and Irhzo, A. (1994). "Natural formation of a protective layer on copper and copper brazing in domestic water: structural characterization and electrochemical behaviour." *J. Mater. Sci.*, *29* (20), 5327–5332.

Indyka, P., Beltowska-Lehman, E., Tarkowski, L., Bigos, A. and García-Lecina, E. (2014). "Structure characterization of nanocrystalline Ni–W alloys obtained by electrodeposition." *J. Alloys Compd.*, *590* 75–79.

Iqbal, M. J. and Ashiq, M. N. (2007). "Comparative studies of $SrZr_x Mn_x Fe_{12-2x} O_{19}$ nanoparticles synthesized by co-precipitation and sol–gel combustion methods." *Scr. Mater.*, *56* (2), 145–148.

Jaccaud, M., Leroux, F. and Millet, J. C. (1989). "New chlor-alkali activated cathodes." *Mater. Chem. Phys.*, *22* (1), 105–119.

Jack, W. (1993). *Electrodeposition: The Material Science of Coatings and Substrates*, Noyes Publications, New Jersey.

Jakšić, J. M., Vojnović, M. V. and Krstajić, N. V. (2000). "Kinetic analysis of hydrogen evolution at Ni–Mo alloy electrodes." *Electrochim. Acta*, *45* (25), 4151–4158.

Jha, B. K. and Aina, B. (2016). "Role of induced magnetic field on MHD natural convection flow in vertical microchannel formed by two electrically non-conducting infinite vertical parallel plates." *Alexandria Eng. J.*, *55* (3), 2087–2097.

Juškėnas, R., Valsiūnas, I., Pakštas, V., Selskis, A., Jasulaitienė, V., Karpavičienė, V. and Kapočius, V. (2006). "XRD, XPS and AFM studies of the unknown phase formed on the surface during electrodeposition of Ni–W alloy." *Appl. Surf. Sci.*, *253* (3), 1435–1442.

Jüttner, K. (1984). "Oxygen reduction electrocatalysis by underpotential deposited metal atoms at different single crystal faces of gold and silver." *Electrochim. Acta*, *29* (11), 1597–1604.

Kanani, N. (2004). Electroplating: basic principles, processes and practice, Elsevier, USA.

Kaninski, M. P. M., Nikolic, V. M., Tasic, G. S. and Rakocevic, Z. L. (2009). "Electrocatalytic activation of Ni electrode for hydrogen production by electrodeposition of Co and V species." *Int. J. Hydrogen Energy*, *34* (2), 703–709.

Kedzierzawski, P., Oleszak, D. and Janik-Czachor, M. (2001). "Hydrogen evolution on hot and cold consolidated Ni–Mo alloys produced by mechanical alloying." *Mater. Sci. Eng. A*, *300* (1), 105–112.

Keita, B. and Nadjo, L. (1985). "Activation of electrode surfaces: Application to the lectrocatalysis of the hydrogen evolution reaction." *J. Electroanal. Chem. Interfacial Electrochem.*, *191* (2), 441–448.

Khabouri, S. A., Harthi, S. A., Maekawa, T., Nagaoka, Y., Elzain, M. E., Hinai, A. A., Al-Rawas, A. D., Gismelseed, A. M. and Yousif, A. A. (2015). "Composition, Electronic and Magnetic Investigation of the Encapsulated $ZnFe_2O_4$ Nanoparticles in Multiwall Carbon Nanotubes Containing Ni Residuals." *Nanoscale Res. Lett.*, *10* (1), 262.

Khan, H. R. and Petrikowski, K. (2001). *Magnetic field effects on electrodeposition of cobalt film and nanowires*. In: Materials Science Forum, Trans Tech Publications, Switzerland, pp 725–728.

Kirihara, S., Umeda, Y., Tashiro, K., Honma, H. and Takai, O. (2016). "Development of Ni-W alloy plating as a substitution of hard chromium plating." *Trans. Mater. Res. Soc. Jpn.*, *41* (1), 35–39.

Kiuchi, D., Matsushima, H., Fukunaka, Y. and Kuribayashi, K. (2006). "Ohmic resistance measurement of bubble froth layer in water electrolysis under microgravity." *J. Electrochem. Soc.*, *153* (8), E138–E143.

Kondo, K., Ohgishi, A. and Tanaka, Z. (2000). "Electrodeposition of Zinc-SiO_2 Composite." *J. Electrochem. Soc.*, *147* (7), 2611–2613.

Kötz, E. R. and Stucki, S. (1987). "Ruthenium dioxide as a hydrogen-evolving cathode." *J. Appl. Electrochem.*, *17* (6), 1190–1197.

Koza, J. A., Mogi, I., Tschulik, K., Uhlemann, M., Mickel, C., Gebert, A. and Schultz, L. (2010). "Electrocrystallisation of metallic films under the influence of an external homogeneous magnetic field—Early stages of the layer growth." *Electrochim. Acta*, *55* (22), 6533–6541.

Koza, J. A., Mühlenhoff, S., Uhlemann, M., Eckert, K., Gebert, A. and Schultz, L. (2009). "Desorption of hydrogen from an electrode surface under influence of an external magnetic field – In-situ microscopic observations." *Electrochem. Commun.*, *11* (2), 425–429.

Koza, J. A., Mühlenhoff, S., Żabiński, P., Nikrityuk, P. A., Eckert, K., Uhlemann, M., Gebert, A., Weier, T., Schultz, L. and Odenbach, S. (2011). "Hydrogen evolution under the influence of a magnetic field." *Electrochim. Acta*, *56* (6), 2665–2675.

Koza, J. A., Uhlemann, M., Gebert, A. and Schultz, L. (2008). "The effect of magnetic fields on the electrodeposition of Co-Fe alloys." *Electrochim. Acta*, *53* (16), 5344–5353.

Krause, A., Koza, J., Ispas, A., Uhlemann, M., Gebert, A. and Bund, A. (2007). "Magnetic field induced micro-convective phenomena inside the diffusion layer during the electrodeposition of Co, Ni and Cu." *Electrochim. Acta*, *52* (22), 6338–6345.

Krstajić, N. V., Gajić-Krstajić, L., Lačnjevac, U., Jović, B. M., Mora, S. and Jović, V. D. (2011a). "Non-noble metal composite cathodes for hydrogen evolution. Part I: the Ni–MoO$_x$ coatings electrodeposited from Watt's type bath containing MoO$_3$ powder particles." *Int. J. Hydrogen Energy*, *36* (11), 6441–6449.

Krstajić, N. V., Lačnjevac, U., Jović, B. M., Mora, S. and Jović, V. D. (2011b). "Non-noble metal composite cathodes for hydrogen evolution. Part II: The Ni–MoO$_2$ coatings electrodeposited from nickel chloride–ammonium chloride bath containing MoO$_2$ powder particles." *Int. J. Hydrogen Energy*, *36* (11), 6450–6461.

Kuang, D., Xu, L., Liu, L., Hu, W. and Wu, Y. (2013). "Graphene–nickel composites." *Appl. Surf. Sci.*, *273* 484–490.

Kubisztal, J. and Budniok, A. (2008). "Study of the oxygen evolution reaction on nickel-based composite coatings in alkaline media." *Int. J. Hydrogen Energy*, *33* (17), 4488–4494.

Kumar, C. P., Venkatesha, T. V. and Shabadi, R. (2013). "Preparation and corrosion behavior of Ni and Ni–graphene composite coatings." *Mater. Res. Bull.*, *48* (4), 1477–1483.

Kumar, U. P., Kennady, C. J. and Zhou, Q. (2015). "Effect of salicylaldehyde on microstructure and corrosion resistance of electrodeposited nanocrystalline Ni–W alloy coatings." *Surf. Coat. Technol.*, *283* 148–155.

Lasia, A. and Rami, A. (1990). "Kinetics of hydrogen evolution on nickel electrodes." *J. Electroanal. Chem. Interfacial Electrochem.*, *294* (1-2), 123–141.

Ledendecker, M., Clavel, G., Antonietti, M. and Shalom, M. (2015). "Highly Porous Materials as Tunable Electrocatalysts for the Hydrogen and Oxygen Evolution Reaction." *Adv. Funct. Mater.*, *25* (3), 393–399.

Lee, H.B. (2013). "Synergy between corrosion and wear of electrodeposited Ni–W coating." *Tribol. Lett., 50* (3), 407–419.

Lee, S., Choi, M., Park, S., Jung, H. and Yoo, B. (2015). "Mechanical Properties of Electrodeposited Ni-W Thin Films with Alternate W-Rich and W-Poor Multilayers." *Electrochim. Acta*, *153* 225–231.

Leisner, P., Nielsen, C. B., Tang, P. T., Dörge, T. C. and Møller, P. (1996). "Methods for electrodepositing composition-modulated alloys." *J. Mater. Process. Technol.*, *58* (1), 39–44.

Li, B., Zhang, W., Zhang, W. and Huan, Y. (2017). "Preparation of Ni-W/SiC nanocomposite coatings by electrochemical deposition." *J. Alloys Compd.*, *702* 38–50.

Li, D., Levesque, A., Franczak, A., Wang, Q., He, J. and Chopart, J. P. (2013). "Evolution of morphology in electrodeposited nanocrystalline Co–Ni films by in-situ high magnetic field application." *Talanta*, *110* 66–70.

Li, H. and Ebrahimi, F. (2003). "Synthesis and characterization of electrodeposited nanocrystalline nickel–iron alloys." *Mater. Sci. Eng. A*, *347* (1), 93–101.

Li, H., Wang, W., Gong, Z., Yu, Y., Chen, H., Xia, J. and others (2015). "Shape-controlled synthesis of nickel phosphide nanocrystals and their application as hydrogen evolution reaction catalyst." *J. Phys. Chem. Solids*, *80* 22–25.

Li, J., Jiang, J., He, H. and Sun, Y. (2002). "Synthesis, microstructure, and mechanical properties of TiO_2/Ni nanocomposite coatings." *J. Mater. Sci. Lett.*, *21* (12), 939–941.

Li, J., Sun, Y., Sun, X. and Qiao, J. (2005). "Mechanical and corrosion-resistance performance of electrodeposited titania–nickel nanocomposite coatings." *Surf. Coat. Technol.*, *192* (2), 331–335.

Li, X. and Li, Z. (2003). "Nano-sized Si_3N_4 reinforced NiFe nanocomposites by electroplating." *Mater. Sci. Eng. A*, *358* (1), 107–113.

Liebreich, E. (1935). "The effects of film formation on the structure of electro-deposited metallic coatings." *Trans. Faraday Soc.*, *31* 1188–1194.

Lima, F., Mescheder, U. and Reinecke, H. (2012). "Simulation of Current Density for Electroplating on Silicon Using a Hull Cell." *Solar Cells*, *6* 7.

Lin, M. Y. and Hourng, L. W. (2014). "Effects of magnetic field and pulse potential on hydrogen production via water electrolysis." *Int. J. Energy Res.*, *38* (1), 106–116.

Lin, M. Y., Hourng, L. W. and Kuo, C. W. (2012). "The effect of magnetic force on hydrogen production efficiency in water electrolysis." *Int. J. Hydrogen Energy*, *37* (2), 1311–1320.

Liu, C., Wang, K., Luo, S., Tang, Y. and Chen, L. (2011). "Direct Electrodeposition of Graphene Enabling the One-Step Synthesis of Graphene–Metal Nanocomposite Films." *Small*, *7* (9), 1203–1206.

Liu, Y. R., Hu, W. H., Li, X., Dong, B., Shang, X., Han, G. Q., Chai, Y. M., Liu, Y. Q. and Liu, C. G. (2016). "Facile one-pot synthesis of CoS_2-MoS_2/CNTs as efficient electrocatalyst for hydrogen evolution reaction." *Appl. Surf. Sci.*, *384* 51–57.

Livage, J. (1999). "Sol-gel synthesis of hybrid materials." *Bull. Mater. Sci.*, *22* (3), 201–205.

Low, C. T. J., Wills, R. G. A. and Walsh, F. C. (2006). "Electrodeposition of composite coatings containing nanoparticles in a metal deposit." *Surf. Coat. Technol.*, *201* (1–2), 371–383.

Lozano-Morales, A. and Podlaha, E. J. (2004). "The Effect of Al_2O_3 Nanopowder on Cu Electrodeposition." *J. Electrochem. Soc.*, *151* (7), C478–C483.

Lu, G. and Zangari, G. (2002). "Corrosion resistance of ternary Ni-P based alloys in sulfuric acid solutions." *Electrochim. Acta*, *47* (18), 2969–2979.

Luo, J. K., Pritschow, M., Flewitt, A. J., Spearing, S. M., Fleck, N. A. and Milne, W. I. (2006). "Effects of process conditions on properties of electroplated Ni thin films for microsystem applications." *J. Electrochem. Soc.*, *153* (10), D155–D161.

Luo, Q., Peng, M., Sun, X., Luo, Y. and Asiri, A. M. (2016). "Efficient electrochemical water splitting catalyzed by electrodeposited NiFe nanosheets film." *Int. J. Hydrogen Energy*, *41* (21), 8785–8792.

Lupi, C., Dell'Era, A. and Pasquali, M. (2009). "Nickel–cobalt electrodeposited alloys for hydrogen evolution in alkaline media." *Int. J. Hydrogen Energy*, *34* (5), 2101–2106.

Lyons, M. E. and Brandon, M. P. (2008). "The oxygen evolution reaction on passive oxide covered transition metal electrodes in aqueous alkaline solution. Part 1-Nickel." *Int. J. Electrochem. Sci.*, *3* 1386–1424.

Ma, M., Donepudi, V. S., Sandi, G., Sun, Y. K. and Prakash, J. (2004). "Electrodeposition of nano-structured nickel–21% tungsten alloy and evaluation of oxygen reduction reaction in a 1% sodium hydroxide solution." *Electrochim. Acta*, *49* (25), 4411–4416.

Madore, C. and Landolt, D. (1996). "Blocking inhibitors in cathodic leveling II. Experimental investigation." *J. Electrochem. Soc.*, *143* (12), 3936–3943.

Mahalingam, T., Raja, M., Thanikaikarasan, S., Sanjeeviraja, C., Velumani, S., Moon, H. and Kim, Y. D. (2007). "Electrochemical deposition and characterization of Ni–P alloy thin films." *Mater. Charact.*, *58* (8), 800–804.

Mansfeld, F. (1990). "Electrochemical impedance spectroscopy (EIS) as a new tool for investigating methods of corrosion protection." *Electrochim. Acta*, *35* (10), 1533–1544.

Masdek, N. R. N. and Alfantazi, A. (2010). "Review of Studies on Corrosion of Electrodeposited Nanocrystalline Metals and Alloys." *ECS Trans.*, *28* (24), 249–260.

Matsushima, H., Ispas, A., Bund, A. and Bozzini, B. (2008). "Magnetic field effects on the initial stages of electrodeposition processes." *J. Electroanal. Chem.*, *615* (2), 191–196.

Matsushima, H., Kiuchi, D. and Fukunaka, Y. (2009). "Measurement of dissolved hydrogen supersaturation during water electrolysis in a magnetic field." *Electrochim. Acta*, *54* (24), 5858–5862.

Mirkova, L., Pashova, V. P. and Monev, M. H. (2011). "Study of Hydrogen Evolution Reaction on Ni/Co3O4 Composite Electrode in Alkaline Solution." *ECS Trans.*, *35* (21), 77–84.

Mohanta, S. and Fahidy, T.Z. (1976). "Mass transfer in cylindrical magnetoelectrolytic cells." *Electrochim. Acta*, *21* (2), 149–152.

Mohanta, S. and Fahidy, T. Z. (1978). "Hydrodynamic and mass transport phenomena in a multiple-electrode magnetoelectrolytic cell." *J. Appl. Electrochem.*, *8* (1), 5–10.

Möller, A. and Hahn, H. (1999). "Synthesis and characterization of nanocrystalline Ni/ZrO$_2$ composite coatings." *Nanostruct. Mater.*, *12* (1-4), 259–262.

Monzon, L. M. and Coey, J. M. D. (2014). "Magnetic fields in electrochemistry: The Lorentz force. A mini-review." *Electrochem. Commun.*, *42* 38–41.

Mooradian, A. (1969). "Photoluminescence of metals." *Phys. Rev. Lett.*, *22* (5), 185.

Mulfinger, L., Solomon, S. D., Bahadory, M., Jeyarajasingam, A. V., Rutkowsky, S. A. and Boritz, C. (2007). "Synthesis and study of silver nanoparticles." *J. Chem. Educ.*, *84* (2), 322.

NabiRahni, D. M. A., Tang, P. T. and Leisner, P. (1996). "The electrolytic plating of compositionally modulated alloys and laminated metal nano-structures based on an automated computer-controlled dual-bath system." *Nanotechnol.*, *7* (2), 134–143.

Narayan, R. and Mungole, M. N. (1985). "Electrodeposition of Ni-P alloy coatings." *Surf. Technol.*, *24* (3), 233–239.

Naseh, M. V., Khodadadi, A. A., Mortazavi, Y., Sahraei, O. A., Pourfayaz, F. and Sedghi, S. M. (2009). "Functionalization of carbon nanotubes using nitric acid oxidation and DBD plasma." *World Academy of Science, Engineering and Technology*, *49* 177–179.

Ngamlerdpokin, K. and Tantavichet, N. (2014). "Electrodeposition of nickel–copper alloys to use as a cathode for hydrogen evolution in an alkaline media." *Int. J. Hydrogen Energy*, *39* (6), 2505–2515.

Nørskov, J. K., Bligaard, T., Logadottir, A., Kitchin, J. R., Chen, J. G., Pandelov, S. and Stimming, U. (2005). "Trends in the exchange current for hydrogen evolution." *J. Electrochem. Soc.*, *152* (3), J23–J26.

O'M, B. J. and Reddy, A. (1970). *Modern Electrochemistry, Vol. 2*, MacDonald Technical &. Scientific, London.

Ogihara, T., Ikeda, M., Kato, M. and Mizutani, N. (1989). "Continuous processing of monodispersed titania powders." *J. Am. Ceram. Soc.*, *72* (9), 1598–1601.

Omi, T., Kokunai, S. and Yamamoto, H. (1976). "Structure of Amorphous Ni–P Electrodeposits." *Trans. Jpn. Inst. Met.*, *17* (6), 370–377.

Parthasaradhy, N. (1989). *Practical Electroplating Handbook*, Prentice-Hall, USA, p. 1444.

Paseka, I. and Velicka, J. (1997). "Hydrogen evolution and hydrogen sorption on amorphous smooth Me-P$_{(x)}$ (Me-Ni, Co and Fe-Ni) electrodes." *Electrochim. Acta*, *42* (2), 237–242.

Pavithra, G. P. and Hegde, A. C. (2012). "Magnetic property and corrosion resistance of electrodeposited nanocrystalline iron–nickel alloys." *Appl. Surf. Sci.*, *258* (18), 6884–6890.

Peeters, P., Hoorn, G. V. D., Daenen, T., Kurowski, A. and Staikov, G. (2001). "Properties of electroless and electroplated Ni–P and its application in microgalvanics." *Electrochim. Acta*, *47* (1), 161–169.

Pentland, N., Bockris, J. and Sheldon, E. (1957). "Hydrogen evolution reaction on copper, gold, molybdenum, palladium, rhodium, and iron mechanism and measurement technique under high purity conditions." *J. Electrochem. Soc.*, *104* (3), 182–194.

Pérez-Alonso, F. J., Adán, C., Rojas, S., Peña, M. A. and Fierro, J. L. G. (2015). "Ni–Co electrodes prepared by electroless-plating deposition. A study of their electrocatalytic activity for the hydrogen and oxygen evolution reactions." *Int. J. Hydrogen Energy*, *40* (1), 51–61.

Pillai, A. M., Rajendra, A. and Sharma, A. K. (2012). "Electrodeposited nickel–phosphorous (Ni–P) alloy coating: an in-depth study of its preparation, properties, and structural transitions." *J. Coat. Technol. Res.*, *9* (6), 785–797.

Pletcher, D. (1984). "Electrocatalysis: present and future." *J. Appl. Electrochem.*, *14* (4), 403–415.

Poursaee, A. (2010). "Determining the appropriate scan rate to perform cyclic polarization test on the steel bars in concrete." *Electrochim. Acta*, *55* (3), 1200–1206.

Prather, M. J. (2003). "An environmental experiment with H_2?" *Science*, *302* (5645), 581–582.

Pu, Z., Wei, S., Chen, Z. and Mu, S. (2016). "Flexible molybdenum phosphide nanosheet array electrodes for hydrogen evolution reaction in a wide pH range." *Appl. Catal. B: Environ.*, *196* 193–198.

Qiu, J., Jin, Z., Liu, Z., Liu, X., Liu, G., Wu, W., Zhang, X. and Gao, X. (2007). "Fabrication of TiO_2 nanotube film by well-aligned ZnO nanorod array film and sol–gel process." *Thin Solid Films*, *515* (5), 2897–2902.

Ragsdale, S. R., Grant, K. M. and White, H. S. (1998). "Electrochemically generated magnetic forces. Enhanced transport of a paramagnetic redox species in large, nonuniform magnetic fields." *J. Am. Chem. Soc.*, *120* (51), 13461–13468.

Raj, I. A. (1992a). "Nickel based composite electrolytic surface coatings as electrocatalysts for the cathodes in the energy efficient industrial production of hydrogen from alkaline water electrolytic cells." *Int. J. Hydrogen Energy*, *17* (6), 413–421.

Raj, I. A. (1992b). "On the catalytic activity of Ni-Mo-Fe composite surface coatings for the hydrogen cathodes in the industrial electrochemical production of hydrogen." *Appl. Surf. Sci.*, *59* (3-4), 245–252.

Raj, I. A. (1993). "Nickel-based, binary-composite electrocatalysts for the cathodes in the energy-efficient industrial production of hydrogen from alkaline-water electrolytic cells." *J. Mater. Sci.*, *28* (16), 4375–4382.

Raj, I. A. and Vasu, K. I. (1990). "Transition metal-based hydrogen electrodes in alkaline solution—electrocatalysis on nickel based binary alloy coatings." *J. Appl. Electrochem.*, *20* (1), 32–38.

Raj, I. A. and Vasu, K. I. (1992). "Transition metal-based cathodes for hydrogen evolution in alkaline solution: electrocatalysis on nickel-based ternary electrolytic codeposits." *J. Appl. Electrochem.*, *22* (5), 471–477.

Randles, J. E. (1948). "A cathode ray polarograph. Part II.—The current-voltage curves." *Trans. Faraday Soc.*, *44* 327–338.

Rao, V. R. and Hegde, A. C. (2013). "Nanofabricated multilayer coatings of Zn-Ni alloy for better corrosion protection." *Prot. Met. Phys. Chem. Surf.*, *49* (6), 693–698.

Rao, V. R. and Hegde, A. C. (2014). "Role of cadmium on corrosion resistance of Zn-Ni alloy coatings." *Surf. Eng. Appl. Electrochem.*, *50* (1), 63–71.

Rao, V. R., Bangera, K. V. and Hegde, A. C. (2013). "Magnetically induced electrodeposition of Zn–Ni alloy coatings and their corrosion behaviors." *J. Magn. Magn. Mater.*, *345* 48–54.

Reddy, S., Du, R., Kang, L., Mao, N. and Zhang, J. (2016). "Three dimensional CNTs aerogel/MoS$_x$ as an electrocatalyst for hydrogen evolution reaction." *Appl. Catal. B: Environ.*, *194* 16–21.

Revie, R. W. and Uhlig, H. H. (2008). *Corrosion and corrosion control: An introduction to corrosion science and engineering*, John Wiley & Sons, Hoboken, New Jersey.

Roger, I., Shipman, M. A. and Symes, M. D. (2017). "Earth-abundant catalysts for electrochemical and photoelectrochemical water splitting." *Nat. Rev. Chem.*, *1* 0003.

Rosa, J. L., Robin, A., Silva, M. B., Baldan, C. A. and Peres, M. P. (2009). "Electrodeposition of copper on titanium wires: Taguchi experimental design approach." *J. Mater. Process. Technol.*, *209* (3), 1181–1188.

Rosalbino, F., Maccio, D., Angelini, E., Saccone, A. and Delfino, S. (2005). "Electrocatalytic properties of Fe–R (R= rare earth metal) crystalline alloys as hydrogen electrodes in alkaline water electrolysis." *J. Alloys Compd.*, *403* (1), 275–282.

Roy, S. (2009). *Electrochemical Fabrication of Nanostructured, Compositionally Modulated Metal Multilayers (CMMMs)*, In Electrochemistry at the Nanoscale, Springer, New York, pp 349–376.

Saedi, A. and Ghorbani, M. (2005). "Electrodeposition of Ni–Fe–Co alloy nanowire in modified AAO template." *Mater. Chem. Phys.*, *91* (2), 417–423.

Safizadeh, F., Ghali, E. and Houlachi, G. (2015). "Electrocatalysis developments for hydrogen evolution reaction in alkaline solutions–a review." *Int. J. Hydrogen Energy*, *40* (1), 256–274.

Sakai, S., Nakanishi, S. and Nakato, Y. (2006). "Mechanisms of oscillations and formation of nano-scale layered structures in induced co-deposition of some iron-group alloys (Ni-P, Ni-W, and Co-W), studied by an in situ electrochemical quartz crystal microbalance technique." *J. Phys. Chem. B*, *110* (24), 11944–11949.

Sankara Narayanan, T. and Seshadri, S. (2008). *Electro-and electroless plated coatings for corrosion protection*, In: Corrosion Science and Technology: Mechanism, Mitigation and Monitoring. Narosa Publishing House, New Delhi, pp. 177-221.

Schlesinger, M. and Paunovic, M. (2006). *Fundamentals of electrochemical deposition*, Wiley, New Jersey.

Schlesinger, M. and Paunovic, M. (2011). Modern electroplating, John Wiley & Sons, New Jersey.

Schlögl, R. (2012). *Chemical Energy Storage*, Walter De Gruyter, Berlin.

Schwarzacher, W. (2006). "Electrodeposition: a technology for the future." *Interface*, *15* (1), 32–35.

Shaw, B. (2003). *ASM handbook volume 13A: corrosion: fundamentals, testing and protection*, ASM International, Materials Park, Ohio, USA.

Shen, M., Bennett, N., Ding, Y. and Scott, K. (2011). "A concise model for evaluating water electrolysis." *Int. J. Hydrogen Energy*, *36* (22), 14335–14341.

Shervedani, R. K. and Lasia, A. (1997). "Studies of the Hydrogen Evolution Reaction on Ni-P Electrodes." *J. Electrochem. Soc.*, *144* (2), 511–519.

Shervedani, R. K., Alinoori, A. H. and Madram, A. R. (2008). "Electrocatalytic activities of nickel-phosphorous composite coating reinforced with codeposited graphite carbon for hydrogen evolution reaction in alkaline solution." *J. New Mater. Electrochem. Syst.*, *11* (4), 259–265.

Shetty, S. and Hegde, A. C. (2017). "Magnetically Induced Electrodeposition of Ni-Mo Alloy for Hydrogen Evolution Reaction." *Electrocatal.*, 1–10.

Shetty, S., Sadiq, M. M. J., Bhat, D. K. and Hegde, A. C. (2016). "Development of multilayer Sn–Ni alloy coating by pulsed sonoelectrolysis for enhanced corrosion protection." *RSC Adv.*, *6* (81), 77465–77473.

Shibli, S. M. A. and Dilimon, V. S. (2007). "Effect of phosphorous content and TiO_2-reinforcement on Ni–P electroless plates for hydrogen evolution reaction." *Int. J. Hydrogen Energy*, *32* (12), 1694–1700.

Shibli, S. M. A., Harikrishnan, G. J., Anupama, V. R., Chinchu, K. S. and Meena, B. N. (2015). "Development of nano NiO incorporated nickel–phosphorus coatings for electrocatalytic applications." *Surf. Coat. Technol.*, *262* 48–55.

Simunovich, D., Schlesinger, M. and Snyder, D. D. (1994). "Electrochemically layered Copper-Nickel nanocomposites with enhanced hardness." *J. Electrochem. Soc.*, *141* (1), L10–L11.

Slavcheva, E., Mokwa, W. and Schnakenberg, U. (2005). "Electrodeposition and properties of NiW films for MEMS application." *Electrochim. Acta*, *50* (28), 5573–5580.

Spyrellis, N., Pavlatou, E. A., Spanou, S. and Zoikis-Karathanasis, A. (2009). "Nickel and nickel-phosphorous matrix composite electrocoatings." *Trans. Nonferrous Met. Soc. China*, *19* (4), 800–804.

Sridhar, T. M., Eliaz, N. and Gileadi, E. (2005). "Electroplating of Ni_4W." *Electrochem. Solid-State Lett.*, *8* (3), C58–C61.

Steinbach, J. and Ferkel, H. (2001). "Nanostructured $Ni-Al_2O_3$ films prepared by DC and pulsed DC electroplating." *Scr. Mater.*, *44* (8), 1813–1816.

Steiner, U. E. and Ulrich, T. (1989). "Magnetic field effects in chemical kinetics and related phenomena." *Chem. Rev.*, *89* (1), 51–147.

Stöber, W., Fink, A. and Bohn, E. (1968). "Controlled growth of monodisperse silica spheres in the micron size range." *J. Colloid Interface Sci.*, *26* (1), 62–69.

Su, X., Wang, G., Li, W., Bai, J. and Wang, H. (2013). "A simple method for preparing graphene nano-sheets at low temperature." *Adv. Powder Technol.*, *24* (1), 317–323.

Subramanya, B., Ullal, Y., Shenoy, S. U., Bhat, D. K. and Hegde, A. C. (2015). "Novel Co–Ni–graphene composite electrodes for hydrogen production." *RSC Adv.*, *5* (59), 47398–47407.

Sziráki, L., Kuzmann, E., Papp, K., Chisholm, C. U., El-Sharif, M. R. and Havancsák, K. (2012). "Electrochemical behaviour of amorphous electrodeposited chromium coatings." *Mater. Chem. Phys.*, *133* (2–3), 1092–1100.

Tabakovic, I., Riemer, S., Sun, M., Vas'ko, V. A. and Kief, M. T. (2005). "Effect of magnetic field on NiCu electrodeposition from citrate plating solution and characterization of deposit." *J Electrochem. Soc.*, *152* (12), C851–C860.

Tabakovic, I., Riemer, S., Vas'ko, V., Sapozhnikov, V. and Kief, M. (2003). "Effect of magnetic field on electrode reactions and properties of electrodeposited NiFe films." *J. Electrochem. Soc.*, *150* (9), C635–C640.

Tacken, R. A. and Janssen, L. J. J. (1995). "Applications of magnetoelectrolysis." *J. Appl. Electrochem.*, *25* (1), 1–5.

Taglauer, E. and Vickerman, J. C. (1997). *Surface Analysis-The Principle Techniques*, Wiley, Chichester, UK.

Tang, J., Zhao, X., Zuo, Y., Ju, P. and Tang, Y. (2015). "Electrodeposited Pd-Ni-Mo film as a cathode material for hydrogen evolution reaction." *Electrochim. Acta*, *174* 1041–1049.

Taniguchi, T., Sassa, K., Yamada, T. and Asai, S. (2000). "Control of crystal orientation in zinc electrodeposits by imposition of a high magnetic field." *Mater. Trans., JIM*, *41* (8), 981–984.

Tench, D. and White, J. (1984). "Enhanced tensile strength for electrodeposited nickel-copper multilayer composites." *Met. Trans. A*, *15* (11), 2039–2040.

Thangaraj, V., Eliaz, N. and Hegde, A. C. (2009). "Corrosion behavior of composition modulated multilayer Zn–Co electrodeposits produced using a single-bath technique." *J. Appl. Electrochem.*, *39* (3), 339–345.

Thiemig, D. and Bund, A. (2008). "Characterization of electrodeposited Ni–TiO$_2$ nanocomposite coatings." *Surf. Coat. Technol.*, *202* (13), 2976–2984.

Tilak, B. V., Ramamurthy, A. C. and Conway, B. E. (1986). *High performance electrode materials for the hydrogen evolution reaction from alkaline media*, In Proceedings of the Indian Academy of Sciences-Chemical Sciences, Springer, New York, pp 359–393.

Tobias, C. W., Eisenberg, M. and Wilke, C. R. (1952). "Diffusion and convection in electrolysis—a theoretical review." *J. Electrochem. Soc*, *99* (12), 359C–365C.

Trasatti, S. (1972). "Work function, electronegativity, and electrochemical behaviour of metals: III. Electrolytic hydrogen evolution in acid solutions." *J. Electroanal. Chem. Interfacial Electrochem.*, *39* (1), 163–184.

Trasatti, S. (1995). "Electrochemistry and environment: The role of electrocatalysis." *Int. J. Hydrogen Energy*, *20* (10), 835–844.

Trotochaud, L., Young, S. L., Ranney, J. K. and Boettcher, S. W. (2014). "Nickel–iron oxyhydroxide oxygen-evolution electrocatalysts: The role of intentional and incidental iron incorporation." *J. Am. Chem. Soc.*, *136* (18), 6744–6753.

Tsyntsaru, N., Cesiulis, H., Donten, M., Sort, J., Pellicer, E. and Podlaha-Murphy, E. J. (2012). "Modern trends in tungsten alloys electrodeposition with iron group metals." *Surf. Eng. Appl. Electrochem.*, *48* (6), 491–520.

Turner, J. A. (2004). "Sustainable hydrogen production." *Science*, *305* (5686), 972–974.

Ullal, Y. and Hegde, A. C. (2014a). "Electrodeposition and electro-catalytic study of nanocrystalline Ni–Fe alloy." *Int. J. Hydrogen Energy*, *39* (20), 10485–10492.

Ullal, Y. and Hegde, A. C. (2014b). "Electrofabrication of multilayer Fe–Ni alloy coatings for better corrosion protection." *Appl. Phys. A*, *116* (4), 1587–1594.

Vargas-Uscategui, A., Mosquera, E., Chornik, B. and Cifuentes, L. (2015). "Electrocatalysis of the hydrogen evolution reaction by Rhenium oxides electrodeposited by pulsed-current." *Electrochim. Acta*, *178* 739–747.

Vasireddy, R., Paul, R. and Mitra, A. K. (2012). "Green synthesis of silver nanoparticles and the study of optical properties." *Nanomater. Nanotechnol.*, *2*, 2–8.

Vasko, A. (1977). *Molybdenum and Tungsten Electrochemistry*, Science Publications, New York..

Venkatakrishna, K. and Hegde, A. C. (2010). "Electrolytic preparation of cyclic multilayer Zn–Ni alloy coating using switching cathode current densities." *J. Appl. Electrochem.*, *40* (11), 2051–2059.

Walsh, F. C. and Ponce de Leon, C. (2014). "A review of the electrodeposition of metal matrix composite coatings by inclusion of particles in a metal layer: an established and diversifying technology." *Trans. IMF*, *92* (2), 83–98.

Wang, L., Gao, Y., Liu, H., Xue, Q. and Xu, T. (2005a). "Effects of bivalent Co ion on the co-deposition of nickel and nano-diamond particles." *Surf. Coat. Technol.*, *191* (1), 1–6.

Wang, L., Gao, Y., Xue, Q., Liu, H. and Xu, T. (2005b). "Effects of nano-diamond particles on the structure and tribological property of Ni-matrix nanocomposite coatings." *Mater. Sci. Eng. A*, *390* (1), 313–318.

Wang, M., Wang, Z., Gong, X. and Guo, Z. (2014). "The intensification technologies to water electrolysis for hydrogen production–A review." *Renewable Sustainable Energy Rev.*, *29* 573–588.

Wang, M., Wang, Z., Yu, X. and Guo, Z. (2015). "Facile one-step electrodeposition preparation of porous NiMo film as electrocatalyst for hydrogen evolution reaction." *Int. J. Hydrogen Energy*, *40* (5), 2173–2181.

Wang, Y., Ju, Y., Wei, S., Gao, W., Lu, W. and Yan, B. (2014). "Au-Ni-TiO$_2$ Nano-Composite Coatings Prepared by Sol-Enhanced Method." *J. Electrochem. Soc.*, *161* (14), D775–D781.

Wasekar, N. P. and Sundararajan, G. (2015). "Sliding wear behavior of electrodeposited Ni–W alloy and hard chrome coatings." *Wear*, *342–343* 340–348.

Waskaas, M. and Kharkats, Y. I. (1999). "Magnetoconvection phenomena: A mechanism for influence of magnetic fields on electrochemical processes." *J. Phys. Chem. B*, *103* (23), 4876–4883.

Wassef, O. and Fahidy, T. Z. (1976). "Magnetoelectrolysis in the presence of bubble formation at the cathode." *Electrochim. Acta*, *21* (10), 727–730.

Watanabe, T. (2004). *Nano-plating: Microstructure Control Theory of Plated Film and Data Base of Plating Film Microstructure*, Elsevier, London.

Webb, P. R. and Robertson, N. L. (1994). "Electrolytic Codeposition of Ni-γAl$_2$O$_3$ Thin Films." *J. Electrochem. Soc.*, *141* (3), 669–673.

Weil, R. and Paquin, R. (1960). "The relationship between brightness and structure in electroplated nickel." *J. Electrochem. Soc.*, *107* (2), 87–91.

Wepasnick, K.A., Smith, B. A., Schrote, K. E., Wilson, H. K., Diegelmann, S. R. and Fairbrother, D. H. (2011). "Surface and structural characterization of multi-walled carbon nanotubes following different oxidative treatments." *Carbon*, *49* (1), 24–36.

Wieckowski, A. (1999). *Interfacial electrochemistry: theory: experiment, and applications*, CRC Press, USA.

Wieckowski, A., Savinova, E. R. and Vayenas, C. G. (2003). *Catalysis and electrocatalysis at nanoparticle surfaces*, CRC Press, USA.

Wilhelm, F. G., Vegt, N. F. A. Van der, Wessling, M. and Strathmann, H. (2001). "Chronopotentiometry for the advanced current–voltage characterisation of bipolar membranes." *J. Electroanal. Chem.*, *502* (1), 152–166.

Williams, R.V. (1966). "Electrodeposited composite coatings." *Electroplating Met. Finish.*, *19* (3), 326–329.

Wolfson, A. and Dlugy, C. (2009). "Glycerol as an alternative green medium for carbonyl compound reductions." *Org. Commun.*, *2* 34–41.

Wu, G., Li, N., Dai, C. S. and Zhou, D. R. (2004). "Electrochemical preparation and characteristics of Ni–Co–LaNi$_5$ composite coatings as electrode materials for hydrogen evolution." *Mater. Chem. Phys.*, *83* (2), 307–314.

Yang, J., Wang, S. C., Zhou, X. Y. and Xie, J. (2012). "Electrochemical behaviors of functionalized carbon nanotubes in LiPF$_6$/EC+ DMC electrolyte." *Int. J. Electrochem. Sci.*, *7* 6118–6126.

Yang, L. (2008). *Techniques for corrosion monitoring*, Elsevier, USA.

Yang, W. M. C., Tsakalakos, T. and Hilliard, J. E. (1977). "Enhanced elastic modulus in composition-modulated gold-nickel and copper-palladium foils." *J. Appl. Phys.*, *48* (3), 876–879.

Yao, Y., Yao, S., Zhang, L. and Wang, H. (2007). "Electrodeposition and mechanical and corrosion resistance properties of Ni–W/SiC nanocomposite coatings." *Mater. Lett.*, *61* (1), 67–70.

Yogesha, S., Bhat, R. S., Venkatakrishna, K., Pavithra, G. P., Ullal, Y. and Hegde, A. C. (2011). "Development of Nano-structured Zn-Ni Multilayers and their Corrosion Behaviors." *Synthesis and Reactivity in Inorganic, Metal-Organic, and Nano-Metal Chemistry*, *41* (1), 65–71.

You, B., Jiang, N., Sheng, M., Gul, S., Yano, J. and Sun, Y. (2015). "High-Performance Overall Water Splitting Electrocatalysts Derived from Cobalt-Based Metal–Organic Frameworks." *Chem. Mater.*, *27* (22), 7636–7642.

Younes, O. and Gileadi, E. (2000). "Electroplating of High Tungsten Content Ni/W Alloys." *Electrochem. Solid-State Lett.*, *3* (12), 543–545.

Younes, O. and Gileadi, E. (2002). "Electroplating of Ni/W Alloys I. Ammoniacal Citrate Baths." *J. Electrochem. Soc.*, *149* (2), C100–C111.

Younes, O., Zhu, L., Rosenberg, Y., Shacham-Diamand, Y. and Gileadi, E. (2001). "Electroplating of Amorphous Thin Films of Tungsten/Nickel Alloys." *Langmuir*, *17* (26), 8270–8275.

Younes-Metzler, O., Zhu, L. and Gileadi, E. (2003). "The anomalous codeposition of tungsten in the presence of nickel." *Electrochim. Acta*, *48* (18), 2551–2562.

Yu, Q., Zeng, Z., Liang, Y., Zhao, W., Peng, S., Han, Z., Wang, G., Wu, X. and Xue, Q. (2015). "Ni–P synergetic deposition: electrochemically deposited highly active Ni as a catalyst for chemical deposition." *RSC Adv.*, *5* (35), 27242–27248.

Yu, X., Wang, M., Wang, Z., Gong, X. and Guo, Z. (2016). "3D multi-structural porous NiAg films with nanoarchitecture walls: high catalytic activity and stability for hydrogen evolution reaction." *Electrochim. Acta*, *211* 900–910.

Yuan, X. -Z. R., Song, C., Wang, H. and Zhang, J. (2009). "Electrochemical impedance spectroscopy in PEM fuel cells: fundamentals and applications, Springer Science & Business Media, Germany.

Zabludovsky, V. A. and Shtapenko, E. F. (1997). "The obtaining of cobalt multilayers by programme-controlled pulse current." *Trans. IMF*, *75* 203–204.

Zabludovsky, V. A., Fedotova, N. V. and Shtapenko, E. F. (1996). "Structure, texture and properties of metallic multilayers deposited by a program-controlled pulse current method." *Trans IMF*, *74* 106–107.

Zemanová, M., Kurinec, R., Jorík, V. and Kadlečíová, M. (2012). "Ni-W alloy coatings deposited from a citrate electrolyte." *Chem. Pap.*, *66* (5), 492–501.

Zeng, K. and Zhang, D. (2010). "Recent progress in alkaline water electrolysis for hydrogen production and applications." *Prog. Energy Combust. Sci.*, *36* (3), 307–326.

Zhang, W., Qi, J., Liu, K. and Cao, R. (2016). "A Nickel-Based Integrated Electrode from an Autologous Growth Strategy for Highly Efficient Water Oxidation." *Adv. Energy Mater.*, *6* (12), doi: 10.1002/aenm.201502489.

Zhao, L. and Gao, L. (2004). "Coating multi-walled carbon nanotubes with zinc sulfide." *J. Mater. Chem.*, *14* (6), 1001–1004.

Zheng, Z., Li, N., Wang, C.-Q., Li, D.-Y., Zhu, Y.-M. and Wu, G. (2012). "Ni–CeO$_2$ composite cathode material for hydrogen evolution reaction in alkaline electrolyte." *Int. J. Hydrogen Energy*, *37* (19), 13921–13932.

Zhu, L., Younes, O., Ashkenasy, N., Shacham-Diamand, Y. and Gileadi, E. (2002). "STM/AFM studies of the evolution of morphology of electroplated Ni/W alloys." *Appl. Sur. Sci*, *200* (1–4), 1–14.

Zhu, X., Cui, X., Che, Z., Jin, X. and Li, M. (2015). "Thermal Decomposition Fabrication of Fe$_2$O$_3$ Nanoparticle-Sensitized TiO$_2$ Nanotube Arrays and Their Photoelectrochemical Properties." *J. Nanosci. .Nanotechnol.*, *15* (12), 9717–9720.

Zimmerman, A. F., Clark, D. G., Aust, K. T. and Erb, U. (2002a). "Pulse electrodeposition of Ni–SiC nanocomposite." *Mater. Lett.*, *52* (1), 85–90.

Zimmerman, A. F., Palumbo, G., Aust, K. T. and Erb, U. (2002b). "Mechanical properties of nickel silicon carbide nanocomposites." *Mater. Sci. .Eng. A*, *328* (1), 137–146.

Zou, X. and Zhang, Y. (2015). "Noble metal-free hydrogen evolution catalysts for water splitting." *Chem. Soc. Rev.*, *44* (15), 5148–5180.

LIST OF PUBLICATIONS

IN PEER-REVIEWED JOURNALS

1. **Elias, L.** and Hegde, A. C. (2015). "Electrodeposition of laminar coatings of Ni–W alloy and their corrosion behaviour." *Surface and Coatings Technology*, *283* 61–69.

2. **Elias, L.**, Scott, K. and Hegde, A. C. (2015). "Electrolytic Synthesis and Characterization of Electrocatalytic Ni-W Alloy." *Journal of Materials Engineering and Performance*, *24* (11), 4182–4191.

3. **Elias, L.**, Bhat, K. U. and Hegde, A. C. (2016). "Development of nanolaminated multilayer Ni–P alloy coatings for better corrosion protection." *RSC Advances*, *6* (40), 34005–34013.

4. **Elias, L.** and Hegde, A. C. (2016). "Optimization of Ni-P bath for coatings of maximum hardness and thickness by Taguchi's statistical approach." *Journal for Electrochemistry and Plating Technology*, DOI: 10.12850/ISSN2196-0267.JEPT5393

5. **Elias, L.** and Hegde, A. C. (2016). "Modification of Ni–P alloy coatings for better hydrogen production by electrochemical dissolution and TiO_2 nanoparticles." *RSC Advances*, *6* (70), 66204–66214.

6. **Elias, L.** and Hegde, A. C. (2016). "Induced codeposition of Ni-W alloy coatings using glycerol as additive and their characterization." *International Journal of Chemical Engineering and Processing*, *2* (2), 1–9.

7. **Elias, L.** and Hegde, A. C. (2016) "Development of Ni-P Alloy Coatings for Better Corrosion Protection Using Glycerol as Additive." *Analytical Bioanalytical Electrochemistry*, 8 (5), 629-643.

8. **Elias, L.** and Hegde, A. C. (2016). "Synthesis and characterization of Ni-P-Ag composite coating as efficient electrocatalyst for alkaline hydrogen evolution reaction." *Electrochimica Acta*, *219* 377–385.

9. **Elias, L.**, Cao, P. and Hegde, A. C. (2016). "Magnetoelectrodeposition of Ni–W alloy coatings for enhanced hydrogen evolution reaction." *RSC Advances*, *6* (112), 111358–111365.

10. **Elias, L.** and Hegde, A. C. (2017). "Effect of magnetic field on HER of water electrolysis on Ni-W alloy." *Electrocatalysis*, 1–8.

11. **Elias, L.** and Hegde, A. C. (2017). "Effect of magnetic field on corrosion protection efficacy of Ni-W alloy coatings." *Journal of Alloys and Compounds*, *712* 618–626.

12. **Elias, L.** and Hegde, A. C. (2017). "Effect of graphene oxide on the electrocatalytic activity of Ni-W alloy coating." *Insights in Analytical Electrochemistry*, 3:1.

13. **Elias, L.** and Hegde, A. C. Electrolytic synthesis of Ni-W-MWCNT composite coating for alkaline hydrogen evolution reaction. *Journal of Materials Engineering and Performance.* (Under Review).

14. **Elias, L.** and Hegde, A. C. A comparative study on the electrocatalytic activity of Ni-W-MWCNT and Ni-W-rGO nanocomposite coatings towards alkaline HER. *Materials Today Energy*. (Under Review).

CONFERENCE PROCEEDINGS

1. **Elias, L.** and Hegde, A. C. (2015). "Electrodeposition and Electrocatalytic Study of Ni-W Alloy Coating." *Materials Science Forum*, *830-831* 651–654.

2. **Elias, L.** and Hegde, A. C. (2015). *Effect of Silver Nanoparticle Sol on Electrocatalytic Character of Ni-P Alloy*, In Industrial Applications of Nanostructured Materials, Bloomsbury Publications, India, pp 61-66. *ISBN: 9789385436932.*

3. **Elias, L.** and Hegde, A. C. (2015). *Electrodeposition of TiO₂/Ni-P Composite Electrodes for Efficient Water Electrolysis,* In Recent Advances in Chemical Engineering, Springer, USA, pp 203-209. *ISBN: 978-981-10-1632-5, 978-981-10-1633-2.*

4. **Elias, L.** and Hegde, A. C. (2016). "Electrodeposited Ni-P alloy thin films for alkaline water splitting reaction." *Mater. Sci. Eng.,* 149 (2016) 012179.

5. **Elias, L.** and Hegde, A. C. (2017). *Electrodeposition of Ni-P Thin Films with Alternate P-high and P-low Multilayers*, In Corrosion: Fundamental and Practical Aspects for Mitigation Strategies, Proceedings of CORSYM 2015, pp 40-48. *ISBN No. 978-81-933428-0-0.*

PAPERS PRESENTED IN NATIONAL/INTERNATIONAL CONFERENCES

1. **Liju Elias** and A. Chitharanjan Hegde, Development of composition modulated multilayer Ni-W alloy on mild steel, 17th National Congress on Corrosion Control, held at Karaikudi, Tamil Nadu during August 21-23, 2014.

2. **Liju Elias** and A. Chitharanjan Hegde, Optimization of deposition conditions for electrodeposition of bright Ni-P alloy coating on mild steel using Taguchi's approach, International Conference on Chemistry and Materials (ICCM-14), held at BIT Campus, Anna University, Tiruchirappalli during November 14-15, 2014. (*ISBN: 978-93-81521-49-6*)

3. **Liju Elias** and A. Chitharanjan Hegde, Ni-W alloy Coatings: A Promising Electrode Material, International Conference on Materials Science and Mechanical Engineering (ICMSME-14) held at Bangkok, Thailand during December, 18-19, 2014. *(ISSN: 2010-376X)*

4. **Liju Elias** and A. Chitharanjan Hegde, Electrodeposition and electrocatalytic study of Ni-W alloy coatings, International Conference on Advanced Materials and Manufacturing Processes for Strategic Sectors (ICAMPS-15), held at Thiruvananthapuram, Kerala during May 13-15, 2015.
(DOI: 10.4028/www.scientific.net/MSF.830-831.651)

5. **Liju Elias** and A. Chitharanjan Hegde, Electrodeposition of Ni-P Thin Films with Alternate P-high and P-low Multilayers, International Corrosion Symposium for Research Scholars (CORSYM-15), held at IIT Madras, Chennai, Tamil Nadu during July 31st to August 2nd, 2015. (***Conferred "Best Presentation Award"***)

6. **Liju Elias** and A. Chitharanjan Hegde, Magnetic field induced water splitting on electrodeposited Ni-W alloy, Make in India: Role of Metals and Materials (MIRMM-15), held at NITK Surathkal, Mangalore during October 30-31, 2015. (***Conferred "Best Poster Award"***)

7. **Liju Elias** and A. Chitharanjan Hegde, Electrodeposition and Characterization of Ni-W Alloy Coatings for Better Corrosion Resistance, International Conference and Exhibition on Corrosion (CORCON-15), held at Chennai, Tamil Nadu during November 19 - 21, 2015.

8. **Liju Elias,** Arun Augustin, Udaya Bhat K. and A. Chitharanjan Hegde, Magnetic field Induced HER on Electrodeposited Ni-W alloy, 4th Nano Today Conference, held at Dubai during December 6 -10, 2015.

9. **Liju Elias** and A. Chitharanjan Hegde, Effect of Silver Nanoparticle Sol on Electrocatalytic Character of Ni-P Alloy, International Conference on Nanomaterials and Nanotechnology (NANO-15), held at KSR Campus, Tiruchengode, Tamil Nadu during December 7 - 10, 2015. *(ISBN: 9789385436932)*

10. **Liju Elias** and A. Chitharanjan Hegde, Electrodeposition of TiO_2/Ni-P Composite Electrodes for Efficient Water Electrolysis, International Conference on Advances in Chemical Engineering (ICACE-15), held at NITK Surathkal, Mangalore during December 20 - 22, 2015. *(ISBN: 978-981-10-1632-5, 978-981-10-1633-2)*

11. **Liju Elias** and A. Chitharanjan Hegde, Development of high corrosion protection Ni-W coatings by magnetoelectrolysis, 17th Asian Pacific Corrosion Control Conference (APCCC-16), held at IIT Bombay, India during January 27 - 30, 2016.

12. **Liju Elias** and A. Chitharanjan Hegde, Magnetoelectrodeposited Ni-W alloy coatings for hydrogen evolution reaction, 19th National Convention of Electrochemists (NCE-19), held at NIT Trichy, India during March 28 to 29, 2016.

13. **Liju Elias** and A. Chitharanjan Hegde, Magnetoelectrodeposition - As means to improve the hydrogen energy of Ni-W alloy, 7th International Conference on Hydrogen Production (ICH2P-16), held at Zhejiang University, Hangzhou, China during May 8 to 11, 2016. *(**Participated under the International Travel Support Scheme of TEQIP-II**)*

14. **Liju Elias** and A. Chitharanjan Hegde, Effect of multi-walled carbon nanotubes on electrocatalytic activity of Ni-W alloy electrodes, Second

International Conference on Materials Science and Technology (ICMST-16), held at St. Thomas College, Pala, Kerala during June 5 to 8, 2016.

15. **Liju Elias** and A. Chitharanjan Hegde, Synthesis of Ni-W-Graphene oxide composite coatings for alkaline hydrogen production, International Conference on Advanced Materials and Applications (ICAMA-16), held at BMS College of Engineering, Bengaluru, Karnataka, India during June 15 to 17, 2016.

16. **Liju Elias**, Vinayaka H. Damle and A. Chitharanjan Hegde, Electrodeposited Ni-P alloy thin films for alkaline water splitting reaction, International Conference on Advanced Materials and Manufacturing Applications (IConAMMA-16), held at Amrita Vishwa Vidyapeetham, Bengaluru Campus, Karnataka, India during July 15 to 16, 2016. *(DOI: 10.1088/1757-899X/149/1/012179)*

17. **Liju Elias** and A. Chitharanjan Hegde, Effect of TiO_2 and Ag nanoparticles on hydrogen energy of Ni-P alloy coatings, Conference on Engineering Materials (CEMAT-16), held at IISc Bangalore, India during July 18-19, 2016.

18. **Liju Elias** and A. Chitharanjan Hegde, A comparative study on the electrocatalytic activity of electrodeposited Ni-W and Ni-P alloy coatings, International Conference on Smart Engineering Materials (ICSEM-16), held at RV College of Engineering, Bengaluru, Karnataka, India during October 20 to 22, 2016.

19. **Liju Elias** and A. Chitharanjan Hegde, Electrochemical dissolution- As means to improve the HER efficiency of Ni-P alloy coating, Eleventh International Symposium on Electrochemical Science and Technology (iSAEST-11), held at Chennai, Tamil Nadu, India, during December 8 to 10, 2016.

BIO-DATA

Liju Elias

Permanent address:

Edamalayil House

Ooramana P.O.

Ramamangalam via

Muvattupuzha

Ernakulam - 686663

Kerala, India.

Contact Details:

Email: eliaslaiju@gmail.com

Phone: +91-4852870990, Mob: +919481331330

Academic Qualifications:

Bachelor of Science in Chemistry (2007) from Nirmala College, Muvattupuzha, Ernakulam (Affiliated to Mahatma Gandhi University, Kottayam), Kerala, India.

Master of Science in Chemistry (2009) from Newman College, Thodupuzha, Idukki (Affiliated to Mahatma Gandhi University, Kottayam), Kerala, India.

Awards and Achievements:

1. '*International Travel Support Grant*' from TEQIP-II to present a paper in ICH2P-16, International conference held at Hangzhou, China during May 8 to 11, 2016.

2. Best poster award in MIRMM-2015, International Symposium held at NITK Surathkal, Mangalore, India during October 30-31, 2015.

3. Best Presentation Award in CORSYM-15, International Conference held at IIT Madras, Chennai, Tamil Nadu, India during July 31 to August 1, 2015.

4. Best poster award in National conference on Emerging Trends in Analytical Techniques (ETAT-16), held at Govt. Science College (Autonomous), Hassan, India during March 28-29, 2016.

5. Selected as the best outgoing student in the Department of Chemistry, Nirmala College, Muvattupuzha, Kerala, India during the academic year 2006-07.

Research Publications:

Articles in International Journals   : 17

Conference Proceedings   : 6

Papers presentations in-

National/International conferences   : 22

Experience:

Teaching Experience (2010 to 2013): Faculty at the Post Graduate Dept. of Chemistry, Newman College, Thodupuzha, Idukki, Kerala, India.

Membership in International Organizations:

NACE International, student membership (Member number: 698675)

ACS, Student membership (Member number: 31011565)

Place : NITK Surathkal

Date : 02-08-2017   **LIJU ELIAS**